Satellite observations of Southeast Asia tropical forest responses related to climate seasonality, disturbance, and sun angle geometries

Ngoc Nguyen Tran

A thesis submitted in fulfilment of the requirements for the degree of
Doctor of Philosophy

School of Life Science
Faculty of Science
University of Technology Sydney

July 2019

Certificate of original authorship

I, Ngoc Nguyen Tran, declare that this thesis is submitted in fulfilment of the requirements for the award of the degree of Doctor of Philosophy, in the Faculty of Science at the University of Technology Sydney.

This thesis is wholly my own work unless otherwise reference or acknowledged. In addition, I certify that all information sources and literature used are indicated in the thesis.

This document has not been submitted for qualifications at any other academic institution.

This research is funded by Joint UTS-VIED Scholarship between University of Technology Sydney and Vietnam International Education Development. Also, this research is supported by an Australian Government Research Training Program.

Signature of student:

Production Note:
Signature removed prior to publication.

Date: 15-07-2019

Acknowledgements

First, and most of all, I would like to express my sincere gratitude to my principal supervisor, Distinguished Professor Alfredo Huete for his expertise, assistance, guidance, support, and patience throughout my doctoral candidature progress. As it was a challenging journey, I could not finish my four years' PhD study without his assistance. I thank him for holding me to a high research standard by providing insightful comments, advice, and constructive criticisms at different stages of my thesis research. I am also very grateful for his immense help during my hard times, including the thesis finalisation and the extension of my scholarship. He also provided me with many chances for me to improve my technical skills and background knowledge related to my research area. I would like to extend my special thanks to Professor Qiang Yu, my co-supervisor for his help during my candidature.

Furthermore, my gratitude also goes to many people who contributed to my PhD project. I would like to acknowledge Ekena Rangel Pinage for her help to revise my thesis with useful and constructive comments. I extend my special thanks to other current and past team colleagues for their invaluable academic and technical support. They include Rakhesh Devadas, Xuanlong Ma, Ha Nguyen, Wenjie Zhang, Sicong Gao, Jianxiu Shen, Leandro Giovannini, Paras Sidiqui, Song Leng.

I also want to thank the faculty staff of the Faculty of Science for their administrative assistance. Special thanks go to Shannon Hawkins, who provided wise advice for me during my PhD candidature. I would like to show my greatest appreciation to Graduate Research School for providing research development workshops which helped me to develop knowledge, skills and capabilities I need as a researcher. Also, special thanks go to Capstone Editing for providing professional editing service I used for several chapters of my thesis.

My deepest thank to my family for their support and understanding throughout my candidature. Their continuous support helped me to overcome negative feelings during my PhD candidature.

Finally, I appreciate the University of Technology Sydney and Vietnam International Education Development for their cooperation in providing UTS-VIED Joint Scholarship, which supported my thesis project.

Table of Contents

List of figures

List of tables

Abbreviations

AMP	Seasonal Amplitude
AVHRR	Advanced Very High Resolution Radiometer
BRDF	Bidirectional Reflectance Distribution Function
CERES	Clouds and the Earth's Radiant Energy System
CHIRPS	Climate Hazards Group InfraRed Precipitation with Station data
CV	Coefficient of Variation
DEM	Digital Elevation Model
DT	Dormancy Time
EGS	End of Greening Season
ENSO	El Niño-Southern Oscillation
EVI	Enhanced Vegetation Index
FAO	Food and Agriculture Organization of the United Nations
GRACE	Gravity Recovery and Climate Experiment
IGBP	International Geosphere-Biosphere Programme
LCT	Land Cover Type
LGS	Length of Greening Season
LST	Land Surface Temperature
MODIS	Moderate resolution Imaging Spectroradiometer

NASA	National Aeronautics and Space Administration
NBAR	Bidirectional reflectance distribution function Adjusted Reflectance
NDVI	Normalized Difference Vegetation Index
NIR	Near Infra-Red
PGS	Peak of Greening Season
QA	Quality assessment
RAA	Relative Azimuth Angle
SEA	Southeast Asia
SGS	Start of Greening Season
SSS	Seasonal Sen's Slope
SZA	Sun Zenith Angle
TRMM	Tropical Rainfall Measuring Mission
TWS	Total Water Storage
TWSA	Total Water Storage Anomalies
USGS	United States Geological Survey
VI	Vegetation Index
VZA	View Zenith Angle

Abstract

A mix of evergreen rainforests and deciduous dry forests, the tropical forests in continental Southeast Asia (SEA) have been massively affected by human activities. Despite being highly threatened, very few studies have been conducted on SEA forests compared to the amount of studies conducted on their Amazonian and African counterparts. Consequently, studies on continental tropical forests in SEA need to be urgently conducted to gain a better understanding of their functioning and more specifically, their seasonal and inter-annual dynamics. Satellite data have proven useful in monitoring vegetated landscapes at variable spatial and temporal scales; however, variations of sun-sensor geometry have caused controversies over satellite-based results. Thus, the effect of variable sun-view angles on phenology needs to be investigated to minimise observation artefacts from real vegetation seasonal dynamics.

The primary goal of this thesis is to study the inter- and intra-annual dynamics of continental SEA tropical forests using vegetation indices (VIs) derived from MODIS satellite data while also considering the effects of the bidirectional reflectance distribution function (BRDF) on the retrieved results. To achieve this goal, I first investigated continental SEA forest phenology and the effects of the BRDF on extracted phenological information. Next, I analysed the disturbance contribution in relation to intra-annual forest phenology by comparing seasonal profiles and phenological metrics between disturbed and undisturbed forests. Finally, I analysed the effects of the BRDF on the inter-annual VI variations and the inter-annual responses of SEA forests to climate variability.

The results showed that the BRDF had substantial effects on the retrieved VI data. Thus, it appears that standardising reflectances and VIs at fixed sun-view angles is an essential process in the analysis of tropical forest phenology in the continental SEA region. Correcting the BRDF will prevent any unnecessary controversy in relation to the effects of varying illumination angles and the viewing geometries of satellite-based observations. Regarding the disturbance effects, my findings showed that disturbance affected SEA forest phenology in terms of both seasonal VI profiles and phenological metrics and that the BRDF correction helped to distinguish between disturbed and intact forests. My analyses also revealed that the inter-annual VI variations of SEA forests were affected by both the BRDF effect and climate variability.

This thesis highlights the responses of continental SEA tropical forests to sun-angle geometries, climate seasonality and disturbances related to satellite observations. It makes an essential and significant contribution to understandings of SEA forest phenological diversity.

Chapter 1. Introduction

1.1. Tropical forest roles

1.1.1. Forest biodiversity

Tropical forests are home to over half of the earth's total species (Ehrlich & Wilson, 1991; Lewis, Edwards & Galbraith, 2015). Forests in tropical regions have many more tree species than those in temperate areas. For example, in half a square kilometre of forest in Malaysia, there are as many tree and shrub species as there are in all of the forests in Canada and the United States of America (USA) (Montagnini Florencia, 2005). Plants provide shelter and food for many animals that depend on these tropical forests for their survival. A case study by Ehrlich and Wilson (1991) showed that a single Peruvian tree contained as many species of ants as the British Islands.

The conversion of tropical forests for agriculture, timber production and other uses has generated vast human-dominated landscapes and has had pernicious consequences on tropical biodiversity (Gibson et al., 2011). According to Hansen et al. (2013), tropical forests experienced the greatest forest loss among the four main forest types (i.e., tropical, subtropical, temperate and boreal) in the globe. As the terrestrial biodiversity of Earth is heavily concentrated in tropical forest ecosystems, mass extinction is likely to occur in the tropics due to their high deforestation rates (Alroy, 2017).

1.1.2. Rainfall regulation

The role of forests in sustaining lower surrounding temperatures or higher humidity moistness could affect climate conditions at both local and regional levels (Nobre, Sellers & Shukla, 1991). If significant portions of forests are lost, evaporation and transpiration will likely decrease, which in turn could reduce rainfall and lead to tropical species being replaced by savannas or woodland vegetation. Currently, the consequences of deforestation are not entirely clear. Some authors contend that deforestation may cause local climate change while others argue that the results and signification of the effect are likely to be minimal (Nasi, Wunder & A, 2002).

Recent studies have shown that the extended consequences of deforestation could affect annual rainfall or precipitation patterns (Devaraju, Bala & Modak, 2015). According to Lawrence and Vandecar (2014), large-scale deforestation within the tropics could significantly shift rainfall distribution and temperatures even at locations far from deforestation hotspots. Lawrence and Vandecar showed that rainfall patterns shift rather than reduce when deforestation rates pass certain thresholds and that consequently, the rainfall in some areas have declined while other regions have become wetter. Spracklen, Arnold and Taylor's (2012) study showed that rain could drop up to 21 per cent in the Amazon dry season by 2050 if deforestation rates are maintained. As Figure 1.1 shows, the effect of decreases in precipitation in the dry season will be much worse than that in the wet season over forest areas in the Amazon basin. Additionally, research has shown that wind blowing over vegetation produces twice as much rainfall as wind blowing over open areas (Spracklen et al., 2012).

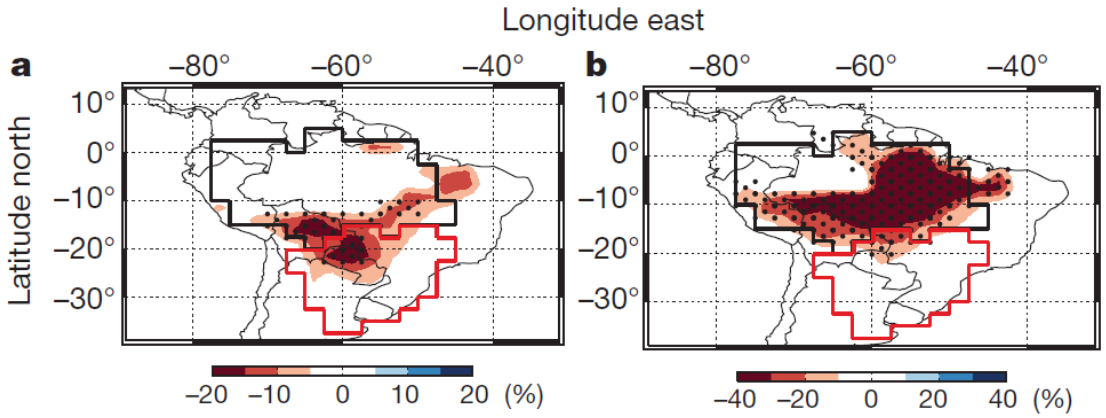

Figure 1.1. *Simulated percentage change in precipitation due to 2000–2050 business-as-usual deforestation of the Amazon basin. A, wet season; B, dry season.*

Note: The stippling denotes regions in which the simulated precipitation anomaly differs from the present day rainfall (1998–2010) by more than one standard deviation. The Amazon and Rio de la Plata basins are marked black and red, respectively (Spracklen et al., 2012).

A significant amount of research has already related the effects of forest loss to changes in intra- and inter-annual rainfall patterns. Deforestation has caused a shift in the seasonality of rainfall in Brazil. Precipitation data obtained from meteorological stations in Rondônia (Brazil) showed a delay in the wet seasons of deforested regions while it

remained in forested areas for over last 30 years (Spracklen et al., 2012). Further, evapotranspiration varies with the leaf area, canopy architecture and rooting depth of the replacement vegetation. Modelling scenarios for the Amazon have indicated that reductions in rainfall are greater following conversions to soybean croplands than those following transformations to pastures (Spracklen & Garcia-Carreras, 2015).

Tree crops, such as palm oil or pulp/paper plantations, currently drive deforestation in Southeast Asia (SEA). Such crops cause less dramatic changes to energy and water balances than conversions to pastures or herbaceous crops (Miettinen, Stibig & Achard, 2014). Suepa (2013) showed that the primary rainfall trend in the SEA Peninsular was mostly downward between 2001 and 2010 (see Figure 1.2). Only a small area in Thailand showed an upward rainfall trend in this period. Thus, most of the tropical forests of SEA are subject to downward trends in precipitation. Such trends could have adverse effects on the phenology of forests and make them more vulnerable to drought and extreme climate events (e.g., El Niño—Southern Oscillation [ENSO]).

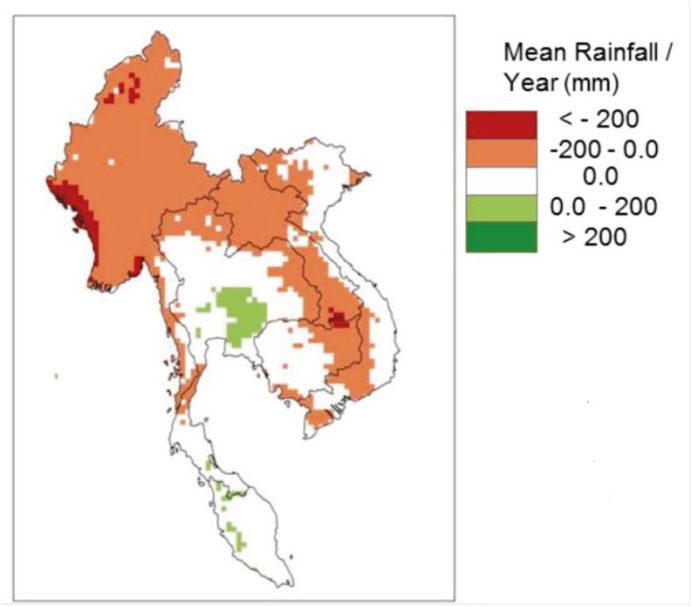

Figure 1.2 *Trend of Peninsular SEA rainfall 2001-2010 (Suepa, 2016)*

Makarieva, Gorshkov, Sheil, Nobre and Li (2013) argued that condensation is an essential driver of winds and that many scientists have ignored condensation for a long time, especially the forest condensation caused by evaporation. The authors suggested that the dense vegetation of natural forests has higher evaporation than oceans. Thus, forests are low-pressure regions, draw moist air from oceans and have high precipitation

in their woods. Deforestation would reduce this hydrological cycle, as transporting less moisture to continental lands would cause a drop in rainfall.

This hypothesis remains controversial but strongly suggests that even small-scale deforestation, if it occurs in coastal areas, could disrupt the movement of moisture from the ocean to the inland and lead to the drying of continental interiors. However, the effects of forest loss on rainfall are unclear in insular SEA where forest cover is scattered across islands rather than over large regions as it is in the Amazon, Congo or continental SEA basins.

1.1.3. Temperature

In addition to shifting rainfall patterns, tropical deforestation could cause an increase in average temperature. By absorbing carbon from the atmosphere, forests reduce the carbon dioxide built-up through the photosynthesis process. During the process of photosynthesis, the cells of green plants use carbon dioxide and solar energy to make sugar molecules, oxygen and other vital plant compounds. Consequently, green plants store carbon in their tissues. As a plant dies, the process of decomposition may cause carbon dioxide or methane to be released into the atmosphere. Alternatively, part of the carbon in plant tissue may become soil organic matter via the decomposition of the plant material.

It is undeniable that clearing forests for wood, crops or other purposes will cause the carbon stored in forests to be released into the atmosphere (Montagnini Florencia, 2005). As a result, there will be a build-up of carbon dioxide, which is considered the primary gas responsible for the ‘greenhouse effect’ and thus the increase in global temperatures. Forest ecosystems are estimated to absorb up to three billion tons of carbon annually. Table 1.1 sets out the carbon stock estimates of the International Panel on Climate Change (IPCC, 2000). Tropical forests represent the most significant carbon (C) pool in vegetation by far, while the boreal forest biome represents the largest carbon (C) stock in soils. For example, the Brazilian Amazon alone accounts for approximately 10 per cent of the world’s terrestrial carbon (Tian et al., 1998). In recent decades, a considerable portion of carbon has returned to the atmosphere through deforestation and forest fires. According to estimations by the Food and Agriculture Organization (FAO,

2001), 25 per cent of carbon emissions from human activities came from tropical deforestation.

Table 1.1 *Global carbon stocks in vegetation and soil carbon pools down to a depth of One Metre (IPCC, 2000)*

Biome	Area (10^9 ha)	Global carbon stocks (Gt C)		
		Vegetation	Soil	Total
Tropical forests	1.76	212	216	428
Temperate forests	1.04	59	100	159
Boreal forests	1.37	88	471	559
Tropical Savannas	2.25	66	264	330
Temperate grasslands	1.25	9	295	304
Deserts and semi-deserts	4.55	8	191	199
Tundra	0.95	6	121	127
Wetlands	0.35	15	225	240
Croplands	1.60	3	128	131

A recent article by Li et al. (2015) used a high-resolution global satellite dataset (MODIS) to gather new evidence on the effects of forests, especially tropical forests, on local temperatures. According to this study, tropical forests cause substantial cooling effects throughout the year. Schneck and Mosbrugger, (2011) predicted a local increase in surface temperature of 1°C due to reduced evaporative cooling after deforestation. The authors also suggested that ocean surface temperatures will fall in some regions due to reduced trade winds and the weakened upwelling of cold deep waters.

1.1.4. Monsoons

Modelling studies of the Indochina peninsula have emphasised the effects of deforestation on the East Asian Summer Monsoon (Omer Lutfi Sen, Wang & Wang, 2004). The complete removal of trees has caused an increase in wind speed and air temperature and a decrease in water vapour, which has led to the weakening of the monsoon flow over east China. At the same time, there has also been a change in the frequency of rainfall, such that there is now a higher rainfall frequency in many areas in

which annual precipitation has increased. Models by Sen et al. (2013) showed that a shift from forest cover to irrigated crops has caused an enhanced monsoonal flow over the upland montane region of mainland SEA, but a weaker flow over the South China Sea. It has also been reported that a significant decrease in summer monsoon rainfall has already occurred in the Indochina peninsula due to extensive lowland deforestation (Kanae, Oki & Musiake, 2001).

1.2. Tropical forest responses to climate change and disturbance

Feedback on the effects of climate change and disturbance on vegetation are critical, as this information can be used to assess the resilience of ecosystems, particularly in tropical forests. Several studies have been conducted on tropical forest responses to climate change and disturbance, notably in the Amazon basin. Betts's (2004) models indicate that tropical forests are drying because of precipitation decreases and global warming. Conversely, Friedlingstein et al.'s (2006) models, which include 11 coupled climate-carbon cycle models, predict that forests are more persistent than expected.

Huete et al. (2006) used the MODIS Enhanced Vegetation Index (EVI) (see Figure 1.3) to show tropical forest 'greening' responses to seasonal dry periods over the Amazon basin. Their discovery was unexpected, as trees should lose their leaves and 'brown' in the dry season. This anomalous phenology is occurring because intact forests have well-developed root structures that help these forests tap deep soil water pools and withstand dry seasonal periods. Additionally, increased sunlight in the dry season increases photosynthesis rates, which together with the sufficient water storage, ensures that these forests 'green-up' in the dry season.

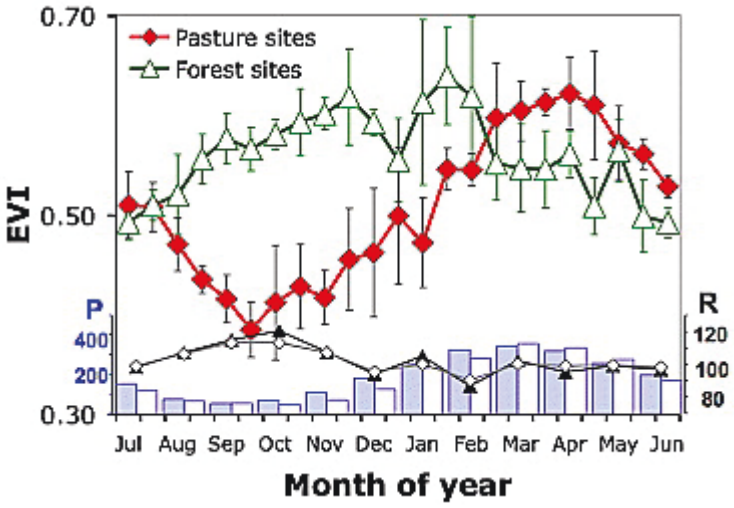

Figure 1.3. *5-year mean seasonal EVI (2000-2005) at Amazon local forest and conversion sites with PAR (lines) and long-term station rainfall (Huete et al., 2006)*

Another study by Huete (2008) showed that water limitations might become dominant in drier tropical areas. The results of satellite and flux tower measurements indicate that equatorial rainforests in Borneo showed 'greening' during dry season while drier Thailand forest areas showed increased water limitations. In a recent article, Zhang et al. (2016) examined a combination of satellite data of solar-induced chlorophyll fluorescence (SIF) and the recent research data of Phompila, Lewis, Clarke and Ostendorf (2014), who studied vegetation changes with the EVI in Lao tropical forests and concluded that Lao's forests are 'greening' due to increased precipitation and that this has little or no relation to temperature.

Evidence of the consequences of extreme climate in SEA was provided in a recent report by Gaveau et al. (2014), which showed that a seasonal two months dry spell in an otherwise rainy year triggered the Indonesian fires of 2013 and that while only 7 per cent of the burned lands were classified as 'forest' before the wildfire event, over half of the burned areas (58 per cent) were forested five years earlier. Thus, even mild drought periods can have large-scale consequences for tropical regions, especially in areas that have already been affected by previous disturbances.

1.3. Tropical forests in mainland of Southeast Asia

Tropical forests are located in the region of the Earth between 23.5 degrees north to 23.5 degrees south of the equator. This part of the planet has only two seasons: wet and

dry. However, even within the tropics, forests may be categorised based on the length of their rainy and dry seasons. Across the broad tropical landscape, the gradual transition from rainforests to dry forests is largely a function of precipitation during the growing season (rainforests receive more rain than dry forests). This transition takes place as one moves away from the equator, where consistent rainfall supports tropical rainforests to the north or the south (Elias & May-Tobin, 2011).

Most rainforests lie close to the equator (i.e., between 10 degrees north and south of the equator). Rainforests have either no or very short dry seasons. The consistent levels of rain the trees receive cause them to remain green and grow throughout the year. Due to their importance of richness in biodiversity and carbon stock, tropical evergreen forests have captured the attention of scientists and have provided a constant source of new scientific discoveries for a very long time.

Unlike rainforests, tropical dry forests are located between 10 and 25 degrees north and south of the equator. At around 10 degrees of latitude, rain becomes more seasonal and land cover tends to transition to dry forests or even savannahs. Dry tropical forests experience longer dry seasons and have deciduous trees that lose some or all their leaves during the dry months. The characteristics of dry forests are dependent on average rainfall; wetter forests have taller trees and more evergreen species than drier forests.

The tropical dry forest map provided by FAO (FAO, 2001) showed that the most significant areas of dry forests are in South America, sub-Saharan Africa and Asia. These areas comprise approximately 42 per cent of the world's subtropical and tropical forests (Murphy & Lugo, 1986). Tropical dry forests are also home to a wide variety of wildlife albeit they are less biologically diverse than rainforests. The poorest people on earth depend on dry forests (Campbell, 1996; Cunningham, 2008). For example, the African miombo woodlands alone sustain the livelihoods of over 100 million people in both city and country areas (Campbell B, 2004; Syampungani, 2009). Additionally, millions of farmers depend on tropical dry forests to aid their agricultural systems, as they supply a wide range of ecosystem services (Gumbo, 2010).

Dry forests are very important to human beings and have a crucial role in nature; however, tropical dry forests are among the most endangered and least studied forested

ecosystems in the world and as a result, are at a higher risk than humid forests (Aide et al., 2013; Gillespie et al., 2012; Janzen, 1988; Miles et al., 2006; Portillo-Quintero & Sánchez-Azofeifa, 2010). For example, Gillespie et al. (2012) showed that tropical dry forests have been reduced to less than 10 per cent of their original cover and that human activities and invasions of exotic species threaten the remaining forests. The goods and services that dry forests provide differ significantly to those that humid forests provide. Consequently, different approaches need to be adopted for their management and conservation (Gumbo, 2010; Nasi et al., 2002). However, very few studies have focused on tropical dry forests. According to Sánchez-Azofeifa et al. (2005), over the last 60 years, only 14 per cent of the articles published on tropical environments have focused on dry forests despite their essential roles. Indeed in both the natural and social sciences, rainforests have received more attention in forest-based discussions and have been subject to more research than tropical dry forests (Malmer, Anders and Nyberg, 2008; Sánchez-Azofeifa et al., 2005).

Of the three major continents of tropical forests (i.e., the Amazon, Africa and SEA), SEA tropical forests are profoundly affected by human activities (Stibig, Achard, Carboni, Raši & Miettinen, 2014) and have endured severe losses. Following the FAO's 2005 report, Vietnam and Laos had the top three highest rates for primary forest loss (FAO 2005). The FAO (2015) further reported that Burma was among the top 10 countries of countries with the highest annual net loss of forest areas. Stibig (2014) showed that the two leading causes of deforestation in SEA were conversion to crop plantation and non-sustainable logging. Despite SEA tropical forests being highly threatened, countries such as Laos and Cambodia are not participating in reserve programs (e.g., the Asian Dry Forests Initiative) (Blackie, 2014). Due to the economic and ecological importance and existing gap in the scientific research about SEA tropical forests, particularly tropical dry forests, there is an urgent need to increase current understandings of the phenology, effects and feedbacks of disturbances in these regions.

1.4. Remote sensing to study forest phenology

1.4.1. Satellite Data and Vegetation Phenology

The science of remote sensing is widely used by environmental scientists. According to Purkis and Klemas (2011), remote sensing might be understood as the practice of obtaining information about the Earth's landscape by using images captured from a distance via the electromagnetic radiation that is reflected or emitted from the surface of the Earth. Remote sensing primarily seeks to understand an object or landscape from a vantage point by capturing and interpreting the information without any direct physical contact. Scales of platforms can be diverse and may range from flux towers (just above the surface of the Earth) to satellites (thousands of miles away in space) (see Figure 1.4). Examples of remote sensing include aerial photography, satellite imagery, radar altimetry and laser bathymetry. Coupled with ground measurements, remote sensing can provide valuable information about the surface of the land, the oceans and the atmosphere.

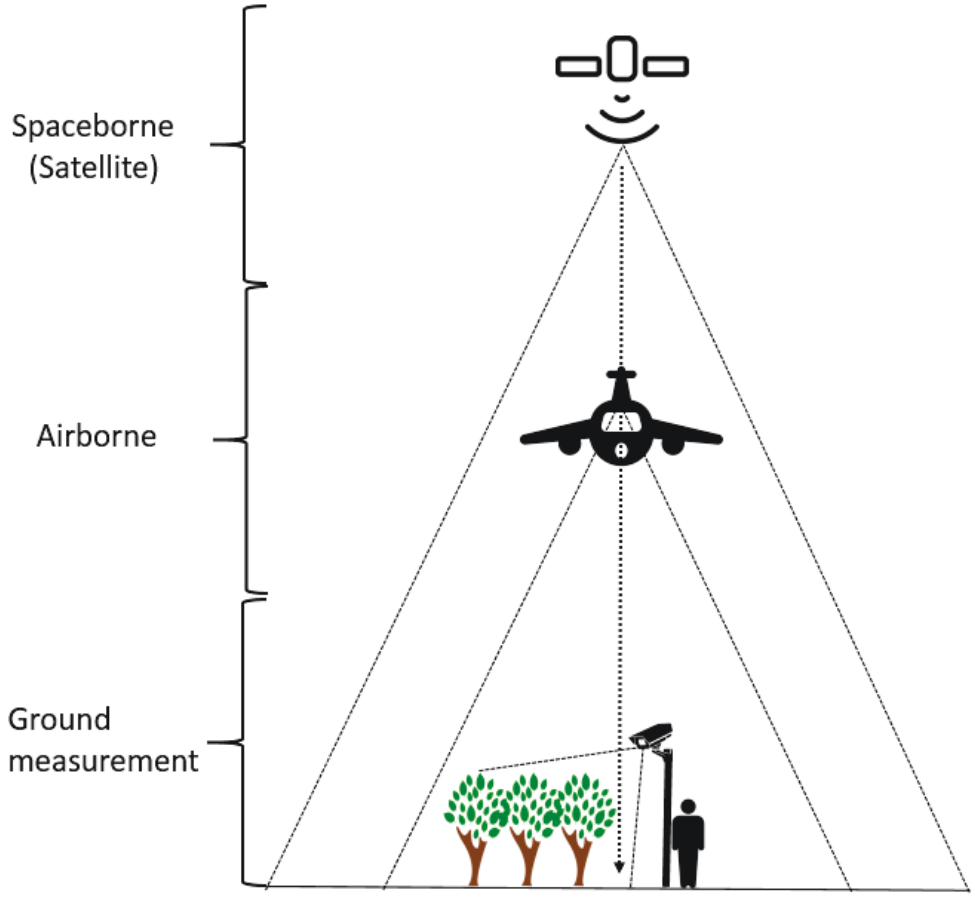

Figure 1.4. *Remote sensing platforms.*

Different remote sensing platforms can bring various benefits to different applications. For example, microwave satellite sensors can be used for applications related to landscape structures, like total above ground biomass (Shi et al., 2008). The advantages of microwave based approaches are the capability of the near all-weather signal capturing and vegetation canopy penetration. However, microwave platform could not directly detect related photosynthesis activities of live green plants because of its wavelengths. Optical remote sensing, though being limited by weather conditions, form images of the earth's surface by capturing the solar radiation reflected from targeted ground using visible, near infrared and shortwave-infrared sensors. It can be used for monitoring vegetation health because of its used spectral region, photosynthetically active radiation (PAR), directly related to the process of photosynthesis of green plants.

Temporal remote sensing products enable the analysis of vegetation time series to monitor the process and the pattern of environmental changes through time and space. The capacity to capture the relationship between temporal and spatial processes is considered the primary advantage of remote sensing data. These data have various spatial and temporal resolutions and enable the adequate monitoring of large-scale vegetation phenology.

In a changing environment, phenology is an essential indicator of ecosystem dynamics (Xiao, Zhang, Yan, Wu & Biradar, 2009). According to Schwartz (2013), plant phenology is the study of periodic biological events in the plant world or the timing of different stages of the seasonal vegetation cycle that are affected by the environment and climate. Phenological information, such as the timing and rate of 'green-up', amplitude or duration of the growing season, is key to understanding climate variability and vegetation trends, both of which are fundamental factors in the global change sciences (Hermance, Jacob, Bradley & Mustard, 2007).

Land surface phenology (LSP) is defined as the seasonal pattern of the spatiotemporal variation in the vegetated land surfaces observed via remote sensing (de Beurs & Henebry, 2010). This definition refers to the aggregated information of plant phenology at the spatial resolution of satellite sensors. LSP is usually considered in relation to the vegetation indices (VIs) of satellite time-series data and its advantage is that it can be assessed globally.

LSP is sensitive to changes in climate. The carbon and water cycles are influenced by changes in the phenology of plants via the photosynthesis and evapotranspiration processes. Differences in phenology trends between ecosystems can be used to assess responsiveness to climate change. The degree of the inter-annual variability of phenology, particularly during severe dry and wet years, is suggestive of an ecosystem's susceptibility to future climate (Bradley & Mustard, 2008). Thus, it is vital that global changes science characterises land cover phenology and understands how phenology responds to inter-annual variability, environment and land use. Phenology analyses often use satellite time-series data to assess regional-scale vegetation variability and identify changes to characterise current patterns of land cover phenology and distinguish between land cover-driven change and inter-annual climate fluctuations (de Beurs & Henebry, 2005b).

1.4.2. Vegetation Index

A VI is a spectral transformation of two or more bands designed to enhance the contribution of vegetation properties (Huete et al., 2002). VI data can be used to monitor land surface biophysical properties and processes, including primary production and land cover conversion. With the right combination of spectral bands, these transformed numbers have a number of advantages over original spectral data. Notably, VI data minimises soil and other background effects, reduces data dimensionality, provides a degree of standardisation for comparison and enhances the vegetation signal (Reed et al., 1994).

Kriegler et al.'s (1969) Normalised Difference Vegetation Index (NDVI) is one of the most well-known VIs and has frequently been used to evaluate the phenological characteristics of vegetation. The NDVI was created based on a vegetation photosynthesis feature: leaf cells mainly absorb visible light for the photosynthetic process while reflecting solar radiation in a near-infrared spectral band that can damage leaf tissues. Thus, the healthy leaves of green plants appear relatively bright in near-infrared and dark in photosynthetically active radiation (PAR) regions (Gates, David M 1980).

The formula of NDVI is based on the following equation (Eq. 2-1)

$$NDVI = \frac{\rho_{NIR} - \rho_{RED}}{\rho_{NIR} + \rho_{RED}} \quad (2\text{-}1)$$

Where ρ_{NIR} and ρ_{RED} stand for the spectral reflectance measurements acquired in the near-infrared and red spectral regions, respectively. These reflectances are ratios of reflected over incoming radiation in each spectral band individually, so they take on values between 0 and 1. By design, NDVI of healthy leaves is higher while stressed or dead ones have lower values. With its simplicity and capacity, NDVI was used to study vegetation phenology in numerous studies for several decades (Yves Julien, Sobrino, & Verhoef, 2006; Smith & Choudhury, 1990; Wu et al., 2018).

Although NDVI is widely used for the study of vegetation and phenology dynamics, it has some disadvantages and is not suitable for specific regions, especially tropical zones. This is due to the variation of atmospheric conditions with aerosols and clouds, and NDVI's sensitiveness to soil background (Xiao, Hagen, Zhang, Keller, & Moore, 2006). Xiao (2009) also indicated the saturation as an additional limitation of NDVI for LSP, in particular for tropical forests and other high biomass regions with large values of leaf area index. EVI is an 'optimised' index designed to enhance the vegetation signal with improved sensitivity in dense biomass regions and to reduce atmospheric effects and soil background. EVI formula (Eq. 2-2) includes the blue reflectance band to correct for the influence of atmospheric aerosols on red reflectance (Huete et al., 2002).

$$EVI = G \times \frac{\rho_{NIR} - \rho_{RED}}{\rho_{NIR} + C_1 \times \rho_{RED} - C_2 \times \rho_{BLUE} + L} \quad (2\text{-}2)$$

Where:

$\rho_{NIR}/\rho_{RED}/\rho_{BLUE}$	are atmospherically-corrected or partially atmospherically-corrected (Rayleigh and ozone absorption) surface reflectances for near-infrared, red and blue spectral regions, respectively,
L	is the canopy background adjustment that addresses non-linear, differential NIR and red radiant transfer through a canopy,
C1	is the coefficients of the aerosol resistance term of Red band
C2	is Atmosphere Resistance Blue Correction Coefficient

G is the gain factor

The coefficients adopted in the MODIS-EVI algorithm are L=1, C1 = 6, C2 = 7.5, and G = 2.5.

EVI profiles, which have the potential to represent seasonal and annual dynamics, can be generated to present trends and changes in vegetation conditions. Xiao (2006) noted that time-series MODIS-EVI data successfully detected phenology in a humid tropical region in South America in 2002. Huete (2002) compared the MODIS NDVI and EVI temporal profiles and found that the EVI exhibited a smoother, more symmetrical seasonal vegetation profile with a narrower, well-defined peak greenness period. Further, the EVI was less sensitive to residual atmospheric contamination due to aerosols from the large fires (Xiao et al., 2009) that are common in dry and disturbed tropical forests. Thus, the EVI has been widely used in tropical areas, as it reduces soil and atmospheric effects and was designed to improve sensitivity in high biomass regions and reduce the canopy background signal.

1.4.3. Data smoothing and filtering

VI time-series data are typically composited over a set period to process the growing season or to extract phenological parameters. These composite data often include noise caused by cloud and atmospheric contamination and varying sun and sensor angles. Due to these issues, the removal of outliers and spiked values or the minimisation of the effect of anomalous data are required when using VI time-series data (Jönsson & Eklundh, 2004).

A variety of smoothing methods have been developed to reduce the noise of time-series data from simple linear smoothing window methods to complex analytical curve function methods. Due to the seasonal cycles of phenology, particularly those derived from monthly or daily averaged samples from multiple years, one of the conventional techniques used to analyse phenology is Fourier Transform (FT) (Hermance et al., 2007). However, FT methods depend on symmetric sine and cosine functions that may cause problems when applied to asymmetric VI data. Further, FT analyses fail to identify each annual VI trajectory separately. Consequently, FT analyses can generate false oscillations in VI time-series data (Hird & McDermid, 2009). Another disadvantage of using FT

methods for VI time series relates to potential data gaps. This is a common issue that arises in relation to VI data, as FT methods require that the observed data is sampled at uniform intervals of time (Hermance et al., 2007).

Unlike FT, Asymmetric Gaussian (AG) functions can be applied to non-uniformly sample data in time. AG fits data to a local model function at intervals around maxima and minima in the time series and builds a global function to describe the annual cycles of vegetation (Eklundh & Jönsson, 2015). AG can capture vegetation dynamics at high latitudes (Beck et al., 2007); however, it can be hard to identify an acceptable and consistent set of maxima and minima for local function, especially for data from areas in which there is no apparent seasonality in the VI time series.

The Double Logistic (DL) function is similar to the AG function, as it uses minimum and maximum VI values, two inflection points and parameters depending on the rate of increasing or decreasing VI (Beck et al., 2007). DL also works with biased noise and in approximate winter conditions (Hird & McDermid, 2009). Thus, the DL function is a proper method for studying vegetation phenology in high latitudes (Beck et al. 2006). However, this approach shares the same disadvantages as those of the AG approach. It relies on the linear combination of local and independent intra-annual functions. Additionally, in some cases, it cannot match the global waveform of numerous time series (Carrao et al. 2010).

The high-order spline fitting model is another choice for smoothing time-series data. It applies a recursive least squares procedure for the initial inter-annual fit and then uses the average annual curve as a baseline and asymmetrically weights all the data points above and below the average to fit the upper envelope of the data (Bradley, Jacob, Hermance & Mustard, 2007). This approach may be suitable for getting rapid ‘green-up’; however, it has one critical drawback: it fits data errors that fall outside the time series (Bradley et al., 2007). This method also requires highly computational calculations and is time consuming (Hermance et al., 2007). Thus, this method is not applicable to the EVI, as this VI has less negatively biased noise and more erroneous spikes than the NDVI (Hird & McDermid, 2009).

The Savitzky-Golay (SG) filter (Savitzky & Golay, 1964) provides a potential approach for smoothing VI time-series data. SG filtering performs least squares

polynomial regressions on each point to determine the smoothed value and adapt for the upper envelope of the VI time-series profile (Eklundh & Jönsson, 2015). The SG filter applies an iterative weighted moving average filter to time series and weighting is given as a polynomial of a particular degree (Chen et al., 2004). The major advantage of this method is that it can preserve the features of the distribution and capture rapid phenology changes, such as relative maximums and minimums, which are usually flattened by the other averaging techniques (Jönsson & Eklundh, 2004). More importantly, the SG filter can model the shape of the seasonal VI in uncertain environments with significant variations in magnitude and timing of vegetation growth. It can distinguish the signal from seasonal changes and noise to reconstruct a clear and clean time series by a linear combination of nearby values. Tottrup et al., (2007) showed that SG filtering provided excellent results in capturing phenological parameters for the monsoon climate of SEA , which has multiple annual seasons during a year.

In tropical regions, SG filtering effectively replaces the large numbers of low VI values caused by atmospheric perturbations with higher values that are more typical of vegetation found in these areas (Chen et al., 2004). A comparison of the SG and AG models in relation to smoothing and extracting phenological parameters in Southern Africa (Bachoo & Archibald, 2007) showed that the SG method worked better than the AG method. Tottrup et al. (2007) applied SG filtering to mapping fractional forest cover in SEA and concluded that the technique produced excellent results in smoothing data and extracting phenological parameters. These authors also claimed that SG analysis is suitable for capturing multiple seasons during a year.

However, SG filtering should be used with caution, as this method is sensitive to the choice of the window size. For example, a wide window limits the ability of the filter to acquire rapid changes in ‘green-up’ while a narrow window may cause the result to retain more noise than real signals (Hird & Mc Dermid, 2009). Thus, the size of the window has to be selected and applied carefully and should be tested before the overall data is run (Chen et al., 2004).

1.4.4. Extracting phenological parameters

To gather meaningful phenological information about the vegetation growing season, suitable parameters with smoothed time-series VIs need to be obtained. Myneni

et al. (1997) and Tucker et al. (2001) proposed a set of metrics from satellite-derived NDVI time series that included data on the onset of 'green-up' and senescence, the maximum rates of 'green-up' and senescence and the amplitude of seasonality. Various techniques were developed to capture the transition dates and related information. One of these approaches is the inflection point on a fitted curve (Reed, 2003). This algorithm defined the start of the 'greening' season (SGS) as the time at which the (left) time derivative transitions from zero to a positive number. Similarly, the end of the greening season (EGS) was defined as the time at which the time derivative transitions from a negative to zero (Reed, 2003). Zhang et al., (2003) used this approach to retrieve four transition dates ('green-up', maturity, senescence and dormancy) to monitor vegetation phenology in the northeast of the USA. The major disadvantage of this algorithm is the difficulty it has in extracting the VI for evergreen vegetation and accounting for snow effects and the slow rate of senescence in some biomes (Reed et al. 2003).

Another approach, curve derivation phenology, identifies phenological metrics by investigating the temporal curve at which VI data show a rapid, sustained increase or decrease (Reed et al. 2003). Under this method, the timing of the highest positive derivative in a VI time series is considered the SGS and the lowest derivative is considered the EGS. However, this approach is unable to determine whether rapid changes are the result of the natural variability of the data or represent significant differences. Additionally, under this method, it is also difficult to determine the SGS and the EGS when VI curves lack abrupt and rapid increases or decreases (de Beurs & Henebry, 2010).

The third and most common approach is threshold-based and provides the most practical technique for retrieving phenological metrics. Notably, this approach uses a pre-defined or relative reference value for defining the SGS and the EGS (Reed et al. 2003). The SGS is determined as the day of the year (DOY) that VI crosscuts the threshold in an upward direction. Conversely, the EGS is determined as the DOY when VI crosses the same limit in a downward direction (see Figure 1.5). Various algorithms based on threshold techniques have been developed to extract phenological parameters (e.g., thresholds based on a long-term mean VI, thresholds based on a baseline year, thresholds based on a reference value and thresholds based on VI ratios) (de Beurs & Henebry, 2010).

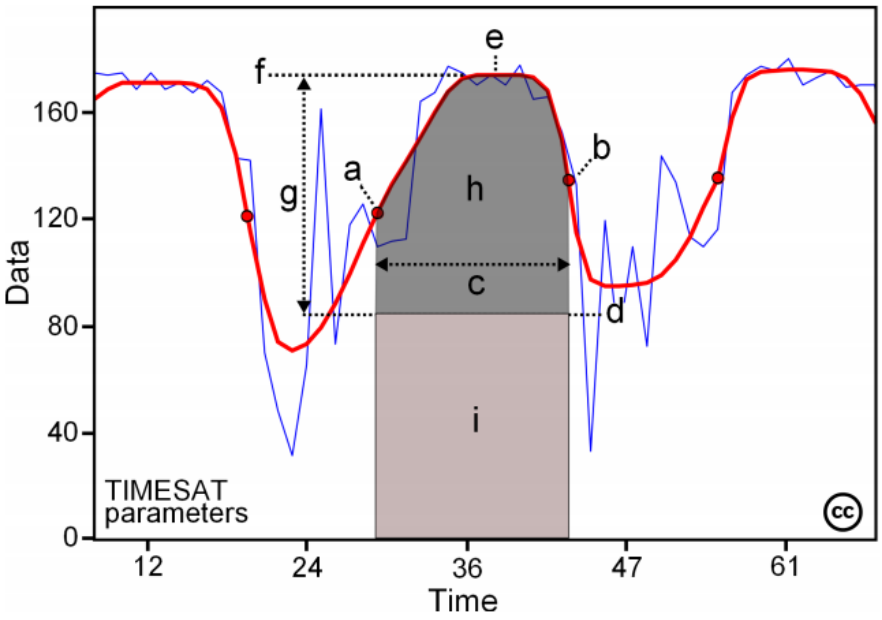

Figure 1.5. *Some of the seasonality parameters generated in TIMESAT: (a) beginning of season, (b) end of season, (c) length of season, (d) base value, (e) time of middle of season, (f) maximum value, (g) amplitude, (h) small integrated value, (h+i) large integrated value. (Eklundh & Jönsson, 2015)*

1.4.5. Trending analysis

Trend analyses of VI time series are crucial to understand inter-annual variations of vegetation dynamics over a long period. These variations reflect both strong and slight changes in vegetation. Strong changes may refer to land cover conversions; for example, deforestation or urbanisation (Martínez & Gilabert, 2009). Conversely, small changes show that the overall land classification is unchanged. Thus, it is still essential to investigate vegetation variation over long-term periods and how it responds to influencing factors, such as climate change or disturbance.

A wide variety of algorithms have been developed for time-series data. Thus, it is important to choose an appropriate technique to study vegetation phenology trends. VI time series are considered as non-stationary data that present frequency components (e.g., seasonal variation and long-term and short-term fluctuation data). VI patterns are generally seasonal (de Beurs & Henebry, 2005). Given these characteristics, a typical procedure, such as a simple linear regression, is not suitable, as the estimated result parameters might not be considerably different from zero and may fail to report the associated and overall errors of the linear regression model. Additionally, linear

regression is very sensitive to extreme values that generally appear in climate or VI time series (Qin 2011).

The Mann-Kendall (MK) trend test is a properly non-parametric trend tests for the non-normally distributed data that are frequently encountered in hydro-meteorological time series (Yue, Pilon & Cavadias, 2002). This algorithm provides the most useful trend analysis statistics for environmental time series (Luus, 2009). Rank-based non-parametric MK statistical tests have been applied to assess significant trends in hydrological and climatological data, including water quality, stream flow, temperature and precipitation data (Latifovic & Pouliot, 2007). The MK trend test has recently been applied to VI time-series analysis (Alcaraz-Segura, Liras, Tabik, Paruelo & Cabello, 2010; Ni, Xie, Zhou, Gao & Ding, 2017; Sobrino & Julien, 2013). The purpose of the MK trend test is to assess whether there is monotonic upward or downward trends in the interest variable over time by examining the signs of all pairwise differences of observed values, which are ranked in chronological order. The sum of sign differences between the observed pairs determines whether the monotonic trend is consistent over time. However, as the test uses the relative magnitude of data and not actual data values, it ignores degrees of changes and only takes into account positive or negative changes. The attributes of the MK trend test enable it to deal with outliers, non-normality and values below detection limits (de Beurs & Henebry, 2005a).

The advantages of the MK trend test have been noted in numerous studies on trends and changing analyses of VI time series. Julien and Sobrino (2009) retrieved local LSP trends for the whole globe and applied the MK trend test to the NDVI time series. In another study, Martínez and Gilabert (2009) noted that the MK method is easy to calculate, robust against non-normality and insensitive to missing values. Additionally, Meng et al. (2011) used the MK trend test to identify patterns of changes in climate variability and the NDVI from 1982 to 2000 in China and reported that the MK method allows abrupt changes to be identified in time series of independent and Gaussian distributed anomalies.

According to Pohlert (2016), the MK test statistic is calculated by:

$$S = \sum_{k=1}^{n-1} \sum_{j=k+1}^{n} sgn(X_j - X_k) \tag{2-3}$$

With

$$sgn(x) = \begin{cases} 1 & if\ x > 0 \\ 0 & if\ x = 0 \\ -1 & if\ x < 0 \end{cases} \tag{2-4}$$

The mean of S is E[S] = 0 and the variance σ^2 is

$$\sigma^2 = \left\{ n(n-1)(2n+5) - \sum_{j=1}^{p} t_j(t_j-1)(2t_j+5) \right\} / 18 \tag{2-5}$$

Where p is the number of the tied groups in the dataset and t_j is the number of data points in the j^{th} tied group. The S value is approximately normally distributed provided that the following Z-transformation is employed:

$$Z = \begin{cases} \dfrac{S-1}{\sigma} & if\ S > 0 \\ 0 & if\ S = 0 \\ \dfrac{S+1}{\sigma} & if\ S < 0 \end{cases} \tag{2-6}$$

Z is used to test the null hypothesis; H_o indicates that there is no trend and H_A indicates that there is a significant downward or upward trend. If $|Z| > Z_{\alpha/2}$, then the null hypothesis of no trend is rejected.

However, the MK test is not suitable for seasonally collected data, as seasonality contaminates the test with inaccurate results. Hirsch (1982) introduced the Seasonal Mann-Kendall (SMK) test, a modified version of the MK test, which takes seasonality into account in the algorithm. The seasonal test runs a separate MK trend test on each 'm' season separately, where m is the number of seasons. The data are only compared to the same season; for example, spring data is only be compared to spring data and summer data is only be compared to summer data. The SMK test first evaluates whether each periodic sub-annual interval (same season) exhibits significant monotonic trends based

on the MK's S score and its variance. A Z score is the computed and heterogeneity test performed to see if this trend is consistent across all sub-annual intervals. De Beurs (2005) recommends the SMK trend test because of its robustness against seasonality, non-normality, heteroscedasticity and missing values. This research uses the SMK test to identify trends in satellite time-series data and understand long-term vegetation dynamics.

The formula for the SMK test is based on the MK statistic for each season as follows:

$$S_g = \sum_{k=1}^{n-1} \sum_{j=k+1}^{n} sgn(X_{jg} - X_{kg}) \quad (2\text{-}7)$$

Adopting Hirsch et al.'s (1982) approach, the seasonal MK statistic for the entire time series is calculated as:

$$S = \sum_{g=1}^{m} S_g \quad (2\text{-}8)$$

1.5. Bidirectional Reflectance Distribution Function

1.5.1. Sun-sensor geometry controversy of satellite-based results

Observation satellites have been used to monitor the Earth's landscape for a long time; however, some issues need to be considered when using satellite data. Two major problems cause uncertainties and noise in satellite data: atmospheric contamination and sun-sensor geometry. The first problem arises due to the clouds and aerosols present in the atmosphere. Clouds and aerosols represent the primary sources of noise in the data capturing process, as these spectral characteristics of the atmosphere affect optical satellite data. Most optical satellites are passive sensors. Consequently, they capture the solar electromagnetic energy that passes through the atmosphere twice (i.e., as it passes from the sun to the Earth's surface and as it is reflected from the Earth's surface to the satellite sensors). Atmospheric gases, aerosols and thin clouds absorb and scatter sunlight, contaminating the signals captured by satellite. Thick clouds may entirely block the sunlight, leaving satellites unable to capture landscape reflected signals. Raw optical

images captured by satellites or airborne platforms reveal the extent of this issue (see Figure 1.6). The removal of atmospheric perturbations and clouds from signal captured by observed satellite sensors is an essential task in obtaining accurate landscape information for Earth observation goals. It has been addressed in many studies and many significant achievements in this area have been made since Landsat (Short, 1982), the first well-known optical satellite system, was launched over 40 years ago.

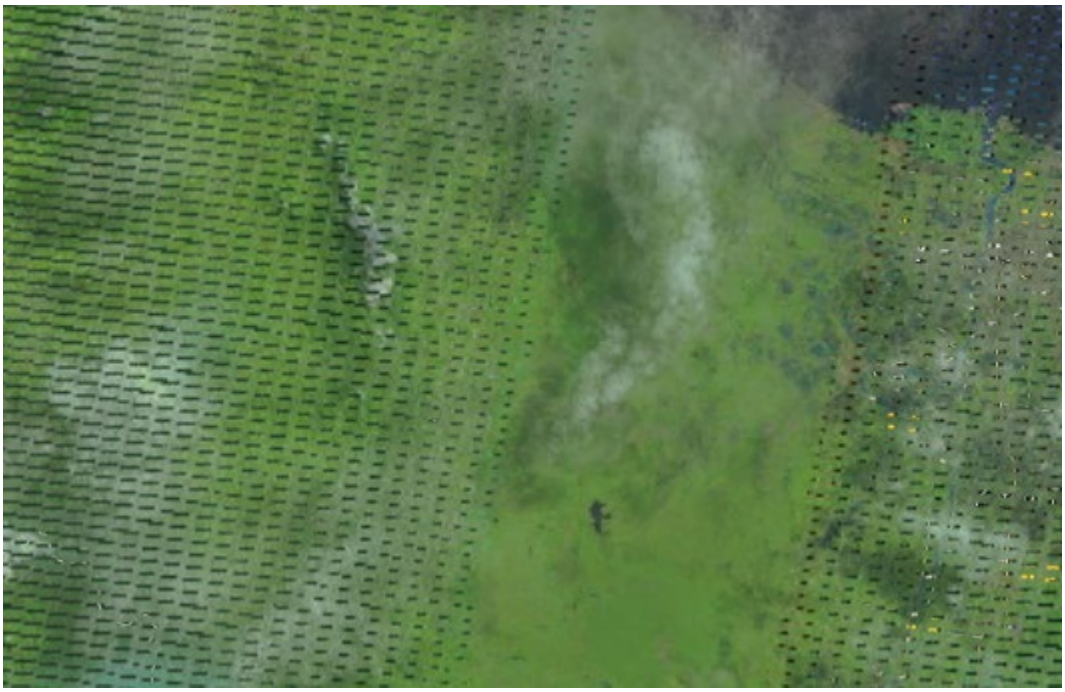

Figure 1.6 *Raw RGB colour Landsat 7 image of parts of Thailand and Malaysia showing clouds, cloud shadows, aerosol and sensor artefacts on 18 June 2019 (captured from EarthExplorer.usgs.gov)*

Sun-sensor geometry causes the second major problem, as it can create artefacts in generating surface reflectances. For example, different results may be produced depending on sun-sensor geometries even in the absence of atmospheric noise. It is a well-known fact that the surface of Earth scatters incident radiation anisotropically at different wavelengths and the intensity of the scattered radiation depends on both illumination and viewing directions. This dependence can be represented by the bidirectional reflectance distribution function (BRDF).

A BRDF is defined as a function of illumination and viewing geometries and describes how light is reflected from a surface (Strahler & Muller, 1999). Nicodemus (1965) first defined BRDF in 1965. To date, it has been quite popular as a computer

graphic due to its photorealistic rendering of synthetic scenes. It has also been applied in computer vision to many inverse problems, such as object recognition or modelling light trapping in solar cells (e.g., using the OPTOS formalism) or in low concentration solar photovoltaic systems (Andrews, Pollard & Pearce, 2013).

In terms of satellite remote sensing, the BRDF has been used to describe the dependence of scattered radiation on illumination and viewing geometry or model characteristics of surface anisotropy. Figure 1.7 provides a simple example of a BRDF effect, the importance of analysing the effects of BRDF on satellite-based outcomes and shows how a forest may look different when viewed and illuminated from different angles.

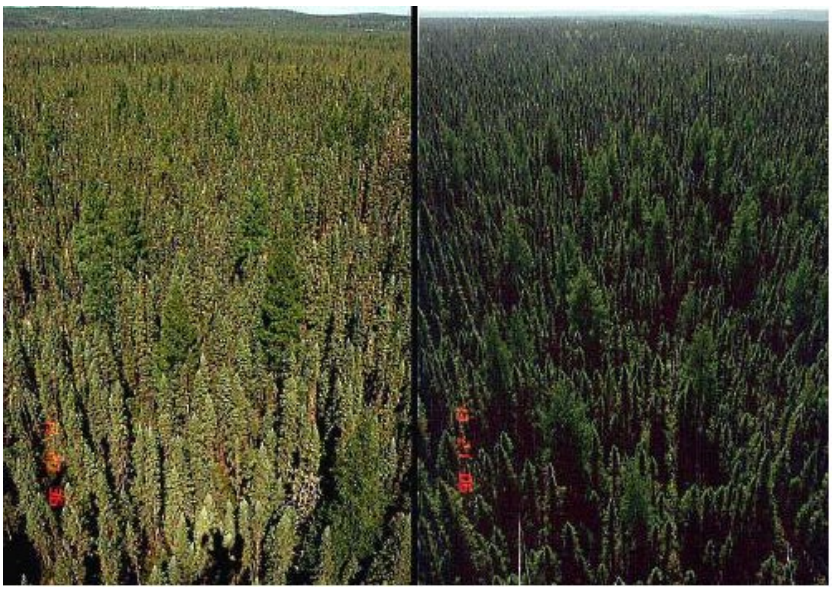

Figure 1.7 *A black spruce forest in the BOREAS experimental region in Canada with various illuminating geometries. Photography by Don Deering, retrieved from https://www.umb.edu.*

The three-dimensional structure of the surface is the primary source of surface anisotropy. The size, shape and geometrical arrangement of the surface objects contribute to the variation of the reflected radiation with variable illumination and view angles (see Figure 1.8). In general, changes in surface reflectance of visible and NIR bands are due to absorption and the scattering of incident light by structures or biochemical composition of surfaces, such as leaf pigments, the water content in vegetation or soil moisture (Croft et al., 2015). In relation to plants, the characteristics of leaves, such as their size, shape or orientation and arrangement within a canopy, determine the angular distribution of

reflected radiation from a vegetation canopy (Bousquet, Lachérade, Jacquemoud & Moya, 2005). In relation to forests, various sun positions can generate different reflectances of the same surface. Differences might result from direct sun angles or indirect shadow caused by angles.

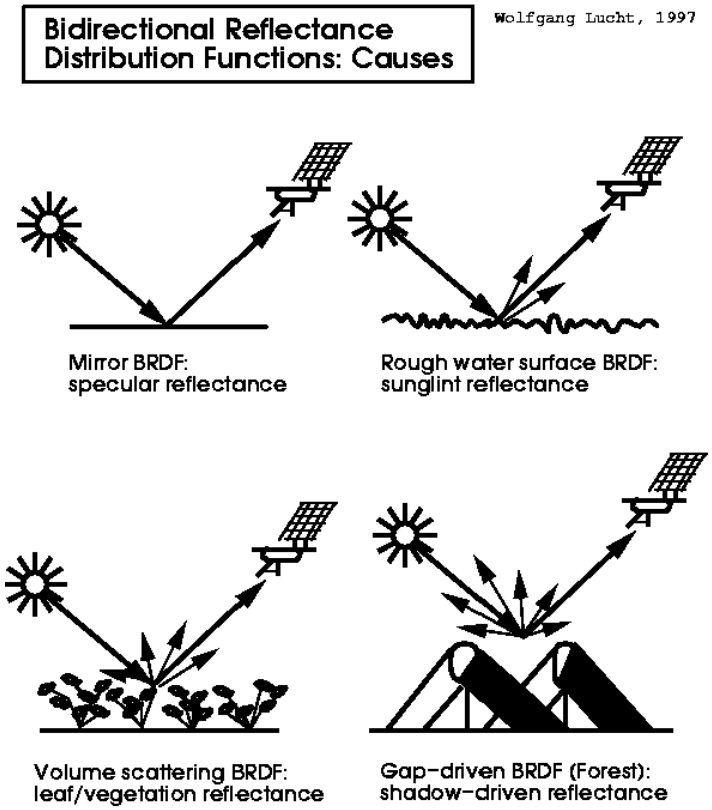

Figure 1.8 *Causes of land surface reflectance anisotropy (Lucht, Schaaf, & Strahler, 2000)*

Some recent studies have raised questions about the BRDF effects on vegetation phenology derived from the EVI time series in dense vegetation areas, such as tropical forests. One significant controversy caused by the BRDF is the hypothesis of the Amazon rainforest 'green-up'. Huete et al. (2006) used the MODIS-EVI and found that Amazon rainforests were 'greening-up' during dry periods, but assumed that this was light driven. Their results were questioned by Morton et al., (2014), who used a BRDF model to exterminate the BRDF effects and concluded that there was no 'green-up' of Amazon rainforests in dry seasons but that the results were an artefact of seasonal variations of sun-view geometries in the Amazon region. Further research supported the light-driven 'green-up' hypothesis, including flux tower and modelling studies that showed increasing productivity in Amazon forests in dry periods. Restrepo-Coupe et al. (2013) observed

Amazon gross primary production (GPP) from eddy flux tower and satellite EVI data and found that greenness was rising during the dry season. Further, Saleska et al. (2016) challenged Morton's conclusion about the non-existence of dry-season 'green-up'. By correcting sun-angle artefacts at several flux tower sites in a comprehensive way, Saleska et al. showed that there was a statistically significant canopy 'greening' during the dry season. Saleska et al. also validated their outcomes with in-situ data that showed that the satellite-based observations were biophysically consistent with the ground-based measurements in relation to increasing leaf amounts (a fraction of the new leaves and canopy photosynthesis capacity was derived from eddy flux towers in the dry season).

The effect of the BRDF on the VI is undeniable; however, it has created controversy. Kaufmann et al. (2000) investigated the effect of changes in solar zenith angles (SZAs) in the NDVI derived from Advanced Very High-Resolution Radiometer (AVHRR) and found that the relationship between the NDVI and sun angles is minimal in dense vegetation canopies; however, the NDVI is considerably related to sun angles in relatively low leaf areas. Galvão et al. (2004) showed that Amazon forests yielded higher NDVI values with increasing sun angles. In terms of the BRDF effects caused by the slope and aspects of the surface, Moreira et al. (2016) showed that the BRDF has less effect on the NDVI than the EVI derived from Landsat images. Thus, any studies in dense vegetation areas, such as forests, that use optical remotely-sensed data should consider the BRDF effects on the outcomes, as neglecting the BRDF effects might lead to false or uncertain results.

A phenological parameter extracted from satellite time series can be different between normal and BRDF-fixed data. Bhandari (2011) found that the NDVI of Queensland forests was sensitive to variations in sun-sensor geometries in relation to seasonal amplitude. Conversely, variable viewing and illumination geometries had lesser effects on the EVI in relation to the annual magnitude but altered time shifts in the seasonal cycle, providing erroneous information on phenology. On a global scale, Los et al. (2005) found that the length of the growing season derived from the AVHRR NDVI was underestimated in the Northern Hemisphere and overestimated in Southern Hemisphere if the BRDF effect was not corrected.

1.5.2. BRDF modelling

A large collection of physical empirical and semi-empirical models have been developed to standardise surface anisotropy to minimise the BRDF effect on monitoring landscapes (He et al., 2012; Roujean, Leroy & Deschamps, 1992; Wanner, W., Li & Strahler, 1995). These models usually use a small number of parameters to model surface BRDF by normalising or correcting multi-angular observations to a commonly observed geometry. By doing so, these models remove reflectance variations caused by illumination and viewing geometries. Additionally, the model parameters estimated from various angular observations can be used to retrieve reflectances at different sun-sensor configurations to study the effects of geometries in surface reflectance retrievals (Strahler & Muller, 1999).

Of the many developed models, the RossThick-LiSparse Reciprocal (RTLSR) model (Wanner, W. et al., 1995) is one of the most common and useful for normalising observed reflectance. It has been applied to MODIS satellite data to provide operational BRDF products with semi-empirical modelled coefficients for spectral bands at a spatial resolution of 500 m to 0.05-degree (C. Schaaf & Wang, 2015a; Crystal B. Schaaf et al., 2002). The theoretical basis of the semi-empirical BRDF model (Roujean et al., 1992) is that land surface reflectance can be modelled as a sum of three kernels representing basic scattering types: 1) isotropic scattering; 2) radiative transfer-type volumetric scattering from horizontally homogenous leaf canopies; and 3) geometric-optical surface scattering from scenes containing three-dimensional objects that cast shadows and are mutually obscured from view at off-nadir angles (X. Li & Strahler, 1992).

The advantages of this model include its simplicity, low implementation costs and accuracy. Additionally, the MODIS team has standardised data and provided BRDF parameters using this model on the global scale since 2000. Thus, it is practical to use the RTLSR model to investigate the effects of the BRDF in forest phenology derived from satellite data.

1.5.3. RossThick-LiSparse Reciprocal model

The BRDF is generally modelled by a linear sum of kernels that characterise different modes of scattering. Strahler et al. (1999) assumed that these modes are spatially

distinct within a scene viewed with little or no cross-coupling and physically distinct within an invariable canopy with an indistinguishable interaction. The resulting BRDF model is called a kernel-based BRDF model (Roujean, 1992; Wanner, 1995):

$$R(\theta, \vartheta, \phi, \Lambda) = \sum_{k} f_k(\Lambda) K_k(\theta, \vartheta, \phi) \tag{2-9}$$

Where θ is Solar Zenith Angle

ϑ is View Zenith Angle

ϕ is View-Sun Relative Azimuth Angle

Λ is waveband Λ of width $\Delta\lambda$ with λ is wavelength

$R(\theta, \vartheta, \phi, \Lambda)$ is bidirectional reflectance distribution function (BRDF) in waveband Λ

$K_k(\theta, \vartheta, \phi)$ is BRDF model kernel k

f_k is BRDF kernel model parameter k in waveband Λ

The Zenith Angle is the angle between the local zenith (i.e., directly above the point of the surface) and the line of sight from that point to the sun or sensor (see Figure 1.9). Thus, the higher the sun/sensor in the sky, the lower the Zenith Angle. The Azimuth Angle is defined as a horizontal angle measured clockwise from the North line (see Figure 1.10). The View-Sun Relative Azimuth Angle is the actual difference between the View Azimuth Angle and the Sun Azimuth Angle.

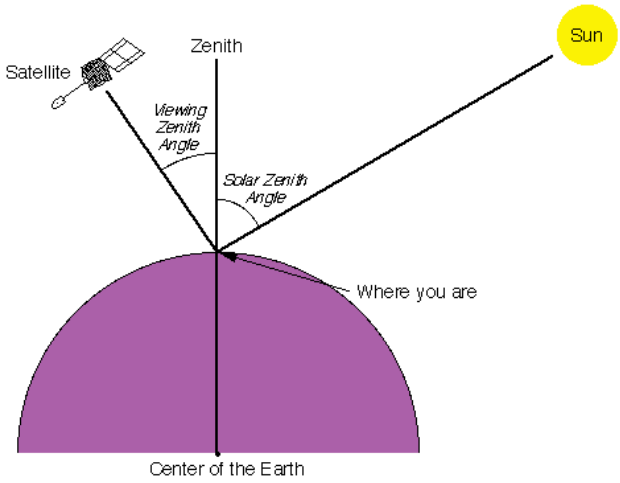

Figure 1.9. *Schematic demonstration of Solar Zenith Angle (SZA) and View Zenith Angle (VZA) for satellite observations. Source: http://sacs.aeronomie.be/info/sza.php.*

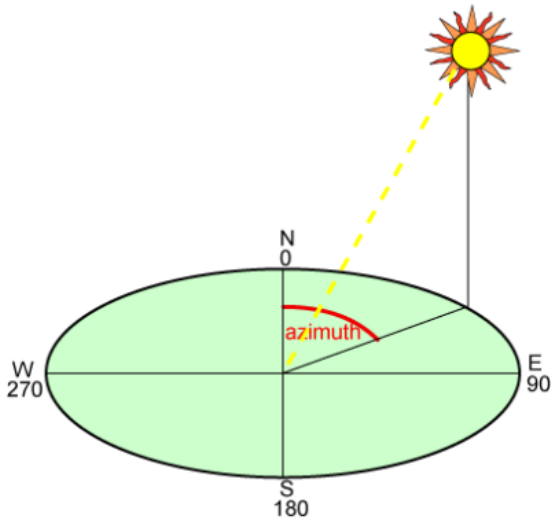

Figure 1.10 *Illustration of Solar Azimuth Angle. Source: www.pveducation.org.*

In this study, a semi-empirical BRDF model was implemented to simulate MODIS surface reflectances acquired at varying view-sun geometries. The theoretical basis of the semi-empirical BRDF model is that the land surface reflectance can be modelled as a sum of three kernels representing basic scattering types: isotropic scattering, volumetric scattering and geometric-optical surface scattering.

Equation 1.2 (Lucht et al., 2000; Roujean et al., 1992; Crystal B. Schaaf et al., 2002; A. Strahler et al., 1999) takes the specific form given by:

$$R(\theta,\vartheta,\phi,\lambda) = f_{iso}(\lambda) + f_{vol}(\lambda)K_{vol}(\theta,\vartheta,\phi) + f_{geo}(\lambda)K_{geo}(\theta,\vartheta,\phi) \quad (2\text{-}10)$$

Where

$R(\theta,\vartheta,\phi,\lambda)$ Reflectance at sun-sensor angles (θ,ϑ,ϕ) and wavelength λ

$f_{iso}(\lambda)$ Isotropic scattering parameter at wavelength λ

$f_{vol}(\lambda)$ Volumetric scattering parameter at wavelength λ

$K_{vol}(\theta,\vartheta,\phi)$ Kernel of volumetric scattering parameter

$f_{geo}(\lambda)$ Geometric-optical surface scattering at wavelength λ

$K_{geo}(\theta,\vartheta,\phi)$ Kernel of geometric-optical surface scattering

Roujean (1992) derived a suitable expression for Kvol called the Ross-Thick kernel, as it assumes a close leaf canopy. This single-scattering approximation of radiative transfer theory by Ross (1981) consists of a layer of small scatterers with uniform leaf angle distribution, a Lambertian background and equal leaf transmittance and reflectance. Its form, normalised to zero for θ = 0, ϑ = 0, is

$$K_{vol} = k_{RT} = \frac{\left(\frac{\pi}{2} - \xi\right)cos\xi + sin\xi}{cos\theta + cos\vartheta} - \frac{\pi}{4} \quad (2\text{-}11)$$

Wanner (1995) derived a suitable express for kgeo that has been found to work well with MODIS observed data. By assuming a sparse ensemble of surface objectives casting shadows on the background, the kernel named LiSparse can be represented. And Li and Strahler (1992) retrieved the kernel from geometric mutual shadow BRDF model. It is given by the fraction of sunlight and shaded scene components in a scene consisting of randomly located spheroids of height-to-centre-crown h/b and crown vertical to horizontal radius ratio b/2 (A. H. Strahler & Muller, 1999). If the sunlight component is assumed to vary as $1/\cos\theta$, the kernel takes on the form to be called LiSparse-R:

$$K_{geo} = k_{LSR} = O(\theta, \vartheta, \phi) - sec\theta' - sec\vartheta' + \frac{1}{2}(1 + cos\xi')sec\theta' sec\vartheta' \quad (2\text{-}12)$$

Where

$$O = \frac{1}{\pi}(t - sint\ cost)(sec\theta' + sec\vartheta')$$

$$cost = \frac{h}{b}\frac{\sqrt{D^2 + (tan\theta' tan\vartheta' sin\phi)^2}}{sec\theta' + sec\vartheta'}$$

$$D = \sqrt{tan^2\theta' + tan^2\vartheta' - 2tan\theta' tan\vartheta' sin\phi}$$

$$cos\xi' = cos\theta' cos\vartheta' + sin\theta' sin\vartheta' cos\phi$$

$$\theta' = tan^{-1}\left(\frac{b}{r}tan\theta\right)\vartheta' = tan^{-1}(\frac{b}{r}tan\vartheta)$$

O, here, is the overlap area between the view and solar shadows. Preselected crown relative height and shape parameters $\frac{h}{b}$ and $\frac{b}{r}$ are set as two and one respectively for MODIS data. In this thesis, the three kernels of the BRDF model, which quantify elemental surface properties at any given areas and within the daily period, were inverted from combined Terra and Aqua MODIS observations (Crystal B. Schaaf et al., 2002).

1.5.4. MODIS BRDF/Albedo product

MCD43 (or MODIS BRDF/Albedo) products supply modelled parameters to characterise the surface anisotropy that can be used to calculate global land surface albedos. The latest version (Collection 6) of the MCD43A1 parameters (C. Schaaf & Wang, 2015a) supplies the weighting parameters associated with the semi-empirical RTLSR BRDF model that best describe the anisotropy of each 500 m pixel at the daily period (Schaaf et al. 2002). Combined data from the MODIS instruments onboard Aqua and Terra satellites (only Terra data are available before mid-2002) provide the parameters of the MCD43A1. Each day, the operational MODIS BRDF/Albedo algorithm (Wanner, 1997; Lucht, Schaaf and Strahler, 2000; Schaaf et al., 2002, 2011; Wang et al., 2012) applies the RTLSR model (Wanner et al., 1995) to 16-day multi-date data from both Terra and Aqua and determines the parameters describing the BRDF of the land surface (Schaaf, 2015). The day of interest is weighted as a function of observation

coverage. From the BRDF parameters of each land surface pixel, the directional reflectance could be calculated by inputting desired sun-view configurations.

When insufficient high-quality reflectances are available (the current threshold is set to less than seven observations) or a poorly representative sampling of high-quality reflectances is obtained (as indicated by the quality of the flags and determined through weights of determination), it is impossible to introduce a full inversion data point. Consequently, a database of archetypal BRDF parameters is used to supplement the observational data available and perform a lower quality magnitude inversion (Strugnell, Lucht, Hyman & Meister, 1998; Wolfgang & Crystal, 2001).

In relation to regional-level analyses, the MCD43C1 Climate Modelling Grid (CMG) BRDF/Albedo Model Parameters Product (MODIS/Terra BRDF/Albedo Parameters Daily L3 Global 0.05Deg CMG) supplies the parameters associated with the RTLSR BRDF model of each 0.05-degree pixel (C. Schaaf & Wang, 2015b) and thus could be a better choice. The three parameters (fiso, fvol, fgeo) are provided for each MODIS spectral band at a 0.05-degree spatial resolution in global files in a geographic (latitude/longitude) projection. Besides the BRDF parameters used for reflectance calculation, the MCD43C1 CMG BRDF/Albedo Model Parameters Product also provides extensive quality information based on quality values of MCD43A1 sub-pixel information. The quality and inversion status of the majority of the underlying 500-m pixels is provided as is the percentage of the underlying snow-covered pixels. Definitions of the QA levels of the MCD43C1 is shown in Table 1.2 (Schaaf & Wang, 2015b).

Table 1.2 *Quality levels of MCD43C1 based on MCD43A1 sub-pixel quality*

Level	Meaning
0	Best quality, 100 per cent with full inversion
1	Good quality, 75 per cent or more with best full inversions and 90 per cent or more with full inversion
2	Relative good quality, 75 per cent or more with full inversions
3	Mixed, 75 percent or less full inversions and 25 percent or less fill values

4	All magnitude inversions or 50 percent or less fill values
5	50 per cent or more fill values
255	Fill Value – 100 percent fill values

Selecting quality level is a critical step when using satellite data like MODIS BRDF/Albedo products. In theory, we should choose the best quality to avoid any noise due to cloud or aerosol contaminations and lower quality levels mean the increasing of data uncertainties. However, it is only practical if we work on clear days without cloud appearance. For some regions, like tropical rainforests where there are no dry seasons, best quality selection results in very few available observations and too many missing data and working on inter- or intra- annual satellite time-series is impractical in those locations. Consequently, we should choose the suitable quality level depending on our applications and study areas.

1.6. Current knowledge gaps and corresponding thesis objectives

As previous research has shown, continental SEA forests are a mix of evergreen rainforests and deciduous tropical dry forests. In recent decades, SEA forests have been massively affected by human activities. Compared to Amazon and African tropical forests, very few studies have been conducted on SEA forests. Continental SEA tropical forests are under great threat and research urgently needs to be conducted to gain a better understanding of their seasonal and inter-annual dynamics.

Satellite data were chosen to analyse SEA forest phenology, as satellite data have proven to be useful in monitoring vegetated landscapes at variable spatial and temporal scales. However, variations in sun-sensor geometry have created controversies about satellite-based results, especially in relation to tropical forests. Thus, the effects of variable sun-view angles on phenology must be investigated to detangle observation artefacts from the real vegetation seasonal dynamics.

To address these gaps in knowledge, this research seeks to study inter- and intra-annual dynamics of continental SEA tropical forests using MODIS satellite data and the effects of the BRDF on the retrieved results. The results should lead to a better

understanding of mainland SEA forest phenology and the BRDF effect on the satellite capability of the MODIS to capture forest seasonal and inter-annual and intra-seasonal dynamics.

This thesis has been divided into chapters to address current issues in this field of study and the corresponding objectives of this research. Chapter 1 provided an introduction to this thesis. It began by describing the broad context of tropical forests, their roles and responses to climate variability and the need to investigate Peninsular SEA tropical forests. To date, there has been a lack of research in this area; however, the anthropogenic activities in this region pose a high threat. Next, the use of satellite data to study phenology of vegetation was considered and a comprehensive literature review was undertaken on data smoothing and phenological metrical extraction. Finally, the controversy of satellite-based results caused by variations of sun-sensor geometry and the BRDF effects in the study of tropical forest dynamics were considered.

Chapter 2 investigates continental SEA forest phenology and the effects of the BRDF on extracted phenological information. The results include an overview of SEA forest phenology and the effects of BRDF on derivative knowledge at a continental scale. Analyses are also undertaken at a higher spatial resolution to gather detailed information on the effects of the BRDF and seasonal forest dynamics. As mainland SEA forests are fragmented due to human activities, intact forests were selected to avoid anthropogenic disturbance contributing to results. The specific objectives of Chapter 2 are to 1) investigate seasonal variations of sun and view angles from MODIS Terra and Aqua sensors; 2) retrieve time series of BRDF-corrected VIs of SEA tropical forests; 3) understand the effects of the BRDF on VI time series, seasonal profiles and the derived phenological parameters of SEA non-disturbed forests; 4) assess the capabilities of the NDVI and the EVI to capture SEA forest phenology, both in terms of the robustness of the BRDF effect and saturation; 5) analyse the seasonal phenology of SEA forests with various rainfall conditions; 6) investigate whether different fixed sun-sensor configurations affect outcomes derived from VI time series; and 7) evaluate the ability of the MODIS BRDF/Albedo to generate reflectance and VIs at specific sun-view angles.

Chapter 3 investigates disturbance contribution to intra-annual forest phenology by comparing seasonal profiles and phenological metrics between disturbed and undisturbed forests. Chapter 3 also includes an investigation of the effects of the BRDF

on disturbed forest sites to determine whether the effects of the BRDF on disturbed forests phenology differs to the effects of the BRDF on intact forests phenology. Specifically, this chapter aims to 1) investigate the effects of disturbance on SEA forest phenology by comparing VI time series and seasonal profiles between non-disturbed and disturbed forests; 2) determine whether the BRDF effects are identical between non-disturbed and disturbed forests; and 3) analyse the effects of various sun-view geometry settings between intact and disturbed forests.

Chapter 4 focuses on the BRDF effects on inter-annual information. The trends or responses of tropical forests to extreme climate events, such as ENSO or droughts, are crucial to explain forest phenology or the vulnerability of forests to climate variability. Thus, it is essential to determine whether variable sun-sensor geometry affects the trends or the inter-annual dynamics of SEA forests. Chapter 4 seeks to 1) investigate inter-annual VI variations of SEA tropical forests over a 16-year period (i.e., from 2001 to 2016); 2) discover responses of SEA tropical forests to inter-annual climate variability; and 3) determine whether the BRDF significantly affects the forest inter-annual phenology information derived from the NDVI and the EVI time series.

Chapter 5 summarises all of the findings set out in the earlier chapters previous and discusses these findings within the broader context. The limitations of this research and directions for future related studies are also considered in this chapter.

1.7. References

Aide, T. M., Clark, M., Grau, R., Lopez-Carr, D., Levy, M., Redo, D., … Muñiz, M. (2013). Deforestation and Reforestation of Latin America and the Caribbean (2001–2010). *Biotropica*, *45*.

Alcaraz-Segura, D., Liras, E., Tabik, S., Paruelo, J., & Cabello, J. (2010). Evaluating the consistency of the 1982-1999 NDVI trends in the Iberian Peninsula across four time-series derived from the AVHRR sensor: LTDR, GIMMS, FASIR, and PAL-II. *Sensors*, *10*(2), 1291–1314. https://doi.org/10.3390/s100201291

Alroy, J. (2017). Effects of habitat disturbance on tropical forest biodiversity. *Proceedings of the National Academy of Sciences*, *114*(23), 6056–6061. https://doi.org/10.1073/pnas.1611855114

Andrews, R. W., Pollard, A., & Pearce, J. M. (2013). Photovoltaic system performance enhancement with non-tracking planar concentrators: Experimental results and BDRF based modelling. *2013 IEEE 39th Photovoltaic Specialists Conference (PVSC)*, 229–234. https://doi.org/10.1109/PVSC.2013.6744136

Bachoo, A., & Archibald, S. (2007). Influence of using date-specific values when extracting phenological metrics from 8-day composite NDVI data. *Proceedings of MultiTemp 2007 - 2007 International Workshop on the Analysis of Multi-Temporal Remote Sensing Images*, 20–23. https://doi.org/10.1109/MULTITEMP.2007.4293044

Beck, P. S. A., Jönsson, P., Høgda, K. A., Karlsen, S. R., Eklundh, L., & Skidmore, A. K. (2007). A ground-validated NDVI dataset for monitoring vegetation dynamics and mapping phenology in Fennoscandia and the Kola peninsula. *International Journal of Remote Sensing*, *28*(19), 4311–4330. https://doi.org/10.1080/01431160701241936

Betts, R. A., Cox, P. M., Collins, M., Harris, P. P., Huntingford, C., & Jones, C. D. (2004). The role of ecosystem-atmosphere interactions in simulated Amazonian precipitation decrease and forest dieback under global climate warming. *Theoretical and Applied Climatology*, *78*(1–3), 157–175. https://doi.org/10.1007/s00704-004-0050-y

Bhandari, S., Phinn, S., & Gill, T. (2011). Assessing viewing and illumination geometry effects on the MODIS vegetation index (MOD13Q1) time series: implications for monitoring phenology and disturbances in forest communities in Queensland, Australia. *International Journal of Remote Sensing*, *32*(22), 7513–7538.

https://doi.org/10.1080/01431161.2010.524675

Blackie, R., Baldauf, C., Gautier, D., Gumbo, D., Kassa, H., Parthasarathy, N. Paumgarten, F.; Sola, P., … Sunderland, T. C. H. (2014). *Tropical dry forests : The state of global knowledge and recommendations for future Tropical dry forests The state of global knowledge and recommendations*. (March), 30. Retrieved from 10.17528/cifor/004408

Bousquet, L., Lachérade, S., Jacquemoud, S., & Moya, I. (2005). Leaf BRDF measurements and model for specular and diffuse components differentiation. *Remote Sensing of Environment*, *98*(2–3), 201–211. https://doi.org/10.1016/j.rse.2005.07.005

Bradley, B. A., Jacob, R. W., Hermance, J. F., & Mustard, J. F. (2007). A curve fitting procedure to derive inter-annual phenologies from time series of noisy satellite NDVI data. *Remote Sensing of Environment*, *106*(2), 137–145. https://doi.org/10.1016/j.rse.2006.08.002

Bradley, B. A., & Mustard, J. F. (2008). Comparison of phenology trends by land cover class: a case study in the Great Basin, USA. *Global Change Biology*, *14*(2), 334–346. https://doi.org/10.1111/j.1365-2486.2007.01479.x

Campbell B, Frost P, Kokwe G, L. B. G., & D., S. S. and T. (2004). Making dry forests work for the poor in Africa – building on success. *Center for International Forestry Research*, 4. Retrieved from http://www.cifor.org/ntfpcd/%0Apdf/b5b.pdf

Campbell, B. M. (1996). The Miombo in Transition: Woodlands and Welfare in Africa. *CIFOR, Bogor, Indonesia*. https://doi.org/10.17528/cifor/000465

Chen, J., Jönsson, P., Tamura, M., Gu, Z., Matsushita, B., & Eklundh, L. (2004). A simple method for reconstructing a high-quality NDVI time-series data set based on the Savitzky-Golay filter. *Remote Sensing of Environment*, *91*(3–4), 332–344. https://doi.org/10.1016/j.rse.2004.03.014

Croft, H., Chen, J., Zhang, Y., Anita, S. M., Noland, T., Nesbitt, N., & Arabian, J. (2015). Evaluating leaf chlorophyll content prediction from multispectral remote sensing data within a physically-based modelling framework. *ISPRS Journal of Photogrammetry and Remote Sensing*, *102*.

Cunningham A, German L, P. F., Chikakula M, Barr C, Obidzinski K, V., & Noordwijk M, de Koning R, Purnomo H, Yatich T, Svensson L, G. A. and P. A. (2008). Sustainable trade and management of forest products and services in the COMESA region: an issue paper. *Center for International Forestry Research,* 91. https://doi.org/10.1146/annurev.ecolsys.33.010802.150507

de Beurs, K. M., & Henebry, G. M. (2005a). A statistical framework for the analysis of long image time series. *International Journal of Remote Sensing*, *26*(8), 1551–1573. https://doi.org/10.1080/01431160512331326657

de Beurs, K. M., & Henebry, G. M. (2005b). Land surface phenology and temperature variation in the International Geosphere–Biosphere Program high-latitude transects. *Global Change Biology*, *11*(5), 779–790. https://doi.org/10.1111/j.1365-2486.2005.00949.x

de Beurs, K. M., & Henebry, G. M. (2010). Spatio-Temporal Statistical Methods for Modelling Land Surface Phenology. In *Phenological Research: Methods for Environmental and Climate Change Analysis* (pp. 177–208). https://doi.org/10.1007/978-90-481-3335-2

Devaraju, N., Bala, G., & Modak, A. (2015). Effects of large-scale deforestation on precipitation in the monsoon regions: Remote versus local effects. *Proceedings of the National Academy of Sciences*, *112*(11), 3257–3262. https://doi.org/10.1073/pnas.1423439112

Ehrlich, P. R., & Wilson, E. (1991). Biodiversity studies: science and policy. *Science (New York, N.Y.)*, *253*(5021), 758–762. https://doi.org/10.1126/science.253.5021.758

Eklundh, L., & Jönsson, P. (2015). *TIMESAT 3.2 with parallel processing Software Manual*.

Elias, P., & May-Tobin, C. (2011). Tropical Forest Regions. *Union of Concerned Scientists*, 3–12. https://doi.org/10.1007/BF00351108

FAO. (2001). Global Forest Resources Assessment 2000 Main Report. *Organization*, *20*(2), 478. https://doi.org/10.1016/S0264-8377(03)00003-6

FAO. (2015). Global Forest Resources Assessment 2015. Desk reference. In *Desk Reference* (Vol. 2005). https://doi.org/10.1002/2014GB005021

Friedlingstein, P., Cox, P., Betts, R., Bopp, L., von Bloh, W., Brovkin, V., … Zeng, N. (2006). Climate-carbon cycle feedback analysis: Results from the C4MIP model intercomparison. *Journal of Climate*, *19*(14), 3337–3353. https://doi.org/10.1175/JCLI3800.1

Galvão, L. S., Ponzoni, F. J., Epiphanio, J. C. N., Rudorff, B. F. T., & Formaggio, A. R. (2004). Sun and view angle effects on NDVI determination of land cover types in the Brazilian Amazon region with hyperspectral data. *International Journal of Remote Sensing*, *25*(10), 1861–1879. https://doi.org/10.1080/01431160310001598908

Ganapathi Subramanian, S., & Crowley, M. (2018). Using Spatial Reinforcement Learning to Build Forest Wildfire Dynamics Models From Satellite Images. *Frontiers in ICT*, *5*, 6. https://doi.org/10.3389/fict.2018.00006

Gaveau, D. L. A., Salim, M. A., Hergoualc'h, K., Locatelli, B., Sloan, S., Wooster, M., … Sheil, D. (2014). Major atmospheric emissions from peat fires in Southeast Asia during non-drought years: evidence from the 2013 Sumatran fires. *Scientific Reports*, *4*. https://doi.org/10.1038/srep06112

Gibson, L., Lee, T. M., Koh, L. P., Brook, B. W., Gardner, T. A., Barlow, J., … Sodhi, N. S. (2011). Primary forests are irreplaceable for sustaining tropical biodiversity. *Nature*, *478*(7369), 378–381. https://doi.org/10.1038/nature10425

Gillespie, T. W., Lipkin, B., Sullivan, L., Benowitz, D. R., Pau, S., & Keppel, G. (2012). The rarest and least protected forests in biodiversity hotspots. *Biodiversity and Conservation*, *21*(14), 3597–3611. https://doi.org/10.1007/s10531-012-0384-1

Gumbo, E. N. C. and D. J. (2010). *The Dry Forests and Woodlands of Africa*. https://doi.org/10.4324/9781849776547

Hansen, M. C., Potapov, P. V, Moore, R., Hancher, M., Turubanova, S. A., Tyukavina, A., … Townshend, J. R. G. (2013). High-Resolution Global Maps of 21st-Century Forest Cover Change. *Science*, *342*(6160), 850–853. https://doi.org/10.1126/science.1244693

He, T., Liang, S., Wang, D., Wu, H., Yu, Y., & Wang, J. (2012). Estimation of surface albedo and directional reflectance from Moderate Resolution Imaging Spectroradiometer (MODIS) observations. *Remote Sensing of Environment*, *119*, 286–300. https://doi.org/10.1016/j.rse.2012.01.004

Hermance, J. F., Jacob, R. W., Bradley, B. A., & Mustard, J. F. (2007). Extracting phenological signals from multiyear AVHRR NDVI time series: Framework for applying high-order annual splines with roughness damping. *IEEE Transactions on Geoscience and Remote Sensing*, *45*(10), 3264–3276. https://doi.org/10.1109/TGRS.2007.903044

Hird, J. N., & McDermid, G. J. (2009). Noise reduction of NDVI time series: An empirical comparison of selected techniques. *Remote Sensing of Environment*, *113*(1), 248–258. https://doi.org/10.1016/j.rse.2008.09.003

Hirsch, R., Slack, J., & Smith, R. (1982). Techniques of trend analysis for monthly water quality data. *Water Resources Research*, *18*(1), 107–121. https://doi.org/10.1029/WR018i001p00107

Huete, A. R., Didan, K., Shimabukuro, Y. E., Ratana, P., Saleska, S. R., Hutyra, L. R., … Myneni, R. (2006). Amazon rainforests green-up with sunlight in dry season. *Geophysical Research Letters*, *33*(6). https://doi.org/10.1029/2005GL025583

Huete, A. R., Restrepo-Coupe, N., Ratana, P., Didan, K., Saleska, S. R., Ichii, K., … Gamo, M. (2008). Multiple site tower flux and remote sensing comparisons of tropical forest dynamics in Monsoon Asia. *Agricultural and Forest Meteorology*, *148*(5), 748–760. https://doi.org/10.1016/j.agrformet.2008.01.012

Huete, Didan, K., Miura, T., Rodriguez, E. P., Gao, X., & Ferreira, L. G. (2002). Overview of the radiometric and biophysical performance of the MODIS vegetation indices. *Remote Sensing of Environment*, *83*(1–2), 195–213. https://doi.org/10.1016/S0034-4257(02)00096-2

IPCC. (2000). IPCC Special Report on Emissions Scenarios. *Change*, *599*, 599. https://doi.org/ISBN: 92-9169-113-5

Janzen, D. H. (1988). Tropical Dry Forests The Most Endangered Major Tropical Ecosystem. In Wilson & E. and P. FM (Eds.), *Biodiversity* (pp. 130–137). Washington, DC: National Academy.

Jensen, J. R. (2007). Remote sensing of the environment: an earth resource perspective. In *Prentice Hall, Upper Saddle River, NJ*.

Jönsson, P., & Eklundh, L. (2004). TIMESAT - A program for analyzing time-series of satellite sensor data. *Computers and Geosciences*, *30*(8), 833–845. https://doi.org/10.1016/j.cageo.2004.05.006

Julien, Y., & Sobrino, J. A. (2009). Global land surface phenology trends from GIMMS database. *International Journal of Remote Sensing*, Vol. 30, pp. 3495–3513. https://doi.org/10.1080/01431160802562255

Julien, Y., Sobrino, J. A., & Verhoef, W. (2006). Changes in land surface temperatures and NDVI values over Europe between 1982 and 1999. *Remote Sensing of Environment*, *103*(1), 43–55. https://doi.org/10.1016/j.rse.2006.03.011

Kanae, S., Oki, T., & Musiake, K. (2001). Impact of Deforestation on Regional Precipitation over the Indochina Peninsula. *Journal of Hydrometeorology*, Vol. 2, pp. 51–70. https://doi.org/10.1175/1525-7541(2001)002<0051:IODORP>2.0.CO;2

Kaufmann, R. K., Zhou, L., Knyazikhin, Y., Shabanov, V., Myneni, R. B., & Tucker, C. J. (2000). Effect of orbital drift and sensor changes on the time series of AVHRR vegetation index data. *IEEE Transactions on Geoscience and Remote Sensing*, *38*(6), 2584–2597. https://doi.org/10.1109/36.885205

Kriegler, F. J., Malila, W. A., Nalepka, R. F., & Richardson, W. (1969). Preprocessing

transformations and their effects on multispectral recognition. *Proceedings of the Sixth International Symposium on Remote Sensing of Environment*, 97–131.

Latifovic, R., & Pouliot, D. (2007). Analysis of climate change impacts on lake ice phenology in Canada using the historical satellite data record. *Remote Sensing of Environment*, *106*(4), 492–507. https://doi.org/10.1016/j.rse.2006.09.015

Lawrence, D., & Vandecar, K. (2014). *The impact of tropical deforestation on climate and links to agricultural productivity*. *5*(January). https://doi.org/10.1038/nclimate2430

Lewis, S. L., Edwards, D. P., & Galbraith, D. (2015). Increasing human dominance of tropical forests. *Science*, *349*(6250), 827–832. https://doi.org/10.1126/science.aaa9932

Li, X., & Strahler, A. H. (1992). Geometric-optical bidirectional reflectance modeling of the discrete crown vegetation canopy: effect of crown shape and mutual shadowing. *IEEE Transactions on Geoscience and Remote Sensing*, *30*(2), 276–292. https://doi.org/10.1109/36.134078

Li, Y., Zhao, M., Motesharrei, S., Mu, Q., Kalnay, E., & Li, S. (2015). Local cooling and warming effects of forests based on satellite observations. *Nature Communications*, *6*, 1–8. https://doi.org/10.1038/ncomms7603

Los, S. O., North, P. R. J., Grey, W. M. F., & Barnsley, M. J. (2005). A method to convert AVHRR Normalized Difference Vegetation Index time series to a standard viewing and illumination geometry. *Remote Sensing of Environment*, *99*(4), 400–411. https://doi.org/10.1016/j.rse.2005.08.017

Lucht, W., Schaaf, C. B., & Strahler, A. H. (2000). An algorithm for the retrieval of albedo from space using semiempirical BRDF models. *IEEE Transactions on Geoscience and Remote Sensing*, *38*(2), 977–998. https://doi.org/10.1109/36.841980

Makarieva, a. M., Gorshkov, V. G., Sheil, D., Nobre, a. D., & Li, B. L. (2013). Where do winds come from? A new theory on how water vapor condensation influences atmospheric pressure and dynamics. *Atmospheric Chemistry and Physics*, *13*(2), 1039–1056. https://doi.org/10.5194/acp-13-1039-2013

Malmer, Anders and Nyberg, G. (2008). Forest and water relations in miombo woodlands. *Finnish Forest Research Institute, Metla*, 70–86.

Martínez, B., & Gilabert, M. A. (2009). Vegetation dynamics from NDVI time series analysis using the wavelet transform. *Remote Sensing of Environment*, *113*(9), 1823–1842. https://doi.org/10.1016/j.rse.2009.04.016

Meng, M., Ni, J., & Zong, M. (2011). Impacts of changes in climate variability on regional vegetation in China: NDVI-based analysis from 1982 to 2000. *Ecological Research*, *26*(2), 421–428. https://doi.org/10.1007/s11284-011-0801-z

Miettinen, J., Stibig, H. J., & Achard, F. (2014, December 1). Remote sensing of forest degradation in Southeast Asia-Aiming for a regional view through 5-30 m satellite data. *Global Ecology and Conservation*, Vol. 2, pp. 24–36. https://doi.org/10.1016/j.gecco.2014.07.007

Miles, L., Newton, A. C., DeFries, R. S., Ravilious, C., May, I., Blyth, S., … Gordon, J. E. (2006). A global overview of the conservation status of tropical dry forests. *Journal of Biogeography*, *33*(3), 491–505. https://doi.org/10.1111/j.1365-2699.2005.01424.x

Montagnini Florencia, J. C. F. (2005). Tropical Forest Ecology. The Basis of Conservation and Management. In *Tropical Forestry*.

Moreira, E. P., Valeriano, M. de M., Sanches, I. D. A., & Formaggio, A. R. (2016). Topographic Effect on Spectral Vegetation Indices From Landsat Tm Data: Is Topographic Correction Necessary? *Boletim de Ciências Geodésicas*, *22*(1), 95–107. https://doi.org/10.1590/S1982-21702016000100006

Murphy, P. G., & Lugo, A. E. (1986). Ecology of Tropical Dry Forest. *Annual Review of Ecology and Systematics*, *17*(1), 67–88. https://doi.org/10.1146/annurev.es.17.110186.000435

Myneni, R. B., Keeling, C. D., Tucker, C. J., Asrar, G., & Nemani, R. R. (1997). Increased plant growth in the northern high latitudes from 1981 to 1991. *Nature*, *386*, 698. Retrieved from http://dx.doi.org/10.1038/386698a0

Nasi, R., Wunder, S., & A, J. C. (2002). Forest ecosystem services: can they pay our way out of deforestation? *Fondo Global Para El Medio Ambiente*, 1–11. Retrieved from http://www.fucema.org.ar/old/gef/forest2.pdf%5Cnhttp://cgspace.cgiar.org/handle/10568/18673

Ni, X., Xie, J., Zhou, Y., Gao, X., & Ding, L. (2017). Evaluating Vegetation Growing Season Changes in Northeastern China by Using GIMMS LAI3g Data. *Climate*, *5*(2), 37. https://doi.org/10.3390/cli5020037

Nicodemus, F. E. (1965). Directional Reflectance and Emissivity of an Opaque Surface. *Appl. Opt.*, *4*(7), 767–775. https://doi.org/10.1364/AO.4.000767

Nobre, Sellers, P. J., & Shukla, J. (1991). Amazonian Deforestation and Regional Climate

Change. *Journal of Climate*, *4*(10), 957–988. https://doi.org/http://dx.doi.org/10.1175/1520-0442(1991)004<0957:ADARCC>2.0.CO;2

Phompila, C., Lewis, M., Clarke, K., & Ostendorf, B. (2014). Monitoring temporal vegetation changes in Lao tropical forests. *7th IGRSM International Remote Sensing & GIS Conference and Exhibition*, *012054*. https://doi.org/10.1088/1755-1315/20/1/012054

Pohlert, T. (2016). Non-Parametric Trend Tests and Change-Point Detection. *R Package*, 26. https://doi.org/10.13140/RG.2.1.2633.4243

Portillo-Quintero, C. A., & Sánchez-Azofeifa, G. A. (2010). Extent and conservation of tropical dry forests in the Americas. *Biological Conservation*, *143*(1), 144–155. https://doi.org/10.1016/j.biocon.2009.09.020

Purkis, S., & Klemas, V. (2011). *Remote sensing and global environmental change*. 757. https://doi.org/10.1002/9781118687659.ch6

Reed, B., White, M., & Brown, J. (2003). *Remote Sensing Phenology*.

Reed, B. C., Brown, J. F., VanderZee, D., Loveland, T. R., Merchant, J. W., & Ohlen, D. O. (1994). Measuring phenological variability from satellite imagery. *Journal of Vegetation Science*, *5*(5), 703–714. https://doi.org/10.2307/3235884

Restrepo-Coupe, N., da Rocha, H. R., Hutyra, L. R., da Araujo, A. C., Borma, L. S., Christoffersen, B., … Saleska, S. R. (2013). What drives the seasonality of photosynthesis across the Amazon basin? A cross-site analysis of eddy flux tower measurements from the Brasil flux network. *Agricultural and Forest Meteorology*, *182–183*, 128–144. https://doi.org/10.1016/j.agrformet.2013.04.031

Ross, J. (1981). *The radiation regime and architecture of plant stands*. Dr. W. Junk, Norwell, MA.

Roujean, J.-L., Leroy, M., & Deschamps, P.-Y. (1992). A bidirectional reflectance model of the Earth's surface for the correction of remote sensing data. *Journal of Geophysical Research*, *97*(D18), 20455. https://doi.org/10.1029/92JD01411

Saleska, S. R., Wu, J., Guan, K., Araujo, A. C., Huete, A., Nobre, A. D., & Restrepo-Coupe, N. (2016). Dry-season greening of Amazon forests. *Nature*, *531*(7594), E4–E5. Retrieved from http://dx.doi.org/10.1038/nature16457

Sánchez-Azofeifa, G. A., Quesada, M., Rodríguez, J. P., Nassar, J. M., Stoner, K. E., Castillo, A., … Cuevas-Reyes, P. (2005). Research priorities for neotropical dry forests. *Biotropica*, *37*(4), 477–485. https://doi.org/10.1111/j.1744-7429.2005.00066.x

Savitzky, A., & Golay, M. J. E. (1964). Smoothing and Differentiation of Data by Simplified Least Squares Procedures. *Analytical Chemistry*, *36*(8), 1627–1639. https://doi.org/10.1021/ac60214a047

Schaaf, C. B., Gao, F., Strahler, A. H., Lucht, W., Li, X., Tsang, T., … Roy, D. (2002). First operational BRDF, albedo nadir reflectance products from MODIS. *Remote Sensing of Environment*, *83*(1–2), 135–148. https://doi.org/10.1016/S0034-4257(02)00091-3

Schaaf, C. B., Liu, J., Gao, F., & Strahler, A. H. (2011). Aqua and Terra MODIS Albedo and Reflectance Anisotropy Products. In B. Ramachandran, C. O. Justice, & M. J. Abrams (Eds.), *Land Remote Sensing and Global Environmental Change: NASA's Earth Observing System and the Science of ASTER and MODIS* (pp. 549–561). https://doi.org/10.1007/978-1-4419-6749-7_24

Schaaf, C., & Wang, Z. (2015a). *MCD43A1 MODIS/Terra+Aqua BRDF/Albedo Model Parameters Daily L3 Global - 500m V006*. NASA EOSDIS Land Processes DAAC.

Schaaf, C., & Wang, Z. (2015b). *MCD43C1 MODIS/Terra+Aqua BRDF/AlbedoModel Parameters Daily L3 Global 0.05Deg CMG V006 [Data set]*. https://doi.org/10.5067/MODIS/MCD43C1.006

Schneck, R., & Mosbrugger, V. (2011). Simulated climate effects of Southeast Asian deforestation: Regional processes and teleconnection mechanisms. *Journal of Geophysical Research: Atmospheres*, *116*(11). https://doi.org/10.1029/2010JD015450

Schwartz, M. (2013). Introduction. In M. Schwartz (Ed.), *Phenology: An Integrative Environmental Science* (pp. 1–5). Springer.

Sen, O. L., Bozkurt, D., Vogler, J. B., Fox, J., Giambelluca, T. W., & Ziegler, A. D. (2013). Hydro-climatic effects of future land-cover/land-use change in montane mainland southeast Asia. *Climatic Change*, *118*(2), 213–226. https://doi.org/10.1007/s10584-012-0632-0

Sen, O. L., Wang, Y., & Wang, B. (2004). Impact of Indochina deforestation on the east Asian summer monsoon. *Journal of Climate*, *17*(6), 1366–1380. https://doi.org/10.1175/1520-0442(2004)017<1366:IOIDOT>2.0.CO;2

Shi, J., Jackson, T., Tao, J., Du, J., Bindlish, R., Lu, L., & Chen, K. S. (2008). Microwave vegetation indices for short vegetation covers from satellite passive microwave sensor AMSR-E. *Remote Sensing of Environment*, *112*(12), 4285–4300. https://doi.org/10.1016/j.rse.2008.07.015

Short, N. M. (1982). *The Landsat tutorial workbook: basics of satellite remote sensing* (p. viii, 553 p.). p. viii, 553 p. Retrieved from file://catalog.hathitrust.org/Record/011409073

Smith, R. C. G., & Choudhury, B. J. (1990). On the correlation of indices of vegetation and surface temperature over south-eastern Australia. *International Journal of Remote Sensing*, *11*(11), 2113–2120. https://doi.org/10.1080/01431169008955164

Sobrino, J. A., & Julien, Y. (2013). Trend Analysis of Global MODIS-Terra Vegetation Indices and Land Surface Temperature Between 2000 and 2011. *IEEE Journal of Selected Topics in Applied Earth Observations and Remote Sensing*, *6*(5), 2139–2145. https://doi.org/10.1109/JSTARS.2013.2239607

Spracklen, D. V., Arnold, S. R., & Taylor, C. M. (2012). Observations of increased tropical rainfall preceded by air passage over forests. *Nature*. https://doi.org/10.1038/nature11390

Spracklen, D. V, & Garcia-Carreras, L. (2015). The impact of Amazonian deforestation on Amazon basin rainfall. *Geophysical Research Letters*, *42*(21), 9546–9552. https://doi.org/10.1002/2015GL066063

Stibig, H., Achard, F., Carboni, S., Raši, R., & Miettinen, J. (2014). Change in tropical forest cover of Southeast Asia from 1990 to 2010. *Biogeosciences*, *11*(2), 247–258. https://doi.org/10.5194/bg-11-247-2014

Strahler, A., Gopal, S., Lambin, E., & Moody, A. (1999). MODIS Land Cover Product Algorithm Theoretical Basis Document (ATBD) MODIS Land Cover and Land-Cover Change. *Change*, (May), 72. Retrieved from http://modis.gsfc.nasa.gov/data/atbd/atbd_mod12.pdf

Strahler, A. H., & Muller, J. P. (1999). MODIS BRDF Albedo Product : Algorithm Theoretical Basis Document. *MODIS Product ID: MOD43*, *Version 5*.(April), 1–53. https://doi.org/http://duckwater.bu.edu/lc/mod12q1.html

Strugnell, N. C., Lucht, W., Hyman, A. H., & Meister, G. (1998). Continental-scale albedo inferred from land cover class, field observations of typical BRDFs and AVHRR data. *Geoscience and Remote Sensing Symposium Proceedings, 1998. IGARSS '98. 1998 IEEE International*, *2*, 595–597 vol.2. https://doi.org/10.1109/IGARSS.1998.699522

Suepa, T. (2013). *SATELLITE TIME-SERIES DATA FOR VEGETATION PHENOLOGY DETECTION AND ENVIRONMENTAL ASSESSMENT IN SOUTHEAST ASIA*. Michigan State University.

Suepa, T., Qi, J., Lawawirojwong, S., & Messina, J. P. (2016). Understanding spatio-temporal

variation of vegetation phenology and rainfall seasonality in the monsoon Southeast Asia. *Environmental Research*, *147*, 621–629. https://doi.org/10.1016/j.envres.2016.02.005

Syampungani, S. , Chirwa, P. W., Akinnifesi, F. K., Sileshi, G. and Ajayi, O. C. (2009). The miombo woodlands at the cross roads: Potential threats, sustainable livelihoods, policy gaps and challenges. *Natural Resources Forum*, *33*(2), 150–159. https://doi.org/10.1111/j.1477-8947.2009.01218.x

Tian, H., Melillo, J. M., Kicklighter, D. W., McGuire, A. D., Helfrich III, J. V. K., Moore III, B., & Vörösmarty, C. J. (1998). Effect of interannual climate variability on carbon storage in Amazonian ecosystems. *Nature*, *396*, 664. Retrieved from http://dx.doi.org/10.1038/25328

Tottrup, C., Rasmussen, M. S., Eklundh, L., & Jönsson, P. (2007). Mapping fractional forest cover across the highlands of mainland Southeast Asia using MODIS data and regression tree modelling. *International Journal of Remote Sensing*, *28*(1), 23–46. https://doi.org/10.1080/01431160600784218

Tucker, C. J., Slayback, D. A., Pinzon, J. E., Los, S. O., Myneni, R. B., & Taylor, M. G. (2001). Higher northern latitude normalized difference vegetation index and growing season trends from 1982 to 1999. *International Journal of Biometeorology*, *45*(4), 184–190. https://doi.org/10.1007/s00484-001-0109-8

Wang, Z., Schaaf, C. B., Chopping, M. J., Strahler, A. H., Wang, J., Román, M. O., … Shuai, Y. (2012). Evaluation of Moderate-resolution Imaging Spectroradiometer (MODIS) snow albedo product (MCD43A) over tundra. *Remote Sensing of Environment*, *117*, 264–280. https://doi.org/https://doi.org/10.1016/j.rse.2011.10.002

Wanner, W., Li, X., & Strahler, A. H. (1995). On the derivation of kernels for kernel-driven models of bidirectional reflectance. *Journal of Geophysical Research: Atmospheres*, *100*(D10), 21077–21089. https://doi.org/10.1029/95JD02371

Wanner, W., Strahler, A. H., Hu, B., Lewis, P., Muller, J.-P., Li, X., … Barnsley, M. J. (1997). Global retrieval of bidirectional reflectance and albedo over land from EOS MODIS and MISR data: Theory and algorithm. *Journal of Geophysical Research: Atmospheres*, *102*(D14), 17143–17161. https://doi.org/10.1029/96JD03295

Wolfgang, L., & Crystal, S. (2001). A global albedo data set derived from AVHRR data for use in climate simulations. *Geophysical Research Letters*, *28*(1), 191–194. https://doi.org/doi:10.1029/2000GL011580

Wu, M., Yang, C., Song, X., Hoffmann, W. C., Huang, W., Niu, Z., … Yu, B. (2018).

Monitoring cotton root rot by synthetic Sentinel-2 NDVI time series using improved spatial and temporal data fusion. *Scientific Reports*, *8*(1), 2016. https://doi.org/10.1038/s41598-018-20156-z

Xiao, X., Hagen, S., Zhang, Q., Keller, M., & Moore, B. (2006). Detecting leaf phenology of seasonally moist tropical forests in South America with multi-temporal MODIS images. *Remote Sensing of Environment*, *103*(4), 465–473. https://doi.org/10.1016/j.rse.2006.04.013

Xiao, Zhang, J., Yan, H., Wu, W., & Biradar, C. (2009). Land surface phenology convergence of satellite and CO2 eddy flux observations. In *Phenology of Ecosystem Processes: Applications in Global Change Research* (pp. 247–270). https://doi.org/10.1007/978-1-4419-0026-5_11

Yue, S., Pilon, P., & Cavadias, G. (2002). Power of the Mann-Kendall and Spearman's rho tests for detecting monotonic trends in hydrological series. *Journal of Hydrology*, *259*(1–4), 254–271. https://doi.org/10.1016/S0022-1694(01)00594-7

Zhang, X., Friedl, M. A., Schaaf, C. B., Strahler, A. H., Hodges, J. C. F., Gao, F., … Huete, A. (2003). Monitoring vegetation phenology using MODIS. *Remote Sensing of Environment*, *84*(3), 471–475. https://doi.org/10.1016/S0034-4257(02)00135-9

Zhang, Y., Zhu, Z., Liu, Z., Zeng, Z., Ciais, P., Huang, M., … Piao, S. (2016). Seasonal and interannual changes in vegetation activity of tropical forests in Southeast Asia. *Agricultural and Forest Meteorology*, *224*, 1–10. https://doi.org/10.1016/j.agrformet.2016.04.009

Chapter 2. Intact forests seasonality and BRDF effect on forest phenology in continental Southeast Asia

2.1. Introduction

Tropical forests play significant roles in global climate and biodiversity. They help stabilise the world's climate; provide a home to many plants and animals; and protect against flood, drought, and erosion. Understanding tropical forest phenology is critical because of recent climate change or extreme events. Among three major tropical forest regions, Southeast Asia is the least studied area compared to Amazon or Central Africa forests (Blackie et al., 2014).

Tropical forests can be classified as tropical rainforests and tropical dry forests. In mainland Southeast Asia (SEA), 30 per cent of forests were classified as dry forests (Poffenberger, 2000). While tropical dry forests comprised a third of tropical forest coverage, only 14 per cent of articles published in tropical environments for the over 60 years focused on dry forests (Sánchez-Azofeifa et al., 2005). Therefore, investigating forest phenology in Peninsular SEA region is a critical need due to the large gap in ecological knowledge about this region.

Spaceborne optical sensors provide a global perspective for the study of seasonal and inter-annual changes in vegetation phenology by capturing landscape reflectance. However, optical satellite sensors usually have critical issues of clouds, aerosols and BRDF effects, especially in tropical forests due to the harsh atmospheric conditions with aerosol contamination from fires in dry seasons and clouds in wet seasons. That is why it is troublesome to extract annual profiles of tropical forest dynamics with low temporal resolution satellites, such as Landsat (Short, 1982). The Moderate Resolution Imaging Spectroradiometer (MODIS), a payload scientific instrument launched in 1999 (Terra) and 2002 (Aqua), generates daily global scenes and provides 16-day composited vegetation indices (Kamel Didan, 2015a), spectral transformations of two or more bands that offer useful tools to study vegetation dynamics, including seasonality and inter-annual variation (Huete et al., 2002).

Pinter *et al.*, (1987) suggested that a perfect time-series of spectral vegetation index should maintain maximum sensitivity to real landscape characteristics while being relatively unaffected by solar angles, atmospheric turbidity, topography and view angles. But MODIS, like other space observation instruments, often acquires images over a wide range of the sensor and solar geometric configurations. These changes in illumination and viewing geometry potentially cause intra- and inter-annual variations of surface reflectances and vegetation indices that are disassociated with canopy photosynthesis activity (Bhandari, Phinn, & Gill, 2011; Moura, Galvão, dos Santos, Roberts, & Breunig, 2012). Field measurements, models, and remote sensing data have shown that surface reflectances, and vegetation indices are solar angle-dependent (Chen & Cihlar, 1997; Alfredo R. Huete, 1987; Elizabeth M Middleton, 1991), and deriving phenological metrics without proper correction of sun-angle effect can produce inaccurate results that reflect false ground vegetation dynamics (Morton et al., 2014).

Moreover, sun-sensor geometry artefacts rose controversial results among scientists. One crucial controversy was whether Amazon rainforest green-up during dry seasons. According to Huete et al. (2006), the majority of Amazon rainforests was greening-up in the dry season and suggested that sunlight might have a stronger influence than precipitation on phenology and productivity of Amazon rainforests. Morton *et al.* (2014) questioned light-driven suggestion by claiming that dry-season green-up of Amazon forests was an artefact of seasonal variations in sun-sensor geometry. However, other studies counter-questioned Morton conclusion as flux tower and modelling results showed that productivity of Amazon forests was increasing in dry periods. According to Restrepo-Coupe et al. (2013), both observed Amazon GPP from eddy flux tower, and satellite EVI increased during the dry season, whereas modelled results decreased during the same period.

Furthermore, by correcting sun angle artefacts at several flux tower sites in a comprehensive way, Saleska et al. (2016) illustrated that there was a statistically significant canopy greening during the dry season. The result was validated with in-situ data shown a consistent correlation between satellite-based observations and ground-based measurements of increasing leaf amount, fractions of new leaves and canopy photosynthesis capacity derived from eddy flux towers in the dry season**.** Consequently, BRDF correcting optical remote sensing data is essential to extract the actual response of vegetation and avoid unnecessary controversy.

Products derived from MODIS data include MODIS BRDF/Albedo that provides modelled parameters to estimate albedo and reflectance of the landscape at varying sun-view geometries. The dataset uses the three-parameter semi-empirical RossThick-LiSparse-Reciprocal (RTLSR) BRDF model, one of the most commonly used models for characterising the anisotropic reflectance of land surfaces (Lucht, Schaaf, & Strahler, 2000; C. B. Schaaf et al., 2002). Using MODIS BRDF/Albedo product to generate vegetation indices at a fixed sun-view configuration and comparing with standard MODI Vegetation Indices products could answer the questions about the impact of BRDF on VI time-series of vegetation landscapes and related phenological metrics derived from VI time-series.

The primary purpose of this chapter is to gain a better understanding of sun-angle influences on time-series vegetation indices of Southeast Asia tropical forests for improving monitoring of forest phenology with MODIS data. The specific objectives of this chapter are: (1) Investigate seasonal variations of sun and view angles from MODIS Terra and Aqua sensors; (2) Retrieve time-series of BRDF-corrected vegetation indices of SEA tropical forests; (3) Understand the BRDF impact on VI time-series, seasonal profiles and derived phenological parameters of SEA non-disturbed forests; (4) Assess NDVI and EVI capabilities in capturing SEA forest phenology, both in terms of robustness to BRDF effect and saturation; (5) Analyse seasonal phenology of SEA forests with various rainfall conditions; (6) Investigate whether different fixed sun-sensor configurations affect outcomes derived from VI time-series; and (7) Evaluate MODIS BRDF/Albedo ability in generating reflectance and VIs at specific sun-view angles.

2.2. Methodology

2.2.1. Study areas

MCD12 products (Friedl & Sulla-Menashe, 2015) are among the most common land cover type (LCT) maps to get forest coverage. These products provide global LCT maps at a yearly interval from 2001 to 2016 derived from MODIS Nadir BRDF-Adjusted Reflectance using supervised classification algorithms. We used the LCT map at 0.05-degree resolution (Friedl & Sulla-Menashe, 2015) to get a continental scale overview of SEA forests in 2016. However, as these forests are highly endangered and threatened by human activities (Blackie, 2014), they are currently heterogeneous and scattered at small patches mixing intact and disturbed forests (Dong et al., 2014).

In this chapter, we only focus on influences of sun-sensor geometries on MODIS VIs in mainland SEA tropical forests and do not account for other factors, especially disturbance. Therefore, we selected intact forest areas to avoid anthropogenic interference on forest phenology. While MODIS LCT map can provide data at only 500m or 0.05-degree spatial resolution (Sulla-menashe & Friedl, 2018), it is difficult to separate between intact forests and disturbed areas in Southeast Asia at this scale because of their high fragmentation levels (Dong et al., 2014).

Hansen *et al.* (2013) introduced the first global forest cover change map between 2000 and 2013 using a combination of MODIS and Landsat data. Later the cover change map was updated until 2016. Using these highly detailed forest coverage maps at 30m, Tyukavina *et al.* (2016) proposed a method of mapping undisturbed global tropical forests, called hinterland forests, based on Hansen's product. Hinterland forests were defined as forest areas without disturbance in near-term history from 2000 to 2012. By applying various criteria, for example, distance from disturbance, size threshold and connectivity of hinterland forest patches, the study provided a quality mapping of undisturbed tropical forests, including mainland SEA tropical forests.

Undisturbed forest sites were chosen from hinterland forest map across whole mainland Southeast Asia. Because Tyukavina's study derived intact forests map for the 2001-2012 period, sites with patches larger than 100 square kilometres and containing no extra forest-loss pixels from updated Hansen cover map (2016) were selected. The set of study areas included 30 sites covering the entire continental Southeast Asia and representing all forest phenology types with varying dry-season lengths. Figure 2.1 highlights chosen undisturbed sites and SEA forest coverage based on MCD12C1 Land Cover Type (Friedl & Sulla-Menashe, 2015). We also selected a subset of four sites at different latitudes to examine seasonal variations of sun and view angles derived from MODIS Terra and Aqua sensors (Figure 2.3). All selected 30 sites were used to investigate BRDF impact on derived phenological parameters.

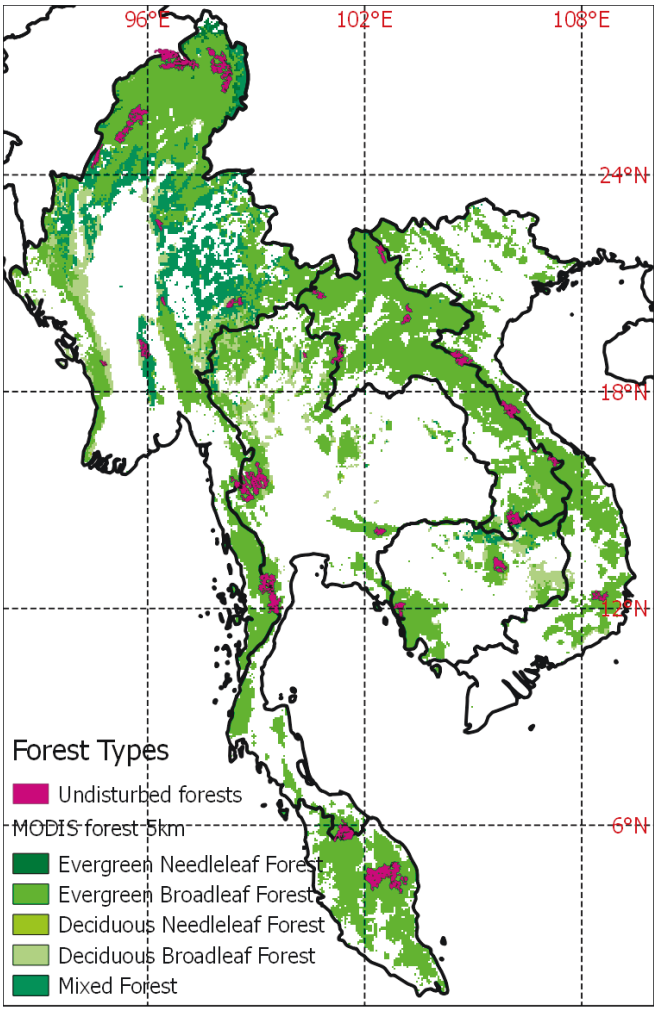

Figure 2.1 *Selected undisturbed sites (red areas) associated with forest pixels derived from MCD12C1 data (2016). The size of the selected undisturbed sites varies from 1000 to over 40000 square kilometres.*

2.2.2. BRDF Model

The surface reflectance can be described using a bidirectional reflectance distribution function (BRDF). It is a function to represent how the reflectance depends on view and solar angles, concerning a reference direction (Roujean, Leroy, & Deschamps, 1992). This anisotropy is strongly affected by solar illumination angle (E. M. Middleton, 1992) as well as canopy structural geometry and wavelength (Elizabeth M Middleton, 1991). BRDF can be used to standardise surface reflectance observations with varying sun-view geometries to a standard geometry (Vermote, Justice, & Breon, 2009).

In this study, we implemented a semi-empirical BRDF model called RossThick-LiSparse Reciprocal to similar MODIS reflectances as acquired at varying solar zenith angles. The basis of the BRDF model is that the land surface can be modelled as a

combination of three parameters representing three scattering types: isotropic scattering, radiative transfer-type volumetric scattering, and geometric-optical surface scattering (Roujean et al., 1992; Strahler & Muller, 1999). A detailed description of the BRDF model can be found in the BRDF section of chapter one of this document and Lucht et al. (2000).

2.2.3. Vegetation Indices

Two famous vegetation indices, Normalized Difference Vegetation Index (NDVI) and Enhanced Vegetation Index (EVI), are widely used as representatives of canopy "greenness", a combined property of green leaf coverage, canopy structure and chlorophyll content of green pigments (Myneni, Hall, Sellers, & Marshak, 1995). These vegetation indices are robust and seamless biophysical measurements used for deriving vegetation phenological parameters at regional to global scale (Broich et al., 2015; de Beurs & Henebry, 2010; Jeganathan, Dash, & Atkinson, 2014; X. Zhang et al., 2003). While NDVI is a simple indicator used to analyse vegetation dynamics for over 40 years since the first well-known study of (Rouse, Hass, Schell, & Deering, 1973), EVI was used as an optimised version of NDVI reducing the impact of soil background and atmospheric noise variations effectively (Huete et al., 2002). The equations defining NDVI and EVI for MODIS data are

$$NDVI = \frac{\rho_{NIR} - \rho_{RED}}{\rho_{NIR} + \rho_{RED}} \quad (2\text{-}1)$$

$$EVI = 2.5 \times \frac{\rho_{NIR} - \rho_{RED}}{\rho_{NIR} + 6 \times \rho_{RED} - 7.5 \times \rho_{BLUE} + 1} \quad (2\text{-}2)$$

Where ρ_{NIR},ρ_{RED}, and ρ_{BLUE} are atmospherically-corrected surface reflectance at near-infrared (841 – 876nm), red (620 – 670nm), and blue (459 – 479nm) bands of MODIS sensors respectively.

2.2.4. Datasets

2.2.4.1. MODIS Vegetation Indices data

MODIS Vegetation Indices datasets provide the NDVI and EVI measurements to monitor biophysical or biochemical states of vegetated surfaces effectively. There are various VI products at varying spatial (500m, 0.05-degree) and temporal (16-day, monthly) resolutions to meet the requirements of research application communities. In

this study, we used MOD13C2/MYD13C2 at 0.05 degrees resolution to analyse minimum and peak timing of tropical forests in the whole continental Southeast Asia, while MOD13A1/MYD13A1 were used to investigate forest phenology in a smaller scale at 500-m spatial resolution (K. Didan, 2015a, 2015b, Kamel Didan, 2015a, 2015b).

Sixteen-year (2001 – 2016) MODIS VI data were downloaded and processed from the U.S. Geological Survey (https://e4ftl01.cr.usgs.gov/). MODIS Terra/Aqua 500m products are 16-day composited images of VIs. We obtained 2944 MOD13A1 Terra and 2688 MYD13A1 Aqua (Collection 6) scenes for the period January 2001 (July 2002 for Aqua) to December 2016, for 8 MODIS tiles covering the entire continental Southeast Asia. We also retrieved 192 Terra and 179 Aqua global scenes of MODIS Vegetation Indices CMG Collection 6 for analysing phenology at 0.05-degree scale.

MODIS Vegetation Indices are provided with related quality reliability to rank the confidence of captured VI values for each pixel (A. Huete & Justice, 1999). In this chapter, we selected only VI measurements with acceptable quality levels and removed all cloudy or snowy pixels. We chose the acceptable quality rather than the best quality because of the fact that our study areas were mixing of tropical rainforests where there are no dry seasons and dry tropical forests having prolonged raining seasons. Selecting the best quality level would result in too many missing data during wet periods and it would be difficult to retrieve the seasonal VI profiles of our sites even we processed on large-sized forest sites. Moreover, VI data filtered by acceptable quality level also include the best quality data. Eventually, with this selection, we could maximise data availability in wet season while retaining good quality data during dry periods when we got more clear observations.

2.2.4.2. MODIS BRDF/Albedo products

To analyse BRDF impact on vegetation indices, we needed to standardise surface reflectances and VIs with varying sun-view geometries to a standard geometry (Vermote et al., 2009). MCD43 (or MODIS BRDF/Albedo) products supply modelled parameters to characterise the surface anisotropy that can be used to calculate global land surface reflectance and related vegetation indices.

In this study, we used the latest version (Collection 6) of MODIS BRDF/Albedo products at both CMG (Climate Modelling Grid) and 500-m scales to generate reflectance and VI to common geometries. Focusing on the impact of seasonal variations in SZA on

surface reflectances and VIs, view zenith angle (VZA) was normalised to zero and solar zenith angle (SZA) was fixed at 0º,15º, 30º, and 45º degrees (termed as SZ0, SZ15, SZ30 and SZ45 respectively) to capture the broadest possible ranges of SZA over the Southeast Asia region.

We used MODIS BRDF MCD43A1product (C. Schaaf & Wang, 2015) sourced from the U.S. Geological Survey (https://e4ftl01.cr.usgs.gov/) to provided BRDF parameters at 500-m spatial resolution. We downloaded and pre-processed 46752 MCD43A1 Collection 6 scenes for continental SEA regions during our study period (2001 – 2016). In addition, 192 images of sixteen-year MODIS BRDF/Albedo CMG data were retrieved for CMG analyses.

For our study, only data satisfying the condition of magnitude inversion of the Ross-Li BRDF model based on the QC information were selected (Strahler & Muller, 1999). Our reason of choosing magnitude inversion over full inversion (the best quality) is similar to the quality selection of MODIS VI product, data limitation in wet seasons. Setting QC level to full inversion would cause long periods of data gaps. While our study focused on intra- and inter- annual time-series VI and derived phenological metrics, long periods of missing data would cause the inaccurate seasonal VI profiles and make our results unreliable. Moreover, selecting magnitude inversion level would not exclude full-inversion data, especially during dry season. So choosing magnitude inversion of QC level can increase data availability in wet seasons and not cause significant lacks to data of dry seasons.

2.2.4.3. Precipitation dataset

The Tropical Rainfall Measuring Mission (TRMM) is a space mission between NASA and Japan Aerospace Exploration Agency (JAXA) planned to monitor tropical and subtropical precipitation and the associated release of energy. TRMM was part of NASA's Mission to Planet Earth, a coordinated research effort to study Earth as a global system. The mission uses five instruments: Precipitation Radar (PR), TRMM Microwave Imager (TMI), Visible and Infrared Scanner (VIRS), Clouds and the Earth's Radiant Energy Sensor (CERES), and Lightning Imaging Sensor (LIS).

Observed data of these instruments are used in an algorithm to generate TRMM Combined Instrument (TCI) calibration dataset from which the TRMM Multisatellite Precipitation Analysis (TMPA), finer-scale precipitation estimated dataset, is created.

TMPA provides monthly (3B43) and daily (3B42) precipitation averages, probably the most relevant TRMM-related products for climate research (Huffman & Pendergrass, 2017).

Compared to previous rainfall datasets like Global Precipitation Climatology Project (GPCP), TMPA is available in excellent spatial resolution (0.25^{o}) covering all tropical and subtropical regions from 50^{o}N to 50^{o}S (Huffman et al., 2007). TMPA provides high spatial and temporal resolution precipitation estimates over a relatively extended period of record since 1998. With its broad coverage, TMPA can be applied to investigate the climatological distribution of precipitation, and its frequency and intensity, especially for tropical regions.

TMPA was excellent to offer good regional rainfall estimates over African and Amazon tropical forests. However, its 0.25-degree spatial resolution makes TMPA an improper dataset for monitoring precipitation in heterogeneous areas. SEA tropical forests are fragmented because of high rates of deforestation in recent decades (Dong et al., 2014). Figure 2.1 shows considerable evidence of the fragmentation level in the SEA.

Climate Hazards Group InfraRed Precipitation with Station data (CHIRPS) is a 30+ year precipitation dataset from 1981 until now. It incorporated satellite information, including TRMM data, with in-situ station data to generate gridded rainfall datasets at 0.05-degree spatial resolution. Higher spatial resolution data could help to minimise the mixing areas of both disturbed and non-disturbed forest caused by coarse spatial datasets. Furthermore, CHIRPS algorithm was designed to focus on trend analysis and seasonal drought monitoring (C. C. Funk et al., 2014; Shukla, McNally, Husak, & Funk, 2014). Therefore, it is a more suitable precipitation dataset for studying phenology of non-disturbed forests in a highly fragmented region such as Southeast Asia.

Using monthly CHIRPS time-series data (C. Funk et al., 2015), spatial distribution of rain were generated to represent 16-year mean annual precipitation and rainfall seasonality parameters for both rainy and dry season (start of the rainy season (SRS), end of the rainy season (ERS), and length of rainy season (LRS)). We defined the wet season as the period in which monthly rainfall was higher than 100mm, while months with precipitation lower than 100mm were considered the dry season. These criteria represent the minimum rain needed for maintaining an evergreen rainforest (Sternberg, 2001) and is also commonly used for ecological-economic zoning (Sombroek, 2001).

2.2.5. Data smoothing and filtering

As VI time-series usually have noise caused by cloud, atmospheric contaminations or variations of solar-sensor angles, smoothing functions needs to be applied to minimise noise effect or abnormal data. Firstly, a median filter was used to remove spikes and outliers as these noises might affect the accuracy of data.

Then Savitz-Golay (SG) filter was applied to smooth noise and irregular values of original VI data due to clouds or atmospheric conditions. SG filter is a digital filter that can be used to smooth data without substantially distorting the signal. SG filter fits successive sub-sets of adjacent data points with a low-degree polynomial by computing least-squares polynomial regression. SG can be mathematically represented as:

$$Y_j = \sum_{i=-\frac{m-1}{2}}^{\frac{m-1}{2}} C_i y_{j+i} \qquad (2\text{-}3)$$

Where

Y_j new VI value replaced by averaged VI in the position j

y_{j+i} the original VI value at the j+i position

C_i a coefficient which is dependent on window size and polynomial degree and can be retrieved from SG look-up table

m the width of moving window (odd number)

In contrast to other approaches such as Fourier Transform (Hermance, Jacob, Bradley, & Mustard, 2007), Double Logistic Function (Beck et al., 2007) or high-order spline fitting model (Bradley, Jacob, Hermance, & Mustard, 2007) which are not suitable for VI time-series data in tropics, SG filter can capture vegetation dynamics. It was applied to smooth VI time-series because of its robustness to reconstruct high-quality VI time-series data in tropical areas (Bachoo & Archibald, 2007; Tottrup, Rasmussen, Eklundh, & Jönsson, 2007). SG method can retain features of the distribution and capture rapid phenological changes, and deal with substantial variation in the timing and

magnitude of vegetation growth. Therefore, this method was selected to produce smoothed VI curves.

2.2.6. Extracting phenological parameters

To extract meaningful phenological parameters with smoothed time-series, this research adopted thresholds based on VI ratio (R Reed, White, & Brown, 2003) to study SEA forest seasonal dynamics and investigate BRDF impact of retrieved information such as specific phenological dates and seasonal amplitude. The key phenological metrics of SEA tropical forests extracted with MODIS time-series data are defined as:

- Start of Greening Season (SGS): the beginning date of growing season. It was defined as when vegetation indices reach the values equals the minimum values before the growing season plus 20% of seasonal amplitude during green-up phrase.
- Peak of Greening Season (PGS): the date of maximum vegetation productivity for forest vegetation assemblage
- End of Greening Season (EGS): the end date of growing season. EGS was determined as when VI crosses the value equal to the minimum value plus 20% of amplitude during brown down phase.
- Dormancy Timing (DT): the timing when VI reaches the bottom value (Rankine, Sánchez-Azofeifa, Guzmán, Espirito-Santo, & Sharp, 2017)
- Length of Greening Season (LGS): duration of growing season, defined as the differences between EGS and SGS
- Amplitude of Greening Season (AGS): the amplitude of greening seasonality, determined as the difference between minimum and maximum productivity of vegetation
- The maximum (MAX): the maximum value of vegetation index
- The minimum (MIN): the minimum value of vegetation index

We use these metrics to investigate SEA forest phenology and determine how BRDF might change these parameters. While MODIS BRDF/Albedo parameters are daily estimates, MODIS Terra/Aqua Vegetation Indices are provided at16-day interval data only. Thus, we interpolated standard 16-day VI time-series to daily data and derived phenological metrics from that interpolated estimation.

2.2.7. Analyses

2.2.7.1. Phenology and BRDF impact analyses at CMG (0.05-degree) resolution

To provide an overview of BRDF impact on VI measurements and phenological parameters of continental SEA forests, we used monthly CMG VI data (MOD13C2 and MYD13C2 products) to derive the timing of minimum and maximum values for both NDVI and EVI. Figure 2.2 describes how we produced our analyses at 0.05-degree resolution. . We generated VI data fixing sun angles to 15, 30 and 45 degrees (SZ15, SZ30 and SZ45 respectively) at 0.05-degree resolution, converted daily MODIS BRDF CMG VI to monthly data and then derived the timing of minimum and maximum measurements of retrieved VIs. By comparing between the phenological timing of BRDF-corrected and -uncorrected Vis, we provided an overview of BRDF impact on the derived phenology of SEA tropical forests at CMG scale (Fig. 2.2A and 2.2B). We also compared results between various SZA settings to detect significant timing variations of minimum and maximum VIs potentially caused by different SZA configurations (Fig. 2.2C).

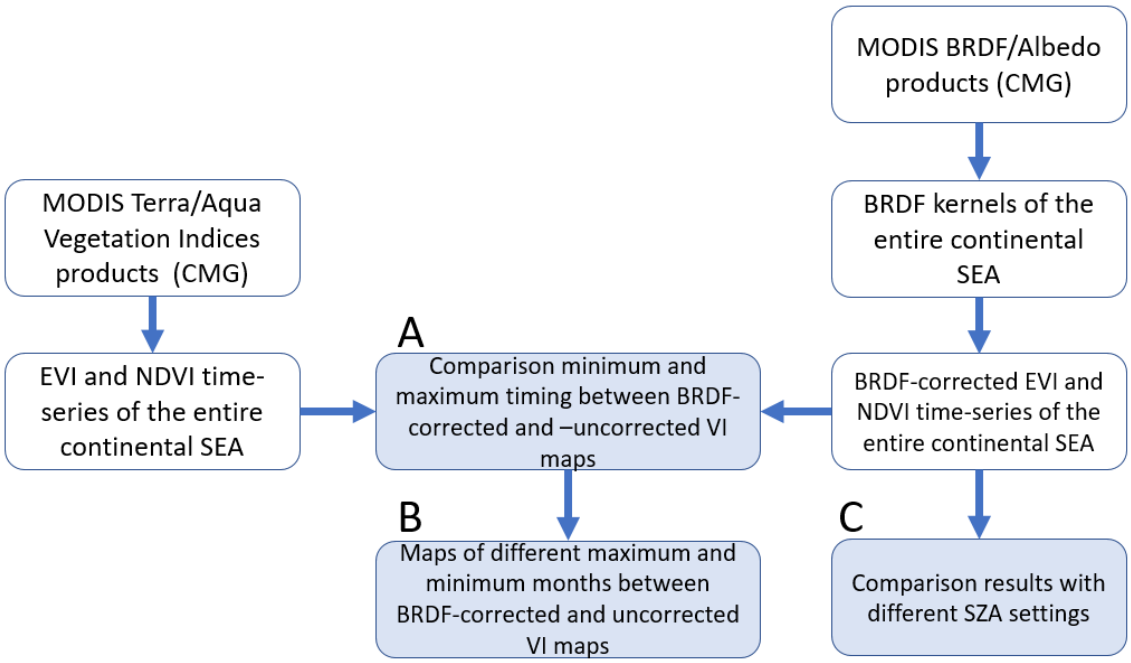

Figure 2.2 *Diagram of CMG VI time-series analyses for BRDF influence on phenological timing. Coloured background boxes are outcomes*

2.2.7.2. Phenology and BRDF impact analyses at 500m resolution

We analysed at 500m resolution with detailed information about forest phenology and BRDF impact on phenological metrics (Figure 2.3). We firstly extracted VI time-

series of 30 selected sites with 500-m scaled data and retrieved all phenological parameters for fully analysing BRDF impact on phenophase dates. Secondly, we chose a sampled subset of 30 sites with various lengths of dry seasons to convey time-series and seasonal profiles of BRDF-corrected and -uncorrected VIs (Fig. 2.3A). Results of this step provided the means to analyse the differences between time-series of corrected and uncorrected VIs and inter- and intra-annual variations.

Later, cross-site correlation plots were used to analyse the variations of phenological metrics caused by BRDF influence. BRDF might produce the shifting of phenophase dates and variability of maximum and minimum measurements, and thus can alter the results about SEA tropical forests phenology (Fig 2.3B). We also used cross-site correlation plots to analyse differences caused by various SZA settings (Fig. 2.3C). Biases were calculated to quantify average shifts and variations of VI measurements.

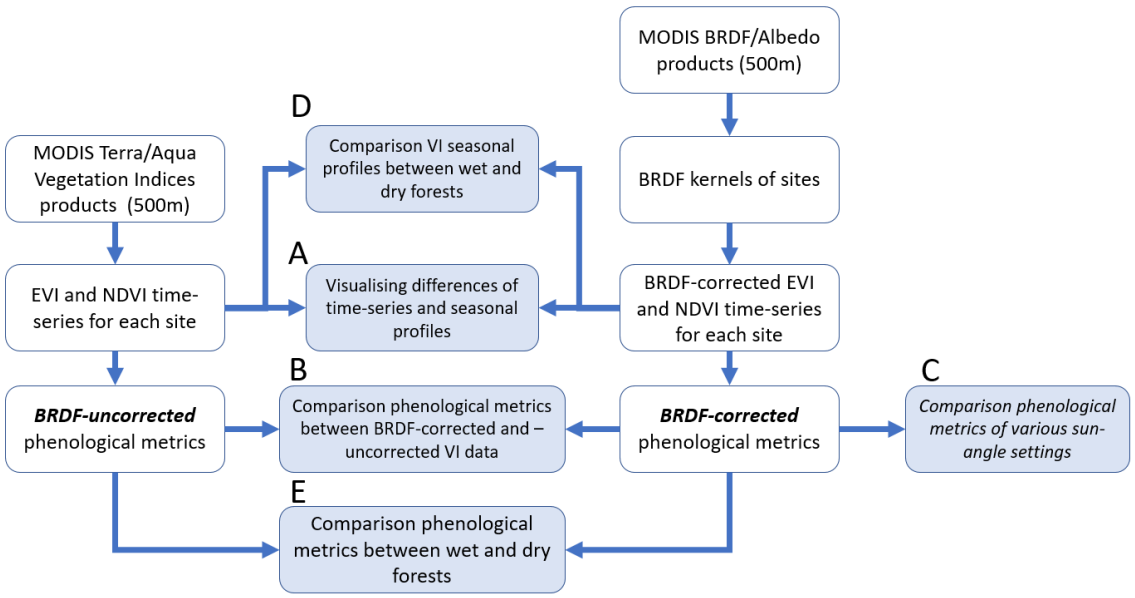

Figure 2.3 *Diagram of 500-m analyses for BRDF influence on phenological timing and dependence of forest phenology on seasonal rainfall patterns. Coloured background boxes are outcomes*

To analyse the dependency of forest phenology on rainfall, we classified forests to groups based on precipitation information. There are two major forest types in tropics: rainforests that have either no or short dry season and dry tropical forests with their pronounced dry seasons (Elias & May-Tobin, 2011). Pennington (2006) defined tropical dry forests as forested areas that experience a minimum dry season period of 5–6 months with strongly seasonal ecological functions. Moreover, Allen et al. (2017) mentioned that

forests having dry seasons of six months or more could affect forest ecosystem functions. Based on different criteria of distinguishing moist and dry tropical forests, we classified SEA forests to three classes based on the length of dry seasons: 0-2 dry months represents rainforests, 3-5 dry months represents medium dry season forests, and 6-7 dry months represents the long dry season forests.

We also used a second classification depending on water deficit during the dry season. Water deficit is the lack of enough water for vegetation to continue regular physiological activity (Vicente-Serrano et al., 2013). As dry periods in tropic regions are defined as rainfall dropped under 100 mm/month; we consider dry water deficit as the lack of rain to reach the threshold of 100 mm/month during the dry periods. The formula of water deficit can be defined as

$$D = (100 - R) * L \quad (2\text{-}4)$$

Where D is water deficit, R is average monthly rainfall during the dry periods, and L is the length of dry seasons.

After that, we calculated VI seasonal profiles and phenological metrics of different forest types and investigated the differences between forests categories with varying water conditions (Fig. 2.3D). Results are supposed to inform about the relationship between seasonal forest VI profiles and rainfall conditions. Moreover, we will be able to understand the impact of BRDF on various forest types phenology by comparing results derived from BRDF-corrected and -uncorrected VI time-series (Fig. 2.3E).

2.2.7.3. Evaluation of the performance of the MODIS BRDF model in estimating surface reflectance at desired sun-view angles

The efficiency of the MODIS BRDF model in generating reflectances and VI with varying sun-view geometries has been validated with multiple methods from in situ to airborne measurements (Che et al., 2017; Liang et al., 2002; Liu et al., 2009; Maignan, Bréon, & Lacaze, 2004; Wang et al., 2012). However, uncertainties about the use of BRDF parameters to model surface reflectance and vegetation indices were found in previous studies (Román et al., 2009; H. Zhang, Jiao, Dong, & Li, 2015). Consequently, it is still necessary to evaluate MODIS BRDF performance in estimating vegetation

indices at desired sun-view geometry and derived phenological metrics in the continental SEA.

Instead of using a standardised sun-view geometry, we used specific sun-view angles extracted from MODIS Terra/Aqua to re-generate vegetation indices for tropical forest sites. MODIS Vegetation Indices are provided with observed sun-view angles (sun zenith angle, view zenith angle and relative azimuth angle) each pixel. We use these angle combinations as inputs to generate reflectance and vegetation indices (Fig 2.4). While estimated- and standard- VI time-series are theoretically indistinguishable, the comparison of derived estimated- and standard- VI results can evaluate the performance of MODIS BRDF model in estimating VI measurements.

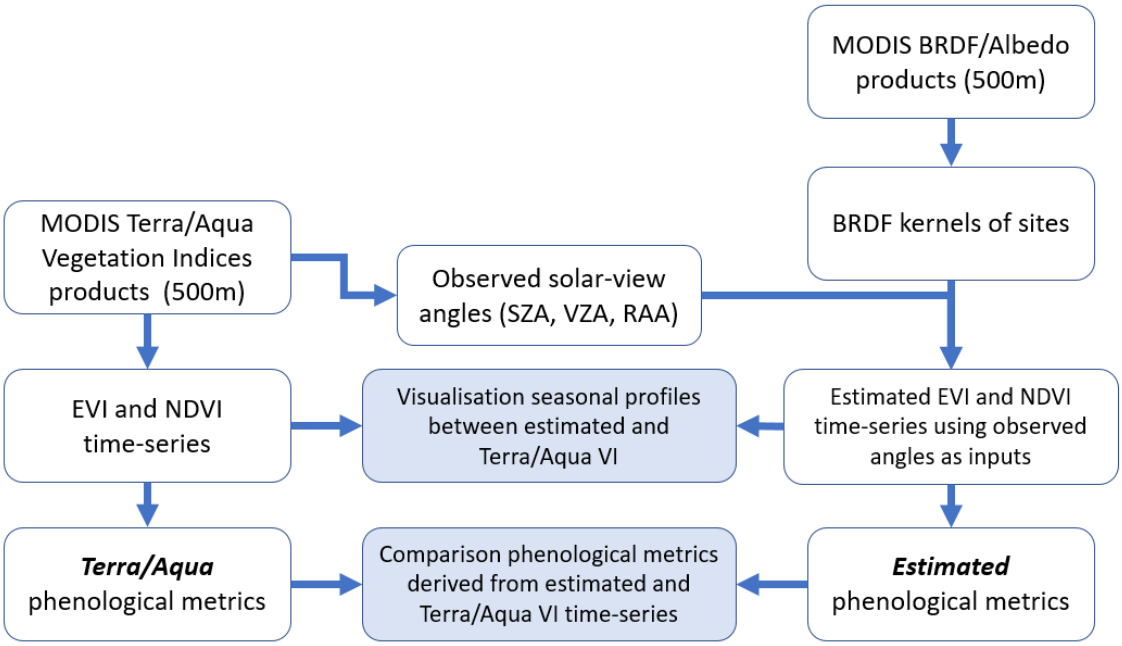

Figure 2.4 *Diagram of 500-m analyses for evaluating MODIS BRDF data in generating VI at desired sun-view configuration. Coloured background boxes are outcomes*

2.2.8. Tools and software

All scripts were programmed on R (R Core Team, 2013) and Python languages. Data was mainly downloaded and pre-processed on eResearch High-Performance Computing Cluster of the University of Technology Sydney. R was used to smooth data, extract phenological parameters, and generating plots. We used several extra packages, including ggplot2 (Wickham, 2009) for plotting, raster (Hijmans, 2016) for processing and reading raster files and pracma (Borchers, 2017) for applying Savitz-Golay

smoothing filter to VI time-series. Also, we used QGIS software (Team, 2017) to produce maps to show results at the continental scale.

2.3. Results

2.3.1. SEA rainfall patterns

Southeast Asia (SEA) rainfall profiles are shown in Figure 2.5. In the majority of the continental SEA, annual precipitation range is between 1000 and 3000 mm/y. High-intensity rainfall (over 3000 mm/y) was found in the coastal regions in Myanmar, Malaysia, Laos and Vietnam and also northern Myanmar (Fig. 2.5F).

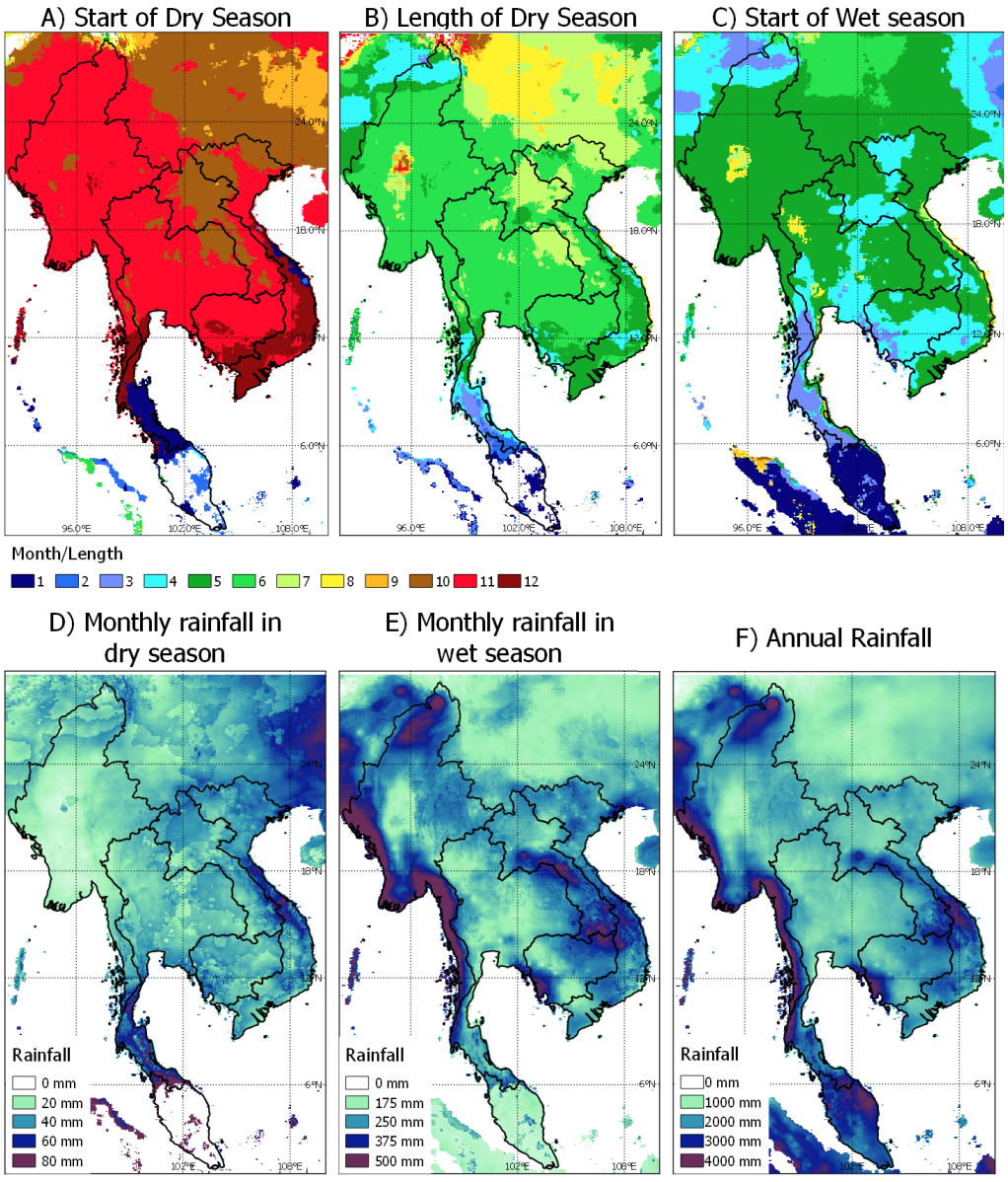

Figure 2.5 *Southeast Asia rainfall profiles retrieved from CHIRPS monthly data (2001 – 2016) with 100mm/month as the criteria for the dry season. A) Start of Dry Season. B) Length of Dry Season. C) Start of Wet Season. D) Monthly rainfall in dry season (mm/month). E) Monthly rainfall in wet season (mm/month). F) Annual rainfall (mm/y)*

The rainy season in SEA generally starts in April or May, except in some areas such as central Myanmar and Thailand where it begins lately in July or August (Fig. 2.5A and 2.5C). The length of dry season for most continental SEA is 5-7 months (Fig. 2.5B). Other areas with shorter dry seasons are northern and southern Myanmar and Thailand. Peninsular Malaysia has more precipitation and more extended rainy season resulting from its wet tropical climate and proximity to the Equator. There is no or short dry season in this area, with the length of the rainy season being 11-12 months.

Monthly rainfall of dry season shows that driest areas were central and coastal Myanmar with only 20 mm/month during dry seasons (Fig. 2.5D). Moreover, the coastal Myanmar areas experience the largest rainfall gaps between rain and dry seasons regarding the monthly rainfall (Fig 2.5D and 2.5E). Intense rainfall during wet periods also happens in northern Myanmar and some areas of Laos, Vietnam and Cambodia. These variations in rainfall patterns undoubtedly influence continental SEA vegetation, including tropical forests.

2.3.2. VZA and SZA seasonal variations

To investigate seasonal angle variations of Peninsular SEA tropical forests, we selected four sites (Figure 2.6, Table 2.3) with various latitudinal ranges, as seasonal sun angles are dependent on latitude. Latitudes of chosen sites range from 27.27° N (site 1) to 5.82° N (site 4).

Table 2.1 *Location of selected sites.*

No	Latitude	Longitude
1	27.27	96.76
2	20.50	96.43
3	12.65	99.36
4	5.82	101.29

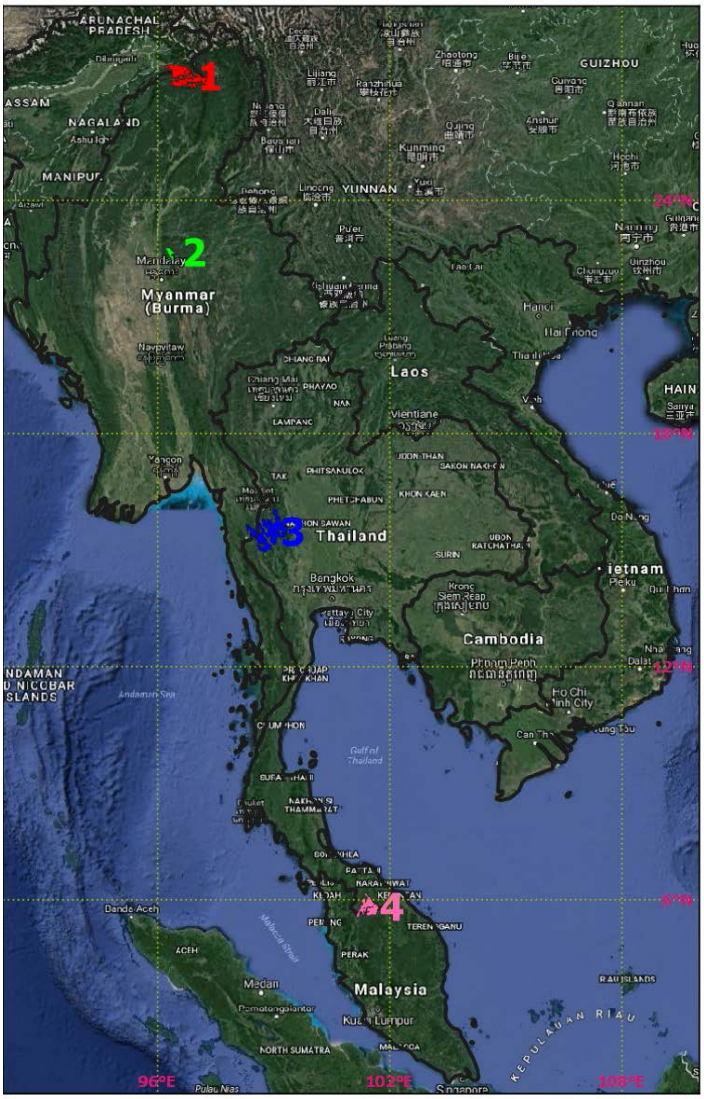

Figure 2.6 *Location of selected sites for angle variation analysis*

Solar zenith angles (SZA) derived from Terra and Aqua sensors exhibited a seasonal cycle and varied among sites (Fig 2.7). Site latitudes mainly caused these variabilities as Terra and Aqua satellites capture images on fixed local time (10h30 AM for Terra and 1h30 PM for Aqua). The range of seasonal variations in SZA increases with latitude, with SZA-Terra ranging from 20-38^{o} at the southernmost site in Peninsular Malaysia to 16-53^{o} at the first site in northern Myanmar. In addition, seasonal SZA patterns tended to have two seasonal peaks in the site closer to the Equator (Site 4). Captured SZA reached peak values around southern solstice time in December while the lowest SZA values were detected at northern solstice time on summer. The less seasonal SZA area (site 4) exhibited peak times at solstices while minimum SZA was in equinox time in March and September.

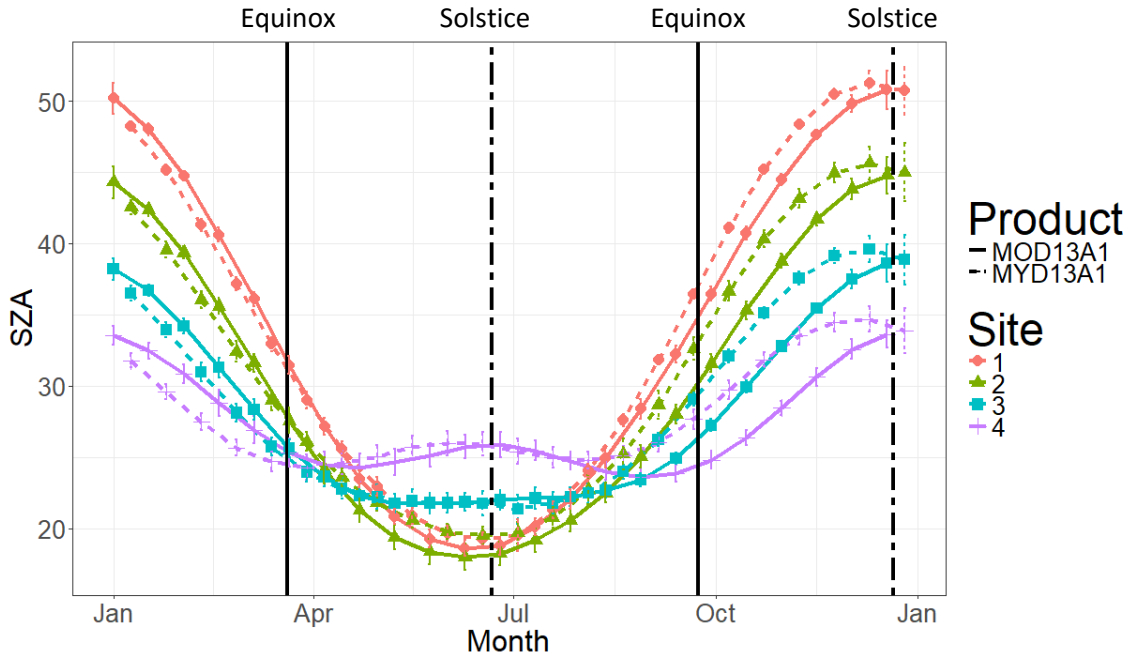

Figure 2.7. *Seasonal variation of SZA extracted from MODIS Terra and Aqua images averaged for 2001 – 2016 period. Continuous lines denote equinox and dashed lines denote solstice. Error bars represent SZA standard deviation of 16-year averaging.*

Averaged seasonal view zenith angle (VZA) profiles for our four forest sites are illustrated in Figure 2.8. VZAs are generally maximised in June or July for all sites and minimised at the end of the year. However, inter-seasonal variations of VZA were weaker than SZA, as seasonal VZA ranged from 5-15 degrees. In contrast, inter-annual VZA variations, represented as standard deviations (SD), were stronger than SZA variations. While SZA SD were only 1-2 degrees, VZA SD could reach over 8 degrees. As MODIS satellites observed over landscapes at fixed local times (10:30 for Terra and 1:30 for Aqua), this result suggests that SZA changes might cause seasonal variations of observations and VZA changes might cause inter-annual observed differences.

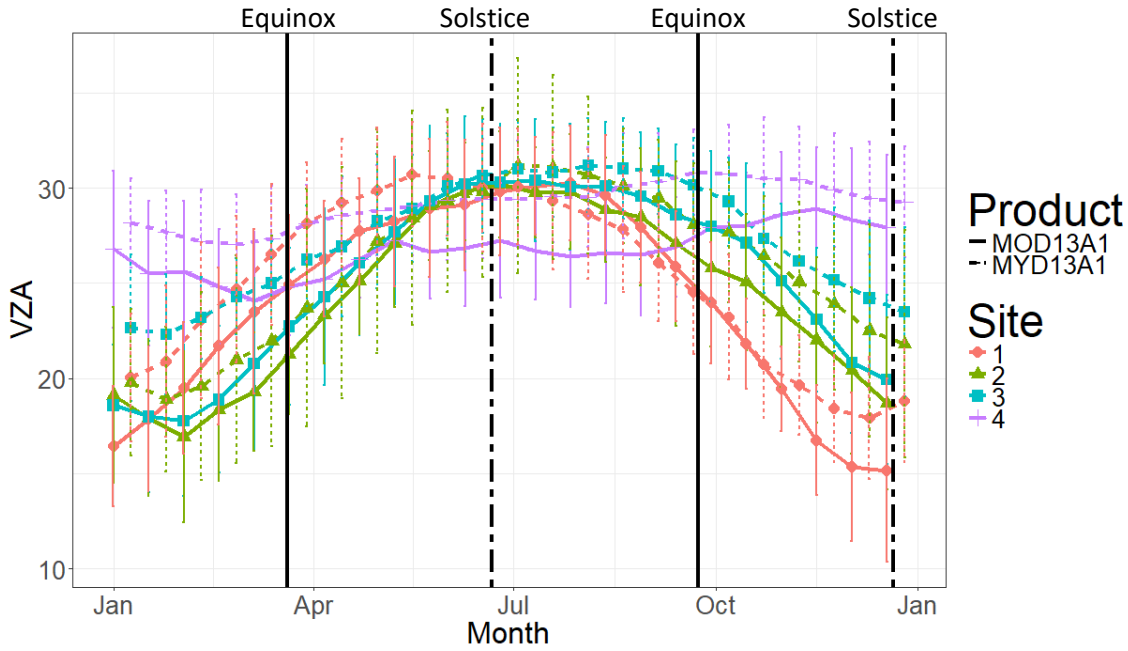

Figure 2.8 *Seasonal variation of VZA extracted from MODIS Terra, and Aqua images averaged for 2001 – 2016 period. Continuous lines denote equinox and dashed lines denote solstice. Error bars represent SZA standard deviation of 16-year averaging.*

Figure 2.9 shows the histograms of Terra SZA and VZA for each quarter of a year. It shows the same SZA seasonal differences as in Figure 2.7 with the distribution of SZA dependent on the season. High SZA appeared at the end of a year (NDJ), and sun positioned at high altitude in the middle of a year (MJJ), except site four that is located close to the Equator. In contrast, VZA was mainly distributed in lower values from 0 to 20 degrees, similar to seasonal profiles of VZAs.

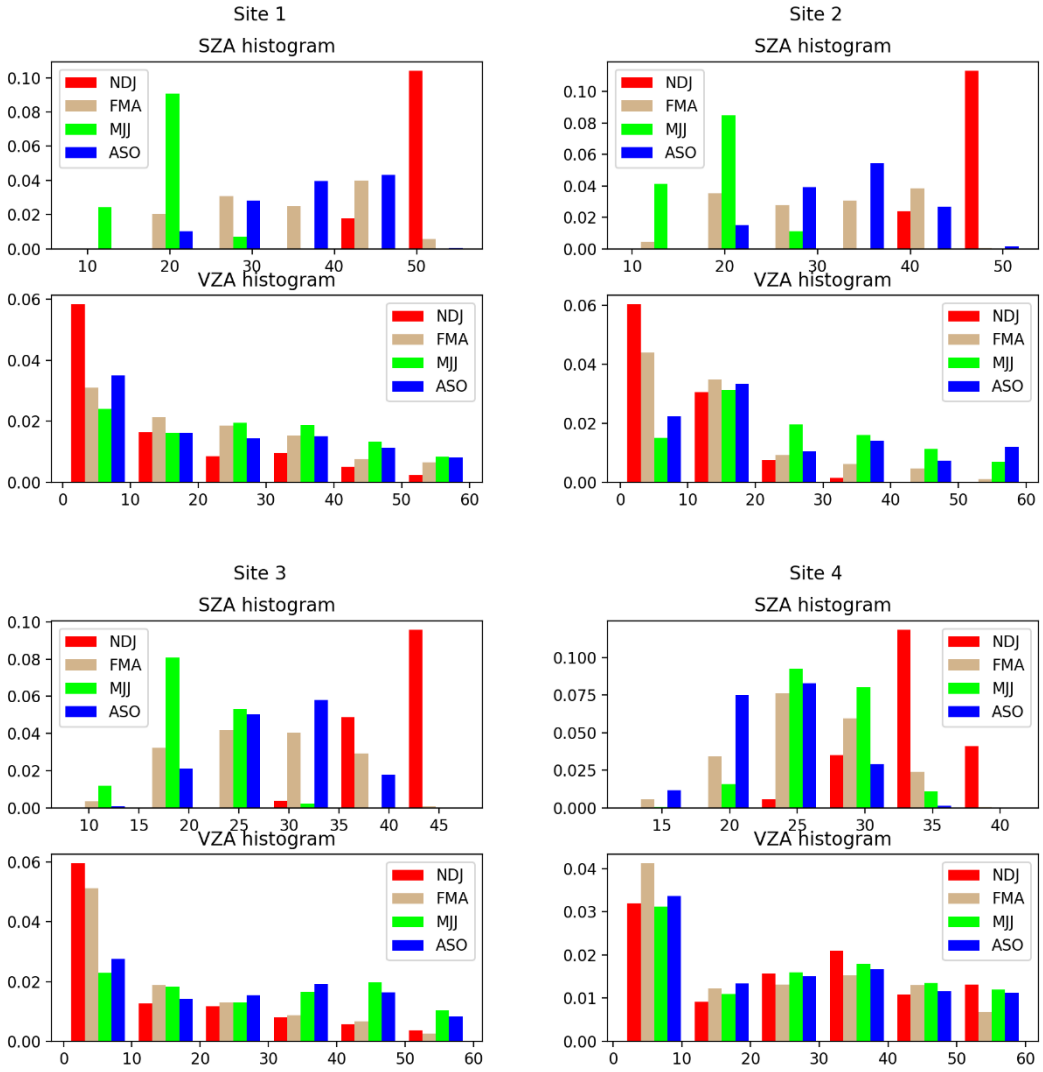

Figure 2.9 *Histograms of SZA and VZA seasonal variations for MODIS Terra (2001 – 2016) with ten bin-widths. NDJ: November-December-January; FMA: February-March-April; MJJ: May-June-July; ASO represents August-September-October.*

Variations in seasonal SZA were much stronger than that of VZA. Intra-annual variability of VZA varied among sites. VZA values of the fourth site were stable regarding seasonal changes while VZA values of the other three northern sites showed minor seasonal differences, with the SZA distribution of solstices concentrated in the range of 0-20 degrees and equinoxes scattered in an extended range of 0-60 degrees.

The distribution of VZA values tended to be concentrate on low-values. The differences were dependent on the algorithm of MODIS Vegetation Index Collection 6. One critical step of the algorithm is the selection of data points when more than one quality observation is available. In that case, the observed value with the highest NDVI and smallest VZA is chosen (Kamel Didan, Munoz, & Huete, 2015).

According to the BRDF model applied to BRDF MODIS data (described in chapter one), the role of SZA and VZA can be interchangeable. Consequently, BRDF impacts on SEA vegetation VI should be dominated by variations of seasonal SZA rather than seasonal VZA. These results suggest that BRDF products only fix view and relative angles to a standardised configuration, like MODIS Nadir BRDF Adjusted Reflectance (NBAR) ones, and that might not minimise BRDF influence as the major seasonal factor caused BRDF remains.

2.3.3. BRDF impact on SEA forest phenology at CMG resolution (0.05-degree)

2.3.3.1. Impact of BRDF on forest phenological metrics derived from time series of VIs

The timing of minimum forest EVI tended to correlate with latitude, as shown in Figure 2.10. Northern forests (North Myanmar) showed their minimum EVI from March to May, while Southern forests' (Peninsular Malaysia) EVI minimum values were found in December or January. When we compared minimum EVI timing between BRDF-uncorrected (Terra/Aqua) and BRDF-corrected EVI, minimised months of BRDF-corrected EVI occurred later than BRDF-uncorrected EVI, as shown in Figure 2.10D and 2.10E. However, the shifting varied depending on the region. Monthly differences were mixed (positive and negative differences) in Peninsular Malaysia, while the shifting was consistently positive in one and two months in Northern Myanmar forests.

In contrast to EVI, the timing and spatial distribution of minimum NDVI was quite similar between BRDF-uncorrected and -corrected NDVI data (Fig. 2.11A, 2.11B and 2.11C); also, differences between standard and BRDF-corrected VI were observed in a smaller portion of SEA forest coverage (Fig 2.11D and 2.11E), except in mainland Malaysia forests. Therefore, BRDF correction affected minimum monthly EVI but had a weaker influence on minimum NDVI. Considering the timing of the two VIs in SEA forests, Terra/Aqua minimum NDVI values came up later than Terra/Aqua minimum EVI, but the timing of fixed-SZA minimum NDVI was identical to that of minimum EVI. The timing similarity of fixed-SZA NDVI and EVI combining with NDVI independence to SZA variation is a strong indication that fixing sun-sensor geometries might correct the impact of BRDF in minimum EVI timing.

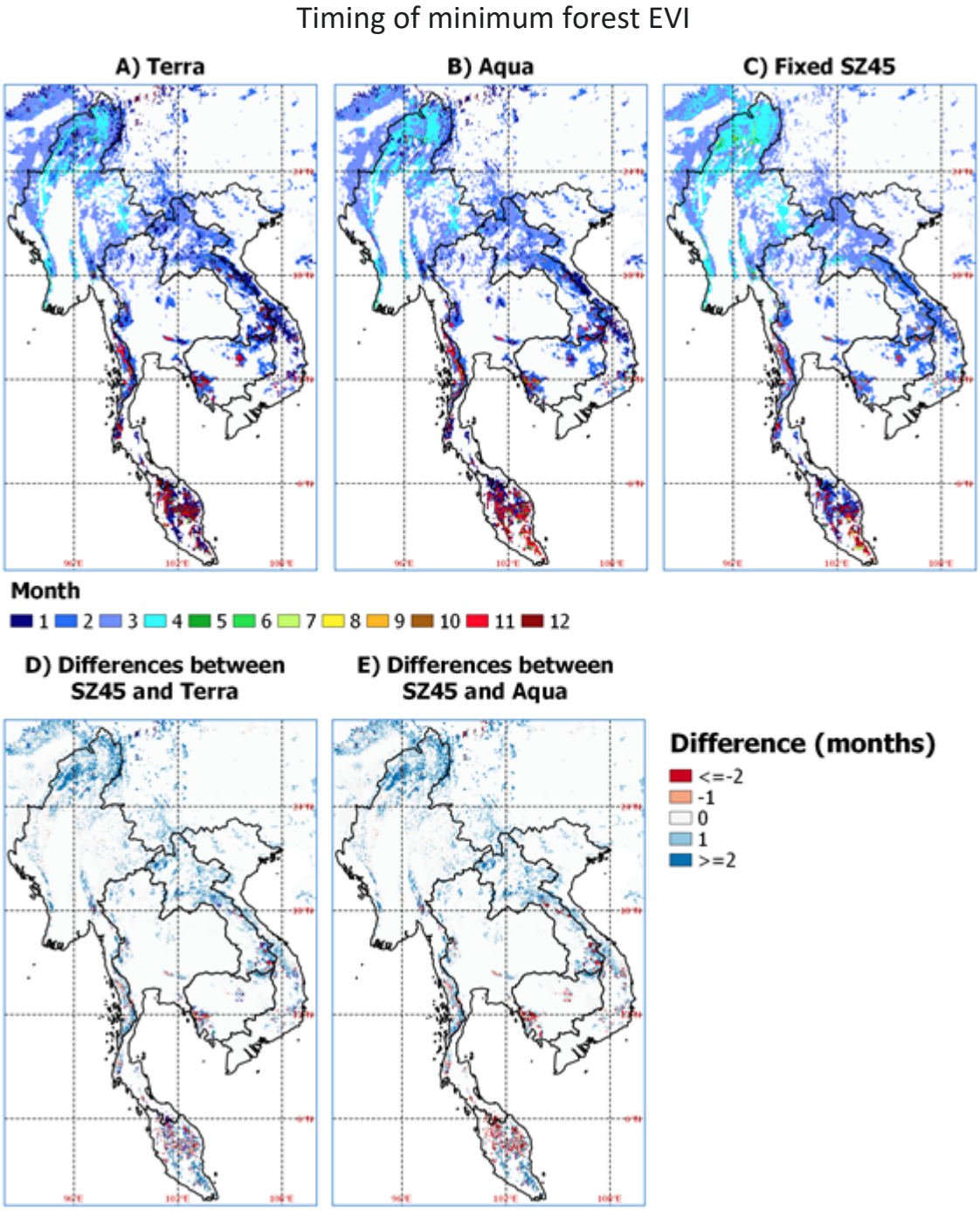

Figure 2.10 *Timing of minimum forest EVI between monthly MODIS CMG Terra, Aqua and BRDF-corrected SZ45 data. Data were calculated from average seasonal VI times-series from 2001 – 2016 (Terra and SZ45) and 2003 – 2016 (Aqua).*

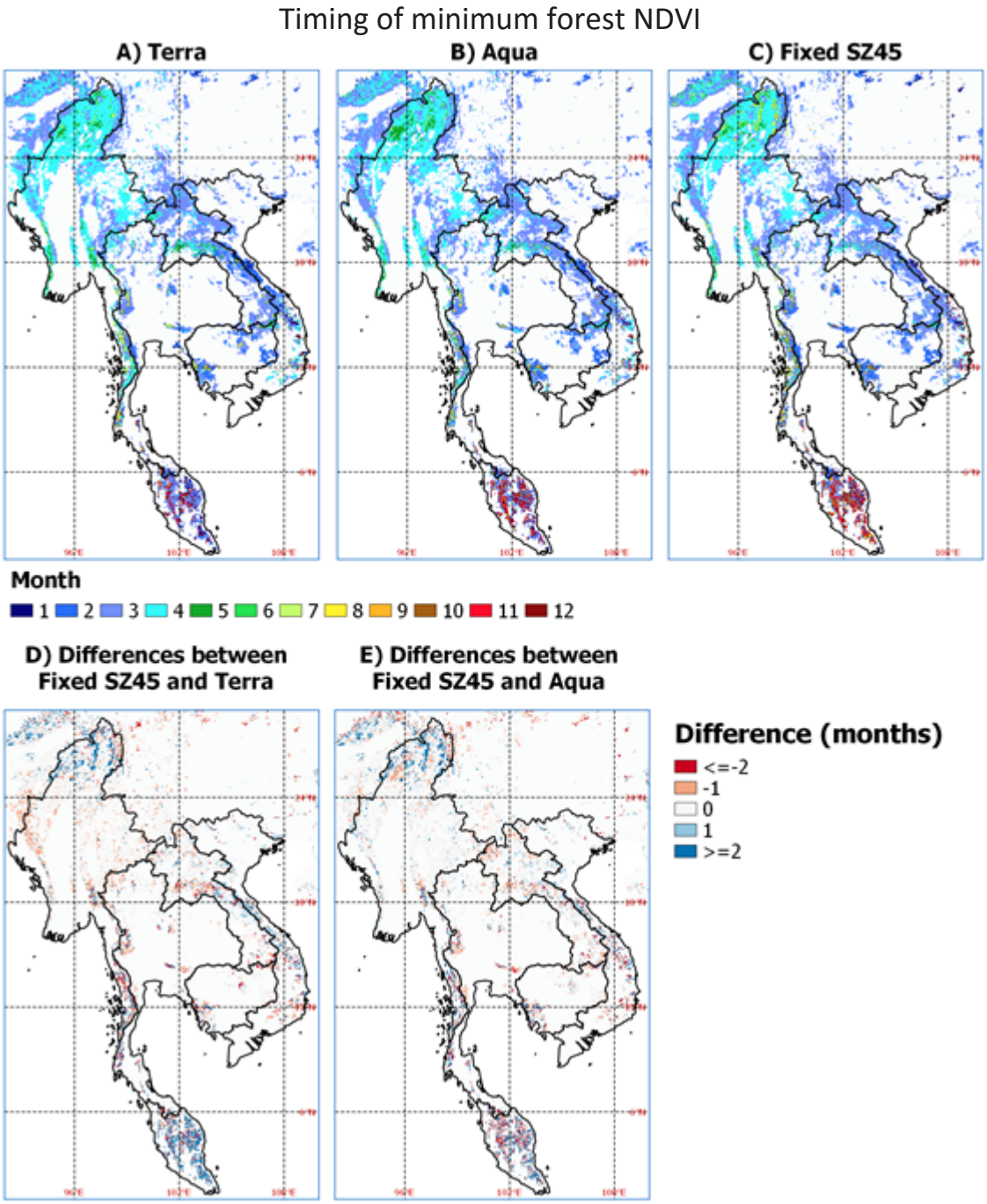

Figure 2.11 *Timing of minimum forest NDVI between monthly MODIS CMG Terra, Aqua and BRDF-corrected SZ45 data. Data were calculated from average seasonal VI times-series from 2001 – 2016 (Terra and SZ45) and 2003 – 2016 (Aqua).*

Regarding the maximum timing, EVI peak timing of SEA forests over the 2001-2016 period is similar between standard and fixed-geometry EVI, except forests of north Myanmar and south of Peninsular Malaysia (Fig. 2.12). In northern Myanmar, forests reached their maximum BRDF-corrected EVI on November-December, while peak months derived from standard EVI were July or August. The maximum timing of

Malaysian forests' EVI highly varied from April to September. In other SEA regions, EVI consistently peaked from June (Southern Laos) to August for both BRDF-corrected and -uncorrected EVI.

Compared to EVI maximum timing, SEA forests' NDVI values tended to peak later. Generally, southern forests reached peak on June-July, and northern forests reached their VI peak values towards the end of the year (October to December). While NDVI minimum timing showed no considerable differences between standard and fixed-geometry retrievals, variable timing of maximum NDVI (Fig 2.13) showed a different outcome. In general, the highest NDVI values of Terra/Aqua products occurred before those of fixed-geometry NDVI, and this early occurrence was more evident with Terra NDVI. This abnormal result is potentially caused by NDVI saturation as forest NDVI values can reach saturation in dense vegetation canopies, especially during wet periods. Moreover, data availability is limited in the wet season because of intense cloud cover. Thus, the peak timings of growing season extracted from NDVI might be imprecise.

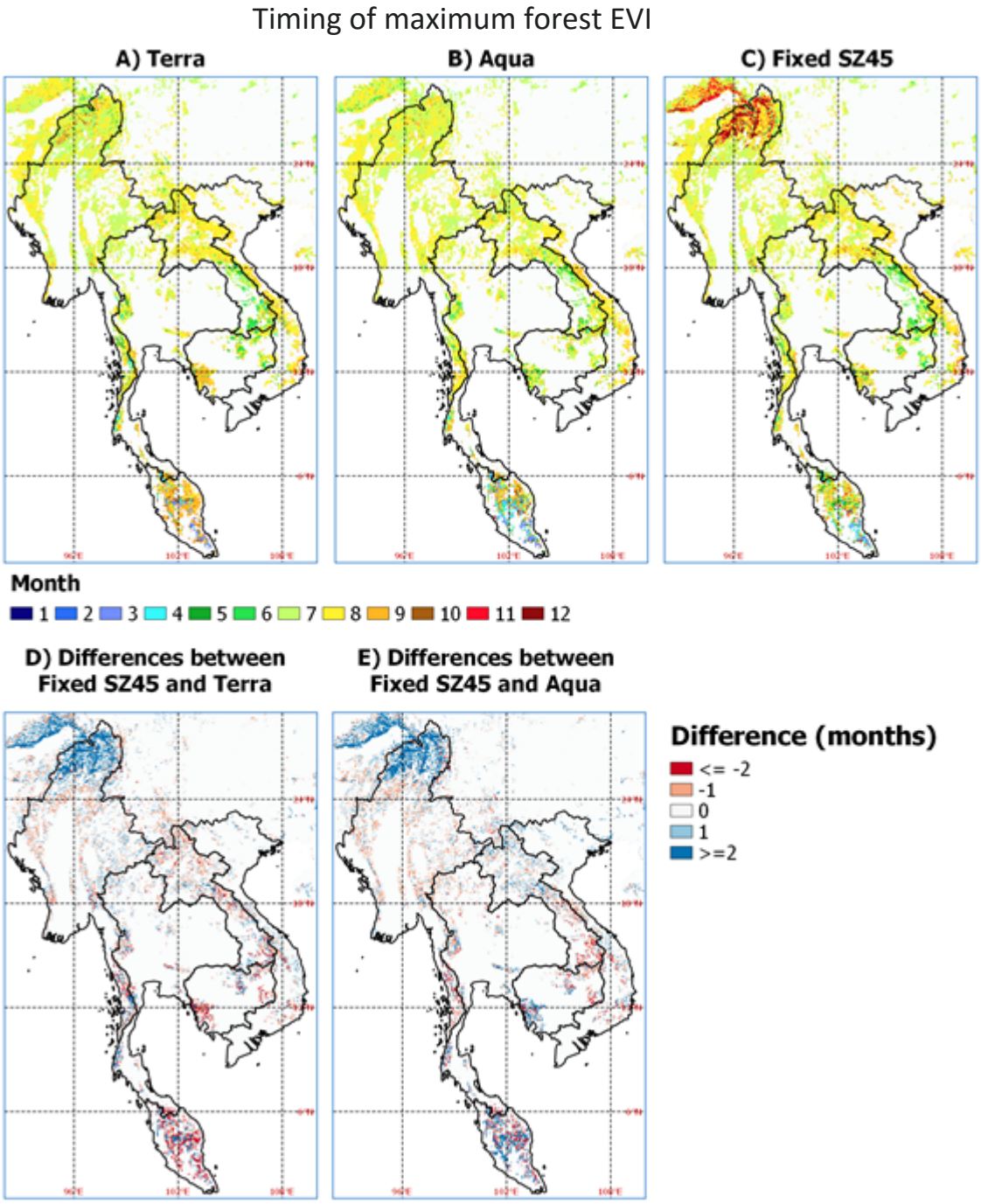

Figure 2.12 *Timing of maximum forest EVI between monthly MODIS CMG Terra, Aqua and BRDF-corrected SZ45 data. Data were calculated from average seasonal VI times-series from 2001 – 2016 (Terra and SZ45) and 2003 – 2016 (Aqua).*

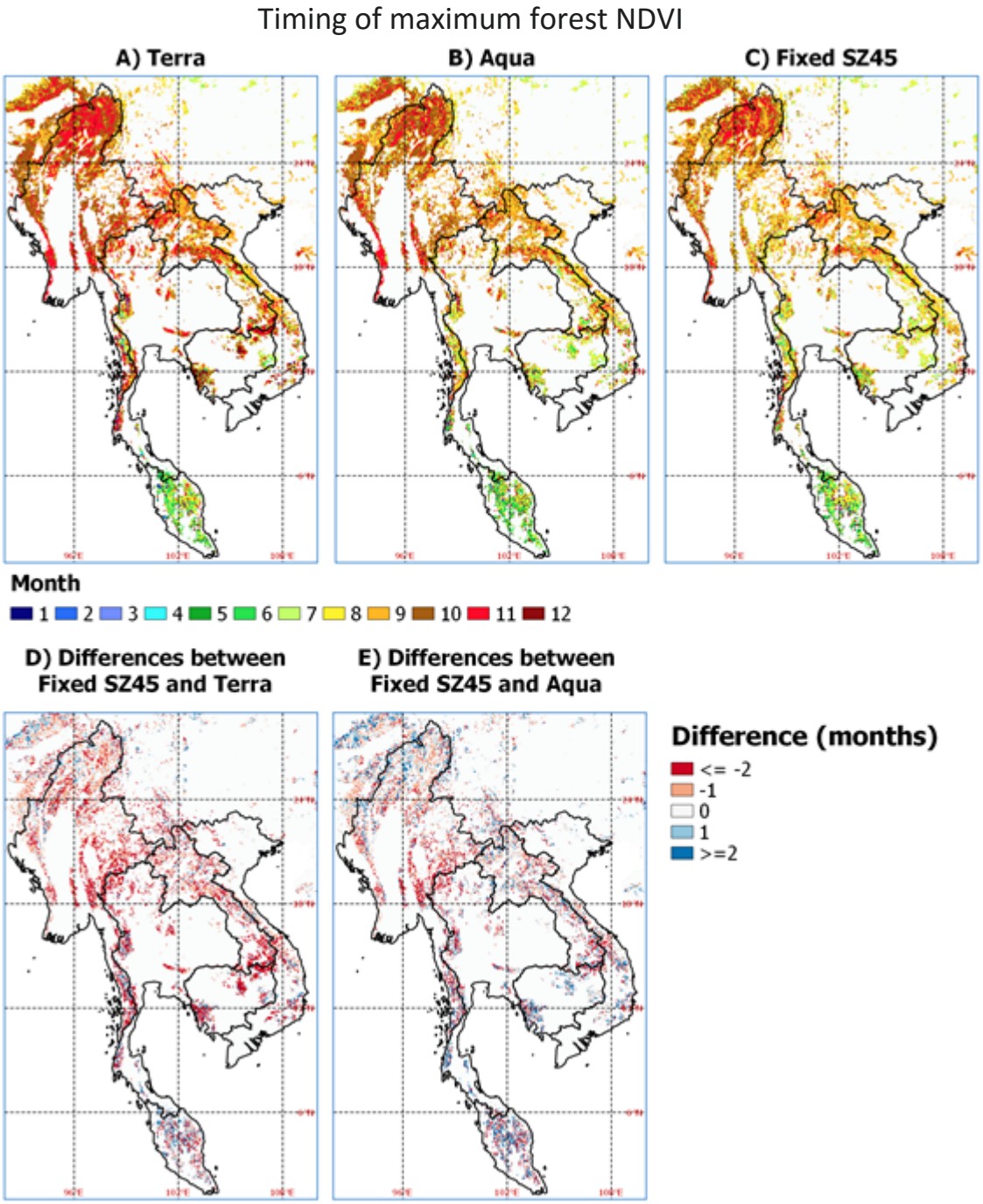

Figure 2.13 *Timing of maximum forest NDVI between monthly MODIS CMG Terra, Aqua and BRDF-corrected SZ45 data. Data were calculated from average seasonal VI times-series from 2001 – 2016 (Terra and SZ45) and 2003 – 2016 (Aqua).*

2.3.3.2. Phenological parameters dependence on variations of sun-angle settings

To analyse the relationship of retrieved phenological parameters on geometric settings, we observed these metrics obtained from various fixed-SZA VI time-series. Results of CMG (0.05-degree) resolution showed that different SZA configurations produce similar minimum and maximum timings for both EVI and NDVI time-series

(Figure 2.14 – 2.17). In particular, it is hard to find differences between the results of different geometry settings. These results provide evidence that different sun-angle choices do not cause significant variations in phenological metrics derived from fixed geometry vegetation indices.

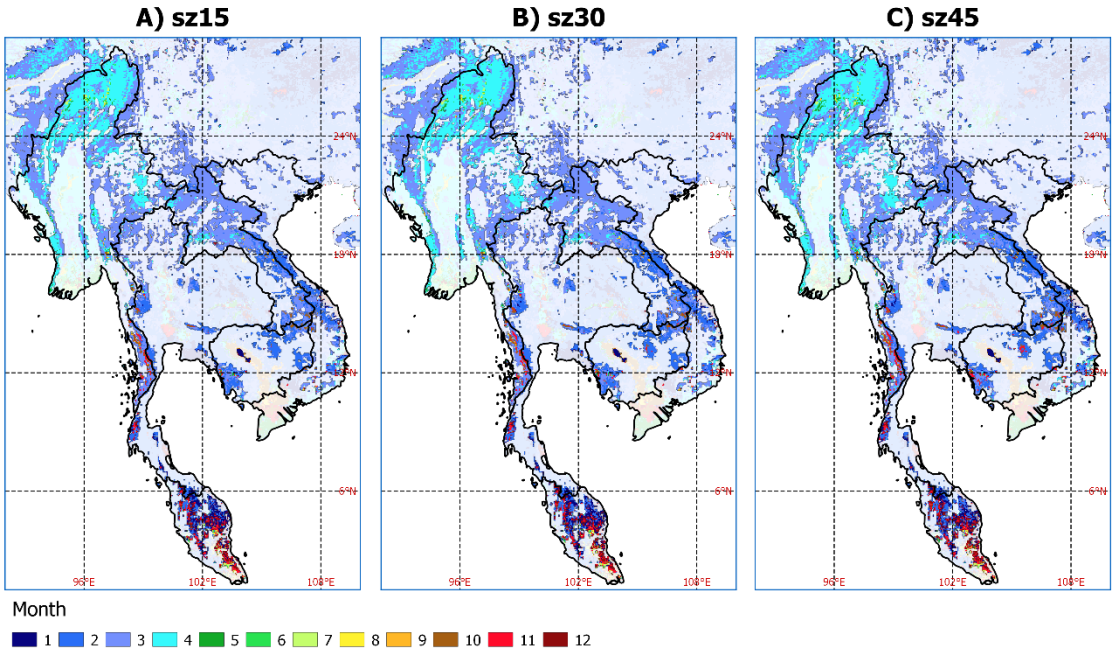

Figure 2.14 *Timing of minimum forest EVI derived from various fixed SZA EVI time-series at 0.05-degree resolution (SZ15-SZ45)*

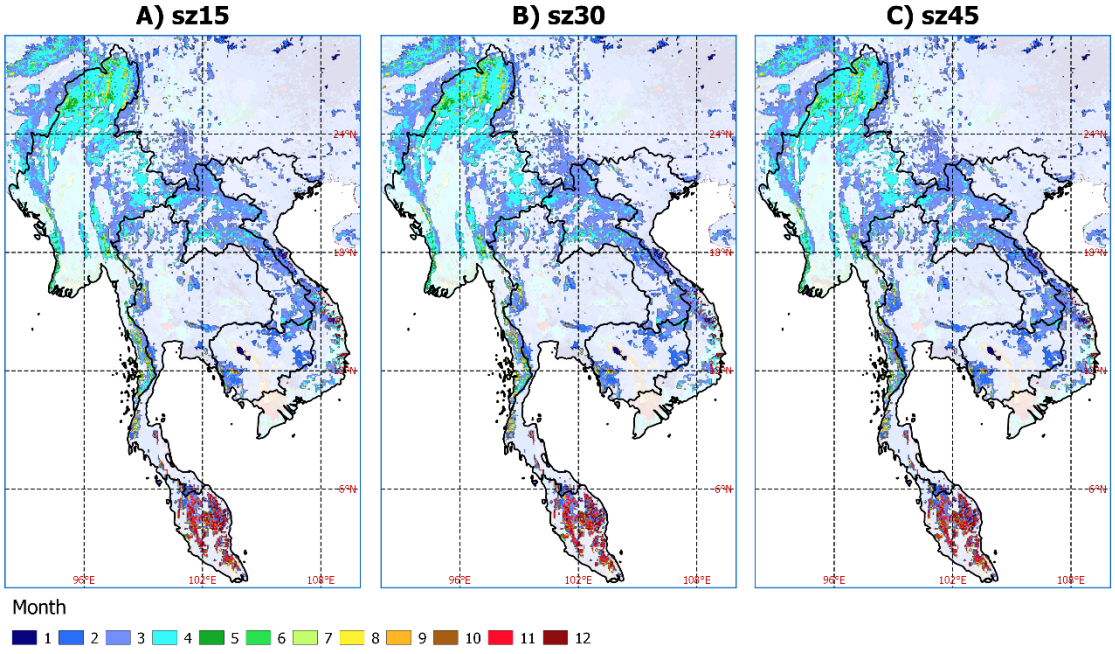

Figure 2.15 *Timing of minimum forest NDVI derived from various fixed SZA NDVI time-series at 0.05-degree resolution (SZ15-SZ45)*

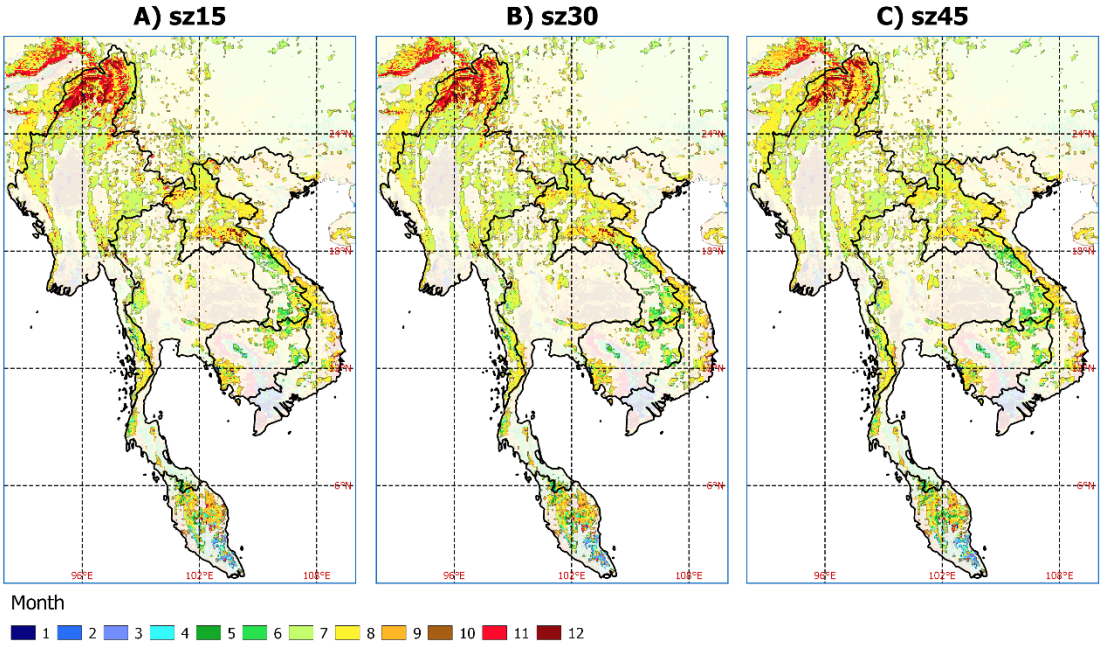

Figure 2.16 *Timing of maximum forest EVI derived from various fixed SZA EVI time-series at 0.05-degree resolution (SZ15-SZ45)*

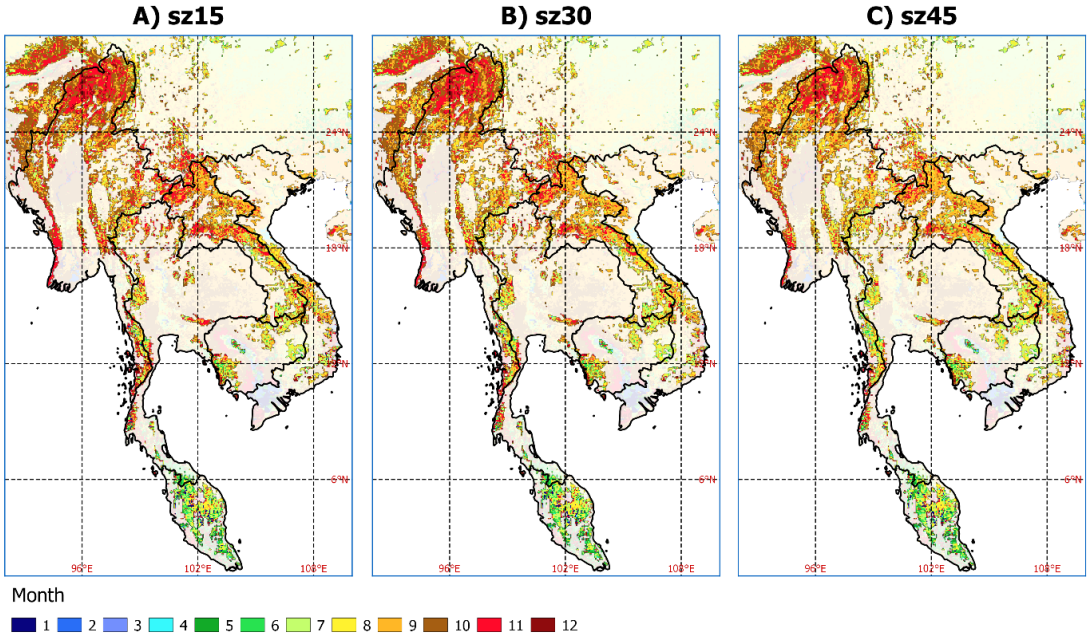

Figure 2.17 *Timing of maximum forest NDVI derived from various fixed SZA NDVI time-series at 0.05-degree resolution (SZ15-SZ45)*

2.3.4. BRDF influence to undisturbed forests at 500m scale

2.3.4.1. Differences of seasonal VI profiles between MODIS Terra/Aqua and fixed sun-sensor geometry data

To analyse the impact of BRDF on phenological parameters, we firstly show filtered NIR band, and then EVI and NDVI time-series of both BRDF-corrected and – uncorrected VI time-series for forest sites with various lengths of dry seasons (Fig. 2.18). We only plotted VI_{sz15} and VI_{sz45} to compare with MODIS Terra and Aqua VI time-series because observed SZAs ranged from 15 to 50 degrees according to our analyses of seasonal sun-view angle changes.

Differences between BRDF-corrected and uncorrected EVI time-series are very large. Also, differences in sun-angle settings result in significant gaps between EVI_{SZ15} and $EVI_{SZ45,}$ but the seasonal patterns are identical. In contrast, gaps between NDVI time-series lines were marginal at the dry forest sites (sites two and three). At the rainforest site (site 1), however, there are considerable differences between BRDF-corrected and – uncorrected NDVI time-series in many periods. These differences are the combination of noise and saturation issues because of higher cloud cover than dry tropical forests and low seasonal NDVI variations ranging only from 0.81 to 0.87.

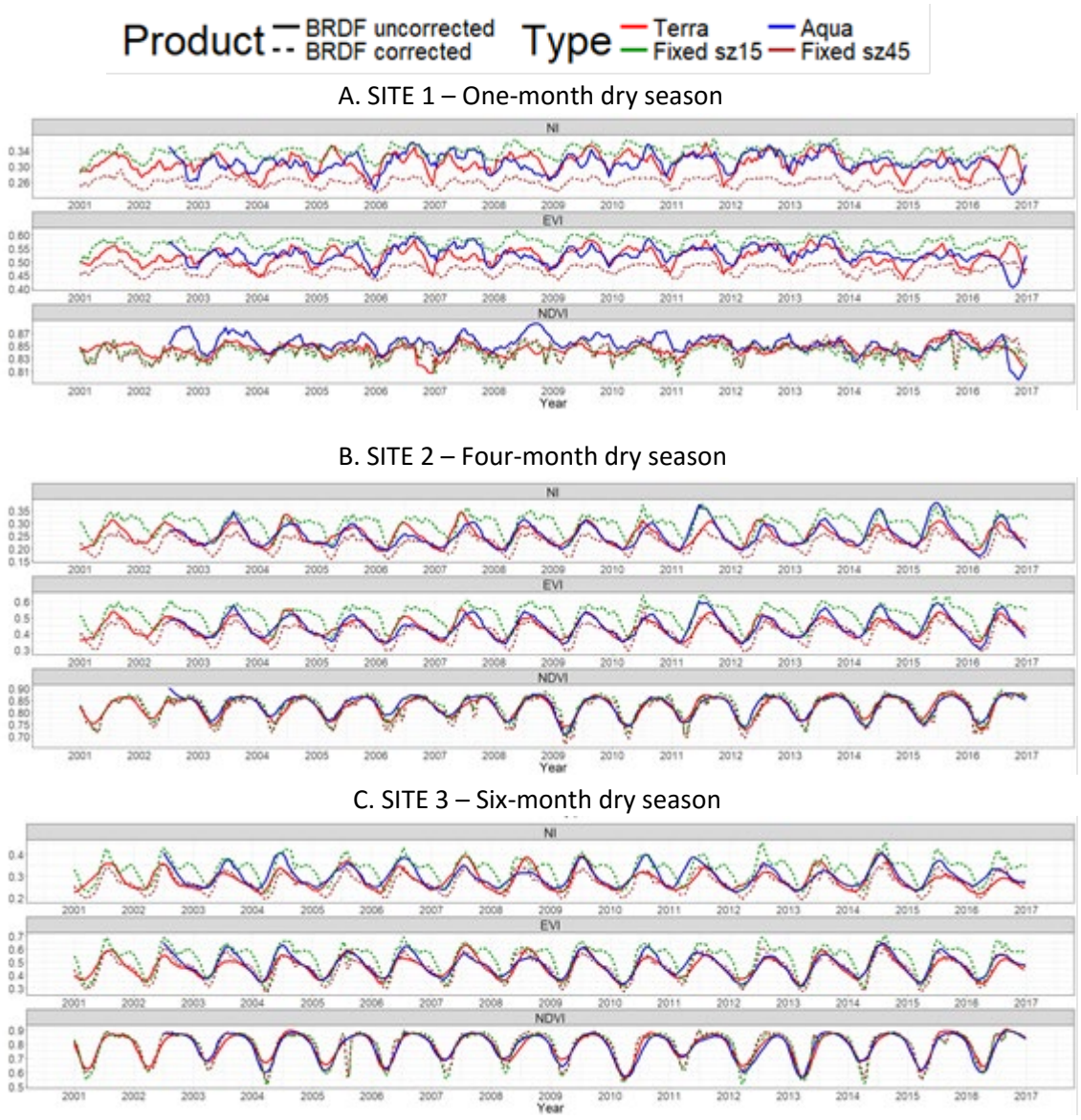

Figure 2.18 *Time-series of NIR band, NDVI and EVI for three forest sites with different lengths of dry season: A. one month (top), B. Four months (middle), and C. Six months (bottom).*

Figure 2.19 shows the seasonal curves of NIR band, NDVI, EVI and SZA of the three selected sites derived by averaging 16-year time-series (2001 – 2016) from standard MODIS Terra/Aqua satellites with various sun-angle configurations while VZA and RZA were to nadir view (VZA and RZA equal to 0). These seasonal profiles showed that NDVI is consistent regardless of SZA changes: all NDVI curves exhibit similar patterns and differences across the various fixed-SZA products are minor compared to variations observed in EVI profiles, which showed to be more affected by SZA. In general, lower SZAs yielded higher VI signals in all forest sites, and the influence of SZA increased with higher EVI values.

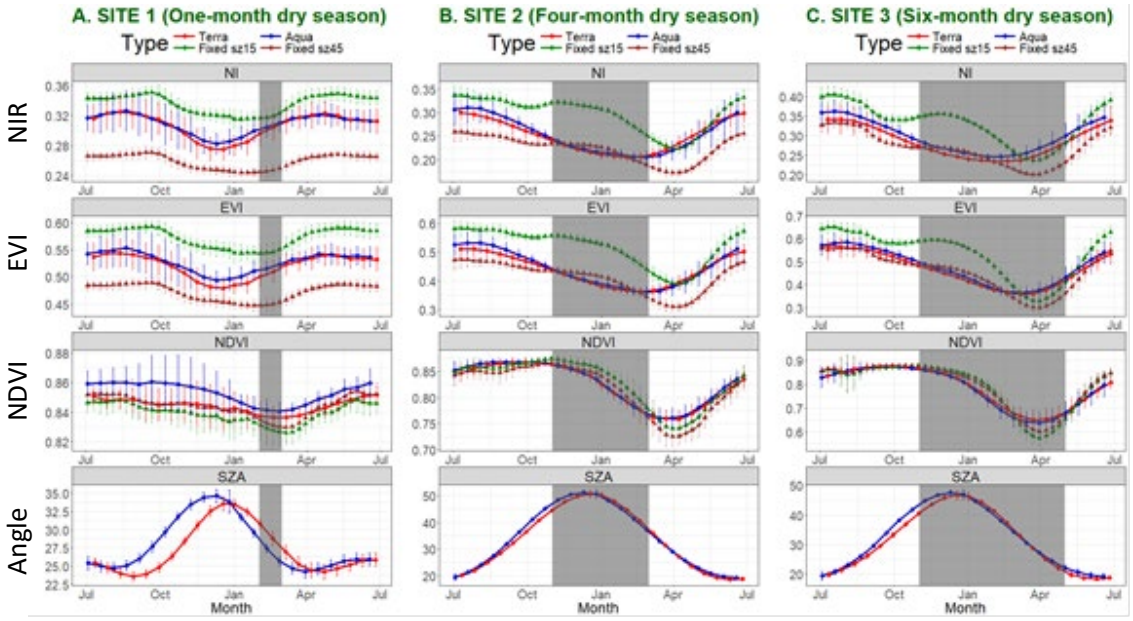

Figure 2.19 *Seasonal NIR/NDVI/EVI/SZA profiles of three sampled forests with various lengths of dry season for BRDF-corrected and uncorrected VIs. Grey areas indicate the dry period. Error bars represent the standard deviation of 16-year averaging. A. One-month. B. Four-months. C. Six-months*

NDVI seems to reach its saturation point around 0.8 - 0.85 and hardly increases beyond this threshold. Consequently, seasonal changes in NDVI are quite small at the rainforest site, with an intra-annual magnitude of only 0.02 (Fig 2.19A). It is troublesome to extract phenological metrics from annual NDVI time-series data at very dense forests: for example, at the rainforest site, EVI displayed marked seasonal signals while NDVI retained a high value (over 0.8) for the entire year. This result suggests that signal saturation aids NDVI robustness to BRDF effect.

There are considerable differences in both the shape and magnitude of phenological profiles between fixed-SZA and Terra/Aqua EVI (Fig. 2.19). Standard Terra and Aqua EVI tended to match with lower fixed-SZA EVI (EVI_{sz45}) while SZA was high and reversed with lower SZA. However, the matching varied depending on the SZA values. Terra and Aqua EVI value approximately equals to EVI_{sz45} with SZA around 45 degrees, indicating that the BRDF model was accurate in this case and confirming the impact of sun-sensor geometries on standard EVI. However, standard EVI and EVI_{sz15} lines do not intersect around 15-20 degrees of SZA, except at the second site. The imprecision of the BRDF model or cloud issues in the wet season is potential causes of

this issue. Moreover, the intra-annual variability of VZA might contribute to this imprecision, though VZA seasonal variation is much lower than SZA annual variation.

Another noteworthy evidence of sun-angle impacts on EVI can be seen from April-to-September EVI values of the rainforest site. Terra and Aqua EVI of that period show a correlation with sun-angle: lower SZA generates higher EVI while BRDF-corrected EVI was stable over the same period.

2.3.4.2. Impact of rainfall on VI seasonal profiles of SEA tropical forests

The EVI seasonal profiles of forests with lengths of dry season are showed in Figure 2.20. BRDF-uncorrected annual EVI profiles of forests with 3-5 month and 6-7 month lengths of dry season are identical, especially in wet season. The EVI maximums are indistinguishable between these two forest types. With BRDF correction, patterns of seasonal EVI measurements are different between forests with 3-5 month and 6-7 month lengths of the dry season. The longer the length of dry seasons, the stronger the EVI seasonality exhibited by the forest types. Moreover, drier forests having longer lengths of dry seasons showed lower EVI in dry seasons and higher EVI during rain periods, greater than rainforests.

Seasonal EVI profiles of forests with different water deficit during dry periods exhibited the same behaviour as profiles based on length of dry seasons (Fig. 2.21). Higher water deficit resulted in stronger seasonality with lower EVI values in the dry season and higher EVI in the wet season (Fig. 2.21A). The distinction among forest types was less apparent without BRDF-correction as maximum EVI values were similar among them. This outcome confirms the impact of BRDF on seasonal EVI profiles of SEA forests.

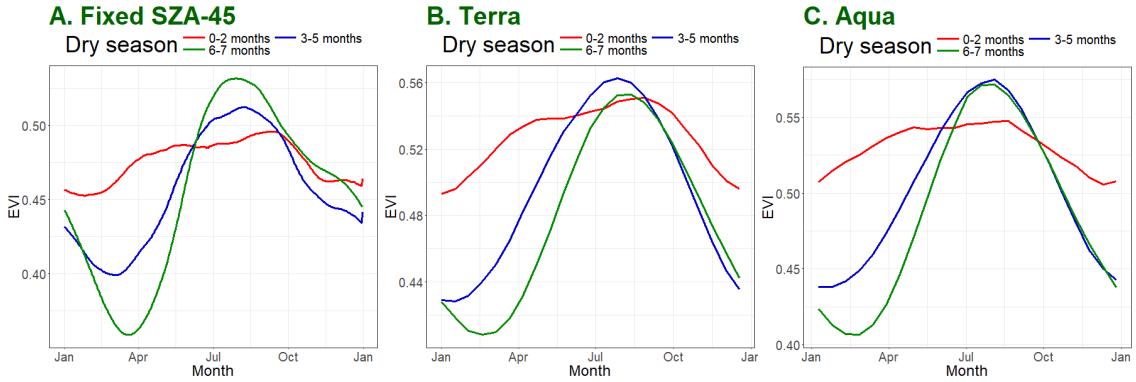

Figure 2.20 *EVI seasonal profiles of forests with different lengths of dry season. A. BRDF-corrected EVI at SZ45. B. Terra EVI. C. Aqua EVI*

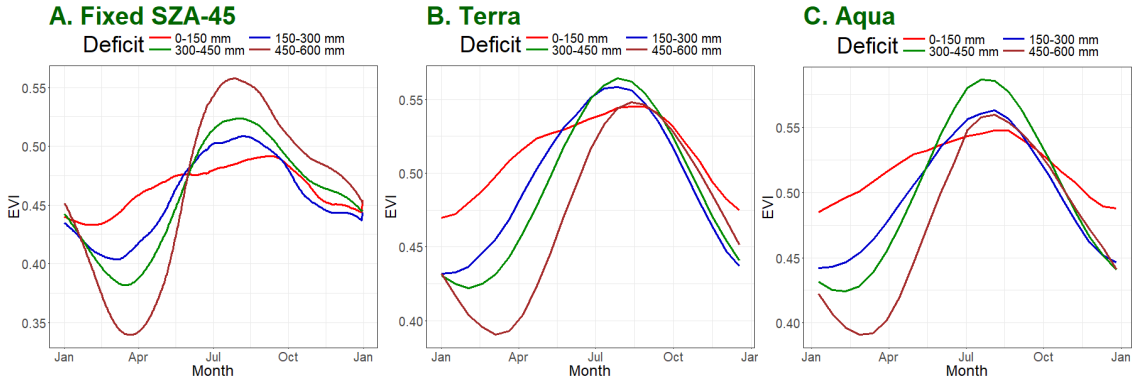

Figure 2.21 *EVI seasonal profiles of forests with different water deficit during the dry season. A. BRDF-corrected EVI at SZ45. B. Terra EVI. C. Aqua EVI*

Seasonal NDVI profiles illustrate that the differences between BRDF-corrected and -uncorrected VI seasonal profiles are marginal because NDVI is robust to BRDF influence (Fig. 2.22 and 2.23). Regarding seasonal NDVI profiles among forest classes, maximum NDVIs are similar at very high values of 0.85 – 0.87 for all forest types during the rainy periods. The differences among forest classes, however, are distinguishable in the dry season. Drier forests represented by longer dry seasons and higher water deficit have lower NDVI during the dry periods, are similar to EVI seasonal profiles. Also, the drier forests' maximum NDVI has not clearly exceeded the rainforest's maximum NDVI in the wet season as it was observed in EVI.

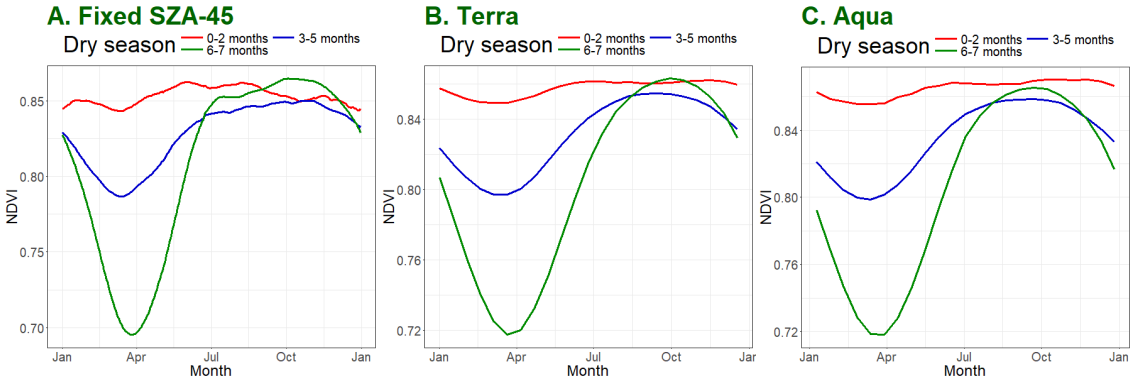

Figure 2.22 *NDVI seasonal profiles of forests with different lengths of dry season. A. BRDF-corrected NDVI at SZ45. B. Terra NDVI. C. Aqua NDVI*

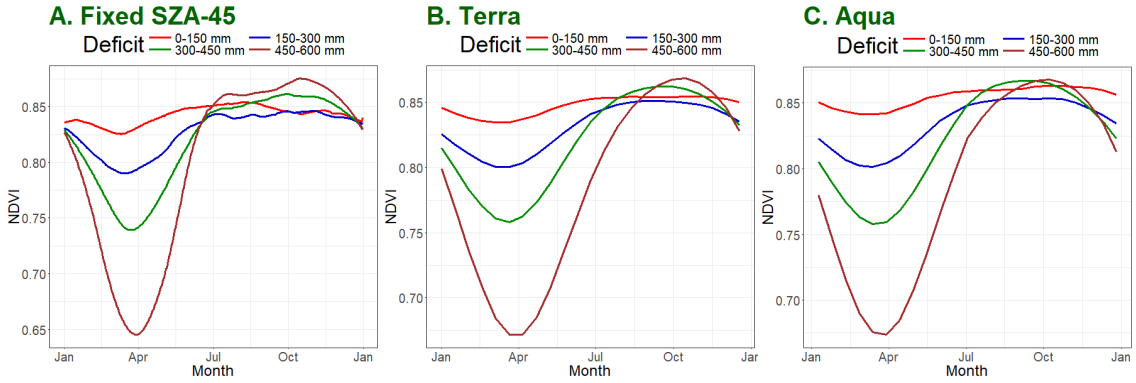

Figure 2.23 *NDVI seasonal profiles of forests with various water deficit during the dry season. A. BRDF-corrected NDVI at SZ45. B. Terra NDVI. C. Aqua NDVI*

2.3.4.3. Impact of BRDF on forest phenological metrics derived from time series of VIs

The cross-site comparisons between phenological parameters derived from standard and SZA-45 EVI for 30 intact forest sites (depicted in Fig. 2.1) are shown in Figure 2.24. In general, the start of greening occurred earlier with MODIS Terra/Aqua EVI while SGS derived from SZA-45 EVI occurred later (Fig 2.24A). More specifically, SEA forests started their greening from December (DOY360) to April (DOY110) with standard EVI and from March (DOY60) to April (DOY120) with BRDF-corrected EVI. The shifting varied from marginal five days to considerable two months. Moreover, SGS variation of MODIS Terra/Aqua EVI among sites was up to 125 days while this range was only 60 days for SZA-45 EVI.

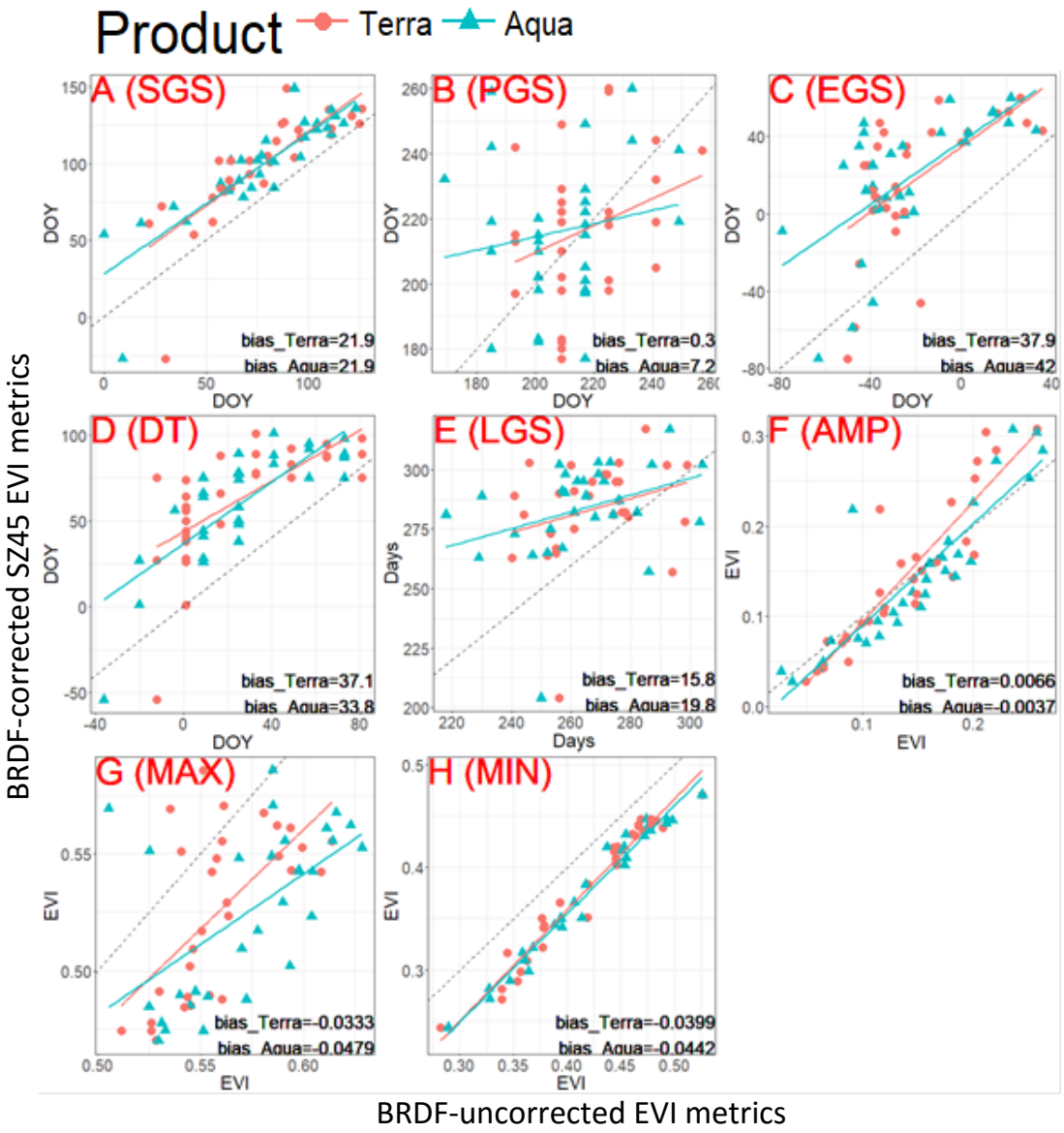

Figure 2.24 *Cross-sited (30 sites) correlation of derived phenological metrics between standard and fixed SZA-45 EVI at 500m scale. A) Start of Greening Season (SGS). B) Peak of Greening Season (PGS). C) End of Greening Season (EGS). D) Dormancy Timing (DT). E) Length of Greening Season (LGS). F) Seasonal amplitude (AMP). G) Maximum (Peak) value. H) Minimum (Dormant) value.*

Similarly, EGS extracted from SZA-45 EVI was delayed when comparing to the same metric derived from normal EVI (Fig 2.24C). Differences between standard and fixed sun-sensor geometric EVI ranged from 10 days to 80 days. As delaying time of EGS acquired from SZA-45 EVI seems to be longer than SGS, SZA-45 EVI time-series tended to have longer greening season except for one site (Fig 2.24E). Unlike other two phenological timing dates (SGS and EGS), the seasonal shift of peak greening between

EVI products was not consistent as there was no dominant shift to early or later in the year (Fig 2.24B).

In regards to seasonal amplitude (Fig 2.24F), annual profiles of standard EVI tended to have stronger seasonality than fixed-SZA EVI. Mainland SEA is located in the northern hemisphere, and its solar altitude is higher (lower SZA) from March to September and lower (higher SZA) from September to March. SEA tropical forests started their growing season in March or April (Fig 2.24A), reached peak from July to September (Fig 2.24B), and then browned down. Consequently, dates of maximum EVI occurred on low SZA timing, while the dates of minimum EVI occurred on high SZA timing. In other words, MODIS Terra/Aqua sensor provided higher maximum with low SZA and lower minimum EVI with high SZA than fixed sun-sensor geometry EVI.

Unlike other phenological parameters, there is no clear evidence about BRDF effect to peak timing (PGS) of SEA forests (Fig. 2.24B). Also, slopes of regression lines are nearly horizontal, meaning low PGS correlation between standard and fixed-SZA EVI. Noisy data in the wet season, which coincides with peak VIs, possibly cause this phenomenon. As shown in seasonal profiles (Fig 2.19), standard deviation (SD) was much smaller in dry period than in the wet season.

The cross-site comparisons between phenological parameters derived from standard and SZA-45 NDVI for 30 intact forest sites are shown in Figure 2.25. Excepting anomalous sites, there is little difference of SGS dates obtained from fixed-geometry and standard NDVI (Fig 2.25A). Likewise, EGS retrieved from Terra/Aqua NDVI is comparable to $NDVI_{sz45}$, except at 2-3 outlier sites. Although EGS and SGS differences among various NDVI products are generally marginal, there is an unclear relationship between PGS extracted from $NDVI_{Standard}$ and $NDVI_{sz45}$, with Aqua data showing very low and Terra data showing moderate correlations with BRDF-corrected NDVI. On the other hand, AMP correlation plot (Fig 2.25F) demonstrated very high correlations between standard NDVI and fixed-geometry NDVI.

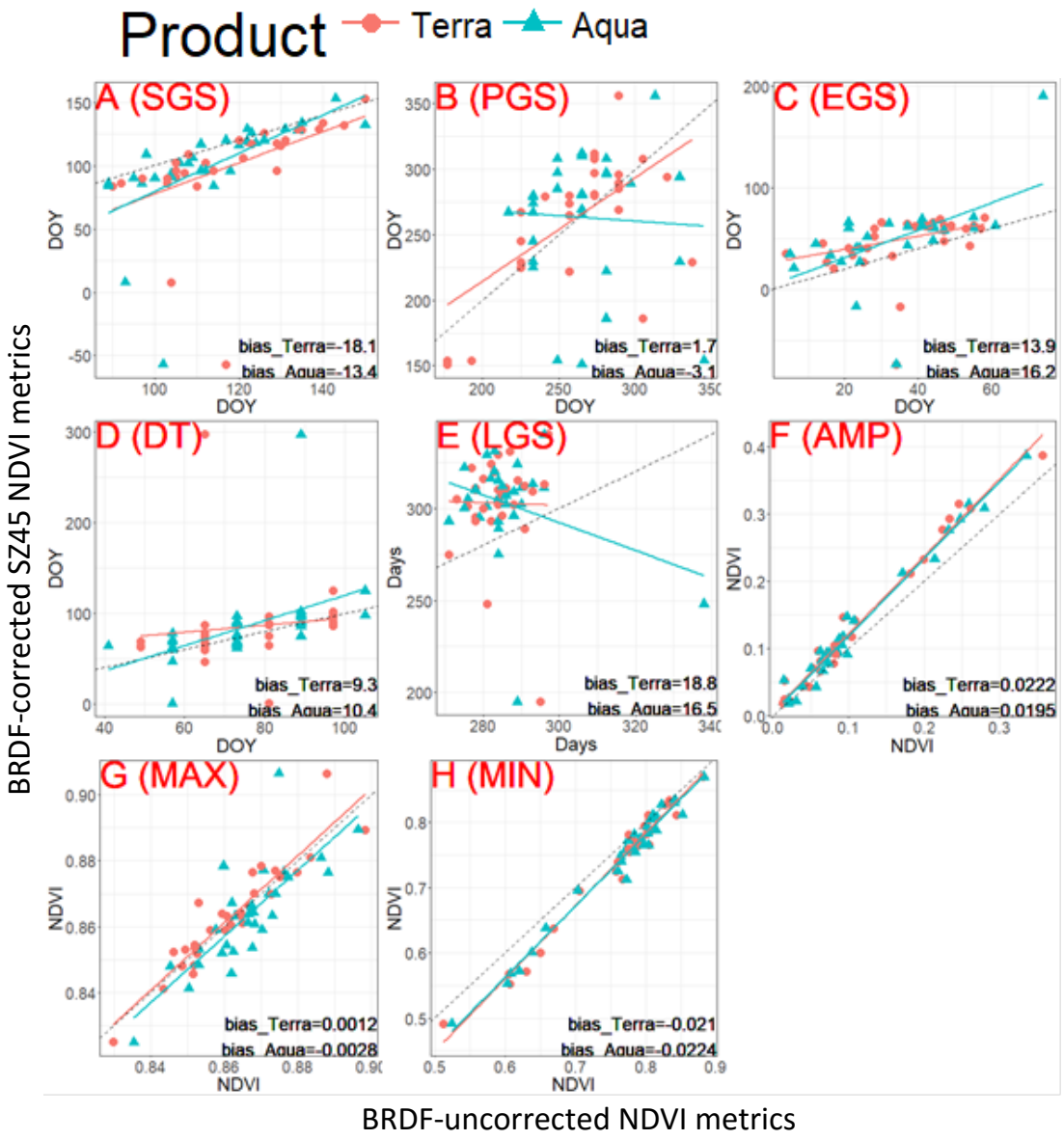

Figure 2.25 *Cross-site (30 sites) correlation of derived phenological metrics between standard and fixed SZA-45 NDVI at 500m resolution. A) Start of Greening Season (SGS). B) Peak of Greening Season (PGS). C) End of Greening Season (EGS). D) Dormancy Timing (DT). E) Length of Greening Season (LGS). F) Seasonal amplitude (AMP). G) Maximum (Peak) value. H) Minimum (Dormant) value.*

Comparison between variations of derived phenological metrics between NDVI and EVI is shown in Figure 2.26. Regarding the onset of forest photosynthesis activity, SGS_{EVI} extracted from standard VI products was earlier than SGS_{NDVI}. In contrast, fixed-SZA EVI and NDVI derived similar Julian dates of start of the greening season. This similarity suggested that SGS dates captured from NDVI and EVI were identical after correcting sun-view angles.

However, the relationship of NDVI and EVI in capturing dates of other growth stages (PGS, EGS) were not the same as SGS. The timing of peak and end of greening season derived from NDVI was later than EVI timing, and these differences remained after correcting for BRDF influence (Fig 2.26B, 2.26C). LGS_{NDVI} tended to be longer than LGS_{EVI} for both standard and fixed-geometry vegetation indices. Regarding seasonal amplitudes between two VIs (Fig 2.26F), AMP_{EVI} showed higher amplitude than AMP_{NDVI} at sites with weak seasonality (low amplitudes). On the other hand, AMP_{NDVI} was higher than AMP_{EVI} of strong seasonality at forest sites with strong seasonal differences (over 0.2).

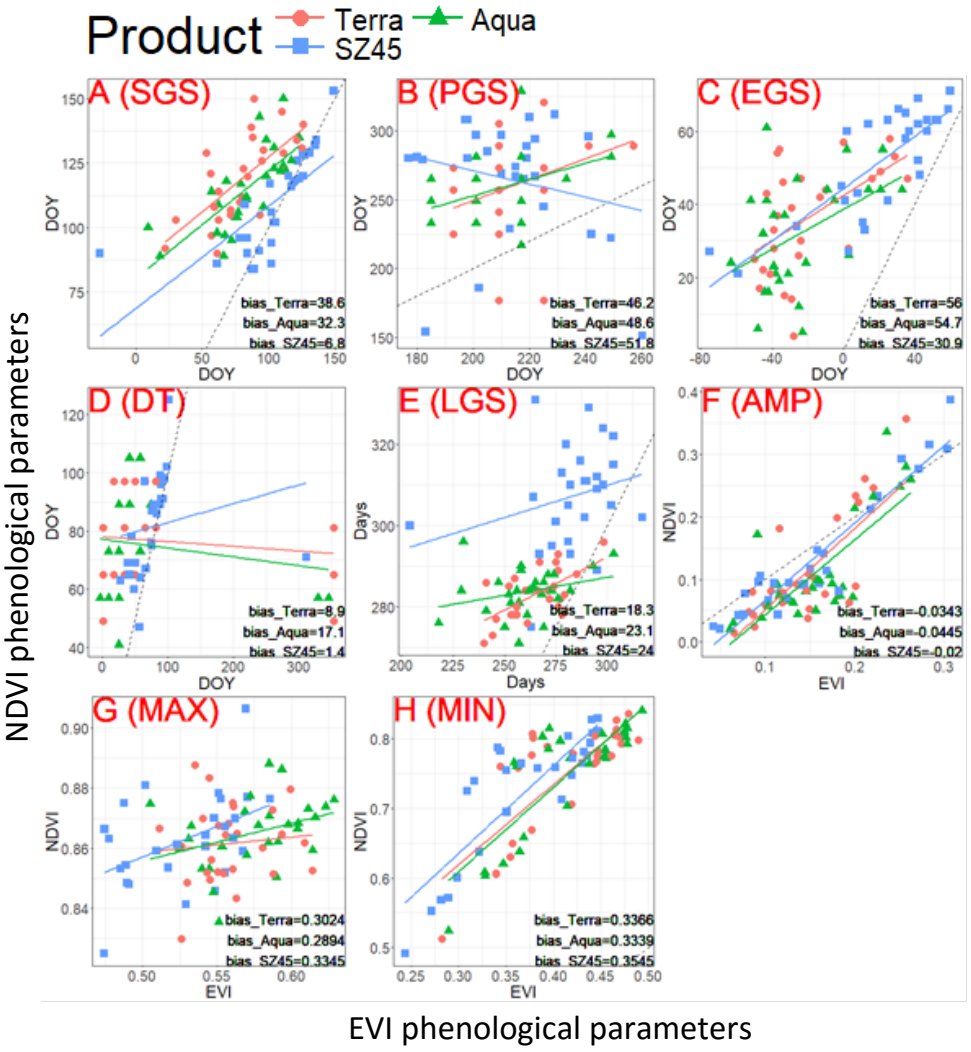

Figure 2.26. *Cross-site (30 sites) correlation of derived phenological metrics between two vegetation indices: EVI and NDVI at 500m resolution. A) Start of Greening Season (SGS). B) Peak of Greening Season (PGS). C) End of Greening Season (EGS). D) Dormancy Timing (DT). E) Length of Greening Season (LGS). F) Seasonal amplitude (AMP). G) Maximum (Peak) value. H) Minimum (Dormant) value.*

2.3.4.4. Phenological metrics variations with different forest types

We show the phenological metrics of forests with different dry season lengths and water deficits to investigate phenology variations of SEA forests depending on water availability (Fig. 4.27 – 4.30). We observed that the onset of the greening season happened earlier with wet tropical forests while drier forests started their growing seasons later (Fig. 2.27A and 2.28A). SGS of wet forests ranged from DOY50 to DOY75 while SGS of other forests ranged from DOY80 to DOY150. However, maximum EVI timing of rainforests occurred later than other forests, especially after doing BRDF correction (Fig. 2.27B and 2.28B). Regarding LGS, rainforests had longer greening season compared with drier forests (Fig. 2.27E and 2.28E). Also, the drier forests had stronger EVI amplitudes because of lower EVI during dry seasons and higher EVI during rain seasons.

Phenological parameters of different forest types obtained from NDVI measurements illustrate that the rainforests exhibit a very distinct profile compared to the drier forests in regards to BRDF-corrected and Terra/Aqua NDVI (Fig. 2.29 and 2.30). For example, the differences of phenophase metrics like SGS, PGS or EGS between $NDVI_{Terra/Aqua}$ and $NDVI_{SZ45}$ were large for forests having short dry seasons (0-2 months) or very low water deficit (0-150 mm/y). This result suggests that NDVI saturation is a severe problem in monitoring SEA rainforest phenology.

The comparison of phenological metrics derived from NDVI time-series among forest types revealed similar results as those obtained from EVI. For example, wetter forests started the greening season before forests with more water limitation during the dry periods (Fig. 2.29A and 2.30A). Moreover, drier forests had stronger seasonality because of lower minimum NDVI than wetter forests (Fig. 2.29FH and 2.30FH). Maximum NDVI measurements, however, were not clearly distinguishable among forest types (Fig. 2.29FG and 2.30FG).

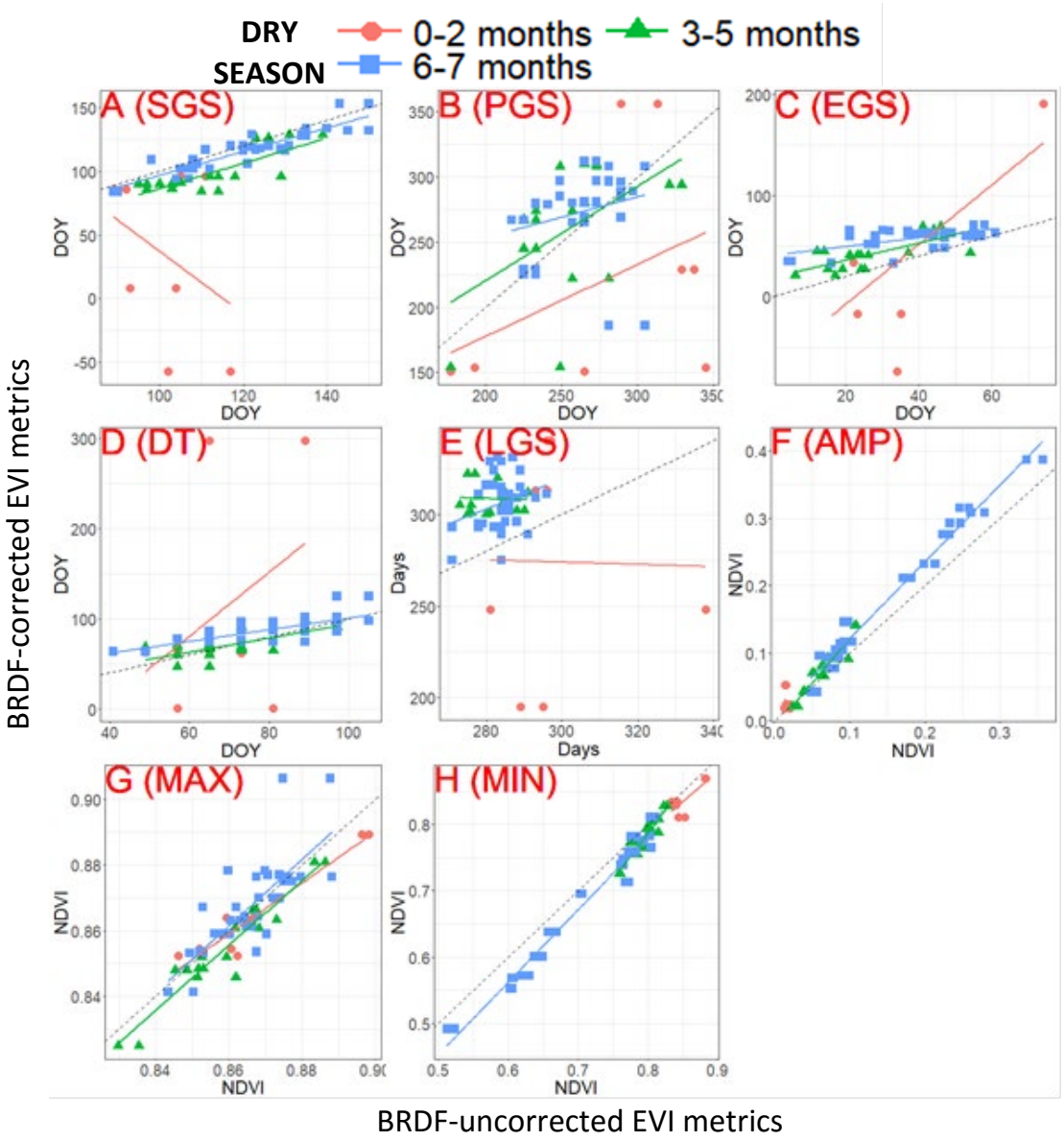

Figure 2.27 *Cross-sited (30 sites) correlation of derived phenological metrics between BRDF-corrected and -uncorrected EVI at 500m resolution with forest groups based on the length of the dry season. A) Start of Greening Season (SGS). B) Peak of Greening Season (PGS). C) End of Greening Season (EGS). D) Dormancy Timing (DT). E) Length of Greening Season (LGS). F) Seasonal amplitude (AMP). G) Maximum (Peak) value. H) Minimum (Dormant) value.*

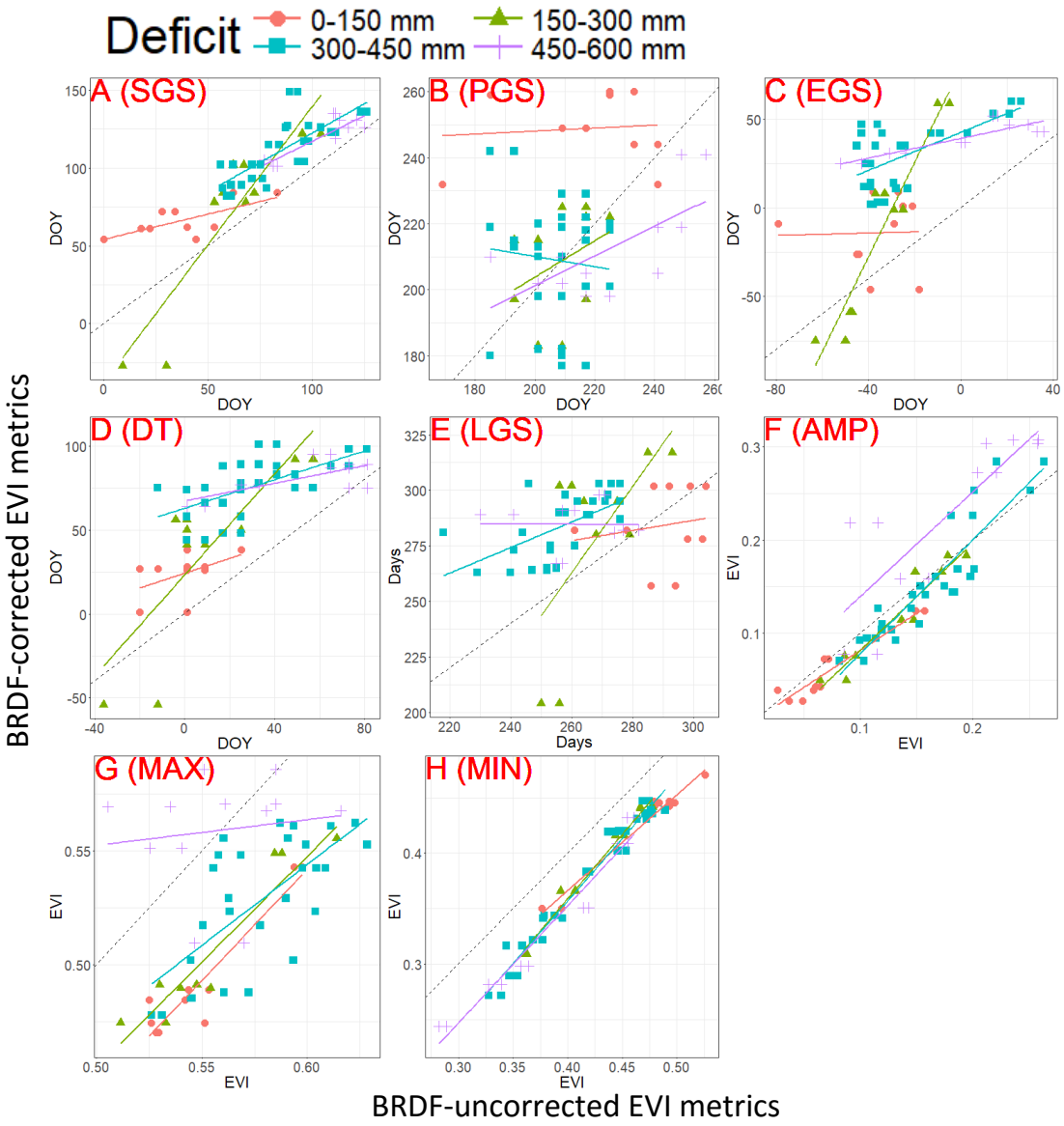

Figure 2.28 *Cross-sited (30 sites) correlation of derived phenological metrics between BRDF-corrected and -uncorrected EVI at 500m resolution with forest groups based on water deficit. A) Start of Greening Season (SGS). B) Peak of Greening Season (PGS). C) End of Greening Season (EGS). D) Dormancy Timing (DT). E) Length of Greening Season (LGS). F) Seasonal amplitude (AMP). G) Maximum (Peak) value. H) Minimum (Dormant) value.*

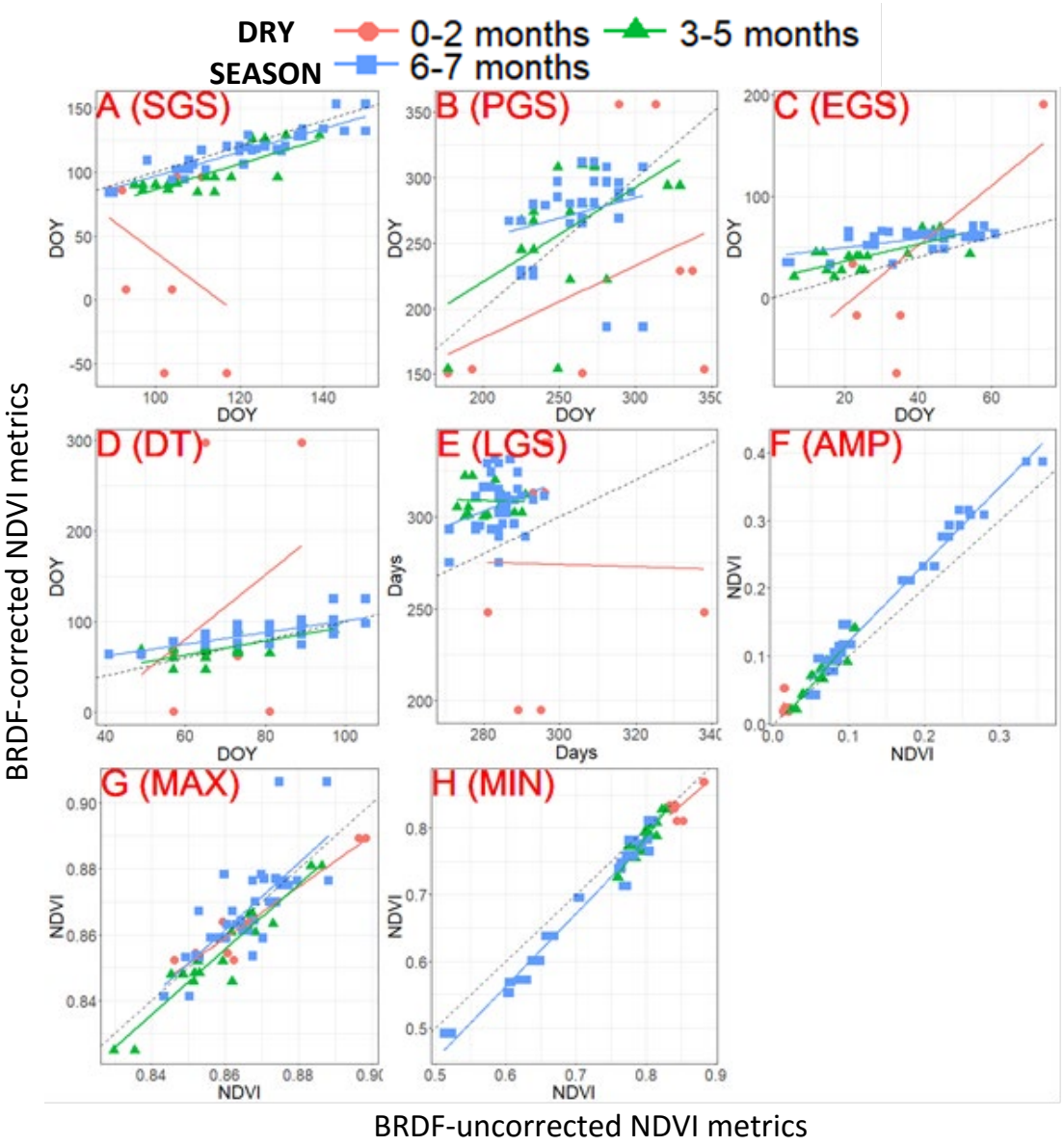

Figure 2.29 *Cross-sited (30 sites) correlation of derived phenological metrics between BRDF-corrected and -uncorrected NDVI at 500m resolution with forest groups based on the length of dry season. A) Start of Greening Season (SGS). B) Peak of Greening Season (PGS). C) End of Greening Season (EGS). D) Dormancy Timing (DT). E) Length of Greening Season (LGS). F) Seasonal amplitude (AMP). G) Maximum (Peak) value. H) Minimum (Dormant) value.*

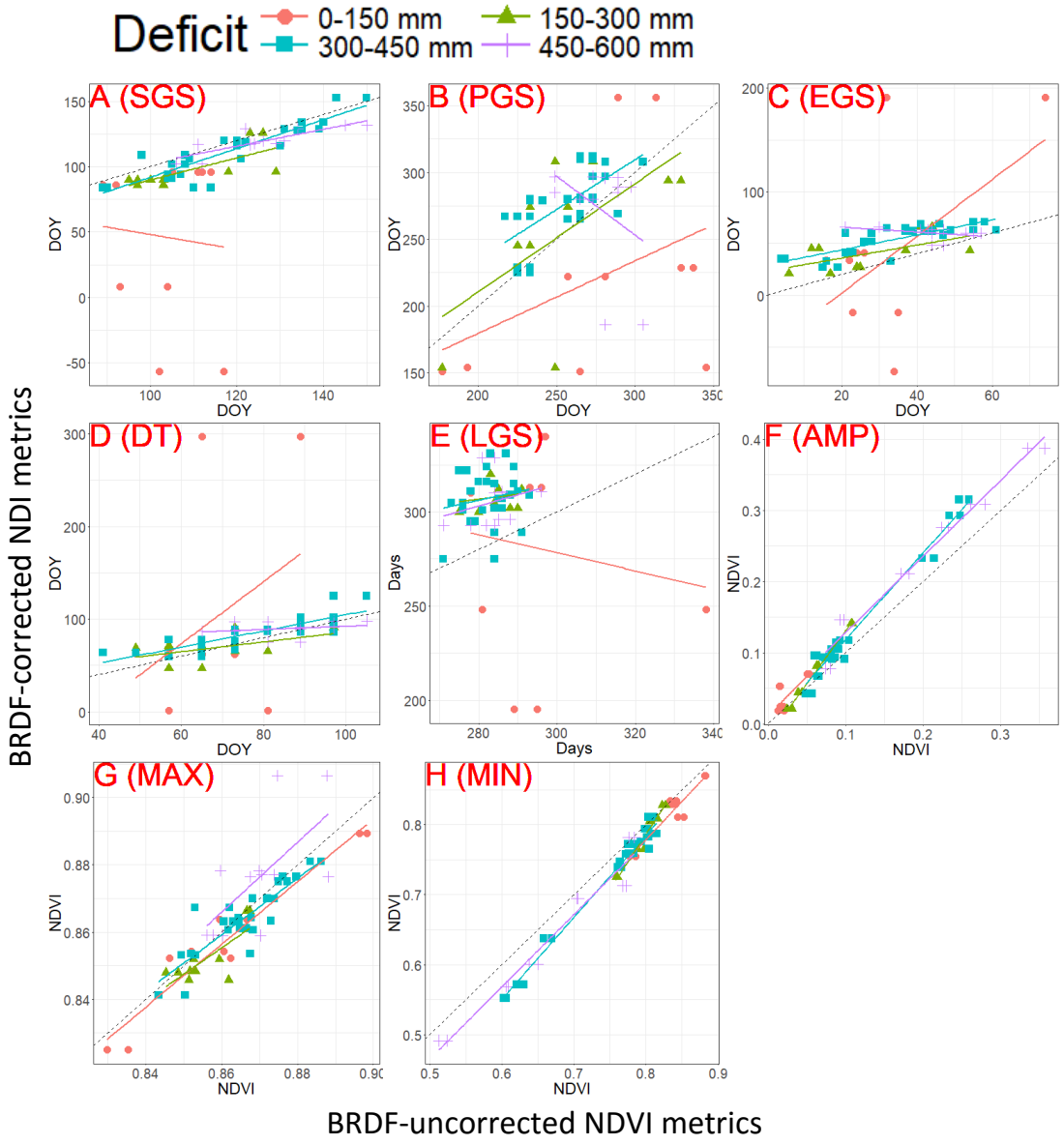

Figure 2.30 *Cross-sited (30 sites) correlation of derived phenological metrics between BRDF-corrected and -uncorrected NDVI at 500m resolution with forest groups based on water deficit. A) Start of Greening Season (SGS). B) Peak of Greening Season (PGS). C) End of Greening Season (EGS). D) Dormancy Timing (DT). E) Length of Greening Season (LGS). F) Seasonal amplitude (AMP). G) Maximum (Peak) value. H) Minimum (Dormant) value.*

2.3.4.5. Phenological parameters dependence on variations of sun-angle settings

The dependence of retrieved EVI phenological metrics to different sun-angle configurations from 2001 to 2016 for 30 undisturbed sites is illustrated in Figure 2.31. The impact of fixing SZA angles on phenological metrics is varied. Among three phenological transition dates, varied sun angles had minor or no impact on SGS and PGS (Fig. 2.31A and B), while there are noticeable differences between EGS derived from VIs with varied SZA (Fig. 2.31C), especially for SZ45. Differences of various-SZA SGS dates were from 0 up to 4 days, while the PGS variation was 10 days. In contrast, EGS exhibited a higher dependency on sun-angle as higher solar altitude caused positive biases (Fig 2.31C). Shifts in EGS dates were up to 30 days when comparing between EVI_{sz0} and EVI_{sz45}. Consequently, as shown in Fig 2.31E, LGS are generally longer with lower SZA values because of the delay in EGS.

Similarly, cross-site analysis of phenological parameters extracted from seasonal NDVI time-series is illustrated in Figure 2.32. Different configurations of SZAs did not affect the start of growing season (SGS) derived from EVI and NDVI. Lower SZA seemed to be anticipating the end timing of growing season for both NDVI and EVI, with a stronger influence of SZA in EVI. Consequently, the length of growing season (LGS) derived from both NDVI and EVI was shorter with lower SZA. Considering seasonal amplitude, lower SZA yielded stronger seasonality for both NDVI and EVI, with weaker impact to NDVI. Surprisingly, the peak timing of NDVI was much more dependent on SZA (Fig 2.32B), than PGS derived from EVI(Fig. 2.31B).

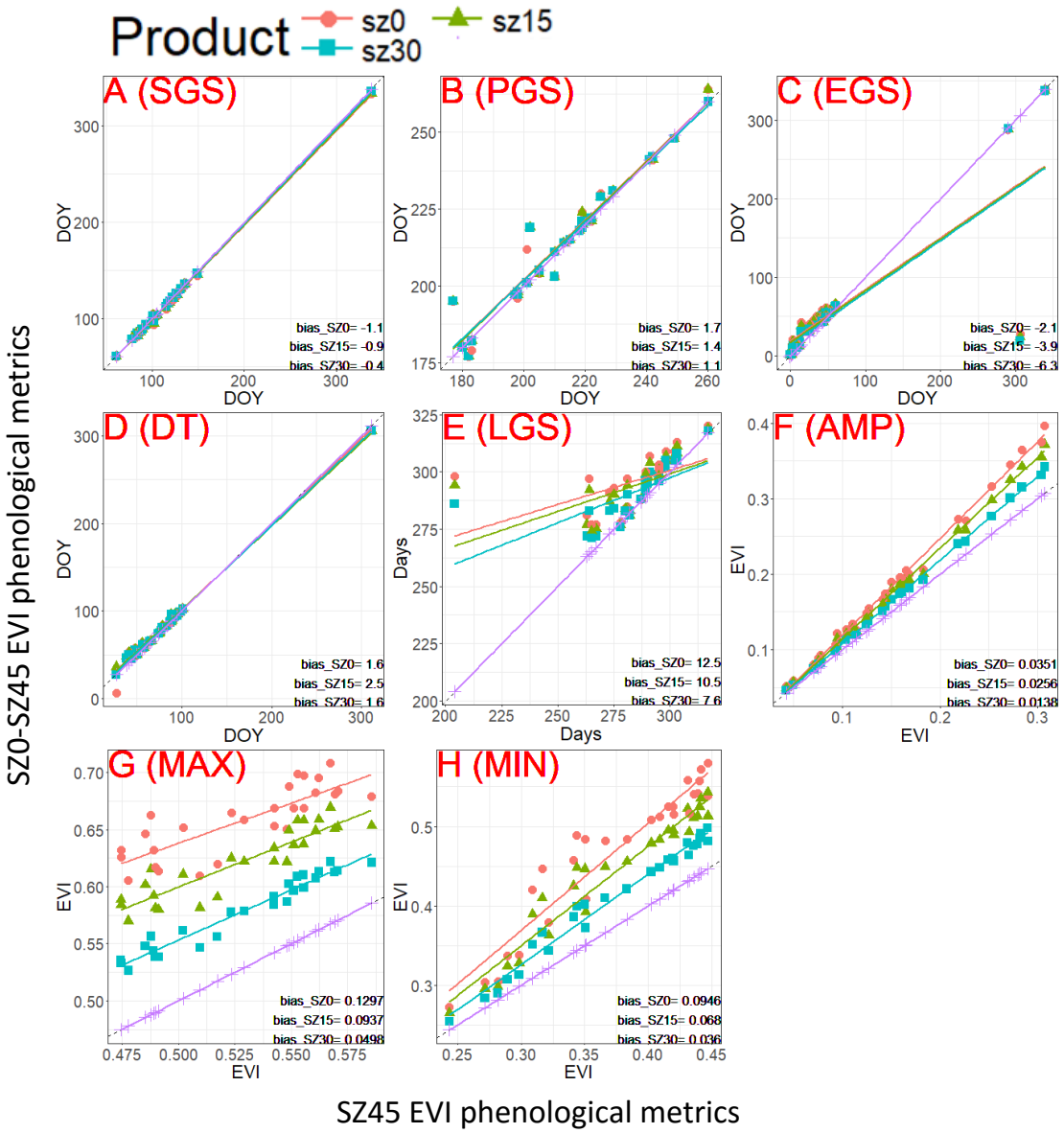

Figure 2.31. *Cross-site correlation of derived phenological metrics between various sun-angle configurations of EVI. A) Start of Greening Season (SGS). B) Peak of Greening Season (PGS). C) End of Greening Season (EGS). D) Dormancy Timing (DT). E) Length of Greening Season (LGS). F) Seasonal amplitude (AMP). G) Maximum (Peak) value. H) Minimum (Dormant) value.*

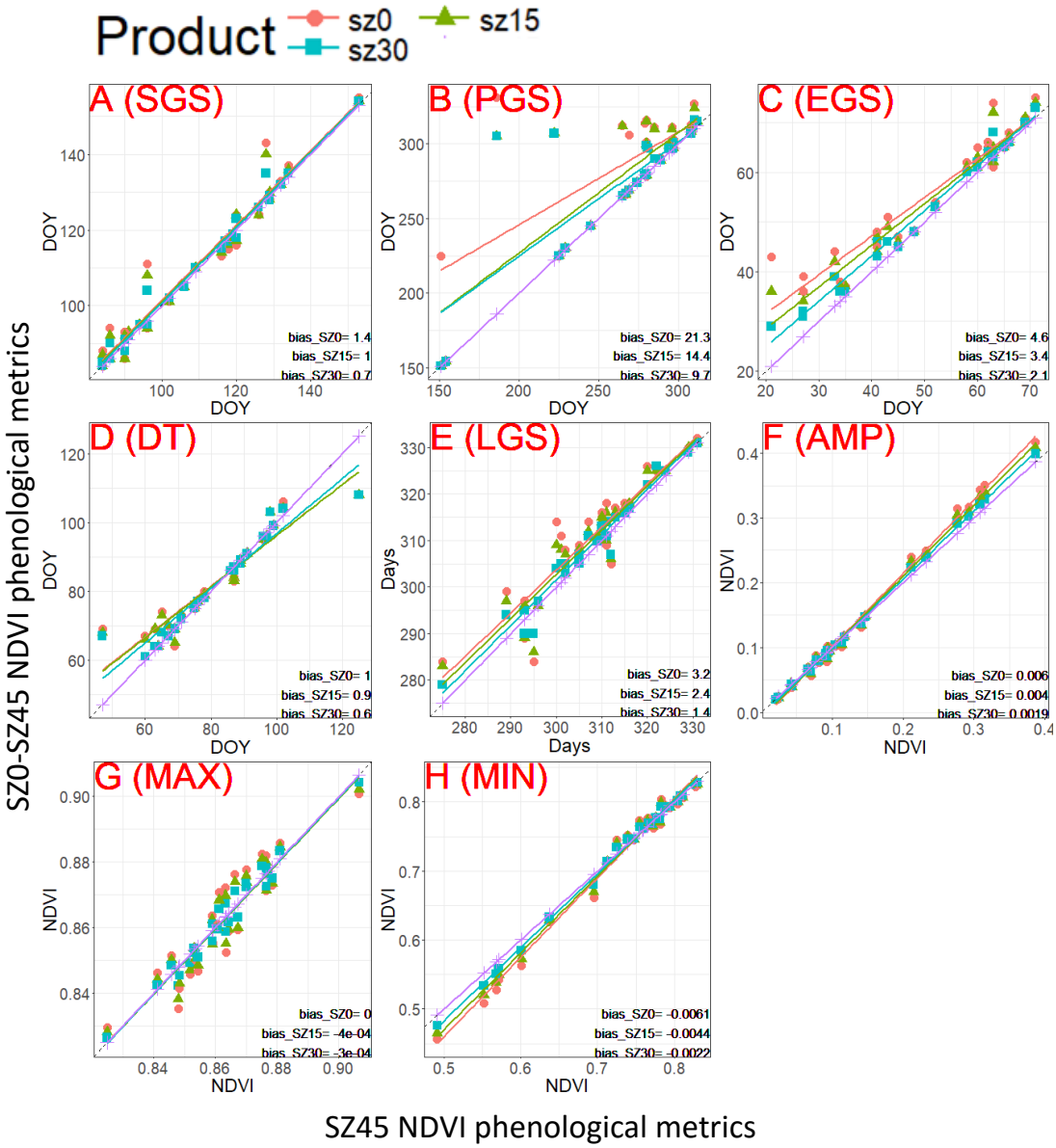

Figure 2.32 *Cross-sited correlation of derived phenological metrics between various sun-angle configurations of NDVI. A) Start of Greening Season (SGS). B) Peak of Greening Season (PGS). C) End of Greening Season (EGS). D) Dormancy Timing (DT). E) Length of Greening Season (LGS). F) Seasonal amplitude (AMP). G) Maximum (Peak) value. H) Minimum (Dormant) value.*

2.3.4.6. Evaluation of RossThick-LiSparse model in retrieving seasonal profiles, and phenological metrics of SEA tropical forests

We used observation angles extracted from MODIS Terra/Aqua metadata to estimate vegetation indices for tropical forest sites. Comparison of VI time-series and derived phenological metrics between BRDF-corrected and standard Terra/Aqua VI would evaluate the ability of MODIS BRDF parameterised data in generating reflectances and vegetation indices at desired illumination and viewing angles.

Figure 2.33 illustrates seasonal profiles between estimated and Terra/Aqua NDVI and EVI of three sample sites with different lengths of the dry season. In general, the BRDF model is accurate to model annual profiles of vegetation indices for SEA tropical forests. Observed seasonal profiles are similar regarding both shapes and magnitudes as modelled VI patterns in the three selected sites.

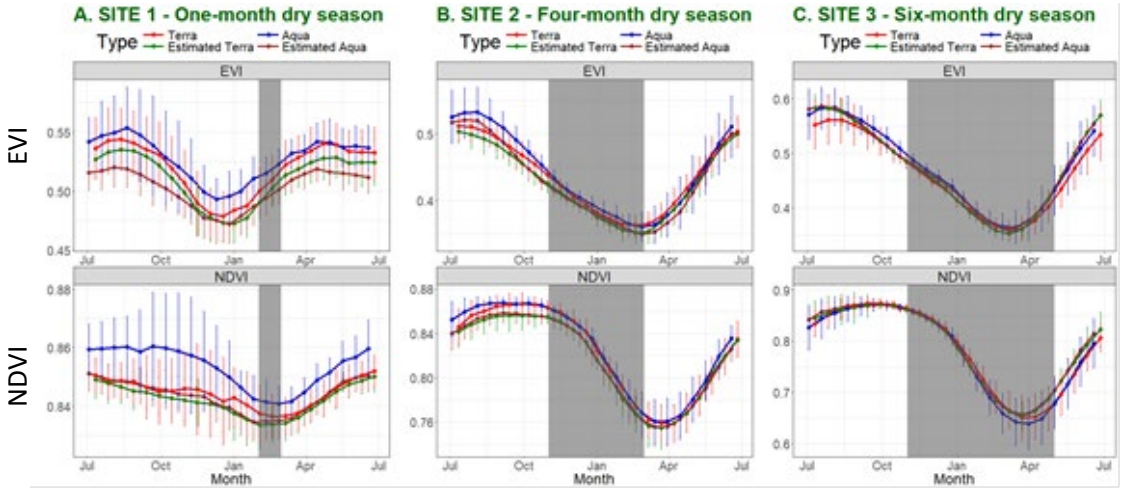

Figure 2.33 *Seasonal profiles between estimated and Terra/Aqua Vegetation Indices of three sample sites with different lengths of dry season at 500m resolution. Grey areas indicate the dry period. Error bars represent VI standard deviation of 16-year averaging. A. One-month. B. Four-months. C. Six-months*

However, the accuracy of the BRDF model used for MODIS products varied across seasons. Standard NDVI and EVI values are indistinguishable from modelled ones in dry season. In the wet season, however, there are gaps between modelled and measured VIs for both NDVI and EVI, especially at the rainforest site (Fig. 2.33A). The differences are likely due to noisy data caused by intense cloud cover in the wet season. Highly dense clouds in wet periods limit available observations needed for RossThick-LiSparse model to provide corrected BRDF parameters. Larger standard deviations (SD) in wet seasons for both standard NDVI and EVI time-series (Fig. 2.33) also illustrate this limitation. This

dissimilarity between dry and wet seasons affects retrievals of phenological parameters from seasonal profiles or time-series.

Cross-sited correlations of derived phenological metrics between modelled and standard EVI annual profiles are shown in Fig. 2.34. Among the parameters related with phenophase dates, the peak of the greening season (PGS) exhibited the largest uncertainty of BRDF model, with high RMSE (14 days with Terra and 16 days with Aqua). Other phenological dates derived from modelled EVI time-series are well correlated with phenological metrics derived from Terra, and less correlated with Aqua EVI times-series, which had RMSE values typically lower than 17 days. Regarding greenness metrics (AMP, MAX, and MIN), there are some differences especially in MAX, but the RMSE values range is small from 0.009 to 0.037.

Comparison of NDVI-based parameters showed similar results to metrics derived from EVI time series (Fig. 2.35). The correlation of PGS between estimated and standard NDVI measurements are low with RMSE values over 32 days for both Terra and Aqua comparison. Comparisons of other metrics illustrate high agreement between estimated and standard NDVI measurements with low RMSE (lower than 16 days for dates and 0.016 for VI values).

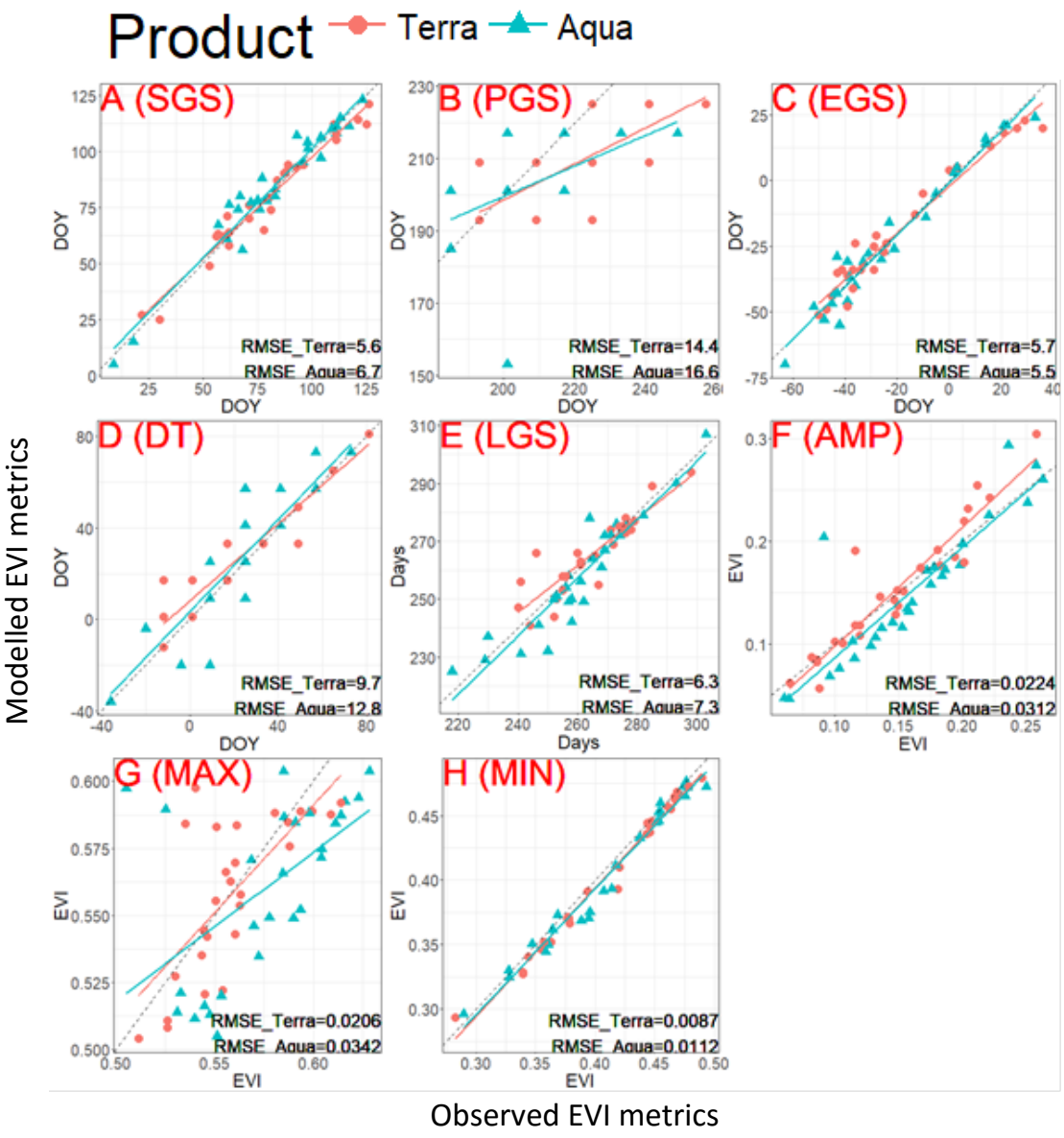

Figure 2.34 *Cross-sited correlation (30 sites) of derived phenological metrics between modelled and Terra/Aqua EVI seasonal profiles at 500m resolution. A) Start of Greening Season (SGS). B) Peak of Greening Season (PGS). C) End of Greening Season (EGS). D) Dormancy Timing (DT). E) Length of Greening Season (LGS). F) Seasonal amplitude (AMP). G) Maximum (Peak) value. H) Minimum (Dormant) value.*

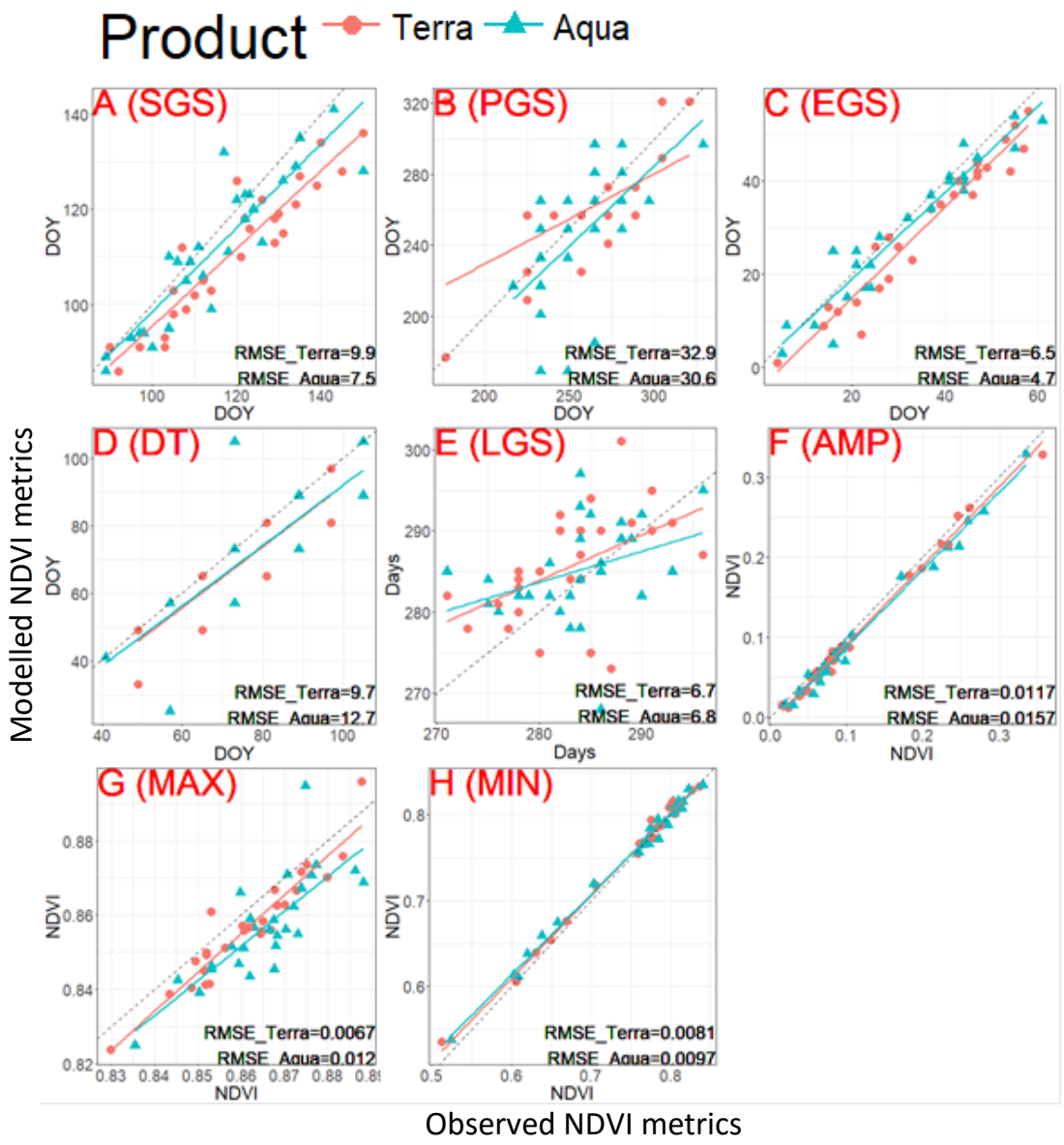

Figure 2.35 *Cross-sited correlation of derived phenological metrics between modelled and Terra/Aqua NDVI seasonal profiles. A) Start of Greening Season (SGS). B) Peak of Greening Season (PGS). C) End of Greening Season (EGS). D) Dormancy Timing (DT). E) Length of Greening Season (LGS). F) Seasonal amplitude (AMP). G) Maximum (Peak) value. H) Minimum (Dormant) value.*

2.4. Discussion

2.4.1. Seasonal sun-angle variations and impact of BRDF to retrieved phenological parameters of SEA tropical forests

One of the objectives of this chapter was to evaluate the sensitiveness of two commonly used vegetation indices, NDVI and EVI, to variable viewing and illumination geometry. The average seasonal profiles of VI time-series showed that NDVI is less affected by seasonal sun-sensor geometries. The shape of the annual growth cycle of Terra and Aqua NDVI is similar to that of normalised NDVI. These findings at SEA tropical forests are in line with previous results by Kaufmann et al. (2000), who investigated the effects of changes in SZA to NDVI derived from Advanced Very High-Resolution Radiometer (AVHRR) and found that the relationship between NDVI and SZA is minimal at dense vegetation canopies.

In contrast, another study by Galvão et al. (2004), which showed that Amazon forests produced higher NDVI values with increasing SZA, partly agreed with our findings as seasonal NDVI profiles were correlated with SZA (Fig 2.19). Also, the seasonal NDVI amplitudes, minimum and maximum were stronger with higher SZA. (Fig 2.32F-2.32H)). However, the differences caused by various SZA settings were marginal and BRDF effect was minimal. Bhandari et al. (2011) found that NDVI of Queensland forests was sensitive to variations of sun-sensor geometry in terms of seasonal amplitude, which was opposite to our outcome of cross-site correlation between $NDVI_{Terra/Aqua}$ and $NDVI_{SZ45}$ (Figure 2.25). However, Bhandari and collaborators included woodlands and discontinuous open forests in the subtropical region (around 25S latitude) for his study. Consequently, NDVI retrieved from those sparse canopy biomes was more sensitive to variable SZA because of the influence of soil-induced effect (Kaufmann et al., 2000). Our study areas, on the other hand, are located in the tropical zone and primarily classified as evergreen broadleaf forests (Figure 2.1), and thus have a high leaf area. Under dense vegetation canopies, the impact of soil-induced effect is minimal or extinguished. BRDF impacts on NDVI measurements might be different in sparse vegetation areas like savannahs or grasslands and thus, should be considered more carefully in those cases (Sims *et al.*, 2011).

However, NDVI was reported by many studies and authors to be saturated in high biomass areas (A.R. Huete, HuiQing Liu, & van Leeuwen, 1997; G. Liu, Liu, & Yin,

2013; Mutanga & Skidmore, 2004; Pei-Yu Chen, Gunar Fedosejevs, 2006). Our results (Fig 2.19) also showed the same issue. NDVI was increasing at the SGS, saturated in June-July, and did not drop until leaf senescence when the dry season started. The long saturated levels ranged from 3-6 months, making it nearly impractical to discriminate forest dynamics in this period with NDVI. Similarly, our correlation plots showed that seasonal forest changes of NDVI were usually lower than changes of EVI in forests with weak seasonality. At forests with seasonal amplitudes higher than 0.2, NDVI seasonal changes tended to be larger than EVI changes (Fig. 2.26F).

EVI, unlike NDVI, is less influenced by the saturation problem. In fact, EVI was designed to enhance sensitivity to vegetation signal in high-vegetation-cover regions and reduce soil background effect (Huete et al., 2002). However, Hilker *et al.* (2015) using statistical methods questioned the use of EVI for detecting seasonal changes of tropical forests without BRDF-correction, and our findings corroborated the fact that EVI was more susceptible to variations in viewing and illumination geometry as compared to NDVI (A. Sims et al., 2011; Morton et al., 2014).

The differences in seasonal EVI patterns between $EVI_{Terra/Aqua}$ and $EVI_{SZ45/SZ15}$ (Fig 2.19) showed a significant impact of BRDF to seasonal EVI. From our results, lower SZA yielded higher EVI for SEA tropical forests with more significant differences between various SZA values than NDVI. The advantage of EVI over NDVI is its unsaturation in tropical forests. Seasonal profiles of EVI showed that EVI maximum was only around 0.6 to 0.7 and not kept its highest level for an extended period like NDVI. SEA forests with weak seasonality also had stronger seasonality while using EVI to retrieve their seasonal dynamics (Fig. 2.26). Therefore, EVI seemed to be more suitable than NDVI to capture SEA forest phenology though it is more sensitive to BRDF effect than NDVI.

NDVI and EVI formulas might explain the trade-off between saturation and BRDF influence. NDVI only includes reflectance of red and NIR bands to compute the vegetation index. Frequently, BRDF influences similarly optical and NIR wavelengths thus BRDF is minimised by the ratio between red and NIR bands in NDVI formula. EVI formula, however, is different: it was designed to solve soil-induced effect, so it has a fixed-number (1) in its denominator. Consequently, this constant factor is unchanged with

variable reflectance due to variations of view and illustration geometry, making EVI easily affected by variable sun-sensor geometries (Sims *et al.*, 2011).

The primary objective of this chapter was to analyse the influence of seasonal sun-sensor geometries on phenological metrics derived from VI time-series. Our results showed that both the shape and magnitude of the annual profiles of EVI were significantly altered by seasonal sun-view geometric variations, resulting in considerable differences among phenological parameters derived from fixed SZA EVI. Specifically, the growing season started and ended later with EVI_{SZ45} compared with normal Terra/Aqua EVI. The shift varied from neglectable 2-3 days up to 2 months. This substantial variation might change our understanding of the dynamics of SEA tropical forests. Moreover, the continental SEA climate is influenced by monsoon and majority of peninsular SEA started its rainy season on late April or May; thus, SGS retrieved from BRDF-corrected EVI showed a more logical connection with the rainy season than SGS from BRDF-uncorrected EVI.

As BRDF impact to derive phenological metrics has been noticed for decades, previous studies (de Beurs & Henebry, 2010; X. Zhang et al., 2003) used vegetation indices calculated from MODIS BRDF nadir-adjust product (MCD43A4) to capture phenological parameters from regional to global scales. This NBAR product, however, only adjusted reflectance to nadir view but SZA remains variable across seasons (C. B. Schaaf et al., 2002). Our outcomes of SZA and VZA histograms showed that seasonal VZA is insignificant in comparison with seasonal variations of SZA (Fig. 2.8 and 2.9). We conclude that BRDF effects were likely caused by variable SZA, rather than variable VZA, and NBAR product is unlikely unable to correct BRDF effect in reflectance values and as a consequence, in vegetation indices.

On a global monitoring scale, the sun-angle effect could result in uncertainties in the estimation of several vital ecological parameters, such as carbon uptake period, grass curing, and crop/forage productions, particularly at high latitudes where seasonal variations in solar zenith angle (SZA) are more significant than at tropical or sub-tropical regions. Los *et al.* (2005) found that the length of growing season derived from AVHRR NDVI to be underestimated in the Northern Hemisphere and overestimated in Southern Hemisphere if BRDF effect was not corrected. Compared to our results, LGS retrieved from $EVI_{Terra/Aqua}$ seemed to be exaggerated by more than one month as compared to LGS

derived from EVI_{SZ45}. However, LGS acquired from seasonal NDVI shared similar findings with EVI, but with smaller overestimation between standard and fixed sun-view geometry. Therefore, it is essential to set sun-view configurations to account for BRDF effects on surface reflectance before extracting phenological metrics from satellite observations. The BRDF correction would help to obtain a more approximate representation of ground vegetation dynamics using satellite data.

2.4.2. Influence of geometry configurations in phenological metrics

BRDF correction is crucial to capture corrected vegetation dynamics. However, the selection of fixed geometry settings, raised by Middleton et al. (1992) is essential. Solar zenith angle is the most important settings to acquire surface reflectance measurements for monitoring vegetation dynamics and estimating canopy structural and functional variables. Previous studies generally defined 45 degrees as an optimal standard SZA (Bréon & Vermote, 2012; E. M. Middleton, 1992). However, a 45 degrees angle would be too large for tropical regions as SZA of low latitude areas was below 45 degrees at any time in the year (Fig 2.7). It is evident that fixing SZA to 45 degrees caused vegetation indices of some SEA forests to be modelled to an unrealistic solar angle that never occurs, and thus cannot be validated through comparison with ground measurements.

Our comparisons between various fixed SZA VI products illustrated the impact of selecting fixed SZA to derive phenological measurements. The influence of SZA choice was mixed among metrics and indices. Different selected SZAs did not affect the start of growing season (SGS) derived from EVI and NDVI. Lower SZA seemed to be left-shifting (anticipating) the end timing of growing season for both NDVI and EVI, with the higher influence of SZA found on EVI. So lower SZA settings produced shorter lengths of the growing season (LGS) for both NDVI and EVI.

SZA values also had a negative correlation with derived seasonal amplitude, with less impact on NDVI. However, the peak timing of NDVI seemed to be positively correlated with SZA values (Fig 2.32B), while PGS derived from EVI was less dependent to variations of SZA setting (Fig. 2.31B). This phenomenon is due to NDVI saturation, causing this VI to be difficult to capture the precise peak timing of high biomass regions like SEA tropical forests. In sum, the choice of SZA had some influence in the retrievals of phenological metrics at SEA tropical forests.

2.4.3. Forest VI seasonal profiles at varying water availability conditions

In this chapter, we also aimed to understand seasonal forest phenology at varying water availability conditions in the continental SEA. Our analyses revealed that seasonal greenness profiles of SEA forests vary according to forest types (Fig. 2.20 – 2.23). Short dry seasons or water deficit resulted in low seasonality. Moreover, the greenness of drier forests was lower in the dry season and higher in the wet season. While tropical dry forests contain a mix of evergreen and deciduous species, the accumulation of water deficit during the dry period causes the defoliation of deciduous trees to adapt with seasonal water stress (Elliott, Baker, & Borchert, 2006; Guan et al., 2015). During the late dry season, water stress is more severe, and the forest greenness represented by VIs drops significantly (Y. Zhang et al., 2016). When new leaves replace lost leaves, forest albedo is expected to increase because old leaves have lower reflectance and decreased transmittance relative to young leaves (Maeda, Heiskanen, Aragão, & Rinne, 2014).

This phenomenon is known as leaf demography and explains why seasonal forests had higher EVI with BRDF correction during wet season, according to our results. Without BRDF correction, EVI measurements of many forest classes were generally identical during wet and dry periods. This finding suggests that BRDF correction is an essential step to capture accurately seasonal EVI profiles of tropical forests. Regarding NDVI of the rainy season, SEA forests' NDVI were nearly indistinguishable among forest types during wet season because of saturation issue. As NDVI is not sensitive to BRDF impact, the role of sun-view angle standardisation is insignificant.

Analyses of phenophase timing showed that out rainforest site started its greening season earlier than dry tropical forests (Fig 2.27 - 2.30). Comparing with SEA rainfall maps (Fig. 2.5), forests having shorter dry seasons are located in Northern Myanmar or Southern Peninsular SEA. These regions started their rainy seasons from January to April, earlier than in other areas. Consequently, the early rainy season is a reasonable reason to explain earlier onset of greening seasons. Regarding the peak timing of tropical forests, humid evergreen forests reached their peak greenness later than drier forests. This outcome indicates that humid evergreen forests with more mature leaves present a slower response to rainfall while dry tropical forests quickly replace lost leaves during the dry season.

Moreover, continental SEA tropical forests reached VI peaks in the middle of rain seasons before the start of the dry season (Fig. 2.10). Our results are correlated with a previous study by Huete *et al.* (2008) that analysed the seasonal and inter-annual changes of three forest sites in Southeast Asia. The changes in pigmentation or reflectance of the mature leaves or the phenological adaptation of plants for the incoming dry season are potential reasons of this phenomenon (Samanta et al., 2012; Y. Zhang et al., 2016).

2.4.4. Evaluation of the BRDF model in generating reflectances and VIs at desired sun-view angles

The accuracy of the BRDF model in generating vegetation indices at desired illumination and viewing angles is crucial as it can affect retrieved information and reported results. We tested the accuracy of RossThick-LiSparse model using observed sun-view angles from MODIS sensor to estimate vegetation indices from MODIS Terra/Aqua products. Our findings are correlated with Bhandari study (2011), which investigated viewing and illumination geometry effects on MODIS VI time-series for monitoring phenology and disturbances in forest communities in Queensland, Australia. The results showed indistinguishable patterns between MODIS VI time-series and modelled VI time-series generated using BRDF parameters for both NDVI and EVI. Our results in the form of seasonal profiles indicated that the BRDF model is reliable to estimate vegetation indices at specific illumination and viewing angles (Fig. 2.33). In general, seasonal VI time-series derived from MODIS sensors have similar shapes and amplitudes to those obtained from modelled VI time-series. However, in the wet period, $VI_{Modelled}$ and VI_{MODIS} were not identical while they were indistinguishable during the dry periods. The differences between the estimated and observed VI measurements were reflected in derived metrics such as peak of the greening season and maximum VI values (Fig. 2.34 – 2.35).

The main reason of BRDF model uncertainty is the limitation of the available data. Wang *et al.* (2014) showed that the lack of available observations caused the increase of BRDF uncertainty in capturing vegetated land surface in wintertime for tundra ecosystems. As RTLSR model relies on the observed data to derive modelled parameters representing BRDF of land surface, limitation of good observed data presumably reduces the accuracy of derived parameters. Another study by Román *et al.* (2009) validated MODIS BRDF/Albedo product in monitoring forest landscapes, and their results

suggested that the variations between MODIS albedos and ground-measured albedos were caused by periods of increased cloudiness during Amazon Monsoon. Román outcomes are well correlated with our results. Cloud issue was seemly evident from standard deviations (SD) of MODIS Terra/Aqua VIs as SD ranges were larger in wet periods than in dry seasons. This finding suggests that MODIS BRDF products should be used carefully in periods with low data availability.

The unmatching results between modelled and standard VI time-series are potentially caused by limited and relatively fixed observations from satellite sensors (H. Zhang et al., 2015). For example, MODIS BRDF parameters are retrieved from 16-day data, which contains insufficient angular observed data to characterise surface anisotropy completely. This issue can cause minor artefacts while estimating surface reflectance and vegetation indices at required sun-view geometries.

Though we should be cautious with results in the wet season, the accuracy of the MODIS BRDF model was proven with identical patterns between $VI_{modelled}$ and $VI_{Terra/Aqua}$. It means that the MODIS BRDF model is precise in estimating vegetation indices at a fixed sun-sensor geometry and the outcome of BRDF correction to derived phenological parameters is reliable in the dry season. Furthermore, the major proportion of forests in Mainland SEA forests are influenced by the available water supply. Thus phenological metrics related to dry period presumably provide invaluable information about forest phenology in this region.

2.5. Conclusion

In this chapter, we generated time-series of NDVI and EVI with different SZA at the regional scale and multiple forest sites at a smaller scale using MODIS BRDF datasets. Then we investigated NDVI and EVI capabilities in capturing SEA forest phenology while considering BRDF impact on phenological metrics derived from vegetation indices. We compared phenological parameters between standard VI products and fixed sun-sensor geometric vegetation indices to analyse how BRDF influenced the retrieved metrics. As variations of seasonal SZA was much stronger than that of VZA, we also inspected the influence of different sun angle settings on phenological parameters.

Our results revealed that there was a trade-off between VI robustness to BRDF effect and saturation, which influenced the retrieval of continental SEA forest phenology.

Specifically, seasonal time-series NDVI was not very sensitive to BRDF impact regarding annual profiles, whereas the main disadvantage of NDVI in monitoring phenology of continental SEA forests was its saturation issue. With long-period saturated values, forest seasonal profiles extracted from NDVI time-series seemed to be unrealistic. In comparison with NDVI, EVI, which was designed for dense vegetation cover analysis, was not saturated in SEA tropical forests but it was sensitive to BRDF impact on the other hand. From our results, higher SZA produced lower EVI and derived phenological metrics were varied. Fixed-SZA EVI showed weaker seasonality regarding seasonal amplitude, while the start and end of the growing seasons were right-shifted (delayed) in comparison with Terra/Aqua EVI.

Different sun-angle configurations also influenced retrieved phenological parameters. While SGS and PGS derived from different fixed-SZA EVI were similar; higher SZA settings yielded stronger seasonality and shorter length of growing season (LGS). Our results provided concrete evidence of BRDF impacts in the retrievals of phenological parameters for tropical forests. Future satellite-based studies of tropical forest phenology are needed to correct for sun-view angles in order to minimise BRDF impacts on retrieved phenological metrics.

Using BRDF-corrected VI data, we found that phenology of SEA forests is dependent on rainfall patterns. Drier forests result in lower EVI during dry seasons and higher EVI during rainy seasons, with evidence for both length of dry season and water deficit criterion. Moreover, the onset of the greening season started earlier at rainforests than at dry tropical forests.

In conclusion, our analyses provided a better understanding of SEA seasonal VI forest phenology related to water availability conditions and BRDF effects. Given the importance of Southeast Asia tropical forest role, our findings might contribute to the accuracy of retrieval forest phenology that can further explore SEA forest fate under the current threat scenarios.

2.6. References

Allen, K., Dupuy, J. M., Gei, M. G., Hulshof, C., Medvigy, D., Pizano, C., … Powers, J. S. (2017). Will seasonally dry tropical forests be sensitive or resistant to future changes in rainfall regimes? *Environmental Research Letters*, *12*(2), 23001. Retrieved from http://stacks.iop.org/1748-9326/12/i=2/a=023001

Bachoo, A., & Archibald, S. (2007). Influence of using date-specific values when extracting phenological metrics from 8-day composite NDVI data. *Proceedings of MultiTemp 2007 - 2007 International Workshop on the Analysis of Multi-Temporal Remote Sensing Images*, 20–23. https://doi.org/10.1109/MULTITEMP.2007.4293044

Beck, P. S. A., Jönsson, P., Høgda, K. -A., Karlsen, S. R., Eklundh, L., & Skidmore, A. K. (2007). A ground-validated NDVI dataset for monitoring vegetation dynamics and mapping phenology in Fennoscandia and the Kola peninsula. *International Journal of Remote Sensing*, *28*(19), 4311–4330. https://doi.org/10.1080/01431160701241936

Bhandari, S., Phinn, S., & Gill, T. (2011). Assessing viewing and illumination geometry effects on the MODIS vegetation index (MOD13Q1) time series: implications for monitoring phenology and disturbances in forest communities in Queensland, Australia. *International Journal of Remote Sensing*, *32*(22), 7513–7538. https://doi.org/10.1080/01431161.2010.524675

Blackie, R., Baldauf, C., Gautier, D., Gumbo, D., Kassa, H., Parthasarathy, N. Paumgarten, F.; Sola, P., … Sunderland, T. C. H. (2014). *Tropical dry forests : The state of global knowledge and recommendations for future Tropical dry forests The state of global knowledge and recommendations*. (March), 30. Retrieved from 10.17528/cifor/004408

Borchers, H. W. (2017). *pracma: Practical Numerical Math Functions*. Retrieved from https://cran.r-project.org/package=pracma

Bradley, B. A., Jacob, R. W., Hermance, J. F., & Mustard, J. F. (2007). A curve fitting procedure to derive inter-annual phenologies from time series of noisy satellite NDVI data. *Remote Sensing of Environment*, *106*(2), 137–145. https://doi.org/10.1016/j.rse.2006.08.002

Bréon, F. M., & Vermote, E. (2012). Correction of MODIS surface reflectance time series for BRDF effects. *Remote Sensing of Environment*, *125*, 1–9. https://doi.org/10.1016/j.rse.2012.06.025

Broich, M., Huete, A., Paget, M., Ma, X., Tulbure, M., Coupe, N. R., … Held, A. (2015). A

spatially explicit land surface phenology data product for science, monitoring and natural resources management applications. *Environmental Modelling and Software*, *64*, 191–204. https://doi.org/10.1016/j.envsoft.2014.11.017

Che, X., Feng, M., Sexton, J. O., Channan, S., Yang, Y., & Sun, Q. (2017). Assessment of MODIS BRDF/albedo model parameters (MCD43A1 Collection 6) for directional reflectance retrieval. *Remote Sensing*, *9*(11), 1–16. https://doi.org/10.3390/rs9111123

Chen, J. M., & Cihlar, J. (1997). A hotspot function in a simple bidirectional reflectance model for satellite application. *Journal of Geophysical Research*, *102*, 907–913.

de Beurs, K. M., & Henebry, G. M. (2010). Spatio-Temporal Statistical Methods for Modelling Land Surface Phenology. In *Phenological Research: Methods for Environmental and Climate Change Analysis* (pp. 177–208). https://doi.org/10.1007/978-90-481-3335-2

Didan, K. (2015a). *MOD13A1 MODIS/Terra Vegetation Indices 16-Day L3 Global 500m SIN Grid V006 [Data set]. NASA EOSDIS LP DAAC*. https://doi.org/10.5067/MODIS/MOD13A1.006

Didan, K. (2015a). *MOD13C2 MODIS/Terra Vegetation Indices Monthly L3 Global 0.05Deg CMG V006*. https://doi.org/10.5067/MODIS/MOD13C2.006

Didan, K. (2015b). *MYD13A1 MODIS/Aqua Vegetation Indices 16-day L3 Global 500m SIN Grid V006*. https://doi.org/10.5067/MODIS/MYD13A1.006

Didan, K. (2015b). *MYD13C2 MODIS/Aqua Vegetation Indices Monthly L3 Global 0.05Deg CMG V006*. https://doi.org/10.5067/MODIS/MYD13C2.006

Didan, K., Munoz, A. B., & Huete, A. (2015). *MODIS Vegetation Index User ' s Guide (MOD13 Series)*. *2015*(June).

Dong, J., Xiao, X., Sheldon, S., Biradar, C., Zhang, G., Duong, N. D., … Moore, B. (2014). A 50-m forest cover map in Southeast Asia from ALOS/PALSAR and its application on forest fragmentation assessment. *PLoS ONE*, *9*(1). https://doi.org/10.1371/journal.pone.0085801

Elias, P., & May-Tobin, C. (2011). Tropical Forest Regions. *Union of Concerned Scientists*, 3–12. https://doi.org/10.1007/BF00351108

Elliott, S., Baker, P. J., & Borchert, R. (2006). Leaf flushing during the dry season: The paradox of Asian monsoon forests. *Global Ecology and Biogeography*, *15*(3), 248–257. https://doi.org/10.1111/j.1466-8238.2006.00213.x

Friedl, M., & Sulla-Menashe, D. (2015). *MCD12C1 MODIS/Terra+Aqua Land Cover Type Yearly L3 Global 0.05Deg CMG V006 [Data set]*. https://doi.org/10.5067/MODIS/MCD12C1.006

Funk, C. C., Peterson, P. J., Landsfeld, M. F., Pedreros, D. H., Verdin, J. P., Rowland, J. D., … Verdin, A. P. (2014). A Quasi-Global Precipitation Time Series for Drought Monitoring. *U.S. Geological Survey Data Series*. https://doi.org/https://dx.doi.org/10.3133/ds832

Funk, C., Peterson, P., Landsfeld, M., Pedreros, D., Verdin, J., Shukla, S., … Michaelsen, J. (2015). The climate hazards infrared precipitation with stations—a new environmental record for monitoring extremes. *Scientific Data*, *2*, 150066. Retrieved from http://dx.doi.org/10.1038/sdata.2015.66

Galvão, L. S., Ponzoni, F. J., Epiphanio, J. C. N., Rudorff, B. F. T., & Formaggio, A. R. (2004). Sun and view angle effects on NDVI determination of land cover types in the Brazilian Amazon region with hyperspectral data. *International Journal of Remote Sensing*, *25*(10), 1861–1879. https://doi.org/10.1080/01431160310001598908

Guan, K., Pan, M., Li, H., Wolf, A., Wu, J., Medvigy, D., … Lyapustin, A. I. (2015). Photosynthetic seasonality of global tropical forests constrained by hydroclimate. *Nature Geoscience*, *8*(4), 284–289. https://doi.org/10.1038/ngeo2382

Hansen, M. C., Potapov, P. V, Moore, R., Hancher, M., Turubanova, S. A., Tyukavina, A., … Townshend, J. R. G. (2013). High-Resolution Global Maps of 21st-Century Forest Cover Change. *Science*, *342*(6160), 850–853. https://doi.org/10.1126/science.1244693

Hermance, J. F., Jacob, R. W., Bradley, B. A., & Mustard, J. F. (2007). Extracting phenological signals from multiyear AVHRR NDVI time series: Framework for applying high-order annual splines with roughness damping. *IEEE Transactions on Geoscience and Remote Sensing*, *45*(10), 3264–3276. https://doi.org/10.1109/TGRS.2007.903044

Hijmans, R. J. (2016). *raster: Geographic Data Analysis and Modeling*. Retrieved from https://cran.r-project.org/package=raster

Hilker, T., Lyapustin, A. I., Hall, F. G., Myneni, R., Knyazikhin, Y., Wang, Y., … Sellers, P. J. (2015). On the measurability of change in Amazon vegetation from MODIS. *Remote Sensing of Environment*, *166*, 233–242. https://doi.org/10.1016/j.rse.2015.05.020

Huete, A., & Justice, C. (1999). Modis Vegetation Index Algorithm Theoretical Basis. *Environmental Sciences*, (Mod 13), 129. https://doi.org/10.1016/j.rse.2007.07.019

Huete, A. R. (1987). Soil and Sun angle interactions on partial canopy spectra. *International*

Journal of Remote Sensing, *8*(9), 1307–1317. https://doi.org/10.1080/01431168708954776

Huete, A. R., HuiQing Liu, & van Leeuwen, W. J. D. (1997). The use of vegetation indices in forested regions: issues of linearity and saturation. *IGARSS'97. 1997 IEEE International Geoscience and Remote Sensing Symposium Proceedings. Remote Sensing - A Scientific Vision for Sustainable Development*, *4*(1), 1966–1968. https://doi.org/10.1109/IGARSS.1997.609169

Huete, A. R., Restrepo-Coupe, N., Ratana, P., Didan, K., Saleska, S. R., Ichii, K., … Gamo, M. (2008). Multiple site tower flux and remote sensing comparisons of tropical forest dynamics in Monsoon Asia. *Agricultural and Forest Meteorology*, *148*(5), 748–760. https://doi.org/10.1016/j.agrformet.2008.01.012

Huete, Didan, K., Miura, T., Rodriguez, E. P., Gao, X., & Ferreira, L. G. (2002). Overview of the radiometric and biophysical performance of the MODIS vegetation indices. *Remote Sensing of Environment*, *83*(1–2), 195–213. https://doi.org/10.1016/S0034-4257(02)00096-2

Huffman, G. J., Bolvin, D. T., Nelkin, E. J., Wolff, D. B., Adler, R. F., Gu, G., … Stocker, E. F. (2007). The TRMM Multisatellite Precipitation Analysis (TMPA): Quasi-Global, Multiyear, Combined-Sensor Precipitation Estimates at Fine Scales. *Journal of Hydrometeorology*, *8*(1), 38–55. https://doi.org/10.1175/JHM560.1

Huffman, G. J., & Pendergrass, A. (2017). The Climate Data Guide: TRMM: Tropical Rainfall Measuring Mission. Retrieved from https://climatedataguide.ucar.edu/climate-data/trmm-tropical-rainfall-measuring-mission

Jeganathan, C., Dash, J., & Atkinson, P. M. (2014). Remotely sensed trends in the phenology of northern high latitude terrestrial vegetation, controlling for land cover change and vegetation type. *Remote Sensing of Environment*, *143*, 154–170. https://doi.org/10.1016/j.rse.2013.11.020

Kaufmann, R. K., Zhou, L., Knyazikhin, Y., Shabanov, V., Myneni, R. B., & Tucker, C. J. (2000). Effect of orbital drift and sensor changes on the time series of AVHRR vegetation index data. *IEEE Transactions on Geoscience and Remote Sensing*, *38*(6), 2584–2597. https://doi.org/10.1109/36.885205

Liang, S., Fang, H., Chen, M., Shuey, C. J., Walthall, C., Daughtry, C., … Strahler, A. (2002). Validating MODIS land surface reflectance and albedo products: Methods and preliminary results. *Remote Sensing of Environment*, *83*(1–2), 149–162. https://doi.org/10.1016/S0034-4257(02)00092-5

Liu, G., Liu, H., & Yin, Y. (2013). Global patterns of NDVI-indicated vegetation extremes and their sensitivity to climate extremes. *Environmental Research Letters*, *8*(2). https://doi.org/10.1088/1748-9326/8/2/025009

Liu, J., Schaaf, C., Strahler, A., Jiao, Z., Shuai, Y., Zhang, Q., … Dutton, E. G. (2009). Validation of moderate resolution imaging spectroradiometer (MODIS) albedo retrieval algorithm: Dependence of albedo on solar zenith angle. *Journal of Geophysical Research Atmospheres*, *114*(1), 1–11. https://doi.org/10.1029/2008JD009969

Los, S. O., North, P. R. J., Grey, W. M. F., & Barnsley, M. J. (2005). A method to convert AVHRR Normalized Difference Vegetation Index time series to a standard viewing and illumination geometry. *Remote Sensing of Environment*, *99*(4), 400–411. https://doi.org/10.1016/j.rse.2005.08.017

Lucht, W., Schaaf, C. B., & Strahler, A. H. (2000). An algorithm for the retrieval of albedo from space using semiempirical BRDF models. *IEEE Transactions on Geoscience and Remote Sensing*, *38*(2), 977–998. https://doi.org/10.1109/36.841980

Maeda, E. E., Heiskanen, J., Aragão, L. E. O. C., & Rinne, J. (2014). Can MODIS EVI monitor ecosystem productivity in the Amazon rainforest? *Geophysical Research Letters*, *41*(20), 7176–7183. https://doi.org/10.1002/2014GL061535

Maignan, F., Bréon, F.-M., & Lacaze, R. (2004). Bidirectional reflectance of Earth targets: evaluation of analytical models using a large set of spaceborne measurements with emphasis on the Hot Spot. *Remote Sensing of Environment*, *90*(2), 210–220. https://doi.org/https://doi.org/10.1016/j.rse.2003.12.006

Middleton, E. M. (1991). Solar zenith angle effects on vegetation indices in tallgrass prairie. *Remote Sensing of Environment*, *38*(1), 45–62. https://doi.org/https://doi.org/10.1016/0034-4257(91)90071-D

Middleton, E. M. (1992). Quantifying reflectance anisotropy of photosynthetically active radiation in grasslands. *Journal of Geophysical Research: Atmospheres*, *97*(D17), 18935–18946. https://doi.org/doi:10.1029/92JD00879

Morton, D. C., Nagol, J., Carabajal, C. C., Rosette, J., Palace, M., Cook, B. D., … North, P. R. J. (2014). Amazon forests maintain consistent canopy structure and greenness during the dry season. *Nature*, *506*(7487), 221–224. https://doi.org/10.1038/nature13006

Moura, Y. M., Galvão, L. S., dos Santos, J. R., Roberts, D. A., & Breunig, F. M. (2012). Use of MISR/Terra data to study intra- and inter-annual EVI variations in the dry season of tropical forest. *Remote Sensing of Environment*, *127*, 260–270.

https://doi.org/https://doi.org/10.1016/j.rse.2012.09.013

Mutanga, O., & Skidmore, A. K. (2004). Narrow band vegetation indices overcome the saturation problem in biomass estimation. *International Journal of Remote Sensing*, *25*(19), 3999–4014. https://doi.org/10.1080/01431160310001654923

Myneni, R. B., Hall, F. G., Sellers, P. J., & Marshak, A. L. (1995). The interpretation of spectral vegetation indices. *IEEE Transactions on Geoscience and Remote Sensing*, *33*(2), 481–486.

Pei-Yu Chen, Gunar Fedosejevs, M. T.-L. and J. G. A. (2006). ASSESSMENT OF MODIS-EVI, MODIS-NDVI AND VEGETATION-NDVI COMPOSITE DATA USING AGRICULTURAL MEASUREMENTS: AN EXAMPLE AT CORN FIELDS IN WESTERN MEXICO. *Environmental Monitoring and Assessment*, *119*(1–3), 69–82. https://doi.org/10.1007/sl0661-005-9006-7

Pennington, R. T., & Ratter, J. A. (2006). *Neotropical Savannas and Seasonally Dry Forests: Plant Diversity, Biogeography, and Conservation*. CRC Press.

Poffenberger, M. (2000). *Communities and Forest Management in South Asia*. IUCN.

R Core Team. (2013). *R: A Language and Environment for Statistical Computing*. Retrieved from http://www.r-project.org/

Reed, B., White, M., & Brown, J. (2003). *Remote Sensing Phenology*.

Rankine, C., Sánchez-Azofeifa, G. A., Guzmán, J. A., Espirito-Santo, M. M., & Sharp, I. (2017). Comparing MODIS and near-surface vegetation indexes for monitoring tropical dry forest phenology along a successional gradient using optical phenology towers. *Environmental Research Letters*, *12*(10). https://doi.org/10.1088/1748-9326/aa838c

Restrepo-Coupe, N., da Rocha, H. R., Hutyra, L. R., da Araujo, A. C., Borma, L. S., Christoffersen, B., … Saleska, S. R. (2013). What drives the seasonality of photosynthesis across the Amazon basin? A cross-site analysis of eddy flux tower measurements from the Brasil flux network. *Agricultural and Forest Meteorology*, *182–183*, 128–144. https://doi.org/10.1016/j.agrformet.2013.04.031

Román, M. O., Schaaf, C. B., Woodcock, C. E., Strahler, A. H., Yang, X., Braswell, R. H., … Wofsy, S. C. (2009). The MODIS (Collection V005) BRDF/albedo product: Assessment of spatial representativeness over forested landscapes. *Remote Sensing of Environment*, *113*(11), 2476–2498. https://doi.org/10.1016/j.rse.2009.07.009

Roujean, J.-L., Leroy, M., & Deschamps, P.-Y. (1992). A bidirectional reflectance model of the

Earth's surface for the correction of remote sensing data. *Journal of Geophysical Research*, *97*(D18), 20455. https://doi.org/10.1029/92JD01411

Rouse, J. W., Hass, R. H., Schell, J. A., & Deering, D. W. (1973). Monitoring vegetation systems in the great plains with ERTS. *Third Earth Resources Technology Satellite (ERTS) Symposium*, *1*, 309–317. https://doi.org/citeulike-article-id:12009708

Saleska, S. R., Wu, J., Guan, K., Araujo, A. C., Huete, A., Nobre, A. D., & Restrepo-Coupe, N. (2016). Dry-season greening of Amazon forests. *Nature*, *531*(7594), E4–E5. Retrieved from http://dx.doi.org/10.1038/nature16457

Samanta, A., Knyazikhin, Y., Xu, L., Dickinson, R. E., Fu, R., Costa, M. H., … Myneni, R. B. (2012). Seasonal changes in leaf area of Amazon forests from leaf flushing and abscission. *Journal of Geophysical Research: Biogeosciences*, *117*(1), 1–13. https://doi.org/10.1029/2011JG001818

Sánchez-Azofeifa, G. A., Quesada, M., Rodríguez, J. P., Nassar, J. M., Stoner, K. E., Castillo, A., … Cuevas-Reyes, P. (2005). Research priorities for neotropical dry forests. *Biotropica*, *37*(4), 477–485. https://doi.org/10.1111/j.1744-7429.2005.00066.x

Schaaf, C. B., Gao, F., Strahler, A. H., Lucht, W., Li, X., Tsang, T., … Roy, D. (2002). First operational BRDF, albedo nadir reflectance products from MODIS. *Remote Sensing of Environment*, *83*(1–2), 135–148. https://doi.org/10.1016/S0034-4257(02)00091-3

Schaaf, C., & Wang, Z. (2015). *MCD43A1 MODIS/Terra+Aqua BRDF/Albedo Model Parameters Daily L3 Global - 500m V006*. NASA EOSDIS Land Processes DAAC.

Short, N. M. (1982). *The Landsat tutorial workbook: basics of satellite remote sensing* (p. viii, 553 p.). p. viii, 553 p. Retrieved from file://catalog.hathitrust.org/Record/011409073

Shukla, S., McNally, A., Husak, G., & Funk, C. (2014). A seasonal agricultural drought forecast system for food-insecure regions of East Africa. *Hydrology and Earth System Sciences*, *18*(10), 3907–3921. https://doi.org/10.5194/hess-18-3907-2014

Sims, D., Rahman, F., Vermote, E., & N. Jiang, Z. (2011). Seasonal and inter-annual variation in view angle effects on MODIS vegetation indices at three forest sites. *Remote Sensing of Environment*, *115*, 3112–3120.

Sombroek, W. (2001). Spatial and Temporal Patterns of Amazon Rainfall: Consequences for the Planning of Agricultural Occupation and the Protection of Primary Forests. *Ambio*, *30*, 388–396.

Sternberg, L. D. S. L. (2001). Savanna-Forest Hysteresis in the Tropics. *Global Ecology and*

Biogeography, *10*(4), 369–378. Retrieved from http://www.jstor.org/stable/2665382

Strahler, A. H., & Muller, J. P. (1999). MODIS BRDF Albedo Product : Algorithm Theoretical Basis Document. *MODIS Product ID: MOD43*, *Version 5*.(April), 1–53. https://doi.org/http://duckwater.bu.edu/lc/mod12q1.html

Sulla-menashe, D., & Friedl, M. A. (2018). *User Guide to Collection 6 MODIS Land Cover (MCD12Q1 and MCD12C1) Product*. (Figure 1), 1–18.

Team, Q. D. (2017). *QGIS Geographic Information System*. Retrieved from http://qgis.osgeo.org

Tottrup, C., Rasmussen, M. S., Eklundh, L., & Jönsson, P. (2007). Mapping fractional forest cover across the highlands of mainland Southeast Asia using MODIS data and regression tree modelling. *International Journal of Remote Sensing*, *28*(1), 23–46. https://doi.org/10.1080/01431160600784218

Tyukavina, A., Hansen, M. C., Potapov, P. V., Krylov, A. M., & Goetz, S. J. (2016). Pan-tropical hinterland forests: Mapping minimally disturbed forests. *Global Ecology and Biogeography*, *25*(2), 151–163. https://doi.org/10.1111/geb.12394

Vermote, E., Justice, C. O., & Breon, F. M. (2009). Towards a Generalized Approach for Correction of the BRDF Effect in MODIS Directional Reflectances. *IEEE Transactions on Geoscience and Remote Sensing*, *47*(3), 898–908. https://doi.org/10.1109/TGRS.2008.2005977

Vicente-Serrano, S. M., Gouveia, C., Camarero, J. J., Begueria, S., Trigo, R., Lopez-Moreno, J. I., … Sanchez-Lorenzo, A. (2013). Response of vegetation to drought time-scales across global land biomes. *Proceedings of the National Academy of Sciences*, *110*(1), 52–57. https://doi.org/10.1073/pnas.1207068110

Wang, Z., Schaaf, C. B., Chopping, M. J., Strahler, A. H., Wang, J., Román, M. O., … Shuai, Y. (2012). Evaluation of Moderate-resolution Imaging Spectroradiometer (MODIS) snow albedo product (MCD43A) over tundra. *Remote Sensing of Environment*, *117*, 264–280. https://doi.org/https://doi.org/10.1016/j.rse.2011.10.002

Wang, Z., Schaaf, C. B., Strahler, A. H., Chopping, M. J., Román, M. O., Shuai, Y., … Fitzjarrald, D. R. (2014). Evaluation of MODIS albedo product (MCD43A) over grassland, agriculture and forest surface types during dormant and snow-covered periods. *Remote Sensing of Environment*, *140*, 60–77. https://doi.org/10.1016/j.rse.2013.08.025

Wickham, H. (2009). *ggplot2: Elegant Graphics for Data Analysis*. Retrieved from

http://ggplot2.org

Zhang, H., Jiao, Z., Dong, Y., & Li, X. (2015). Evaluation of BRDF archetypes for representing surface reflectance anisotropy using MODIS BRDF data. *Remote Sensing*, *7*(6), 7826–7845. https://doi.org/10.3390/rs70607826

Zhang, X., Friedl, M. A., Schaaf, C. B., Strahler, A. H., Hodges, J. C. F., Gao, F., … Huete, A. (2003). Monitoring vegetation phenology using MODIS. *Remote Sensing of Environment*, *84*(3), 471–475. https://doi.org/10.1016/S0034-4257(02)00135-9

Zhang, Y., Zhu, Z., Liu, Z., Zeng, Z., Ciais, P., Huang, M., … Piao, S. (2016). Seasonal and interannual changes in vegetation activity of tropical forests in Southeast Asia. *Agricultural and Forest Meteorology*, *224*, 1–10. https://doi.org/10.1016/j.agrformet.2016.04.009

Zipoli, G., Maracchi, G., & Reginato, R. J. (1987). Influence of topography and sensor view angles on NIR/red ratio and greenness vegetation indices of wheat. *International Journal of Remote Sensing*, *8*(6), 953–957. https://doi.org/10.1080/01431168708948701

Chapter 3. Impact of disturbance and associated BRDF effect on Southeast Asia forest phenology

3.1. Introduction

According to Hansen et al. (2013), the tropics was the only region in the globe that had a significantly positive trend in annual forest loss from 2001 to 2013. As tropical forests have crucial roles in biodiversity, carbon sinks and balancing water cycle on Earth, the deforestation in these regions might cause severe consequences to tropical and global ecosystems.

Satellite remote sensing platforms have become a suitable choice for landscape monitoring and modelling because of their capability in providing extended spatial and temporal resolution observations (Xie, Sha, & Yu, 2008). Remote sensing technologies, integrated with other measurements, offer unique opportunities to study tropical forests (Arturo et al., 2017). In addition, remote sensing was proven useful to investigate tropical forest disturbance, as many previous studies used vegetation indices derived from remotely sensed data to detect and monitor forest disturbance and impact of disturbance on forest phenology (Langner et al., 2018).

Van Leeuwen (2008) illustrated the abrupt decreases in the NDVI time-series of all burned areas after wildfire disturbance in Arizona forests. Setiawan (2014) showed that using MODIS EVI time-series was plausible to separate the dynamic changes of forests caused by deforestation or reforestation in Indonesia. Mildrexler (2007) detected forest disturbance based on distinguishable land surface temperature (LST) and EVI patterns between intact and disturbed forests. Another study by Phompila et al. (2015) revealed that native forests have higher EVI and lower LST than mixed wooded/cleared areas and this characteristic could be used to classify forests and disturbed forests.

In addition, remotely sensed data were applied for monitoring disturbed forest phenology. Cuevas-González *et al.* (2009), using MODIS NDVI time-series to analyse forest regeneration after wildfire disturbance in boreal forests, found that NDVI measurements of burned forests after wildfire disturbance were considerably lower than unburned control sites for both deciduous needle-leaf and evergreen needle-leaf forests.

In contrast, Chen *et al.* (2014) used MODIS NDVI to investigate temporal and spatial features of post-fire forest dynamics in China. He found that NDVI values of burned forests were considerably higher than those of unburned forests and concluded that the growth of young leaves and grasses caused higher productivity and greenness than old leaves from intact forests.

Disturbance might alter the seasonal phenology of forests. Yvonne *et al.* (2006) studied the effects of forest fragmentation on dry tropical forests and found out that disturbed forests started to flower 15-20 days earlier than untouched forests. The probable reason is that these degraded forests have secondary vegetation with no access to deep surface water (Huete *et al.* 2006) and respond faster to first inputs of water than conserved forest covers. A recent study by Martinez (2017) investigated the phenology of disturbed forests in Mexico, and showed similar results, i.e., the start of greening season of degraded forests occurred sooner than of intact forests.

As mentioned in chapters one and two, varying illumination angles and view geometry might influence derived phenological information. Results of chapter two showed a significant impact of BRDF on phenometrics of undisturbed forests, but most studies about forest disturbance have used BRDF-uncorrected reflectance and vegetation indices to conduct their analysis. Compared to undisturbed forests, disturbed forests typically present altered canopy structure. Remote sensing data could capture this change. For example, Langner et al. (2018) used Landsat images to detect canopy changes due to encroachment and selective logging in disturbed areas in SEA.

As anisotropy can be affected by the structure of the Earth's surface, changing canopy of disturbed regions contributes to BRDF impacts on seasonal phenology retrievals of continental Southeast Asia tropical forests. Liu et al. (2009) found that site heterogeneity was one of the significant factors contributing to the disagreement between MODIS albedo and field measurements. Therefore, we should investigate BRDF impact while studying the impact of disturbance on phenology of tropical forests.

Among major domains of tropical forests, tropical forests in mainland Southeast Asia contains a diverse mix of evergreen tropical forests and dry tropical forests. The latter forest type covers about 30 percent of continental SEA forests (Blackie et al., 2014), however, Southeast Asia dry forests are potentially the tropical forests domain that has been most affected by deforestation and degradation due to human activity. A recent study

(Stibig, Achard, Carboni, Raši, & Miettinen, 2014) showed that SEA annually lost 0.67% and 0.59% of its area in the periods 1990-2000 and 2000-2010 respectively. These authors also indicated the deforestation was caused by two primary reasons: forest conversation to crops and non-sustainable logging. Also, tropical forests of Peninsular Southeast Asia seemed to be the most fragmented forest areas in terms of intact forest coverage (Dong et al., 2014).

Undisturbed forest coverage for three major tropical forest regions (Amazon, Central Africa and continental Southeast Asia) derived from the study of Tyukavina *et al.* (2016) is shown in Figure 3.1. The remaining pristine or unaltered tropical forests of Southeast Asia form only small fragments rather than large homogenous areas like Amazon and Africa undisturbed forests. Moreover, there were very few studies focusing on SEA tropical forests, especially on the disturbance effects on forest phenology (Huete et al., 2008). Therefore, it is essential to investigate and compare the phenology of disturbed and intact forests in SEA. The results can improve the current knowledge about the impact of disturbances on forest functioning.

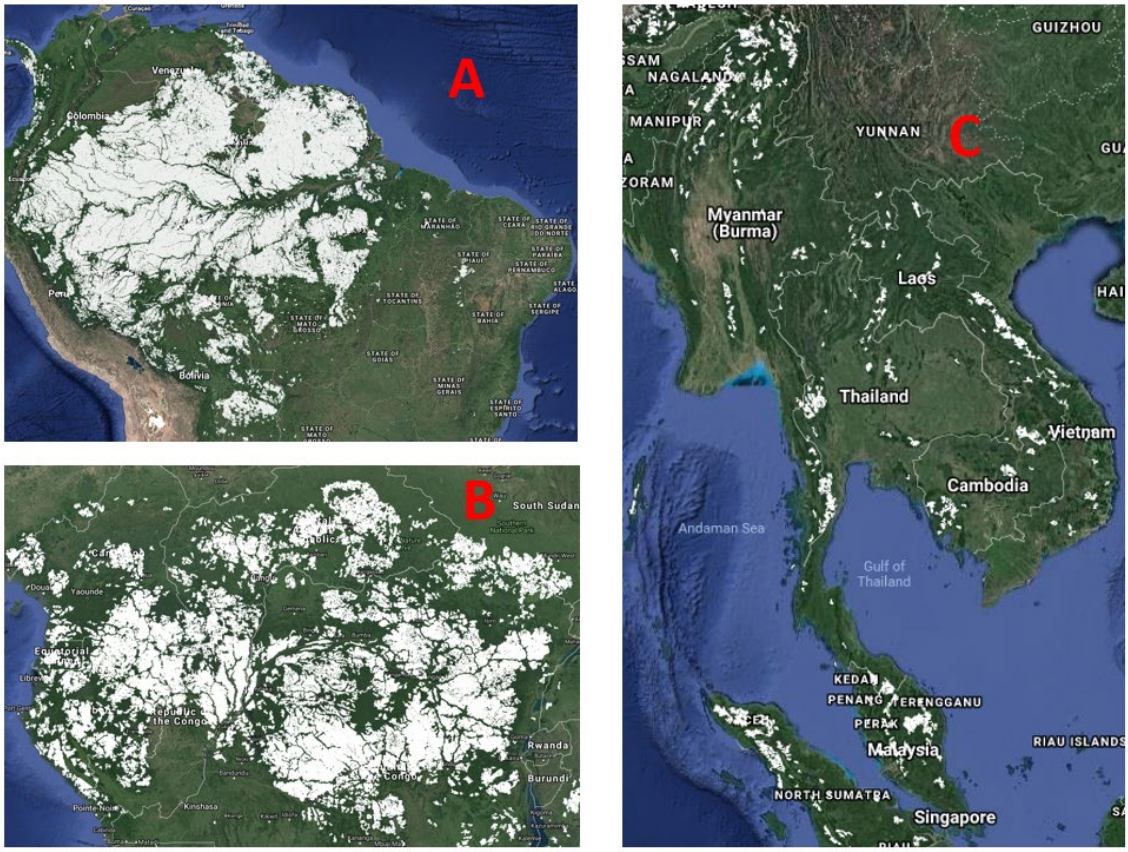

Figure 3.1 *Extent of undisturbed tropical forests for three regions: Amazon (A), Central Africa (B) and Southeast Asia (C). Undisturbed forests are represented as white areas (Images captured from https://earthenginepartners.appspot.com/science-2013-global-forest).*

The primary goal of this chapter is to gain a better understanding of the disturbance contribution to intra-annual forest phenology by comparing seasonal profiles and phenological metrics between disturbed and undisturbed forests. Another purpose of this chapter is to investigate whether BRDF impacts on disturbed and intact forests are different. Specifically, the objectives of this chapter are to (1) assess the impacts of disturbance on phenology of continental SEA forests by investigating the differences of VI time-series and seasonal profiles between disturbed and undisturbed forests; (2) assess BRDF impacts on disturbed VI measurements and whether BRDF influences are similar between disturbed and undisturbed forests and (3) determine whether different sun angle settings influence results when we compare phenology of disturbed and undisturbed forests.

3.2. Methodology

3.2.1. Study areas

SEA forests have been profoundly affected by human activity (Stibig et al., 2014). Its forest coverage is scattered rather than in large patches, and therefore, it is difficult to separate between undisturbed and disturbed forests. We developed a multi-scale approach to accomplish that: firstly, we used the five forest categories of MODIS LCT map at CMG resolution to retrieve forest coverage (Fig. 3.2), which were considered a mix of undisturbed and disturbed forests. Then, we adopted the hinterland or intact forest areas derived by Tyukavina *et al.* (2016) with Landsat data at 30m resolution to extract and separate intact forests.

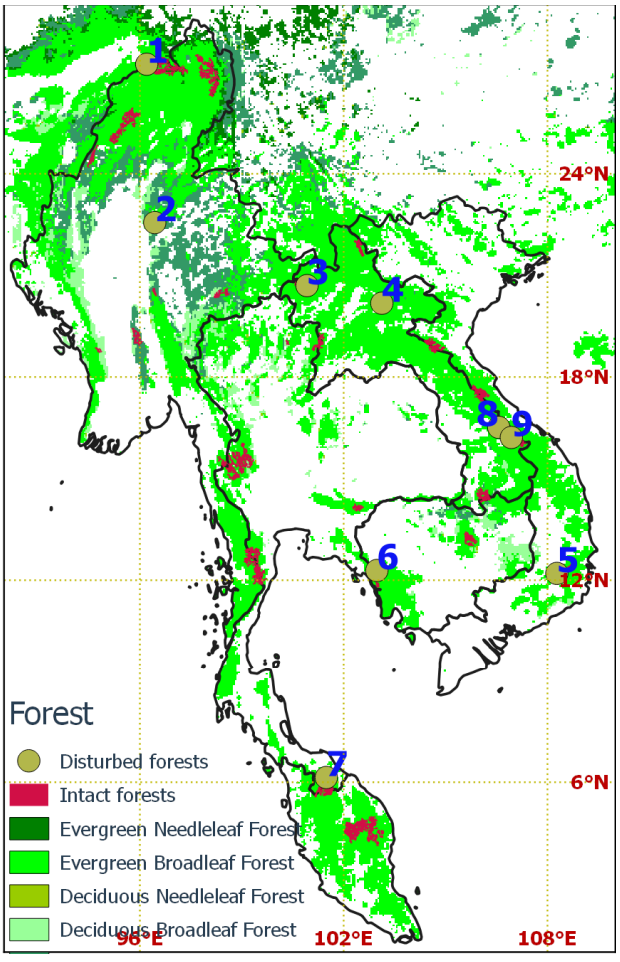

Figure 3.2 *Forest coverage (CMG resolution) represented as green colours, undisturbed sites (30m scale) represented as red areas and disturbed sites (30m scale) represented as yellow points.*

To determine disturbed areas at 30m scale and compare with undisturbed forests at the same spatial resolution, we used forest cover change map (Hansen et al. 2013) to extract disturbed sites adjacent to undisturbed sites. We selected nine sites around continental SEA to conduct our analysis (Locations are shown in Figure 3.2). To extract phenology of disturbed forests, we used a 21x21 MODIS pixels window (10 x 10 km) to retrieve data and then calculate seasonal profiles and phenological metrics. We confirmed that selected disturbed areas were considered forests according to MODIS CMG Land Cover Types.

Figure 3.3 illustrates the window size associated with Hansen's forest loss-year pixels. Hansen's loss-year background pixels present the year when the majority of forest loss happened (Hansen et al., 2013). After visually inspecting Hansen's forest loss map and Google Earth satellite imagery, we had one forest site which was partially converted to other uses, while the other sites experienced forest loss at scattered pixels. Because forest conversion and unsustainable logging are two primary factors causing forest loss in Southeast Asia region, our selected locations seemed to be disturbed by logging as their lost forest areas are represented by scattered points, except that site mentioned above. Another essential characteristic of disturbed sites is that disturbance happened gradually for a long time periods instead of a single event. The continuity of disturbance processes results in complexities in monitoring forest recovery.

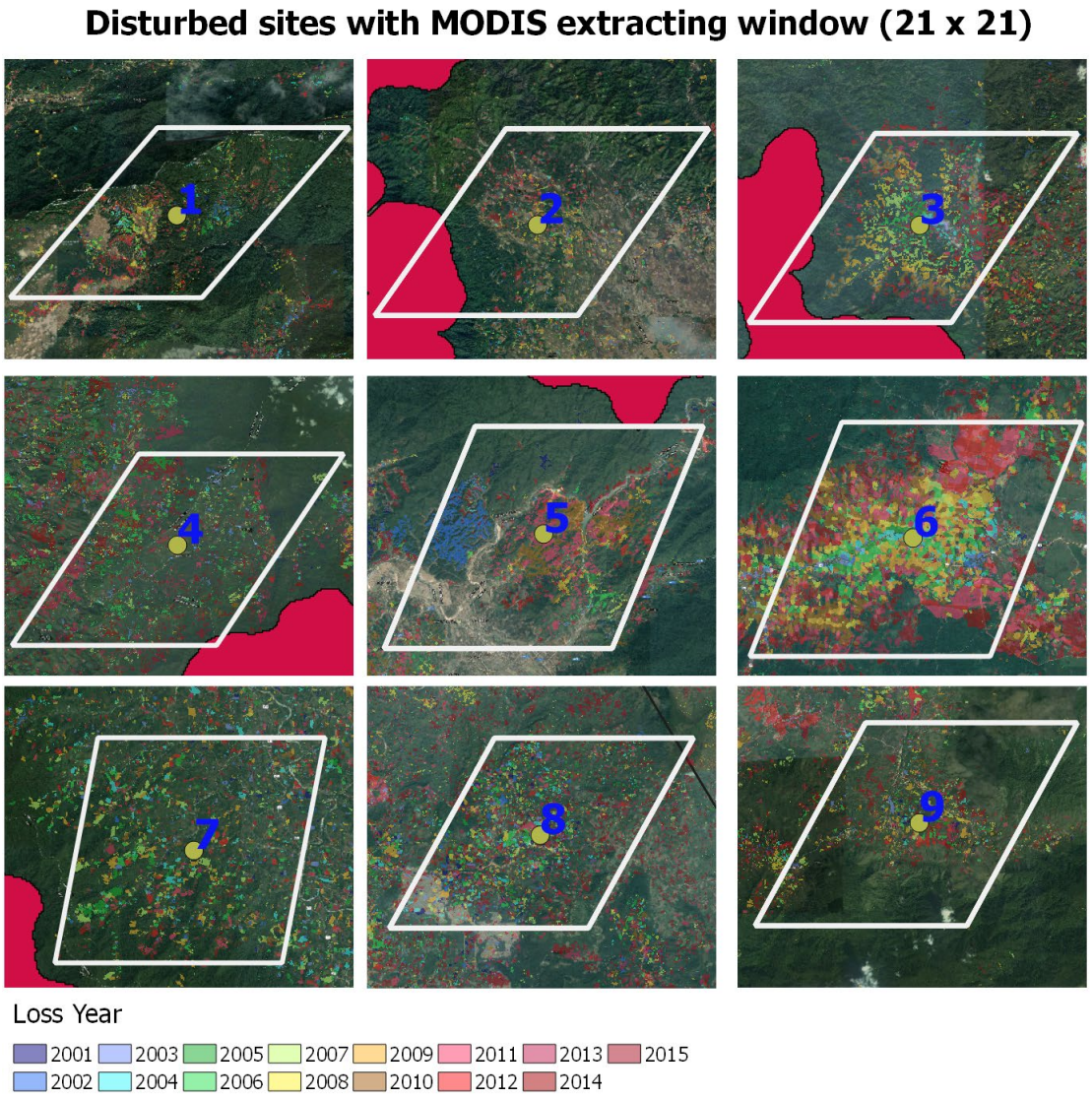

Figure 3.3 *Disturbance sites associated with loss year pixels extracted from Hansen's maps and MODIS extracting window (21 x 21 pixels). Red areas represent neighbour undisturbed forests*

3.2.2. Vegetation Indices

Two common vegetation indices, NDVI and EVI, are widely used as representatives of canopy "greenness", a combined property of green leaf coverage, canopy structure and chlorophyll content of green pigments (Myneni, Hall, Sellers, & Marshak, 1995). These vegetation indices are robust and seamless biophysical measurements used for deriving vegetation phenological parameters at regional to global scale (Broich et al., 2015; de Beurs & Henebry, 2010; Jeganathan, Dash, & Atkinson, 2014; Zhang et al., 2003). While NDVI is a simple indicator used to analyse vegetation dynamic for over 40 years since the first well-known study of Rouse, Hass, Schell, &

Deering (1973), EVI was used as an optimised version of NDVI reducing the impact of soil background and atmospheric noise variations effectively (Huete et al., 2002). The equations defining NDVI and EVI for MODIS data are

$$NDVI = \frac{\rho_{NIR} - \rho_{RED}}{\rho_{NIR} + \rho_{RED}} \quad (2.1)$$

$$EVI = 2.5 \times \frac{\rho_{NIR} - \rho_{RED}}{\rho_{NIR} + 6 \times \rho_{RED} - 7.5 \times \rho_{BLUE} + 1} \quad (2.2)$$

Where ρ_{NIR},ρ_{RED}, and ρ_{BLUE} are atmospherically-corrected surface reflectances at near-infrared (841 – 876nm), red (620 – 670nm), and blue (459 – 479nm) bands of MODIS sensors, respectively.

3.2.3. MODIS datasets

To compare forest phenology between intact and disturbed forests while considering BRDF influences, we used two key MODIS datasets. Firstly, MODIS Vegetation Indices (Terra and Aqua) products were used to derive time-series and phenological information for both undisturbed and disturbed forests at 500m and 0.05degree spatial resolutions and 16-day intervals (Didan, 2015a, 2015b, 2015c, 2015d). To balance between maximising data availability and retaining data quality, we chose the acceptable quality level (useful – 1) and removed all cloudy values (Didan, Munoz, & Huete, 2015).

Secondly, we generated standardised surface reflectances and VIs from MODIS BRDF/Albedo Model Parameters products (C. Schaaf & Wang, 2015a), which supplies the BRDF weighting parameters that describe the anisotropy of each 500m/0.05degree pixel on a daily basis (Schaaf & Wang, 2015b, 2015a; Schaaf et al., 2002; Schaaf, Liu, Gao, & Strahler, 2011; Wang et al., 2012; Wanner et al., 1997). From the BRDF parameters of each land surface pixel, directional reflectance could be calculated by input of desired sun-view configurations. View zenith angle (VZA) was normalised to zero and solar zenith angle (SZA) was fixed at 0º, 15º, 30º, and 45º degrees (termed as SZ0, SZ15, SZ30 and SZ45 respectively) to capture the broadest possible ranges of SZA over the Southeast Asia region.

MODIS BRDF/Albedo products support two quality levels: full inversion with highest quality level and magnitude inversion generated with support of a database of

archetypal BRDF parameters (Strahler & Muller, 1999; Strugnell, Lucht, Hyman, & Meister, 1998; Strugnell, Wolfgang, & Crystal, 2001). As data availability is limited in the wet season of tropical regions, we set the QC level to magnitude inversion level to avoid long-periods of missing data.

3.2.4. Extraction of phenological parameters

This research adopted thresholds based on ratio VIs (R Reed, White, & Brown, 2003) to extract meaningful phenological parameters from MODIS smoothed time-series, and to investigate BRDF impact on retrieved information. These parameters are important indicators of SEA forests seasonal dynamics, and can be defined as:

- Start of Greening Season (SGS): the beginning date of growing season or the onset of photosynthesis activity (Rankine, Sánchez-Azofeifa, Guzmán, Espirito-Santo, & Sharp, 2017). It was defined as when vegetation indices reach the values equal to the minimum values before the growing season plus 20% of seasonal amplitude during green-up phrase
- Peak of Greening Season (PGS): the date of maximum vegetation productivity for forest vegetation assemblage
- End of Greening Season (EGS): the end date of growing season. EGS was determined as when VI crosses the value equal to the minimum value plus 20% of amplitude during brown down phase
- Dormancy Timing (DT): the timing when VI measurements reach the bottom value (Rankine et al., 2017)
- Length of Greening Season (LGS): duration of growing season, defined as the differences between EGS and SGS
- Amplitude of Greening Season (AGS): the amplitude of greening seasonality, determined as the difference between minimum and maximum productivity of vegetation
- Maximum (MAX): the maximum measurement of vegetation index
- Minimum (MIN): the minimum measurement of vegetation index

We use these metrics to investigate SEA forest phenology and assess how BRDF might influence these parameters. While MODIS BRDF/Albedo parameters are daily estimates, MODIS Terra/Aqua Vegetation Indices are provided at 16-day interval data

only. Thus, we interpolated standard 16-day VI time-series to day-to-day data and derived phenological metrics from that interpolated estimation.

3.2.5. Analyses

We calculated seasonal BRDF-uncorrected and –corrected VI profiles for undisturbed forests at 500m resolution and forested areas derived from the CMG (0.05degree resolution) dataset. As we considered CMG forest areas a mix of both undisturbed and disturbed patches, the comparison of seasonal VI profiles between undisturbed and mixed forests provided an overview about disturbance influence on phenology of continental SEA tropical forests. Subsequently, we classified forests into different types based on the length of dry season derived from CHIRPS rainfall dataset (Funk et al., 2015), and analysed the impact of disturbance and BRDF effect on the different forest types.

We also used our selected disturbed sites to compare VI time-series and seasonal profiles of disturbed and undisturbed forests at the 500m spatial resolution. Additionally, we used Hansen's map, which provided a forest loss-year map representing forest loss detected during the 2001 – 2016 period to calculate annual forest loss percentages at each disturbed site.

VI time-series from the disturbed sites at the most disturbed period were retrieved to compare with VI time-series at the beginning of our study period (2001-2003) and with coupled undisturbed sites. We expected that results from this analysis would confirm the findings resulting from the comparison between undisturbed forests and CMG forest areas. The cross-site correlation between undisturbed and disturbed forests at the most disturbed time was also produced to further investigate impact of disturbance and BRDF effect on forest phenology.

3.3. Results

3.3.1. Southeast Asia forest loss from 2001 to 2016

To understand forest loss in Southeast Asia between 2001 to 2016, we used two datasets: forest cover change map derived by Hansen and MODIS Land Cover Type map (product MCD12C1). Figure 3.4 shows changes of forest cover in continental Southeast Asia from 2000 to 2016. In the year 2000, forests mainly covered Peninsular Malaysia,

South Thailand, Laos and West Myanmar (Fig 3.4A). For 16 years, only a limited portion of Malaysia and Northeast Thailand experienced forest gain (Fig 3.4B), while forest loss happened significantly in many regions, especially in Malaysia, Cambodia and Laos. The other countries in SEA experienced less forest loss during the 2000-2016 period.

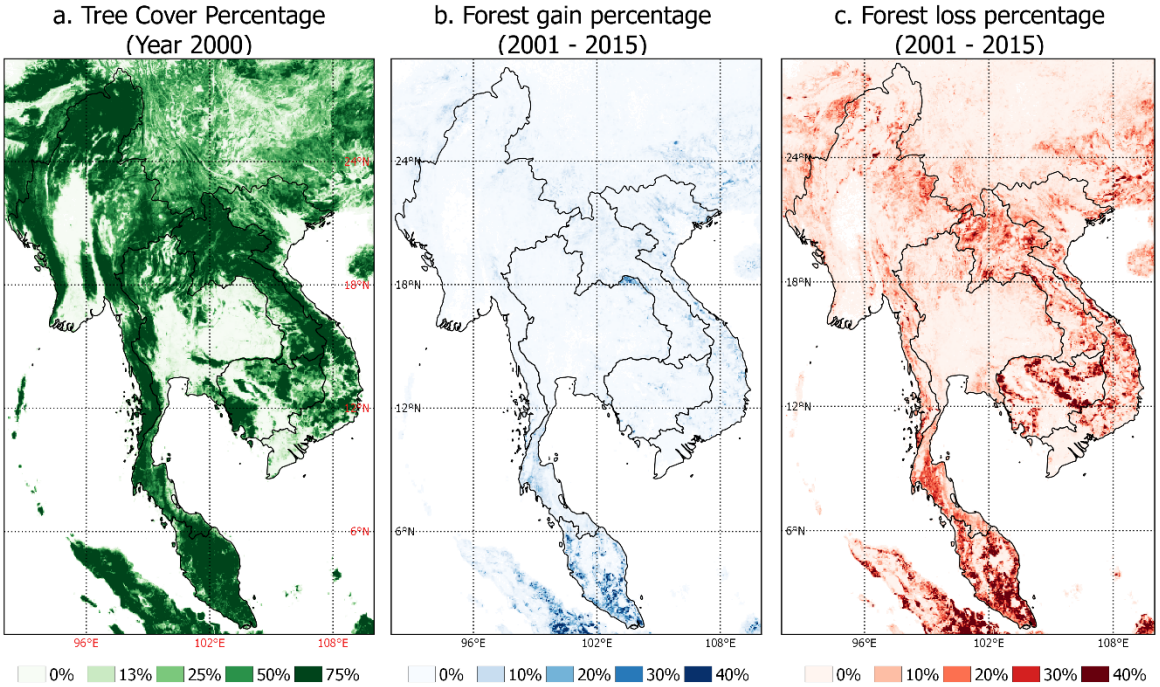

Figure 3.4 *Forest cover change maps (2001 - 2016) derived from Hansen's maps. According to Hansen's criteria, lands with more than 25% of tree cover were considered forests; forest gain/loss maps show the percentage of forest gain or loss during the study period (2001 – 2016).*

In the other hand, MODIS Land Cover Type products presented annual land cover type information and does not focus on forest cover change. The results in Figure 3.5 show that a large proportion of Southeast Asia forests retained their forests class after 16 years, while Hansen's map shows widespread forest loss across the whole SEA continent. Changes of forest coverage derived from MCD12C1 datasets presented major forest loss occurring in Cambodia, but also significant forest disappearance happening in Malaysia and Laos. In Myanmar, there was a mix of forest loss and changes in forest type together. Results from MCD12C1 product and Hansen's maps suggest that forests might experience disturbance and partial loss of canopy cover while they maintain their forest status in the Land Cover Type maps.

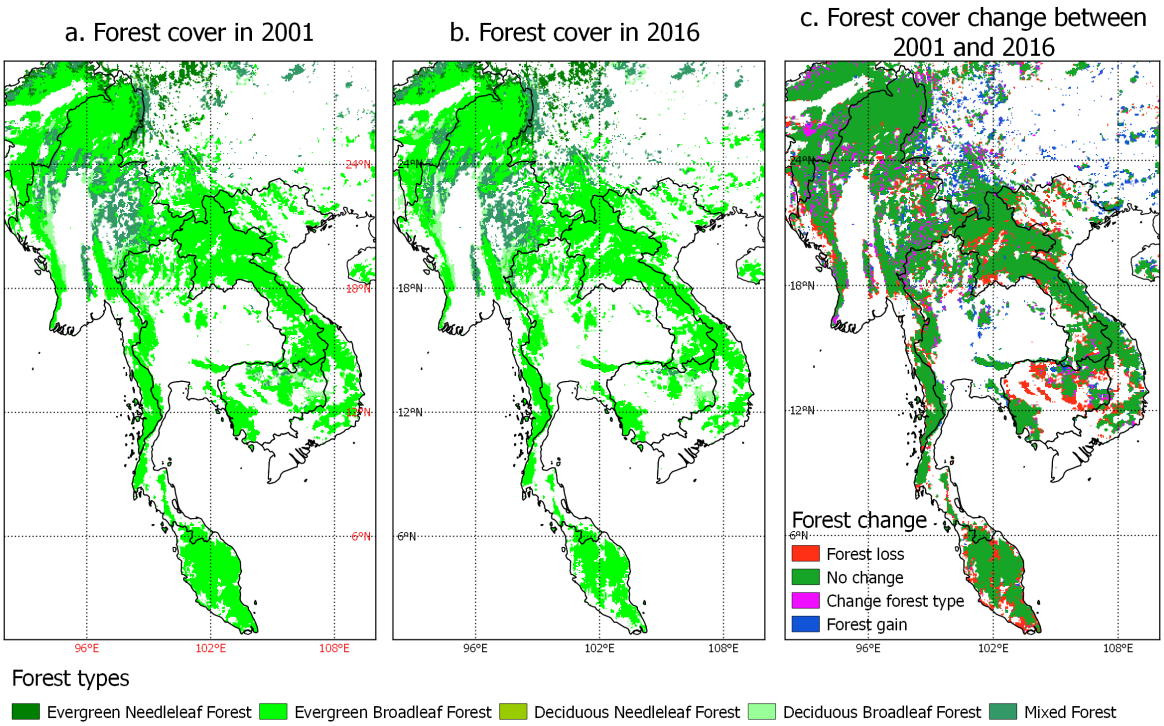

Figure 3.5 *Forest cover changes between 2001 and 2016 extracted from MCD12C1 data.*

3.3.2. Forest phenology of undisturbed and mixed forests of the entire Southeast Asia

We observed the seasonal VI profiles of undisturbed forests and forests represented by MODIS Land Cover Maps (EVI in Fig. 3.6 and NDVI in Fig. 3.7). Forest pixels retrieved from MODIS CMG LCT map represented a mix of intact and disturbed forests because of its coarse resolution. Seasonal BRDF-uncorrected EVI profiles revealed that disturbed forests with long dry season (6-7 months) had stronger seasonality than undisturbed forests (Fig. 3.6B and 3.6C). EVI values of those disturbed forests were lower in late dry season and higher in wet seasons than in intact forests. In regards to the wet forests with the shortest dry season (0-2 months), EVI of forests with disturbance were generally equal or lower than undisturbed forests, but in general followed the same seasonal pattern.

In contrast, BRDF-corrected EVI profiles of wet forests illustrate that intact forests had consistently lower EVI than disturbed forests (Fig. 3.6A). In addition, the EVI differences of drier forests between disturbed and undisturbed types were marginal in the wet season, but more pronounced in the dry season. Annual EVI measurements also indicate changes in phenophase metrics. For example, disturbed forests with 3-5 months

of dry season started the greening season after intact forests with the same length of dry season (blue EVI lines). These findings suggest that forest disturbance might be altering phenological metrics of SEA tropical forests.

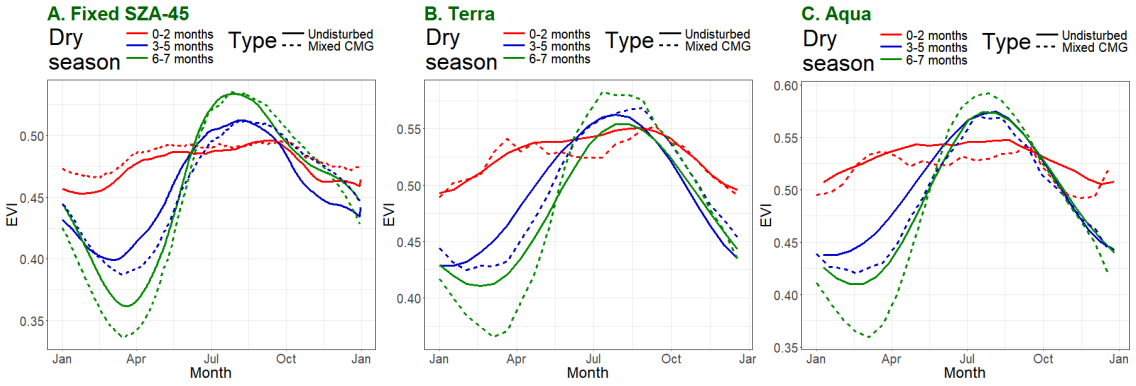

Figure 3.6 *Seasonal EVI profiles of SEA forests for undisturbed forests (500m resolution) and mixed forests at CMG resolution with different lengths of dry season.*

Annual NDVI profiles of SEA tropical forests showed that NDVI of disturbed forests were lower than undisturbed forests in all cases (BRDF-corrected and –uncorrected, all dry season lenghts). Moreover, the relationship between disturbed and undisturbed forests was identical with or without BRDF correction. Another important finding is that the NDVI differences between disturbed and undisturbed forests were higher than EVI differences (0.06 – 0.08 for NDVI and 0.01 – 0.05 for EVI). This result suggests that NDVI is a better choice to detect or map disturbed forest areas based on phenological behavior.

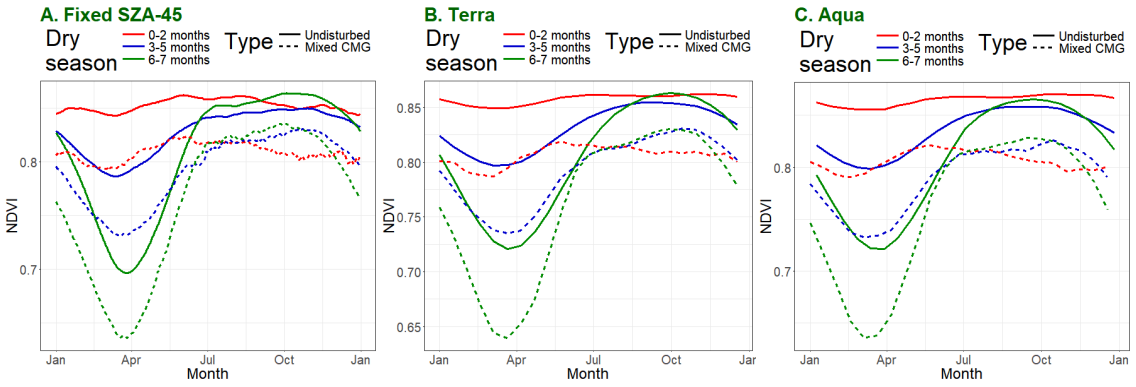

Figure 3.7 *Seasonal NDVI profiles of SEA forests for undisturbed forests (500m resolution) and mixed forests at CMG resolution with different lengths of dry season.*

3.3.3. Impact of disturbance on VI for disturbed and undisturbed forests associated with BRDF influences at 500m resolution

3.3.3.1. Time-series comparison of disturbed and undisturbed forests

To understand how disturbance influences forest VIs, we observed time-series from three coupled sites representing forests with various lengths of dry season (Figure 3.8). The relationship of VI time-series between undisturbed and disturbed forests varied across different sites. For example, EVI time-series of the wet forest site showed that disturbed EVI was higher than undisturbed EVI during our entire study period, while NDVI time-series was undistinguishable and likely contaminated because of NDVI saturation and cloud issues (Fig 3.8A). The result indicates that the disturbed site might have experienced disturbances before 2001.

For coupled sites with four-months dry season, VI time-series of the disturbed and undisturbed sites were similar during the 2001–2003 period, but the patterns of the disturbed site changed later with disturbance (Fig. 3.8B). At the end of our study period, NDVI of the disturbed site was lower and presented stronger seasonality, especially after the peak of forests loss in 2010-2012, while minimum EVI was lower and maximum EVI was higher than EVI from the undisturbed site.

In contrast, the disturbed site with six-month dry season (Fig. 3.8C) showed marginal VI differences between undisturbed and disturbed sites at the end of study period, even though there were significant NDVI decreases with BRDF correction. This result suggests that these disturbed forests recovered its greenness after disturbance quickly, and a potential explanation for these different responses is the disturbance intensity, as site 3 had a smaller degree of forest loss than the site 2.

Regarding BRDF impact on VI time-series and interplay with disturbance, NDVI of disturbed sites showed larger BRDF sensitivity, as BRDF-corrected NDVI dropped to much lower values than BRDF-uncorrected NDVI in many years, while the differences for undisturbed forests were minor. This result indicates that the heterogeneity in canopy structure caused by disturbance might be interacting differently with BRDF at different disturbance levels and lengths of dry season. .

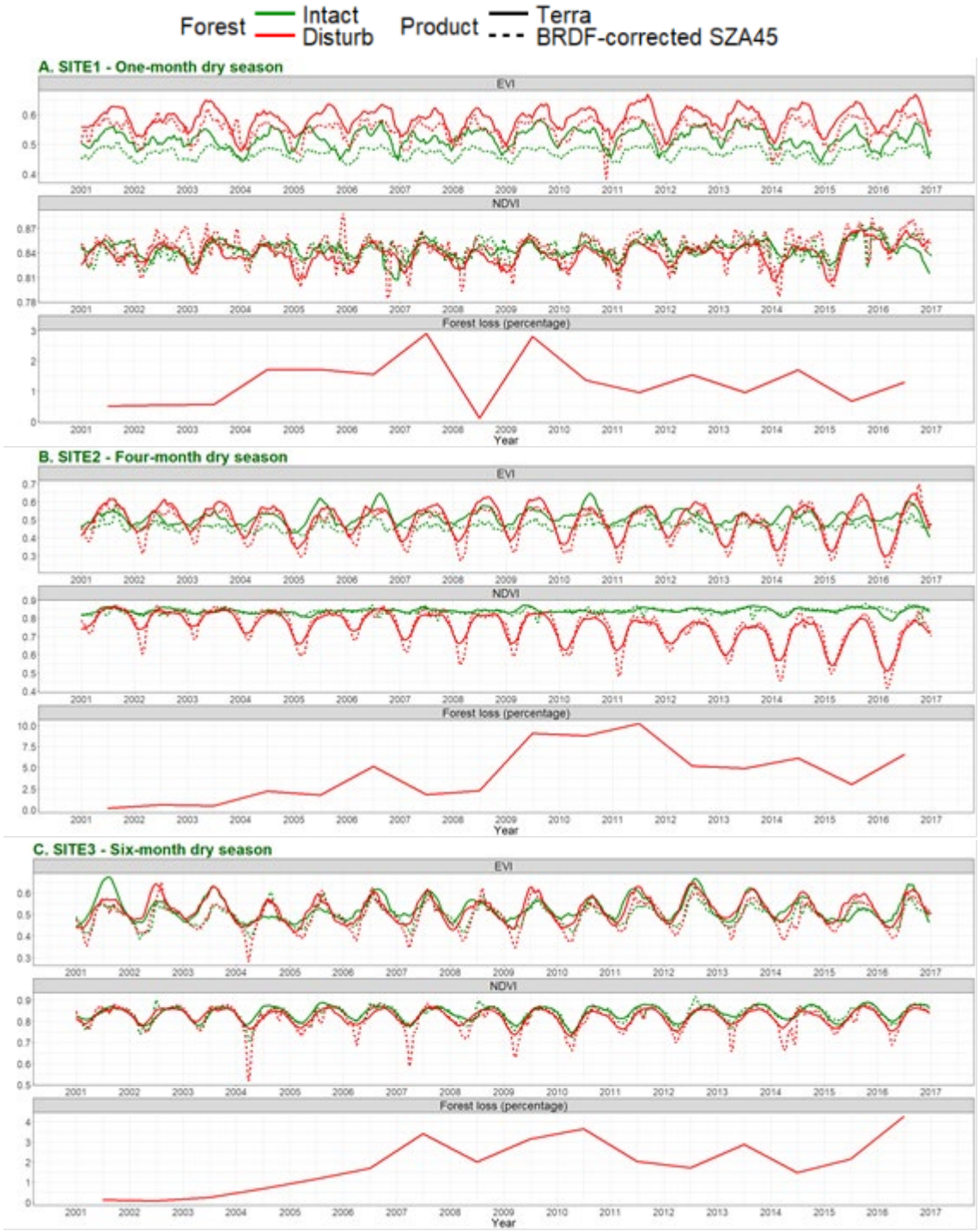

Figure 3.8 *VI time-series and percentage of forest loss of coupled disturbed and undisturbed forests during our study period (2001 – 2016). Annual percentage of forest loss was obtained from Hansen's forest loss map. Forest sites represent different lengths of dry season: A) One month, B) Four months, and C) Six months*

3.3.3.2. Seasonal VI profiles of disturbed sites for the least and most disturbed periods

To further analyse the impact of disturbance events on forest phenology, we observed seasonal VI profiles of three sample disturbed sites between two distinct periods: first three years of our study period (2001-2003), because all the three sites presented nearly zero forest loss in these years, and the most disturbed time period based on annual percentage losses (Figure 3.9). The most disturbed time period of site 1-3 were 2007-2009, 2009-2011 and 2007-2009 periods respectively. Our results revealed that disturbance caused changes in forest phenology with lower VI values during the most disturbed time period compared with the initial 2001-2003 period. However, the differences also varied across sites. For example, the gap was marginal with the wet forest site (Fig. 3.9A) but it was significant with drier sites (Fig. 3.9B and 3.9C). In the comparison between NDVI and EVI differences, NDVI variations between different times of the year were higher than EVI variation.

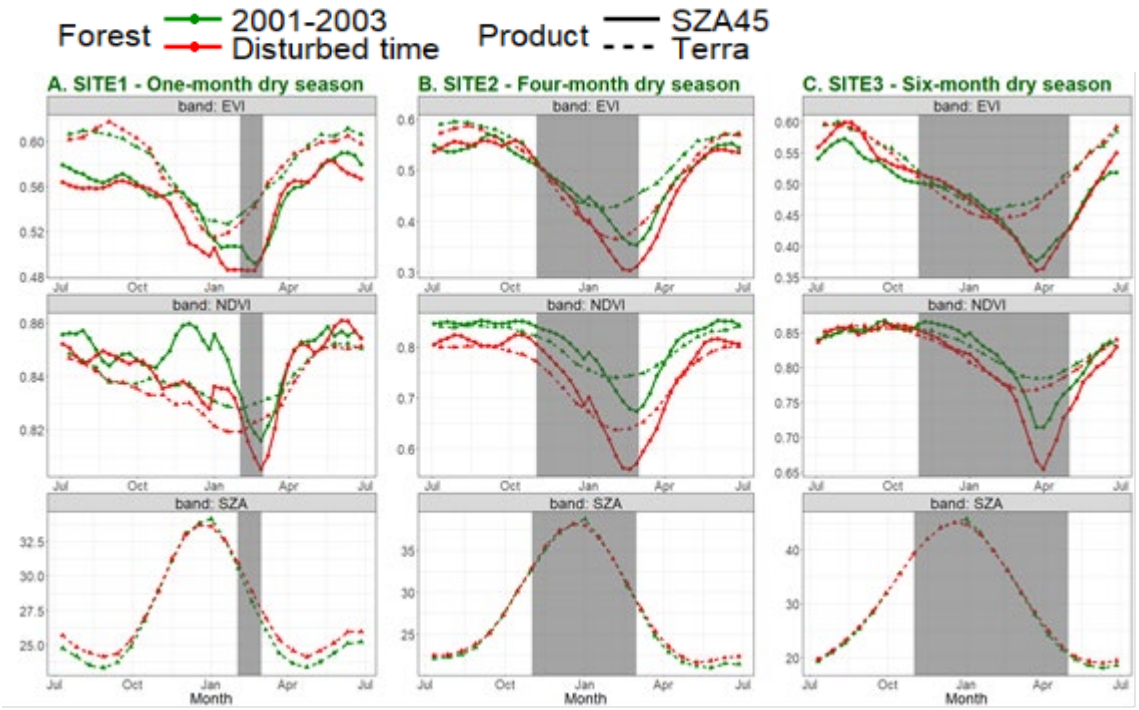

Figure 3.9 *Seasonal VI profiles for disturbed sites between 2001-2003 period and three consecutive years with the greatest level of disturbance based on annual percentage of forest loss. Grey areas represent the dry season.*

In constrast with undisturbed forests, NDVI of disturbed forests exhibited the considerable sensitivity to BRDF impacts. BRDF-corrected NDVI decreased much more than BRDF-uncorrected NDVI during the late dry season. As forest loss is considered the main cause of changes in forest canopy structure, our findings suggest that NDVI robustness to BRDF influence might decrease over heterogeneously vegetated areas.

3.3.3.3. Seasonal profiles of intact and disturbed forests at the most disturbing period

We observed the seasonal VI profiles from undisturbed and disturbed forests at the most disturbing period to investigate VI differences between intact and disturbed forests at 500m resolution (Fig. 3.10). In general, annual NDVI time-series of disturbed forests was lower than of intact forests, except for the rainforest site (one-month dry season). NDVI of disturbed sites tended to match with NDVI of intact forests in wet periods while disturbed NDVI measurements were much lower at the end of dry season. The comparison between BDRF-corrected and -uncorrected NDVI confirmed that NDVI of disturbed forests were sensitive to BRDF influences at the end of the dry season, while NDVI of intact forests was not. In the case of site 3 (six-month dry season), BRDF correction helped to distinguish between undisturbed and disturbed forests in the dry season while BRDF-uncorrected NDVI of the two disturbance categories were identical (Fig. 3.10C).

The comparison of seasonal EVI profiles illustrates different outcomes. At the wet sites, EVI of the disturbed forest was higher than the adjacent undisturbed forest (Fig. 3.10A). In contrast, EVI of disturbed forests was lower at dry season and tended to be higher during wet seasons for the dry tropical forest sites (Fig. 3.10B and 3.10C). These results are well correlated with results of section 3.3.2 as impact of disturbance is similar.

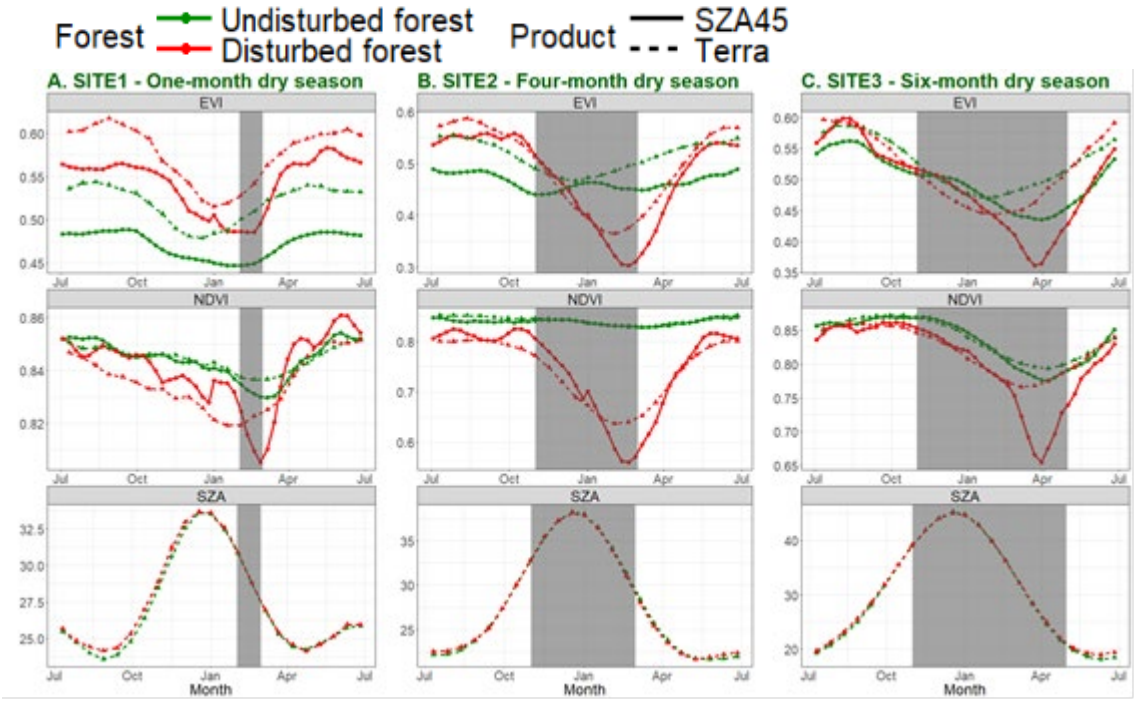

Figure 3.10 *Seasonal VI of disturbed and undisturbed vegetation indices of the three coupled-sites with different dry-season lengths: A) One-month dry-season. B) Four-month dry season C) Six-month dry season. Grey areas represent the dry season.*

3.3.3.4. Comparison of phenological metrics between disturbed and undisturbed forests

We used cross-site correlation plots to compare phenological metrics between disturbed forests and undisturbed forests for the period of maximum disturbance period (EVI in Fig. 3.11 and NDVI in Fig. 3.12). Disturbed forests tended to start their growing season (SGS) later than undisturbed forests (Fig. 3.11A). This delayed start of the greening season possibly indicated a slower response of forests to rain events due to disturbance impact.

The end of growing season (EGS) of disturbed sites also occurred after EGS of undisturbed sites (Figure 3.11C). Correlations of another metric, peak of growing season (PGS), show inconsistent relationships between intact and disturbed sites for EVI_{SZ45}, EVI_{Terra} or EVI_{Aqua} (Fig. 3.11B). The correlated plot of LGS (Fig 3.11E) showed mixed relationships between intact and disturbed forests.

Regarding absolute values of dormancy and maturing, minimum EVI values of disturbed forests were lower than that those of undistubred sites (Fig 3.11H) while

maximum EVI values of disturbed forest were higher than for intact forests (Fig. 3.11G). Consequently, seasonal amplitudes (AMP) of disturbed forests were significantly greater than intact forests (Fig. 3.11F).

Compared to EVI, SGS dates derived from NDVI time-series were identical between intact and disturbed forests (Fig. 3.12A). Regarding derived EGS, there were different relations of disturbed and intact sites among NDVI products (Fig. 3.12C). While EGS of disturbed forests derived from $NDVI_{Terra}$ and $NDVI_{SZ45}$ tended to occur earlier than that of intact forests, the same metric of disturbed sites extracted from $NDVI_{Aqua}$ had no clear earlier or later timing compared to intact forests.

In regards to differences in annual changes (AMP) between the two forest types, amplitudes of intact forests were smaller than amplitudes of disturbed forests. This difference was mainly caused by lower minimum NDVI of disturbed forests (less green foliage), because the correlated plot of maximum NDVI shows this index saturation issues with the small range of maximum values (0.81 – 0.88).

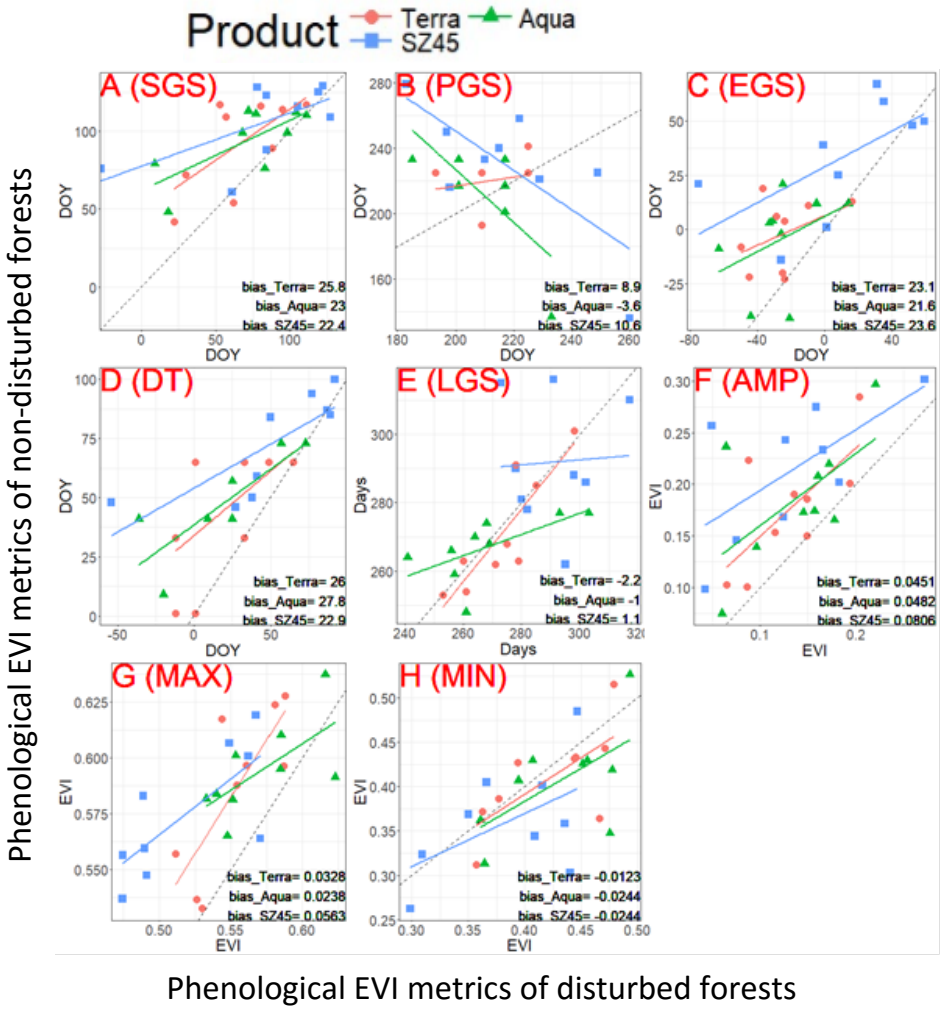

Figure 3.11 *Comparisons of EVI phenological metrics between disturbed and undisturbed forests at the most disturbing period. A) Start of Greening Season (SGS). B) Peak of Greening Season (PGS). C) End of Greening Season (EGS). D) Dormancy Timing (DT). E) Length of Greening Season (LGS). F) Seasonal amplitude (AMP). G) Maximum (Peak) value. H) Minimum (Dormant) value.*

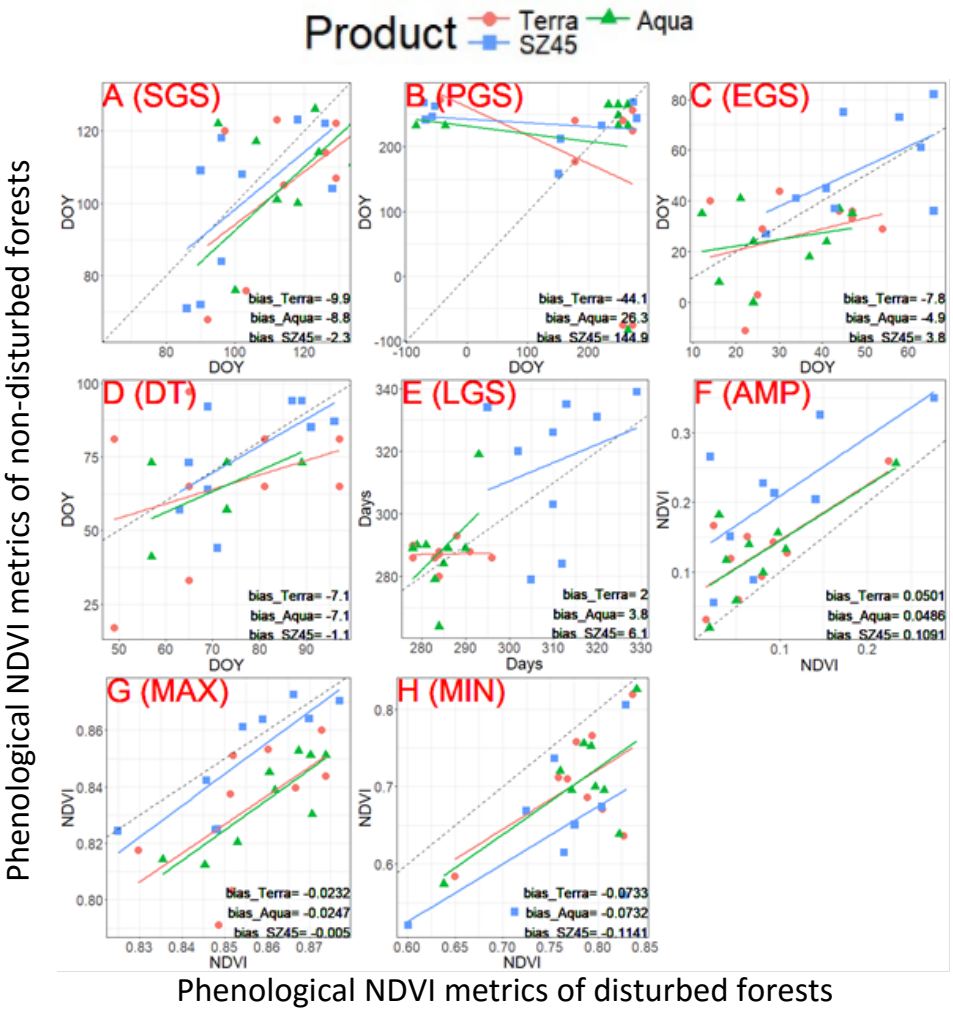

Figure 3.12 *Comparisons of NDVI phenological metrics between disturbed and undisturbed forests at the most disturbing period. A) Start of Greening Season (SGS). B) Peak of Greening Season (PGS). C) End of Greening Season (EGS). D) Dormancy Timing (DT). E) Length of Greening Season (LGS). F) Seasonal amplitude (AMP). G) Maximum (Peak) value. H) Minimum (Dormant) value.*

3.3.3.5. Impact of geometry settings on phenology metrics of intact and disturbed forests

The correlation plots of phenological parameters from disturbed and undisturbed forests with various sun angle configurations provide an opportunity to explore the potential impact of common sun-view angle settings on phenological differences between disturbed and intact forest types (Figure 3.14 for EVI and Figure 3.14 for NDVI). In general, varying SZA selections in EVI metrics yielded similar differences in phenophase metrics between the two forest types, as the shifting days (bias values) are no greater than three days. Specifically, averaged date differences of SGS and EGS are less than one day whereas timings of PGS and DT are shifted up to 3 days. These variations are minor and indicate that influences of varying sun-view settings on differences between the two forest categories are insignificant.

Also, discrepancies of seasonal amplitude (AMP) are less influenced by the variability of SZA. The maximum bias of SZA-0 setting is just 0.01 in comparing SZA-0 and SZA-45 settings. However, the effect of sun angle choice is considerable with the differences of maximum and minimum values. Smaller SZA settings caused maximum and minimum differences of disturbed and undisturbed forests lower than higher SZA settings, which were lower than at larger SZA settings, with highest absolute biases of 0.043 and 0.033 for minimum and maximum EVI, respectively. These variations might change the relationship between undisturbed and disturbed forests. For example, minimum EVI values of eight out of nine disturbed sites were lower than undisturbed forests with SZA fixed at 0 degrees whereas minimum EVI values of four disturbed sites are higher than undisturbed forests with SZA fixed at 45 degrees.

Contrasting with EVI, the impact of different fixed geometries on metrics related to NDVI values were insignificant. Highest absolute bias value is only 0.02, and various sun-view settings do not alter the relationships between undisturbed and disturbed forests (Fig. 3.15). Influences of different geometries on NDVI differences are also minimal as the highest shift of phenophase date was only five days.

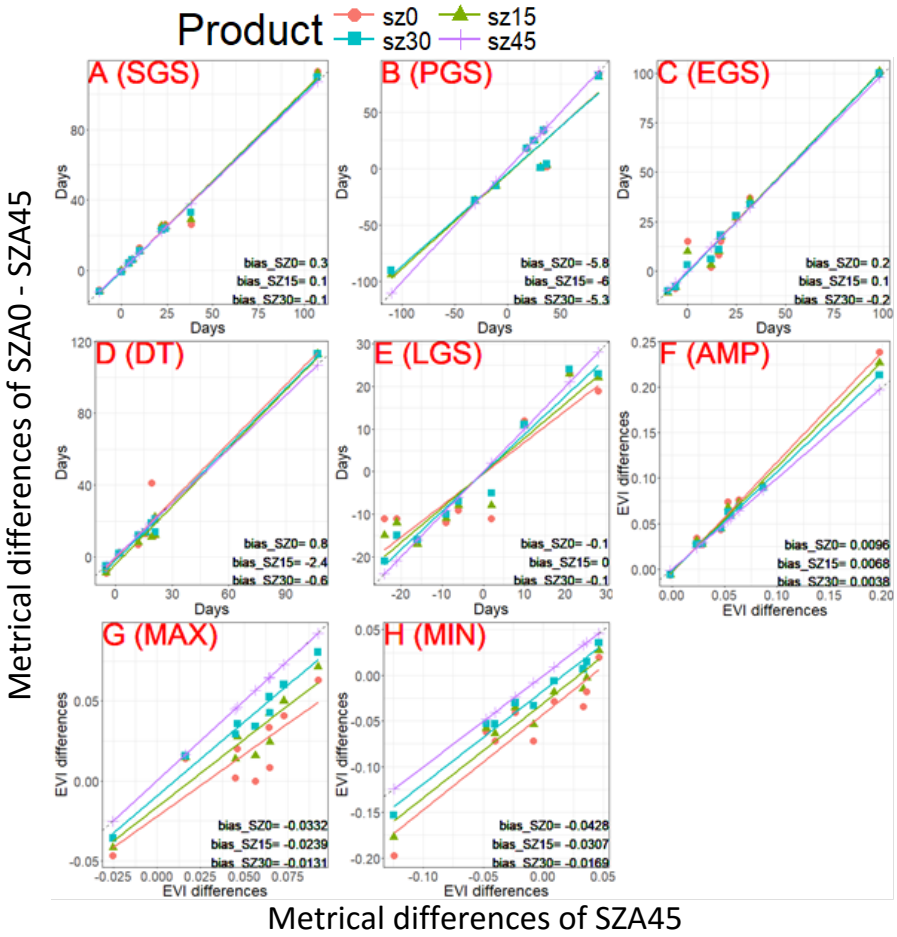

Figure 3.13 *Cross-site correlation plots of the differences in phenological metrics derived from disturbed and undisturbed forests EVI time-series between with various illumination and viewing geometries. A) Start of Greening Season (SGS). B) Peak of Greening Season (PGS). C) End of Greening Season (EGS). D) Dormancy Timing (DT). E) Length of Greening Season (LGS). F) Seasonal amplitude (AMP). G) Maximum (Peak) value. H) Minimum (Dormant) value.*

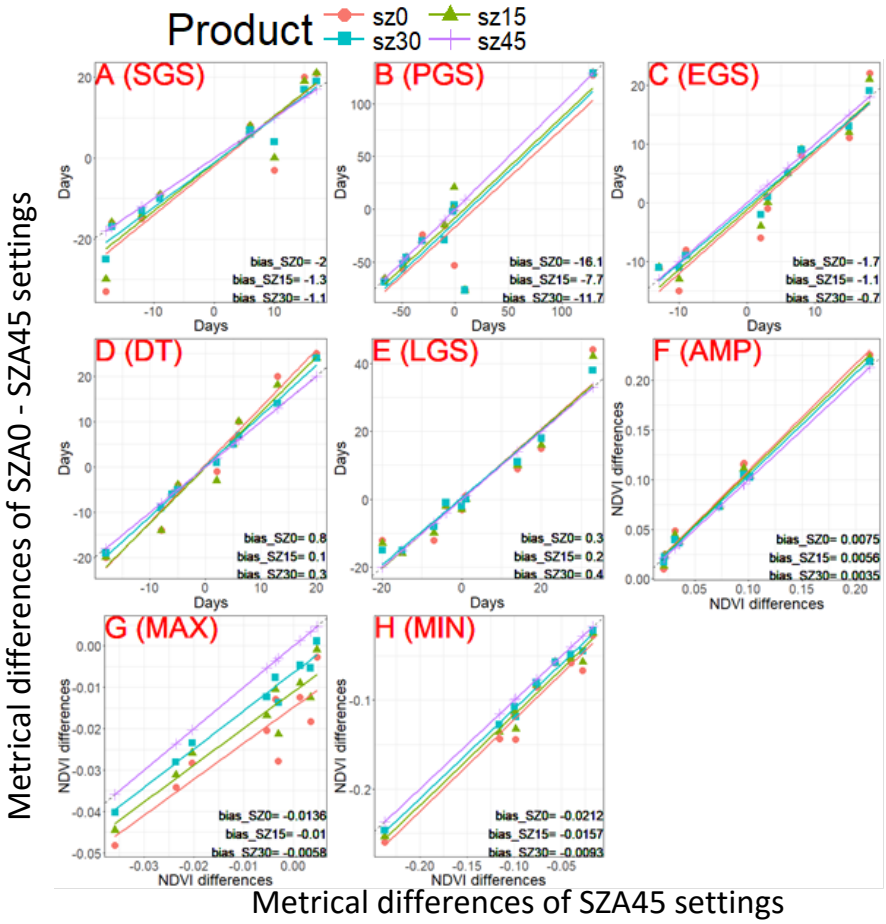

Figure 3.14 *Cross-site correlation plots of differences in phenological metrics derived from disturbed and undisturbed forests NDVI time-series with various illumination and viewing geometries. A) Start of Greening Season (SGS). B) Peak of Greening Season (PGS). C) End of Greening Season (EGS). D) Dormancy Timing (DT). E) Length of Greening Season (LGS). F) Seasonal amplitude (AMP). G) Maximum (Peak) value. H) Minimum (Dormant) value.*

3.4. Discussion

3.4.1. Impact of BRDF on VI time-series and derived phenological parameters of disturbed forests

One of the primary objectives of this chapter is to investigate EVI and NDVI sensitivities of disturbed and undisturbed forests to variable viewing and illumination geometry. Previous research of Kaufmann *et al.* (2000) analysed the influences of SZA changes on NDVI measurements from AVHRR satellite. Their results showed the impact of SZA variations was insignificant for most vegetation types, except shrublands and bushlands. Comparing with our VI time-series and seasonal profiles of disturbed sites (Fig. 3.9), NDVI of SEA disturbed forests seems to be sensitive to variations of sun-sensor geometry, especially during the late dry season.

This BRDF influence contradicts the result of intact forests in chapter two, as NDVI time-series of undisturbed forests were resistant to seasonal sun-angle changes. This finding was well supported by Bhandari et al (2011) who found that NDVI of Queensland forests was also sensitive to changes of sun-sensor geometry. As Bhandari used woodlands and discontinuous open forests in the subtropical region (around 25S latitude) for his study, his research areas presumably shared the same characteristics as disturbed forests in Southeast Asia.

Disturbance likely causes forests to replace trees by more deciduous species like grasses and shrubs that expose bare soil during the dry periods. Exposed soil might contribute to BRDF because NDVI is sensitive to soils at low canopy densities (Huete et al., 2002). Consequently, NDVI retrieved from the sparser canopy of disturbed forests was more sensitive to variable SZA because of the influence of rougher and more porous canopy surface that soil-induced effect (Kaufmann et al., 2000). With undisturbed tropical forests having high biomass and denser canopies, the impact of soil-induced impact is minimal or removed.

Another plausible reason is the temporal resolution difference between MODIS Vegetation Index Products and MODIS BRDF/Albedo products. While latest version (Collection 6) of MODIS VI products maintain a 16-day temporal resolution, MODIS BRDF Collection 6 products provide BRDF parameters at a daily interval. While 16-day interval data might underestimate the VI decreasing during the late of dry season before

raining, daily frequency of MODIS BRDF might have enhanced capability of capturing seasonal vegetation dynamics (Wang, Schaaf, Sun, Shuai, & Román, 2018).

The seasonal profiles of disturbed forests (Fig. 3.10) reflect very well the NDVI saturation issue in high biomass areas (Huete, Liu, & Leeuwen, 1997; Liu, Liu, & Yin, 2013; Chen, Fedosejevs, 2006). Under the impact of disturbances, NDVI values of forest sites are saturated for extended periods in the wet season and discrimination of forest dynamics is nearly unattainable. Another plausible reason for saturation is that the dense and more vigorous understory vegetation can saturate the NDVI in the wet season. The similarity in NDVI values between disturbed and intact forests suggests that disturbed forests still retain high levels of green biomass, especially in the rainy season.

3.4.2. Impact of disturbance on VI time-series, seasonal profiles and derived phenological metrics

Another objective of this chapter is to investigate forest disturbance influences on SEA tropical forest phenology. The comparison of VI time-series revealed that the disturbance impact was varied according to the degree of disturbance. The disturbed forests with greater forest loss percentages changed its NDVI patterns, while the forest with lower forest loss percentages recovered its NDVI dynamics after disturbance (Fig. 3.9). Our results suggest that significant disturbance might alter forest phenology perennially (or at least during the time window analysed in this study), while less disturbed forests can recover their greenness. However, our site selection was based on Hansen's forest cover change maps without any ground validation, so further studies are needed to confirm this finding.

By comparing between disturbed and undisturbed forests, we found that NDVI of disturbed forests were generally lower than NDVI of undisturbed forests, especially in the drier tropical forest sites. Our results are well correlated with previous studies: for example, Cuevas-González *et al.* (2009) showed that MODIS NDVI time-series exhibited significantly lower NDVI values in burned forests compared to undisturbed control sites. Other studies from Van Leeuwen (2008) and Buma (2012) showed abrupt decreases of the NDVI time-series when disturbance occurred.

NDVI time-series with BRDF correction amplified the differences between disturbed and undisturbed forest in the late dry season. In some cases, BRDF correction

helped to separate undisturbed and disturbed forests while BRDF-uncorrected NDVI of disturbed and undisturbed forest were indistinguishable. The main reason for this underestimation is the potential difference of temporal resolutions between MODIS BRDF/Albedo and MODIS Vegetation Indices products. Specifically, MODIS Vegetation Indices data are provided as 16-day interval images (Didan et al., 2015) while the latest version (Collection 6) of MODIS BRDF/Albedo is a daily dataset (Didan et al., 2015; Schaaf & Wang, 2015a; Strahler & Muller, 1999). The Collection V006 product still generates modelled parameters by utilising the 16-day data of directional reflectances around the day of interest but sets the highest temporal weight to the day of interest. Wang *et al.* (2018) evaluated the performance of MODIS BRDF/Albedo Collection 6 product to capture rapid land surface dynamics and found that reflectances derived from BRDF/Albedo product were highly correlated with tower measurements. Consequently, higher temporal resolution potentially captures rapid changes of a vegetation landscape, especially in the highly dynamic post-disturbance period.

Based on the results derived for undisturbed forests, EVI is presumably more suitable to capture forest seasonal dynamics, as it has less saturation issues like NDVI. Gaps between disturbed and undisturbed forests measured with EVI are different from results from NDVI. EVI values of dry disturbed forests are lower in the dry period and higher in the wet season compared to those of undisturbed forests (Fig. 3.11). However, this pattern is reversed in forests that have no pronounced dry season, where EVI measurements of disturbed forests are higher than EVI in intact forests for the whole year.

The role of forest regeneration in the post-disturbance period might explain this apparently contradictory finding. Disturbed forests contain more young trees than intact forests, in response to the increased light abundance in the new gap (Brokaw, 1985). Old leaves have lower reflectance and decreased transmittance relatively to young leaves. As new leaves replace the old ones, forest albedo is expected to increase (Maeda, Heiskanen, Aragão, & Rinne, 2014). In rainforests without distinct dry seasons, young trees and seedling can keep growing with high rainfall intensity for almost the entire a year, causing EVI values of disturbed areas to be higher than those of undisturbed forests. A study from Brando et al. (2010) supported our findings, as the production of new leaves were found to be the reason for increasing plant productivity in the dry season. As EVI was more sensitive to the production of young leaves, it tended to be higher in the regenerating

forests; this result was also corroborated by field measurements that found higher EVI values during the peak of leaf flush in the dry season in the Amazon (Lopes et al., 2016).

In regions with longer dry seasons, water deficit forces deciduous species to lose leaves (Murphy & Lugo, 1986). As forest loss likely increased the amount of young trees and leaves, in the wet season, these forests tend to have higher EVI values than intact forests having old leaves. This strong dependence on precipitation of young trees was shown in previous studies. For example, a research by Vicente, Lucía and Miguel (2009) pointed that young trees of *Juniperus thurifera* species were the most climatically sensitive to rainfall while precipitation influenced less the old trees. Another study of Zhang et al. (2018) showed the sensitivity of young trees to rainfall and temperature in Qilian Mountains. In a tropical example, Giardina *et al.* (2018) studied Amazonian forests and found that tall trees are less sensitive to precipitation variability. Taller forests are known to be older, have more biomass and deeper root systems, which enable them to access deeper soil moisture and make them more resilient to drought.

Our results also illustrate the dependence of young trees to rainfall events. Disturbed forests with younger trees have stronger seasonal magnitudes derived from both NDVI and EVI than intact forests with older trees. Our results indicate that disturbed forests in SEA have stronger seasonality and are more sensitive to rainfall though they have higher EVI measurements. The implications of our findings to the resilience of SEA forests are evident, as the high disturbance levels in this region, combined with the intensification of climate variability, may be pushing these forests to a precipitation threshold that may turn them into other vegetation types.

Another crucial finding of our study is related to the phenophase timing of disturbed forests. We showed that the greening season of disturbed sites derived from EVI time-series started later than in intact sites. This finding is a contrast to past researches. Yvonne *et al.* (2006) studied the effects of forest fragmentation on dry tropical forests and found out that disturbed forests started to flower 15-20 days earlier than untouched forests. The probable reason is that these degraded forests have secondary vegetation with no access to deep surface water (Huete *et al.* 2006) and respond faster to first inputs of water from precipitation than conserved forests. A recent study by Martinez (2017) investigated the phenology of disturbed forests in Mexico and showed similar results as SGS of degraded forests happened sooner than in intact forests.

Our disturbed sites are potentially the primary cause of the disagreement between our results and previous findings. Disturbances occurred continuously for extended periods while previous studies selected disturbed sites with one single disturbance event and monitored their inter-annual and intra-annual dynamics. As unsustainable logging was considered as the leading cause of these repeated forest losses (Stibig et al., 2014), it suggests that consecutive forest losses cause changes of inter-annual forest dynamic with later onset and ending of the greening season.

Our results successfully presented an overview of phenology for the entire SEA region, and for that purpose, we chose to employ MODIS data, as it is a suitable data for regional analysis. However, it is important to highlight that MODIS' coarse resolution present some limitations: it is inarguable that a pixel at either 0.05degree or 500m resolution will contain a mix of different surface targets such as exposed soil and intact and undisturbed forests. As a recommendation for further studies, analysis with finer resolution satellite data could obtain information related to ecological processes that happen at smaller scales, such as tree mortality and leaf demography.

3.4.3. Influences of sun-angle on the differences of derived phenological parameters between undisturbed and disturbed forests

Different fixed geometry settings potentially caused the variability of derived reflectance measurements for monitoring vegetation dynamics. Standardisation of sun-view angles to SZA of 45 degrees with nadir-view has been used in previous studies (Middleton, 1991; Gao, 2014). Middleton (1992) raised the question about the selection of standardised illumination and viewing geometry and concluded that fixing sun angle at 45 degrees was a suitable choice that produced minimum errors in predicting reflectance from off-nadir angles and least variance in a spectral vegetation index versus LAI relationship. Moreover, choosing SZA of 45 degrees avoids the effect of strong directional signature close to the backscatter scenario (Bréon & Vermote, 2012).

However, standardising SZA to 45-degree would be too large for tropical regions as SZA values of low latitude areas are below 45 degrees throughout the year. Results derived from reflectance and VI time-series of this unrealistic solar angle setting cannot be validated through comparison with ground measurements. By comparing results of

various sun-angle configurations, we investigated potential variations caused by different geometry configurations.

Our results for disturbed forests illustrated that sun-angle settings had minor influence on the differences of phenometrics from undisturbed and disturbed forests (Fig 3.14 and 3.15). These variations were generally insignificant as varying sun-angle selection caused the shifting of phenophase dates up to 5 days only, while variation in VI measurements like maximum or minimum were up to 0.04. However, if the differences between disturbed and undisturbed forests are marginal, these small variations should be considered to avoid false results.

3.5. Conclusion

In this chapter, we standardised NDVI and EVI time-series of paired disturbed-undisturbed forests with various SZA settings. Then, we compared seasonal profiles and derived phenological metrics between disturbed and undisturbed forests to get a better understanding of the disturbance influence on SEA tropical forests. We also investigated the potential effect of BDRF on the phenology of disturbed sites and BRDF differences between intact and disturbed forests.

Our results showed that NDVI saturation was still a significant problem in the extraction of accurate seasonal profiles of disturbed forests, similar to the outcome of undisturbed forests. As NDVI measurements were indistinguishable for forests with long wet seasons, annual patterns derived from NDVI time-series were shown to be inaccurate in the rainy season. Unlike undisturbed forests, the BRDF impact on NDVI values of disturbed forests was significant in the dry season, evidenced with minimum values, as fixed sun-angle NDVI yielded lower minimum values compared with standard Terra/Aqua NDVI. These variations are presumably caused by complex canopy structure of disturbed forests and different temporal resolutions between MODIS Vegetation Indices (16-day interval) and BRDF/Albedo products (daily).

The comparison of seasonal profiles and phenological metrics between disturbed and undisturbed forests exhibited considerable differences. NDVI values of disturbed sites were significantly lower than intact sites whereas disturbed EVIs were higher in the wet season than intact EVIs. Stronger seasonality of disturbed forests represented by both

annual EVI and NDVI magnitudes suggests the higher sensitivity of disturbed forests to seasonal climate variability.

Our results also indicate the impact of disturbance on phenophase dates as the onset and end of the greening season of disturbed forests occurred later than of undisturbed sites. The continuous disturbance processes happening in SEA forests are presumably the cause of this finding that contrasts to previous studies. These impacts of disturbance on phenological timings were still observed at various sun-angle settings, though variability of geometry configurations caused some minor variations on derived phenological information.

In conclusion, our results provided knowledge about the impact of disturbance on continental SEA tropical forests phenology, considering BRDF influence on the extracted information.

3.6. References

Arturo, S.-A., Jose, A. G., A., C. C., Saulo, C., Virginia, G.-M., Joanne, N., & Cassidy, R. (2017). Twenty-first century remote sensing technologies are revolutionizing the study of tropical forests. *Biotropica*, *49*(5), 604–619. https://doi.org/10.1111/btp.12454

Bhandari, S., Phinn, S., & Gill, T. (2011). Assessing viewing and illumination geometry effects on the MODIS vegetation index (MOD13Q1) time series: implications for monitoring phenology and disturbances in forest communities in Queensland, Australia. *International Journal of Remote Sensing*, *32*(22), 7513–7538. https://doi.org/10.1080/01431161.2010.524675

Blackie, R., Baldauf, C., Gautier, D., Gumbo, D., Kassa, H., Parthasarathy, N. Paumgarten, F.; Sola, P., … Sunderland, T. C. H. (2014). Tropical dry forests : The state of global knowledge and recommendations for future Tropical dry forests The state of global knowledge and recommendations, (March), 30. Retrieved from 10.17528/cifor/004408

Brando, P. M., Goetz, S. J., Baccini, A., Nepstad, D. C., Beck, P. S. A., & Christman, M. C. (2010). Seasonal and interannual variability of climate and vegetation indices across the Amazon. *Proceedings of the National Academy of Sciences*, *107*(33), 14685–14690. https://doi.org/10.1073/pnas.0908741107

Bréon, F. M., & Vermote, E. (2012). Correction of MODIS surface reflectance time series for BRDF effects. *Remote Sensing of Environment*, *125*, 1–9. https://doi.org/10.1016/j.rse.2012.06.025

Broich, M., Huete, A., Paget, M., Ma, X., Tulbure, M., Coupe, N. R., … Held, A. (2015). A spatially explicit land surface phenology data product for science, monitoring and natural resources management applications. *Environmental Modelling and Software*, *64*, 191–204. https://doi.org/10.1016/j.envsoft.2014.11.017

Brokaw, N. V. L. (1985). Gap-Phase Regeneration in a Tropical Forest. *Ecology*, *66*(3), 682–687. Retrieved from http://www.jstor.org/stable/1940529

Buma, B. (2012). Evaluating the utility and seasonality of NDVI values for assessing post-disturbance recovery in a subalpine forest. *Environmental Monitoring and Assessment*, *184*(6), 3849–3860. https://doi.org/10.1007/s10661-011-2228-y

Chen, W., Moriya, K., Sakai, T., Koyama, L., & Cao, C. (2014). Temporal and spatial monitoring of post-fire forest dynamics using time-series MODIS data. In *2014 IEEE Geoscience and Remote Sensing Symposium* (pp. 772–775).

https://doi.org/10.1109/IGARSS.2014.6946538

Cuevas-González, M., Gerard, F., Balzter, H., & Riaño, D. (2009). Analysing forest recovery after wildfire disturbance in boreal Siberia using remotely sensed vegetation indices. *Global Change Biology*, *15*(3), 561–577. https://doi.org/10.1111/j.1365-2486.2008.01784.x

de Beurs, K. M., & Henebry, G. M. (2010). Spatio-Temporal Statistical Methods for Modelling Land Surface Phenology. In *Phenological Research: Methods for Environmental and Climate Change Analysis* (pp. 177–208). https://doi.org/10.1007/978-90-481-3335-2

Didan, K. (2015a). *MOD13A1 MODIS/Terra Vegetation Indices 16-Day L3 Global 500m SIN Grid V006 [Data set]. NASA EOSDIS LP DAAC*. https://doi.org/10.5067/MODIS/MOD13A1.006

Didan, K. (2015a). MOD13C2 MODIS/Terra Vegetation Indices Monthly L3 Global 0.05Deg CMG V006. NASA EOSDIS LP DAAC. https://doi.org/10.5067/MODIS/MOD13C2.006

Didan, K. (2015b). *MYD13A1 MODIS/Aqua Vegetation Indices 16-day L3 Global 500m SIN Grid V006*. https://doi.org/10.5067/MODIS/MYD13A1.006

Didan, K. (2015b). MYD13C2 MODIS/Aqua Vegetation Indices Monthly L3 Global 0.05Deg CMG V006. NASA EOSDIS LP DAAC. https://doi.org/10.5067/MODIS/MYD13C2.006

Didan, K., Munoz, A. B., & Huete, A. (2015). MODIS Vegetation Index User ' s Guide (MOD13 Series), *2015*(June).

Dong, J., Xiao, X., Sheldon, S., Biradar, C., Zhang, G., Duong, N. D., … Moore, B. (2014). A 50-m forest cover map in Southeast Asia from ALOS/PALSAR and its application on forest fragmentation assessment. *PLoS ONE*, *9*(1). https://doi.org/10.1371/journal.pone.0085801

Funk, C., Peterson, P., Landsfeld, M., Pedreros, D., Verdin, J., Shukla, S., … Michaelsen, J. (2015). The climate hazards infrared precipitation with stations—a new environmental record for monitoring extremes. *Scientific Data*, *2*, 150066. Retrieved from http://dx.doi.org/10.1038/sdata.2015.66

Gao, F., He, T., Masek, J. G., Shuai, Y., Schaaf, C. B., & Wang, Z. (2014). Angular effects and correction for medium resolution sensors to support crop monitoring. *IEEE Journal of Selected Topics in Applied Earth Observations and Remote Sensing*, *7*(11), 4480–4489. https://doi.org/10.1109/JSTARS.2014.2343592

Giardina, F., Konings, A. G., Kennedy, D., Alemohammad, S. H., Oliveira, R. S., Uriarte, M.,

& Gentine, P. (2018). Tall Amazonian forests are less sensitive to precipitation variability. *Nature Geoscience*, *11*(6), 405–409. https://doi.org/10.1038/s41561-018-0133-5

Hansen, M. C., Potapov, P. V, Moore, R., Hancher, M., Turubanova, S. A., Tyukavina, A., … Townshend, J. R. G. (2013). High-Resolution Global Maps of 21st-Century Forest Cover Change. *Science*, *342*(6160), 850–853. https://doi.org/10.1126/science.1244693

Huete, A. R., Didan, K., Shimabukuro, Y. E., Ratana, P., Saleska, S. R., Hutyra, L. R., … Myneni, R. (2006). Amazon rainforests green-up with sunlight in dry season. *Geophysical Research Letters*, *33*(6). https://doi.org/10.1029/2005GL025583

Huete, A. R., HuiQing Liu, & van Leeuwen, W. J. D. (1997). The use of vegetation indices in forested regions: issues of linearity and saturation. *IGARSS'97. 1997 IEEE International Geoscience and Remote Sensing Symposium Proceedings. Remote Sensing - A Scientific Vision for Sustainable Development*, *4*(1), 1966–1968. https://doi.org/10.1109/IGARSS.1997.609169

Huete, A. R., Restrepo-Coupe, N., Ratana, P., Didan, K., Saleska, S. R., Ichii, K., … Gamo, M. (2008). Multiple site tower flux and remote sensing comparisons of tropical forest dynamics in Monsoon Asia. *Agricultural and Forest Meteorology*, *148*(5), 748–760. https://doi.org/10.1016/j.agrformet.2008.01.012

Huete, Didan, K., Miura, T., Rodriguez, E. P., Gao, X., & Ferreira, L. G. (2002). Overview of the radiometric and biophysical performance of the MODIS vegetation indices. *Remote Sensing of Environment*, *83*(1–2), 195–213. https://doi.org/10.1016/S0034-4257(02)00096-2

Jeganathan, C., Dash, J., & Atkinson, P. M. (2014). Remotely sensed trends in the phenology of northern high latitude terrestrial vegetation, controlling for land cover change and vegetation type. *Remote Sensing of Environment*, *143*, 154–170. https://doi.org/10.1016/j.rse.2013.11.020

Kaufmann, R. K., Zhou, L., Knyazikhin, Y., Shabanov, V., Myneni, R. B., & Tucker, C. J. (2000). Effect of orbital drift and sensor changes on the time series of AVHRR vegetation index data. *IEEE Transactions on Geoscience and Remote Sensing*, *38*(6), 2584–2597. https://doi.org/10.1109/36.885205

Langner, A., Miettinen, J., Kukkonen, M., Vancutsem, C., Simonetti, D., Vieilledent, G., … Stibig, H. J. (2018). Towards operational monitoring of forest canopy disturbance in evergreen rain forests: A test case in continental Southeast Asia. *Remote Sensing*, *10*(4), 1–21. https://doi.org/10.3390/rs10040544

Liu, G., Liu, H., & Yin, Y. (2013). Global patterns of NDVI-indicated vegetation extremes and their sensitivity to climate extremes. *Environmental Research Letters*, *8*(2). https://doi.org/10.1088/1748-9326/8/2/025009

Liu, J., Schaaf, C., Strahler, A., Jiao, Z., Shuai, Y., Zhang, Q., … Dutton, E. G. (2009). Validation of moderate resolution imaging spectroradiometer (MODIS) albedo retrieval algorithm: Dependence of albedo on solar zenith angle. *Journal of Geophysical Research Atmospheres*, *114*(1), 1–11. https://doi.org/10.1029/2008JD009969

Lopes, A. P., Nelson, B. W., Wu, J., Graça, P. M. L. de A., Tavares, J. V., Prohaska, N., … Saleska, S. R. (2016). Leaf flush drives dry season green-up of the Central Amazon. *Remote Sensing of Environment*, *182*, 90–98. https://doi.org/10.1016/j.rse.2016.05.009

Maeda, E. E., Heiskanen, J., Aragão, L. E. O. C., & Rinne, J. (2014). Can MODIS EVI monitor ecosystem productivity in the Amazon rainforest? *Geophysical Research Letters*, *41*(20), 7176–7183. https://doi.org/10.1002/2014GL061535

Middleton, E. M. (1991). Solar zenith angle effects on vegetation indices in tallgrass prairie. *Remote Sensing of Environment*, *38*(1), 45–62. https://doi.org/https://doi.org/10.1016/0034-4257(91)90071-D

Middleton, E. M. (1992). Quantifying reflectance anisotropy of photosynthetically active radiation in grasslands. *Journal of Geophysical Research: Atmospheres*, *97*(D17), 18935–18946. https://doi.org/doi:10.1029/92JD00879

Mildrexler, D. J., Zhao, M., Heinsch, F. A., & Running, S. W. (2007). A new satellite-based methodology for continental-scale disturbance detection. *Ecological Applications*, *17*(1), 235–250. https://doi.org/10.1890/1051-0761(2007)017[0235:ANSMFC]2.0.CO;2

Murphy, P. G., & Lugo, A. E. (1986). Ecology of Tropical Dry Forest. *Annual Review of Ecology and Systematics*, *17*(1), 67–88. https://doi.org/10.1146/annurev.es.17.110186.000435

Myneni, R. B., Hall, F. G., Sellers, P. J., & Marshak, A. L. (1995). The interpretation of spectral vegetation indices. *IEEE Transactions on Geoscience and Remote Sensing*, *33*(2), 481–486.

Pei-Yu Chen, Gunar Fedosejevs, M. T.-L. and J. G. A. (2006). Assessment of MODIS-EVI, MODIS-NDVI and Vegetation-NDVI composite data using agricultural measurements: an example at corn fields in western mexico. *Environmental Monitoring and Assessment*, *119*(1–3), 69–82. https://doi.org/10.1007/sl0661-005-9006-7

Phompila, C., Lewis, M., Ostendorf, B., & Clarke, K. (2015). MODIS EVI and LST temporal response for discrimination of tropical land covers. *Remote Sensing*, *7*(5), 6026–6040. https://doi.org/10.3390/rs70506026

Rankine, C., Sánchez-Azofeifa, G. A., Guzmán, J. A., Espirito-Santo, M. M., & Sharp, I. (2017). Comparing MODIS and near-surface vegetation indexes for monitoring tropical dry forest phenology along a successional gradient using optical phenology towers. *Environmental Research Letters*, *12*(10). https://doi.org/10.1088/1748-9326/aa838c

Reed, B., White, M., & Brown, J. (2003). Remote Sensing Phenology.

Martinez Romero, J. J., & Gao, Y. (2017). Forest disturbance analysis by phenology of forest covers in Mexico using time series NDVI data. *Asian Conference on Remote Sensing*, (October).

Rouse, J. W., Hass, R. H., Schell, J. A., & Deering, D. W. (1973). Monitoring vegetation systems in the great plains with ERTS. *Third Earth Resources Technology Satellite (ERTS) Symposium*, *1*, 309–317. https://doi.org/citeulike-article-id:12009708

Schaaf, C. B., Gao, F., Strahler, A. H., Lucht, W., Li, X., Tsang, T., … Roy, D. (2002). First operational BRDF, albedo nadir reflectance products from MODIS. *Remote Sensing of Environment*, *83*(1–2), 135–148. https://doi.org/10.1016/S0034-4257(02)00091-3

Schaaf, C. B., Liu, J., Gao, F., & Strahler, A. H. (2011). Aqua and Terra MODIS Albedo and Reflectance Anisotropy Products. In B. Ramachandran, C. O. Justice, & M. J. Abrams (Eds.), *Land Remote Sensing and Global Environmental Change: NASA's Earth Observing System and the Science of ASTER and MODIS* (pp. 549–561). New York, NY: Springer New York. https://doi.org/10.1007/978-1-4419-6749-7_24

Schaaf, C., & Wang, Z. (2015a). MCD43A1 MODIS/Terra+Aqua BRDF/Albedo Model Parameters Daily L3 Global - 500m V006. NASA EOSDIS Land Processes DAAC.

Schaaf, C., & Wang, Z. (2015b). MCD43C1 MODIS/Terra+Aqua BRDF/AlbedoModel Parameters Daily L3 Global 0.05Deg CMG V006 [Data set]. NASA EOSDIS Land Processes DAAC. https://doi.org/10.5067/MODIS/MCD43C1.006

Setiawan, Y., Yoshino, K., & Prasetyo, L. B. (2014). Characterizing the dynamics change of vegetation cover on tropical forestlands using 250 m multi-temporal MODIS EVI. *International Journal of Applied Earth Observation and Geoinformation*, *26*(1), 132–144. https://doi.org/10.1016/j.jag.2013.06.008

Stibig, H., Achard, F., Carboni, S., Raši, R., & Miettinen, J. (2014). Change in tropical forest

cover of Southeast Asia from 1990 to 2010. *Biogeosciences*, *11*(2), 247–258. https://doi.org/10.5194/bg-11-247-2014

Strahler, A. H., & Muller, J. P. (1999). MODIS BRDF Albedo Product : Algorithm Theoretical Basis Document. *MODIS Product ID: MOD43*, *Version 5*.(April), 1–53. https://doi.org/http://duckwater.bu.edu/lc/mod12q1.html

Strugnell, N. C., Lucht, W., Hyman, A. H., & Meister, G. (1998). Continental-scale albedo inferred from land cover class, field observations of typical BRDFs and AVHRR data. In *Geoscience and Remote Sensing Symposium Proceedings, 1998. IGARSS '98. 1998 IEEE International* (Vol. 2, pp. 595–597 vol.2). https://doi.org/10.1109/IGARSS.1998.699522

Strugnell, N., Wolfgang, L., & Crystal, S. (2001). A global albedo data set derived from AVHRR data for use in climate simulations. *Geophysical Research Letters*, *28*(1), 191–194. https://doi.org/doi:10.1029/2000GL011580

Tyukavina, A., Hansen, M. C., Potapov, P. V., Krylov, A. M., & Goetz, S. J. (2016). Pan-tropical hinterland forests: Mapping minimally disturbed forests. *Global Ecology and Biogeography*, *25*(2), 151–163. https://doi.org/10.1111/geb.12394

Van Leeuwen, W. J. D. (2008). Monitoring the effects of forest restoration treatments on post-fire vegetation recovery with MODIS multitemporal data. *Sensors*, *8*(3), 2017–2042. https://doi.org/10.3390/s8032017

Vicente, R., Lucía, D., & Miguel, O. J. (2009). Sex-specific, age-dependent sensitivity of tree-ring growth to climate in the dioecious tree Juniperus thurifera. *New Phytologist*, *182*(3), 687–697. https://doi.org/10.1111/j.1469-8137.2009.02770.x

Wang, Z., Schaaf, C. B., Chopping, M. J., Strahler, A. H., Wang, J., Román, M. O., … Shuai, Y. (2012). Evaluation of Moderate-resolution Imaging Spectroradiometer (MODIS) snow albedo product (MCD43A) over tundra. *Remote Sensing of Environment*, *117*, 264–280. https://doi.org/https://doi.org/10.1016/j.rse.2011.10.002

Wang, Z., Schaaf, C. B., Sun, Q., Shuai, Y., & Román, M. O. (2018). Capturing rapid land surface dynamics with Collection V006 MODIS BRDF/NBAR/Albedo (MCD43) products. *Remote Sensing of Environment*, *207*, 50–64. https://doi.org/https://doi.org/10.1016/j.rse.2018.02.001

Wanner, W., Strahler, A. H., Hu, B., Lewis, P., Muller, J.-P., Li, X., … Barnsley, M. J. (1997). Global retrieval of bidirectional reflectance and albedo over land from EOS MODIS and MISR data: Theory and algorithm. *Journal of Geophysical Research: Atmospheres*, *102*(D14), 17143–17161. https://doi.org/10.1029/96JD03295

Xie, Y., Sha, Z., & Yu, M. (2008). Remote sensing imagery in vegetation mapping: a review. *Journal of Plant Ecology*, *1*(1), 9–23. https://doi.org/10.1093/jpe/rtm005

YVONNE, H.-D., MAURICIO, Q., E., S. K., & A., L. J. (2006). Effects of Forest Fragmentation on Phenological Patterns and Reproductive Success of the Tropical Dry Forest Tree Ceiba aesculifolia. *Conservation Biology*, *20*(4), 1111–1120. https://doi.org/10.1111/j.1523-1739.2006.00370.x

Zhang, L., Jiang, Y., Zhao, S., Jiao, L., & Wen, Y. (2018). Relationships between tree age and climate sensitivity of radial growth in different drought conditions of Qilian Mountains, northwestern China. *Forests*, *9*(3). https://doi.org/10.3390/f9030135

Zhang, X., Friedl, M. A., Schaaf, C. B., Strahler, A. H., Hodges, J. C. F., Gao, F., … Huete, A. (2003). Monitoring vegetation phenology using MODIS. *Remote Sensing of Environment*, *84*(3), 471–475. https://doi.org/10.1016/S0034-4257(02)00135-9

Chapter 4. Inter-annual variabilities of Southeast Asia tropical forests and BRDF influences

4.1. Introduction

Between 1850 and 2010, the average global temperature increased by approximately 0.8 degrees Celsius. In the last 50 years, the rate of increase doubled (Brohan, Kennedy, Harris, Tett & Jones, 2006). This increase in temperature is closely correlated with a rise in concentration of greenhouse gas. Since 1750, carbon dioxide levels increased by 39 per cent and methane increased by 148 per cent (Riebeek, 2010).

Global warming is significant, with far-reaching effects on the planet. It has the potential to alter rainfall patterns and, for many places, result in more frequent hot days and fewer cold days. A recent study (Wang, Jiang & Lang, 2017) using a CMIP5 daily dataset demonstrated the link between the intensity of global increases in temperature and extreme changes in climate. The number of extreme temperature events was found to increase with a rise in average global temperature. Moreover, the dry season had a tendency to last longer and rainfall intensity became more damaging (Fischer, Beyerle & Knutti, 2013). Fu et al. (2013) observed rain gauge data, which revealed that the length of the dry season in the southern Amazon has increased considerably since 1987, causing concern among scientists about the future of Amazonian forests.

The effect of these changes in climate on ecosystems is evident. In the last few decades, the growing season has become 10 to 20 days longer globally (Linderholm, 2006). Extending the greening season means that plants require more water to grow or they will dry out, increasing the risk of wildfires. Maximum daily temperatures may pass beyond the healthy threshold of many plant and animal species, risking extinction.

Since the phenology of tropical vegetation is dependent on rainfall events (Hannah, 2015), changes in rainfall are considered the essential cause of inter-annual vegetation variability in the tropics. There is an abundance of modelled and observed evidence to indicate that rain regimes in the tropics are changing because of climate change (Allen et al., 2017). Chadwick (2016) used various models to suggest that precipitation in the tropics would considerably change in the twenty-first century. Greve

et al. (2014) analysed land dryness changes with different hydrological datasets, illustrating that drying trends occurred in many tropical regions.

The way in which these changes in rainfall regimes affect tropical forest phenology is a considerable question. Tan et al. (2015) used nine-year eddy flux data to demonstrate that there was no inter-annual trend in water-use efficiency in tropical rainforests. In contrast, Brando et al. (2010) showed the relationship between forest phenology and inter-annual climate variability, as the gross primary productivity expressed as EVI and plant-available water of Amazon forests decreased in the period from 1996 to 2005 and air dryness increased in the period from 2002 to 2005. Additionally, El Niño–Southern Oscillation (ENSO) events affect climate variability in tropical regions, such as the Amazon or SEA. For example, rainfall and temperature variability caused by ENSO events had a critical effect on tropical vegetation activities (Nagai, Ichii & Morimoto, 2007).

In SEA, precipitation variability was primarily controlled by the East Asian summer monsoon. Rainfall season was predicted to be delayed and rainfall variability affected the frequency and intensity of flooding in many places (Loo, Billa & Singh, 2015). Considering the effect of climate variability on SEA vegetation activity, Suepa (2016) demonstrated the downtrend of EVI and precipitation between 2001 and 2010. Another study by Zhang et al. (2016) concluded that the forest NDVI of SEA decreased non-linearly with drought severity in dry seasons.

However, these past studies use either NDVI measurements saturated in densely vegetated landscapes or EVI measurements that are sensitive to the BRDF effect without BRDF correction. Although optical observation satellites provide a global view of intra- and inter-annual variability in vegetation phenology by capturing landscape albedo and reflectance, space-observed instruments acquire signals over a wide range of viewing and illumination geometries. These variations in sun-view angles are likely to cause artefacts, surface reflectances and derived vegetation indices that are incorrectly associated with the photosynthesis process (Bhandari, Phinn & Gill, 2011; Moura, Galvão, dos Santos, Roberts & Breunig, 2012). Combined with the fact that there are few studies on the effects of climate on SEA vegetation (Huete et al., 2008), there is a need to study the inter-annual variability of SEA tropical forest phenology associated with variations in climate factors and the BRDF effect.

Since ENSO conditions affect the climate variability of regions bordering the Pacific Ocean, continental SEA is one of the affected areas. The El Niño event (2014–2016) was one of the strongest El Niño events in history (Becker, 2016). Thirumalai (2017) discovered that amplified temperatures in SEA were caused by El Niño. However, the effect of this strong ENSO event on continental SEA vegetation, including forests, is unknown. Therefore, it is important to investigate the effect of extreme climate events, such as ENSO (2014–2016), on SEA forest phenology.

The primary purpose of this chapter is to investigate the effect of BRDF on inter-annual results on SEA tropical forests. The secondary goal of this chapter is to gain a better understanding of the inter-annual variability of SEA tropical forest phenology and the relationship between inter-annual changes in forest phenology and climate. Specifically, the objectives of this chapter are to: (1) investigate inter-annual vegetation index (VI) changes of SEA tropical forests; (2) analyse the BRDF effect on inter-annual VI changes and determined whether BRDF can influence the detection of wet and dry year anomalies; and (3) understand the relationship between inter-annual variations in forest phenology and climate variability.

4.2. Methodology

4.2.1. Study areas

The study area was located between longitudes 92°E and 110°E and latitudes 1°N and 29°N, covering peninsular SEA. The International Geosphere–Biosphere Programme (IGBP) land cover maps derived from the MODIS land cover type (LCT) product were used to determine forest coverage in continental SEA (Loveland & Belward, 1997; Strahler, Gopal, Lambin & Moody, 1999). Using supervised classification algorithms, MODIS LCT maps were provided annually for the period from 2001 to 2016, derived from MODIS Nadir BRDF-Adjusted Reflectance. The IGBP land cover map of the year for 2016 was extracted from a MCD12C1 0.05 degree product to retrieve the SEA LCT (Friedl & Sulla-Menashe, 2015). All pixels that did not represent forest areas were excluded and the analyses were conducted on the remaining available regions.

However, forest areas retrieved from MODIS LCT map contain both disturbed and non-disturbed forests as SEA forests were heterogeneous and scattered in small

patches (Dong et al., 2014). As presented in Chapter 3, SEA disturbed events were generally unsustainable logging, which occurred continuously, rather than as a single event. These occurrances caused inter-annual forest phenology dominated by disturbance, not the effect of climate variability. We need to obtain non-disturbed forest areas to analyse the inter-annual variations of non-disturbed forests and compare with forests mixing of disturbed and non-disturbed forests

In this chapter, 30 intact forest sites were chosen using a hinterland forest map derived by Tyukavina et al. (2016). Tyukavina designed a novel method of mapping undisturbed tropical forests based on the global cover change map derived from study of Hansen et al. (2013). Undisturbed forest sites were chosen from hinterland forest maps across the entire mainland of SEA. Overall, 30 sites that were greater than 100 square kilometres in size were selected, scattered across the entire continent of SEA and representing all forest phenology in all regions of peninsular SEA. Figure 4.1 highlights the chosen undisturbed sites and SEA forest coverage based on MCD12C1 LCT (Friedl & Sulla-Menashe, 2015).

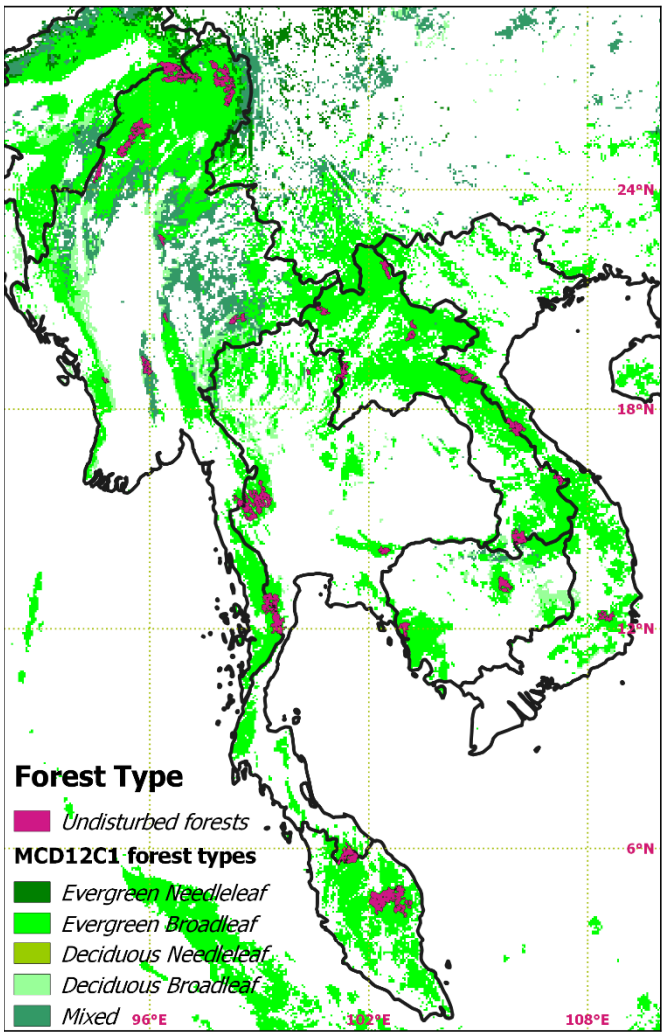

Figure 4.1. *Selected undisturbed sites (red areas) associated with forest pixels derived from MCD12C1 data (2016). Sizes of selected sites vary from 1000 to over 40000 square kilometres.*

4.2.2. Datasets

4.2.2.1. VI datasets

VI are spectral band transformations that strengthen vegetation properties (Huete et al., 2002). NDVI and EVI are two common VIs and are widely used to represent vegetation signal. NDVI, one of the most well-known VIs, has been used to study vegetation activity for over 40 years, since it was first used by Rouse (1973). EVI is an 'optimised' VI that reduces the influence of soil and atmospheric noise variations.

In this chapter, MODIS VI products from both Terra and Aqua sensors are used to extract EVI and NDVI time series to analyse inter-annual changes in SEA tropical forests. First, data was collected from of monthly Collection 6 CMG MODIS Terra (MOD13C2; 2001–2016) and Aqua (MYD13C2; 2003–2016) VI products and used to

analyse inter-annual changes of SEA tropical forest phenology at a 0.05 degree scale (Didan, 2015a, 2015b). Second, to investigate inter-annual VI variations of selected sites, MODIS VI products were used at a 500 m spatial resolution (Didan, 2015a, 2015b).

To analyse the BRDF effect on inter-annual changes in SEA tropical forests, there was a need to generate VI measurements at fixed sun-view geometries. MODIS BRDF/Albedo products provide BRDF parameters using a RossThick-LiSparse Reciprocal BRDF model that best describes the anisotropy of each 500 m pixel at the same daily period (Schaaf et al., 2002; Schaaf, Liu, Gao & Strahler, 2011; Wang et al., 2012; Wanner et al., 1997). MODIS BRDF/Albedo parameters were used at 500 m and averaged CMG 0.05 degree scales (Schaaf & Wang, 2015a, 2015b) to generate NDVI and EVI values at nadir view with various sun-angle settings (SZ15–SZ45) to compare to standard MODIS VI products. Since data availability is limited during the wet season in tropical regions, the QC level was set to magnitude inversion level to avoid long periods missing data (Strahler & Muller, 1999; Strugnell, Lucht, Hyman & Meister, 1998; Wolfgang & Crystal, 2001).

All MODIS VI data were downloaded from the NASA EarthData system (https://search.earthdata.nasa.gov/). MODIS Aqua in 2002 was excluded, due to incomplete data in that year. All cloudy values from extracted VI data were removed to reduce noise in processed data (Kamel, Didan, Munoz & Huete, 2015).

4.2.2.2. Land Surface Temperature (LST)

4.2.2.3. LST

To retrieve the land surface temperature (LST) of SEA forest areas, the latest version (Collection 6) of MODIS LST and emissivity data was used for the periods from 2001 to 2016 (Terra) and 2003 to 2016 (Aqua). Both Terra and Aqua LST were used, as the different captured timings (Terra: 10.30 am, Aqua: 1.30 pm) can produce different results. Both 1 km and 0.05 degree CMG LST data were used for separate scale analyses (Wan, Hook & Hulley, 2015d, 2015c, 2015b, 2015a). MODIS LST data were also retrieved from the NASA EarthData system (https://search.earthdata.nasa.gov/). Data were filtered to remove all noise pixels based on the MODIS Land Surface User's Guide (Zhengming Wan, 2013).

4.2.2.4. Precipitation dataset

Climate Hazards Group InfraRed Precipitation with Station data (CHIRPS) is a near global precipitation dataset from 1981 to near-present. It combines satellite information and includes popularised TRMM data with flux station data to create a gridded rainfall dataset spanning 50°S to 50°N and all longitudes at a five-kilometre scale (Funk et al., 2015; Huffman et al., 2007). As the CHIRPS algorithm was created to target trend analysis and seasonal drought monitoring, it is suitable to obtain rainfall information to study forest phenology in continental SEA due to its climate-based monsoon. Moreover, high spatial resolution (0.05 degree) matches MODIS CMG data, which may increase the reliability of the analyses.

Monthly CHIRPS gridded data (downloaded from ftp://ftp.chg.ucsb.edu/pub/org/chg/products/CHIRPS-2.0) was used for the period from 2001 to 2016. Only forested pixels (as explained in Section 4.2.1) were cropped and selected. The analyses were conducted on pre-processed rainfall data, such as seasonal trending or anomalies.

4.2.2.5. GRACE TWSA dataset

In March 2002, the Gravity Recovery and Climate Experiment (GRACE) was launched to measure gravity field anomalies on Earth. GRACE periodically measures changes in Earth's gravity, and gravitational changes are affected by increasing or decreasing water resources, including groundwater, soil moisture and surface water (e.g., rivers and lakes). Given that GRACE data exploits how regional water storage changes over time, global total water storage anomalies (TWSA) can be obtained by converting observed gravitational data (Famiglietti & Rodell, 2013). As tropical forests can access water reserves with their roots, TWSA data can be a useful water source to investigate the relationship between forest phenology and climate variability.

TWSA data was retrieved from NASA's GRACE Tellus website (https://grace.jpl.nasa.gov/data/get-data/monthly-mass-grids-land/) for the continental SEA region for the period between April 2002 and December 2016. The GRACE TWSA data were pre-processed and provided at one-degree spatial resolution, with the removal of atmospheric and ocean signals (Landerer & Swenson, 2012; Swenson & Wahr, 2006). Sine TWSA data were generated differently by three research centres—NASA Jet

Propulsion Laboratory, (University of Texas), Center for Space Research and the GeoForschungsZentrum (Potsdam)—the averaged TWSA data were calculated from three research centres to minimise the uncertainties associated with data processing progress (Xie et al., 2016). The scaling factors obtained from the National Center for Atmospheric Research's Community Land Model 4.0 were applied for accurate TWSA measurements (Long et al., 2015).

4.2.2.6. CERES shortwave radiation dataset

Aside from water dependency, solar radiation may influence tropical forest activity. Inter-annual variations of solar radiation potentially affect inter-annual tropical forest phenology. In this chapter, data of Clouds and the Earth's Radiant Energy System (CERES) project were used to represent downward shortwave solar radiation on the surface of continental SEA (Wielicki et al., 1998). CERES data provided not only radiation fluxes at the top of the atmosphere, but also those on the surface (Yan, Huang, Minnis, Wang & Bi, 2011). The latest version (4.0) of monthly CERES data was obtained from the CERES website for the period from January 2001 to December 2016 (https://ceres.larc.nasa.gov/index.php). Surface downward shortwave radiation was extracted for continental SEA during the study period for this research (2001–2016).

4.2.2.7. ENSO

The Oceanic Niño Index (ONI) was used to measure ENSO. ONI is a popularised index to characterise ENSO events by measuring sea surface temperature anomalies of the east-central equatorial Pacific Ocean (Marek et al., 2018). The latest version (ERSSTv5) of ONI data was retrieved from the Climate Prediction Center website (http://origin.cpc.ncep.noaa.gov/) with the improved accuracy of sea surface temperature (SST) spatial and temporal variability (Huang, 2017).

4.2.3. Analyses

The Seasonal Mann-Kendall (SMK) test was applied to detect significant trends in VI and climate data of continental SEA. The SMK test was introduced by Hirsch (1982) and is a seasonal version of the Mann-Kendall test, which is well-known for assessing potential trends of time series variables (Yue, Pilon & Cavadias, 2002). The SMK test was selected because it provides the strength and direction of a trend. SMK robustness

against seasonality, non-normality and missing data make it suitable for these data (de Beurs & Henebry, 2005). To measure the linear rate of change, Seasonal Sen's slope (SSS) was used, which is a modified version of the Sen's slope estimator for seasonal time series data (Hirsch et al., 1982; Sen, 1968).

To investigate inter-annual VI changes of SEA tropical forests, pre-processed monthly CMG VI data were applied to the SMK test to demonstrate spatial maps of pixels with significant trending of 90 per cent confidence ($p < 0.05$). Trending maps were used to analyse trending of forest VI, the effect of BRDF on trending results and the correlation between climate and VI trends. Maps of relative standard deviation (coefficient of variation) were estimated to reveal forests with stronger VI inter-annual variations. The VI trends of undisturbed forest sites were further calculated at a 500 m scale and compared with CMG forests (considered mixed forests) to analyse the effect of disturbance on forest trending.

Beside annual VI trends, we also produced VI trend analyses on February – April (Feb-Apr) periods, which considered as VI trends of SEA forests during dry seasons. As continental SEA region contain a mix of rainforests and tropical dry forests, which majorly started their rain season on May, the Feb-Apr trends could revealed the responses of SEA forests due to water limitation during dry periods.

The anomalies of forest VI and climate factors were found to exhibit inter-annual changes during the study period (2001–2016). Although trending represents long-term changes, inter-annual changes show independent annual variations of VI and climate factors, especially during extreme climate events, such as El Niño. VI anomalies were computed at 500 m and 0.05 degree scales to understand the BRDF and disturbance effect on inter-annual VI changes across SEA tropical forests.

To analyse the relationship between inter-annual VI variations and climate variability of SEA tropical forests, rainfall and LST trend maps were generated with CMG (0.05 degree) spatial resolution using the SMK test. Trend maps of GRACE TWSA and CERES solar radiation at one-degree resolution were calculated using the same method. Correlated plots of trend slope between VI and climate variables were used to discover the correlation between VI and climate variability.

Chosen forest sites were further grouped into classes based on the lengths of their dry season to examine the responses of different forest types on inter-annual climate variability. Given the different criterion for distinguishing moist forests and dry tropical forests, SEA forests were grouped into three classes based on the length of their dry seasons: zero to two months represented rainforests, three to five months were medium prolonged dry seasons and six to seven months was considered a long dry season (Pennington & Ratter, 2006; Portillo-Quintero & Sánchez-Azofeifa, 2010; Sánchez-Azofeifa et al., 2005). Inter-annual VI changes associated with climate factors were shown to discover whether different forests responded differently or similarly according to climate variability.

4.3. Results

4.3.1. Effect of BRDF on forest trends in continental SEA

4.3.1.1. Forest VI trending and the effect of BRDF

Figure 4.2 shows the significant Z-score values of the SMK test for continental SEA tropical forest EVI from 2001 to 2016 (Terra and BRDF-corrected EVI) and 2003 to 2016 (Aqua EVI). In general, SEA forest EVI illustrates an upward trend for the annual SMK test (Figure 4.2.I), while the size of SEA forest areas with significant upward or downward trends for the dry season periods was smaller than annual trends (Figure 4.2.II). Moreover, VI trending examined between the February and April periods demonstrated significant downward trends in some forest areas in Laos and Cambodia. The different results of dry seasons could possibly have been caused by the limitation of water during dry season periods.

Regarding VI trends of different forest areas, MODIS Terra EVI mainly yielded a substantial upward trend in Myanmar and Laos, while some forests in east Myanmar experienced a downward trend with MODIS Aqua EVI. The different time ranges between Terra (2001–2016) and Aqua (2003–2016) sensors potentially caused this difference.

Compared to BRDF-uncorrected EVI, BRDF-corrected EVI at SZ45 demonstrates a significant upward trend for most of SEA (Figure 4.2.I.C). This is evidence of BRDF impact on trending analyses of continental SEA tropical forests and

that BRDF-corrected results displayed greater trends. The variations between trends of BRDF-uncorrected and corrected EVI were insignificant in thedry season (February–April). Although forests in eastern Myanmar and northern Laos demonstrate an uptrend, some forests in southern Laos and Cambodia experienced a downtrend for BRDF-corrected and uncorrected EVI.

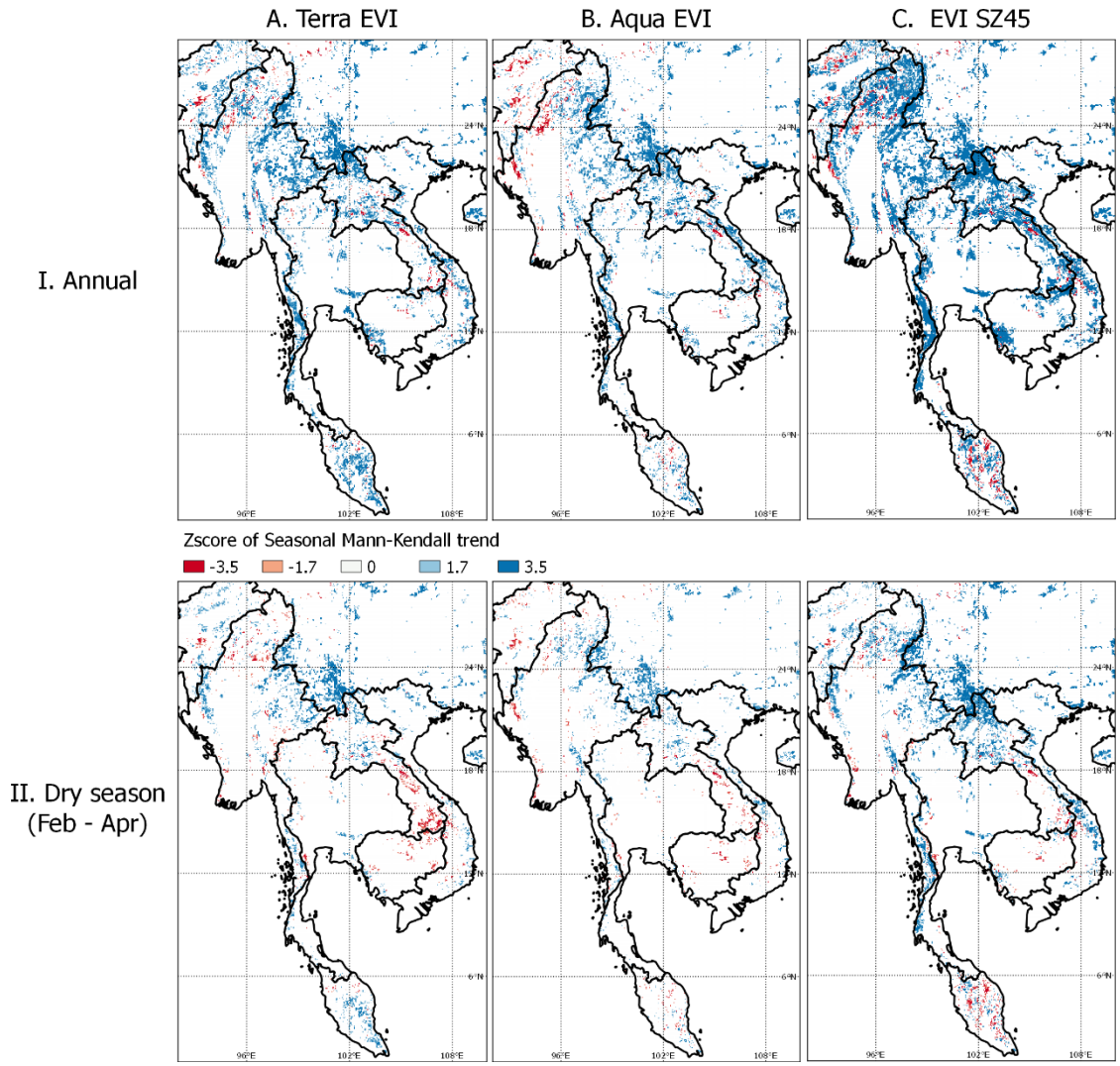

Figure 4.2. *Z-score of forest areas with significant trends ($p < 0.05$) generated from monthly CMG EVI data. MODIS BRDF/Albedo CMG daily data were converted to the monthly interval to match the temporal resolution of MODIS VI CMG data. The SMK tests of Terra and BRDF-corrected time series were calculated for the period from 2001 to 2016, while the Aqua VI time series were limited from 2003 to 2016.*

While BRDF significantly affected SEA forest EVI trends, the EVI SSS demonstrated that the BRDF effect varied with different lengths in SEA tropical forest dry seasons (Figure 4.3). In wet forests with a dry season of zero to two months, BRDF-

corrected EVI data yielded lower increasing trend slopes than BRDF-uncorrected EVI. In contrast, EVI trend slopes were higher, with BRDF correction for forests with a three- to seven-month dry season.

The outcome of the dry season was similar to the annual result. Although EVI trend slopes of the period from February to April were lower than yearly trend slopes, the trend relationship between BRDF-corrected and uncorrected was the same as the annual trends (Figure 4.4). Most continental SEA regions had distinct dry seasons (except southern Thailand and the area of peninsular Malaysia), which explained why the trend map of BRDF-corrected EVI illustrated more forest coverage with significant uptrend during this study period.

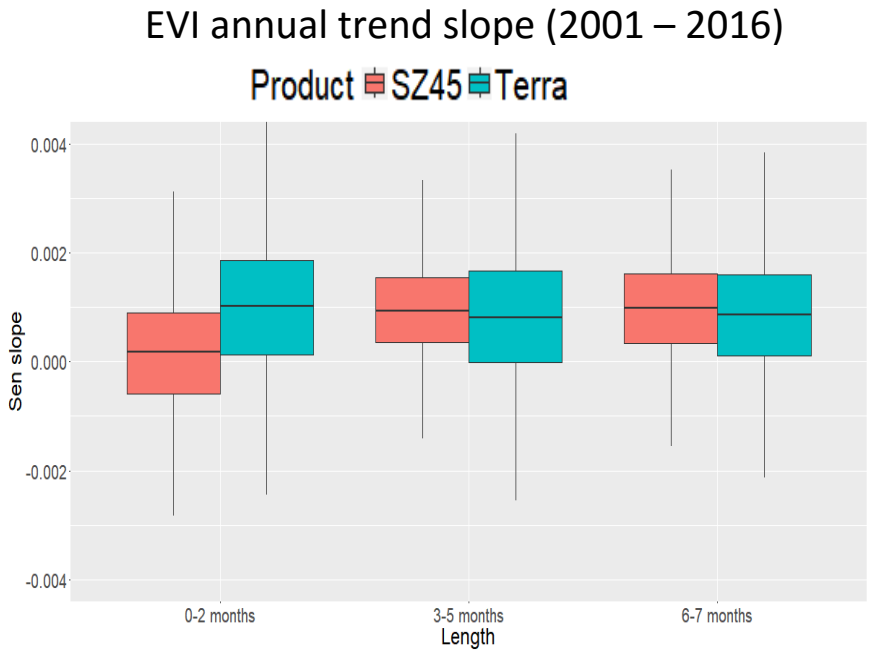

Figure 4.3. *EVI SSS of SEA forests at CMG resolution between MODIS Terra and BRDF-corrected SZ45 with various dry season lengths for 16 years (2001–2016).*

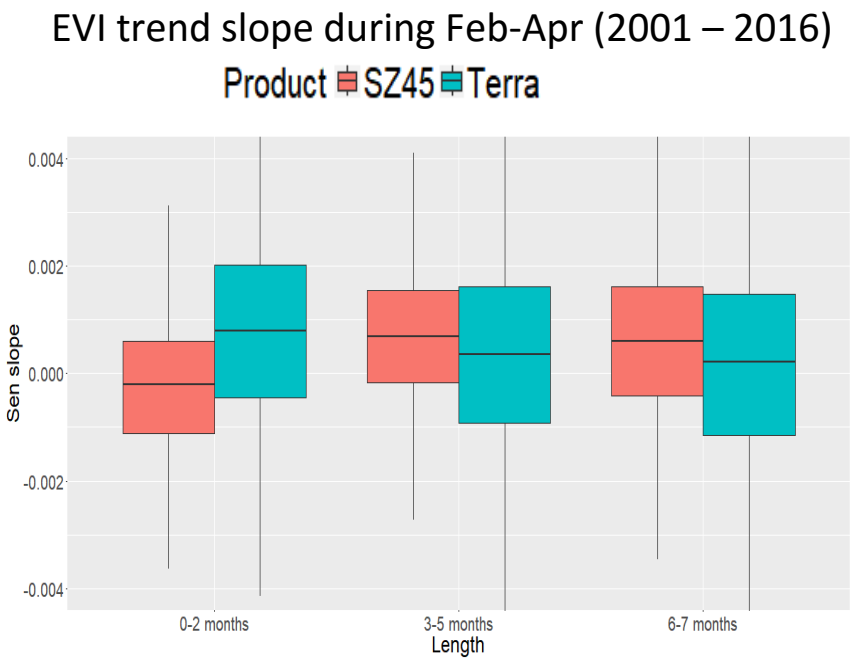

Figure 4.4. *EVI SSS of SEA forests at CMG resolution between MODIS Terra and BRDF-corrected SZ45 with various dry season lengths during the periods from February to April (2001–2016).*

Significant trending areas derived from NDVI time series for SEA forest areas showed the different results between MODIS Terra and Aqua NDVI, less the BRDF influence compared to trend results obtained from EVI time series (Figure 4.4). Although continental SEA forests demonstrate a significant uptrend with Terra NDVI data, tropical forests across northern Myanmar, southern Laos and peninsular Malaysia illustrate downward trends with the Aqua NDVI time series (Figure 4.5.I). The differences in trends derived from Terra and Aqua NDVI time series potentially resulted from the different observed time periods (Terra: 2001–2016, Aqua: 2003–2016). For dry season trending, NDVI trending maps of Aqua and Terra were similar, with some forests demonstrating significant downtrends. The similar results of NDVI and EVI trends confirmed the greening of most SEA tropical forests and downtrends of some forests during dry seasons.

The BRDF effect on NDVI trending results is insignificant, as Z-score trend maps between BRDF-corrected and uncorrected Terra NDVI over the same calculated period (2001–2016) are similar for both inter-annual and dry season trends (Figure 4.5.C). This similarity suggests that the BRDF influence is insignificant, with trending results retrieved from NDVI time series and this outcome similar to the results in Chapter 2.

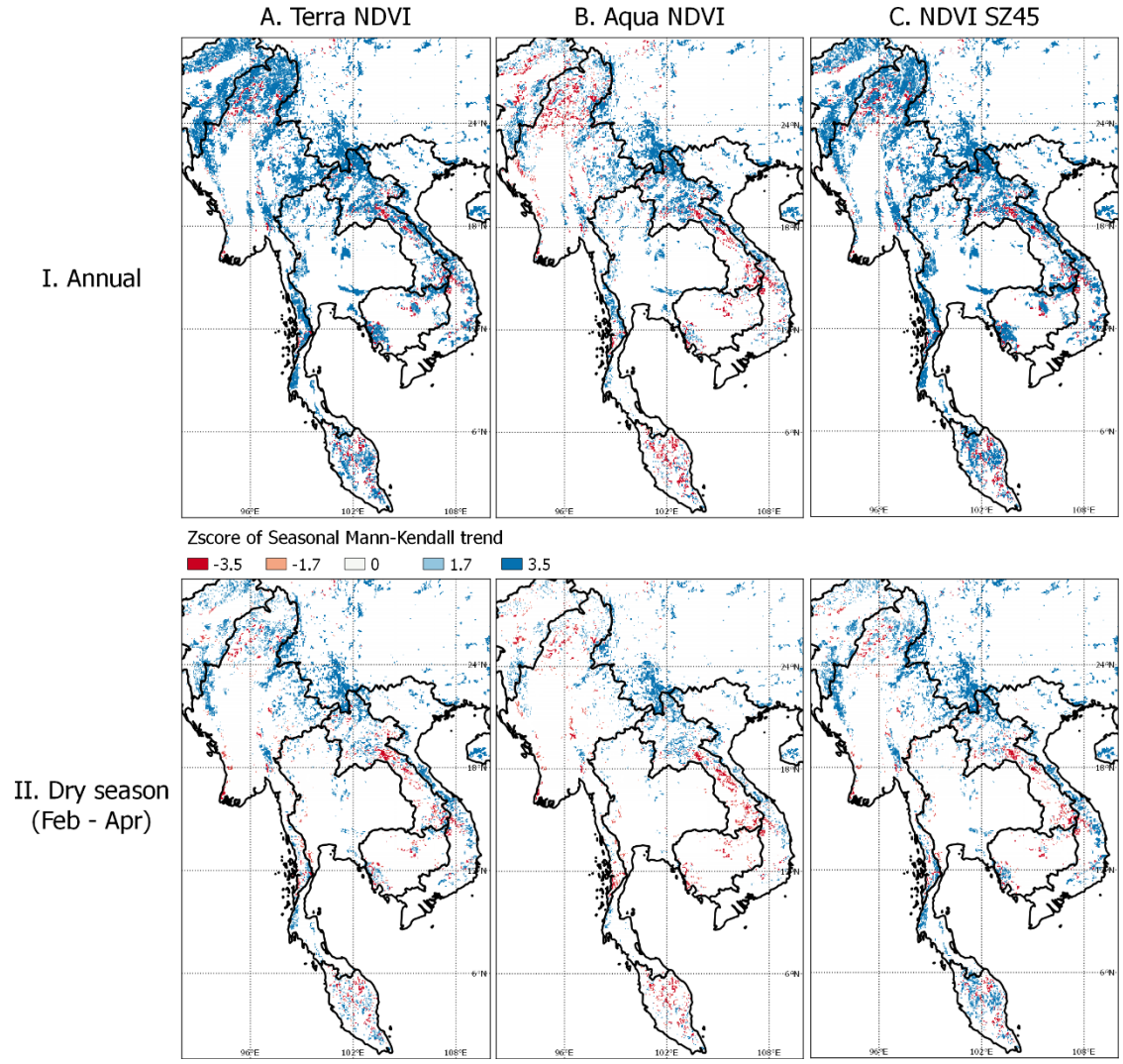

Figure 4.5. *Z-score of forest areas with significant trends ($p < 0.05$) generated from monthly CMG NDVI data. MODIS BRDF/Albedo CMG daily data were converted to the monthly interval to match the temporal resolutions of MODIS VI CMG data. The SMK tests of Terra and BRDF-corrected time series were calculated for the period from 2001 to 2016, while the Aqua VI time series used for the SMK test was limited from 2003 to 2016.*

4.3.1.2. Comparison of EVI trend slopes between undisturbed forests (500 m) and disturbed influenced forests (0.05 degree)

The trends between undisturbed forests and forests with disturbance influence were further investigated by comparing the EVI trend slopes between undisturbed forests at 500 m resolution and CMG forests with various dry season lengths (Figures 4.6 and 4.7). The observed results of annual trends demonstrated in Figure 4.6 revealed that undisturbed forests had lower trend slopes than mixed CMG forests for both BRDF-corrected and uncorrected EVI. EVI trend slopes in the dry season (February–April) presented similar results, as trend slopes of undisturbed forests were lower than forests

with a disturbance effect at 0.05 degree resolution (Figure 4.7). The similarity between annual trends and trends for the period from February to April mean the greening of undisturbed forests was insignificant compared with mixed CMG (0.05 degree) forests during this study period.

Regarding BRDF effect, BRDF-corrections could reverse the SSS patterns. In specific, SSS of forests having short dry season (0-2 months) was positive with BRDF-uncorrected EVI while it was negative with BRDF-corrected SZ45 EVI regardless forest types. Moreover, the SSS gaps between undisturbed and disturbed influenced forests were amplified after applying BRDF-correction. These findings suggest that BRDF correction is needed to capture precise forest VI trends.

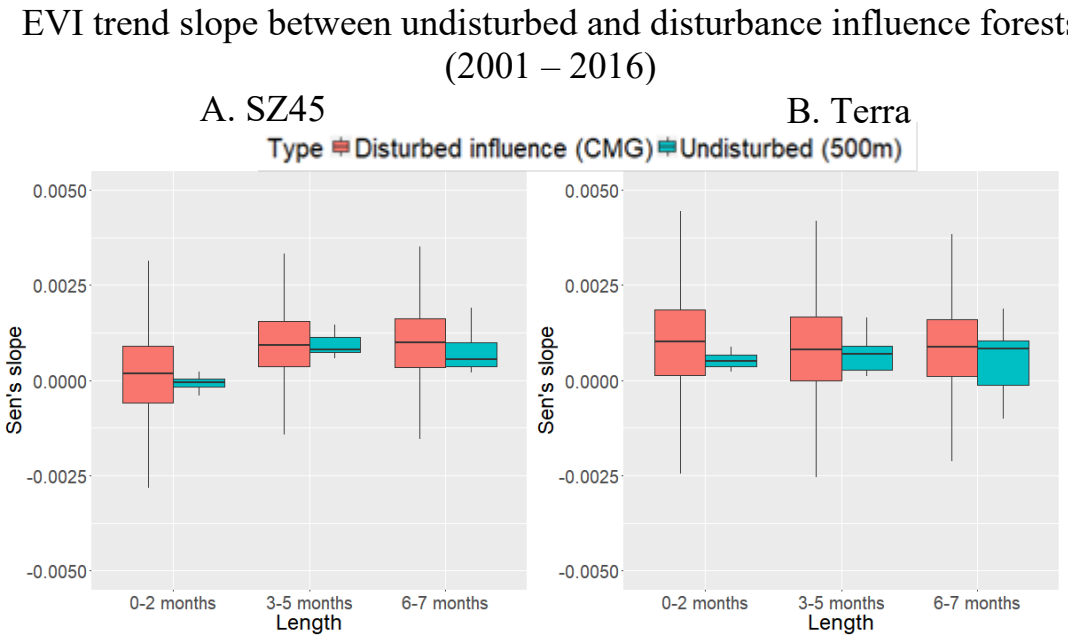

Figure 4.6. *Comparison of EVI SSS between undisturbed forests (500 m scale) and CMG forests with different dry season lengths. A. BRDF-corrected SZ45 EVI. B. MODIS Terra EVI.*

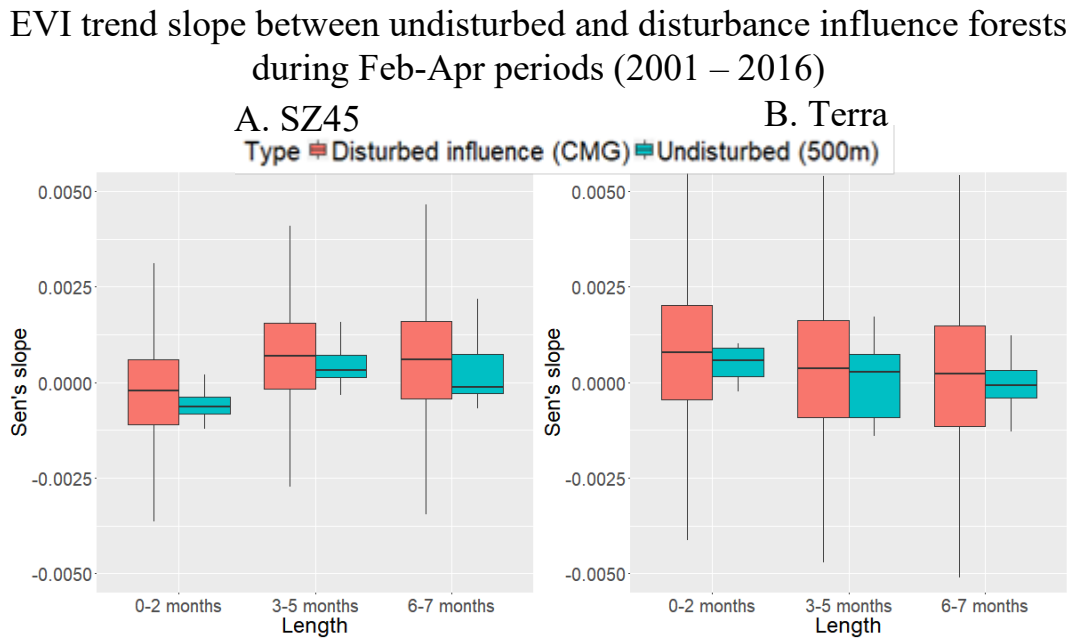

Figure 4.7. *Comparison of EVI SSS between undisturbed forests (500 m scale) and CMG forests with different dry season lengths for the period from February to April. A.BRDF-corrected SZ45 EVI. B.MODIS Terra EVI.*

4.3.1.3. Effect of SZ settings on VI trending of SEA tropical forests

VI trends of various SZ settings (SZ15–SZ45) were calculated and plotted with nadir view to investigate potential result variations between different SZ settings (Figures 4.8 and 4.9). In general, the effect of SZ angle settings was insignificant for the SMK trend test. For most SEA tropical forest areas, Z-score trend maps were similar, with different SZ angles for NDVI and EVI time series.

Forests in peninsular Malaysia are the only forested areas that present considerable differences in trends across various fixed SZ configurations. For EVI trends, Malaysian forest trends decreased with the increasing SZ values for annual and dry season periods (Figure 4.8). In contrast, Z-scores derived from the SMK test on NDVI time series are positively correlated with the increasing of solar zenith angles (Figure 4.9). Given that NDVI is mostly insensitive with BRDF influences and peninsular Malaysia is an area with high annual rainfall and no dry season (Chapter 2), the contrasting results of NDVI and EVI suggest that the variations caused by different SZ settings were potentially the result of cloud issues.

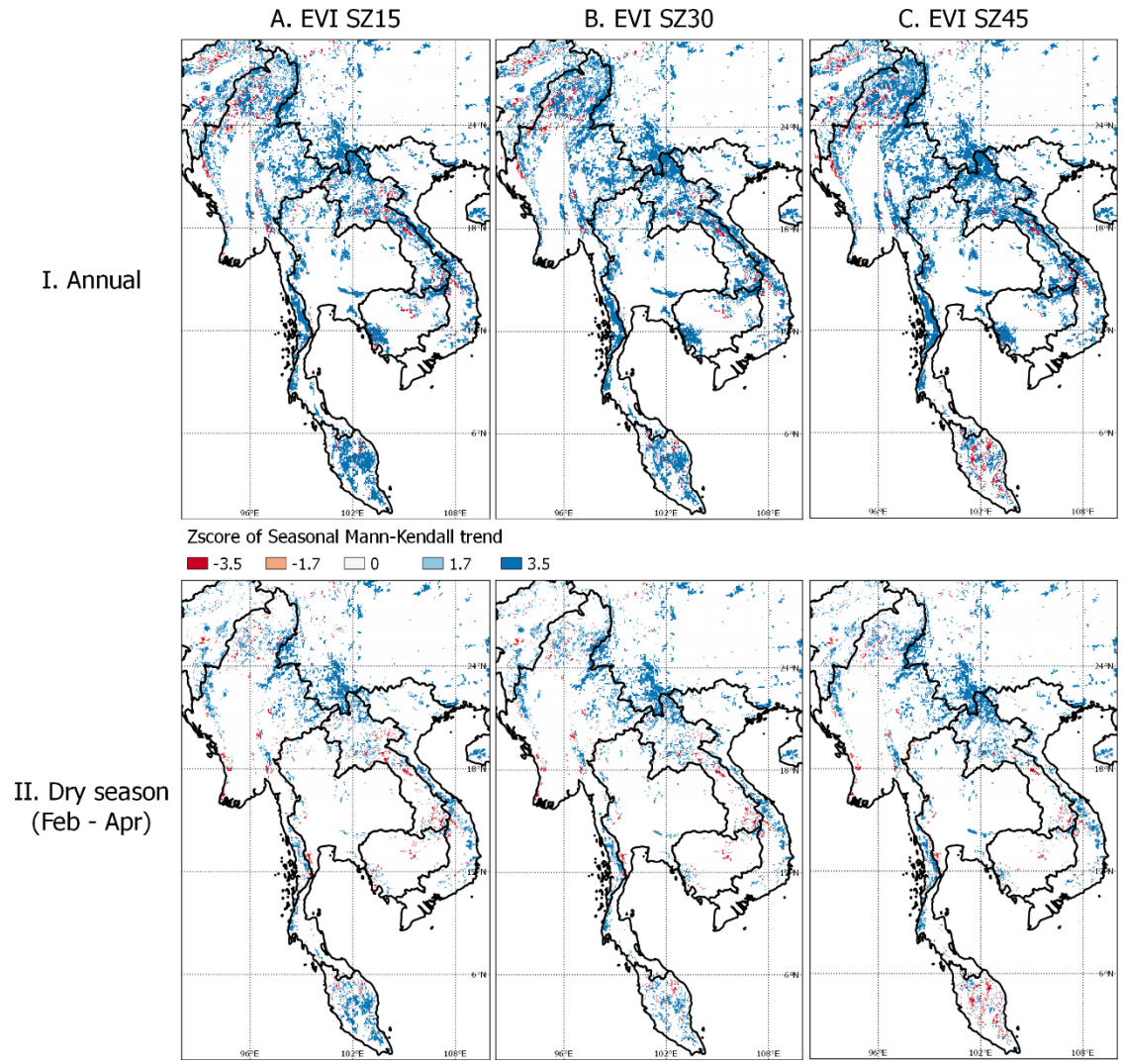

Figure 4.8. *Z-score of forest areas with significant trends ($p < 0.05$) generated from various SZ settings of EVI. MODIS BRDF/Albedo CMG daily data were converted to the monthly interval to match the temporal resolution of MODIS VI CMG data from 2001 to 2016.*

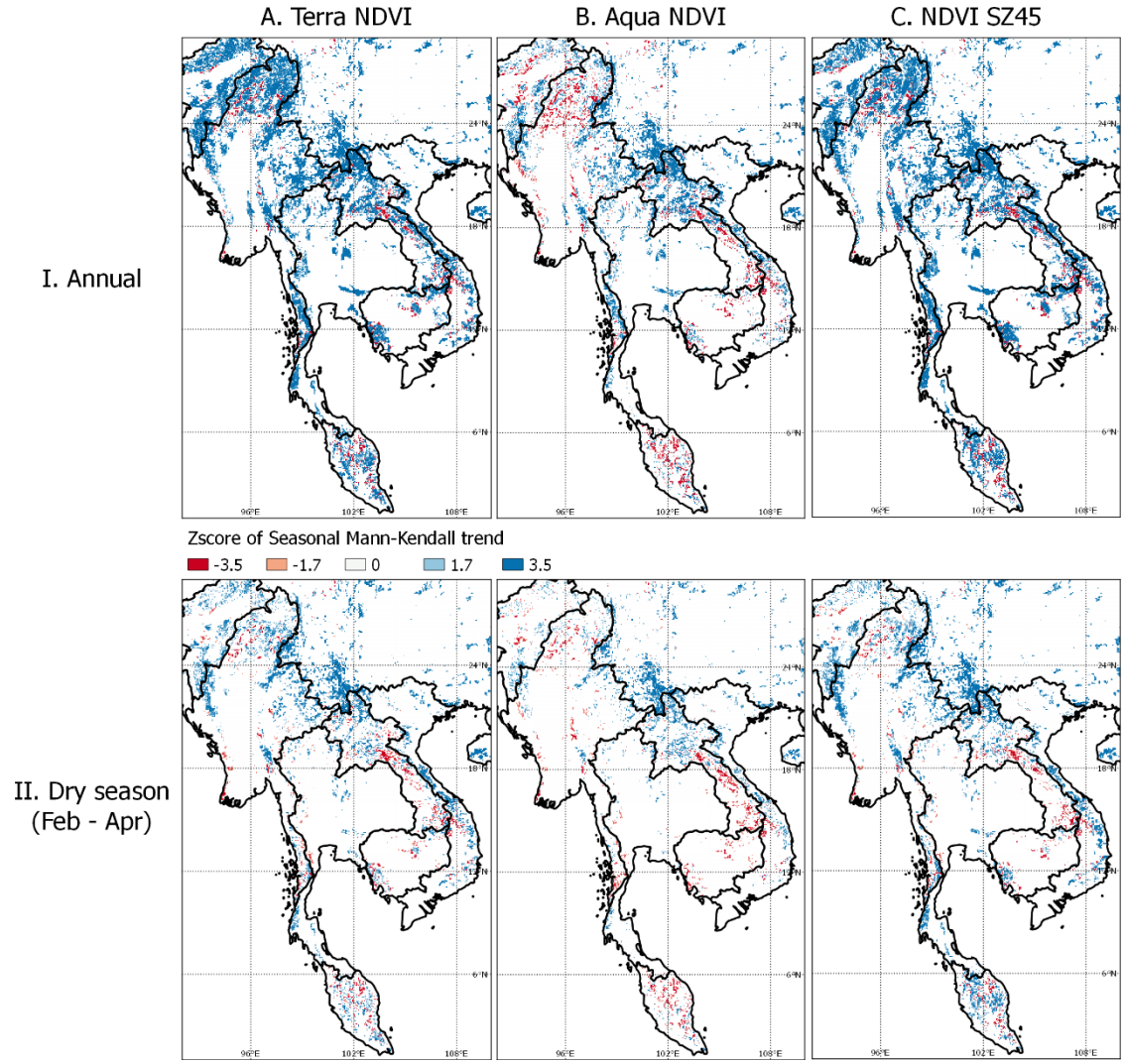

Figure 4.9. *Z-score of forest areas with significant trends ($p < 0.05$) generated from various SZ settings of EVI. MODIS BRDF/Albedo CMG daily data were converted to the monthly interval to match the temporal resolution of MODIS VI CMG data from 2001 to 2016.*

4.3.2. VI anomalies of SEA tropical forests and BRDF influence on results

4.3.2.1. Anomalies of VI for SEA tropical forests

Detailed anomaly VI maps are shown in Figures 4.10 to 4.12 for MODIS Terra, Aqua and BRDF-corrected SZ45, respectively. Annual anomaly maps of Terra VI exhibit yearly spatial changes of forest EVI (Figure 4.10.A) and NDVI (Figure 4.10.B). VI maps have two anomalous years of 2001 (Terra) and 2003 (Aqua), which had the lowest anomaly values for mainland SEA forests. As these years coincides with the beginning working time of Terra and Aqua satellites, we suspect that anomaly maps of these years were uncertainty due to sensor calibration or stabilisation.

Except for the year 2001 (Terra) and 2003 (Aqua), annual changes of VI varied with forest locations. Forests in northern Myanmar experienced the lowest annual VI in 2010, while the minimum VI anomalies of forests in eastern Myanmar occurred between 2008 and 2009. During the study period, the VIs of forests in Laos were low in 2002 and 2008, while VI anomalies of forests in northern Vietnam were lowest in 2011. Forests in Cambodia demonstrated their lowest anomaly VI in the period from 2015 to 2016. In contrast to areas with distinct long dry seasons, VI anomalies of peninsular Malaysia demonstrated insignificant variations during the study period from 2001 to 2016.

Compared to the Terra VI anomaly map, Aqua VI anomaly maps generally exhibited similar annual changes for most SEA forest areas (Figure 4.11). The significant disagreement between Terra and Aqua anomaly VI occurred in 2007. VI anomalies of forests in southern Laos, southern Vietnam and Cambodia were low, with Aqua VI measurements in 2007, while VI anomalies of these forests calculated from Terra VI time series were neutral in the same year.

Annual changing patterns between NDVI and EVI of SEA tropical forests are similar, except for the period from 2004 to 2005. During this period, EVI of many forested areas dropped significantly (Figures 4.10A and 4.11A), while NDVI measurements decreased slightly (Figures 4.10B and 4.11B). This difference suggests that EVI is more sensitive to sudden changes in forested vegetation than NDVI.

Figure 4.12 presents annual anomalies of BRDF-corrected EVI and NDVI fixed at SZ45. It was observed that yearly anomaly maps with BRDF corrections eliminated

strange VI anomalies in 2001 (Terra) and 2003 (Aqua). In addition, the variations of BRDF-corrected VI anomalies appeared to be lower than anomalies of BRDF-uncorrected VI. In terms of annual changes, inter-annual VI changes were similar between BRDF-uncorrected and corrected VIs. For example, EVI anomalies were low from 2004 to 2005 and Cambodian forests showed their low VI anomalies from 2015 to 2016. Another noteworthy example includes the bottom VI anomalies of forests in western Myanmar in 2009, which can be observed in both standard Terra/Aqua and SZ45 VI maps (Figures 4.10–4.12).

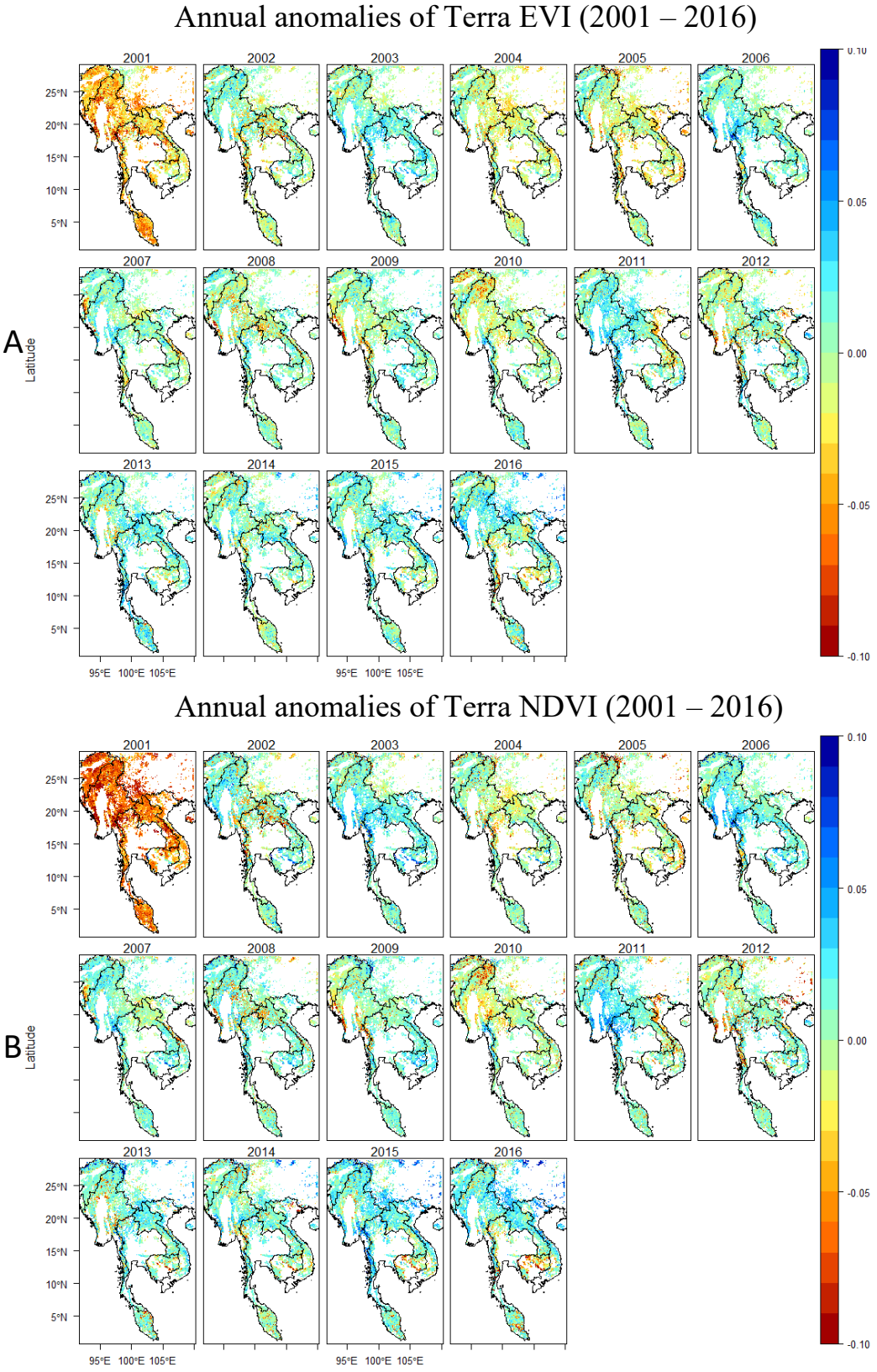

Figure 4.10. *Annual anomalies of forest areas for 16 years (2001–2016) of MODIS Terra VI generated from MODIS Terra CMG monthly data. A.EVI B.NDVI*

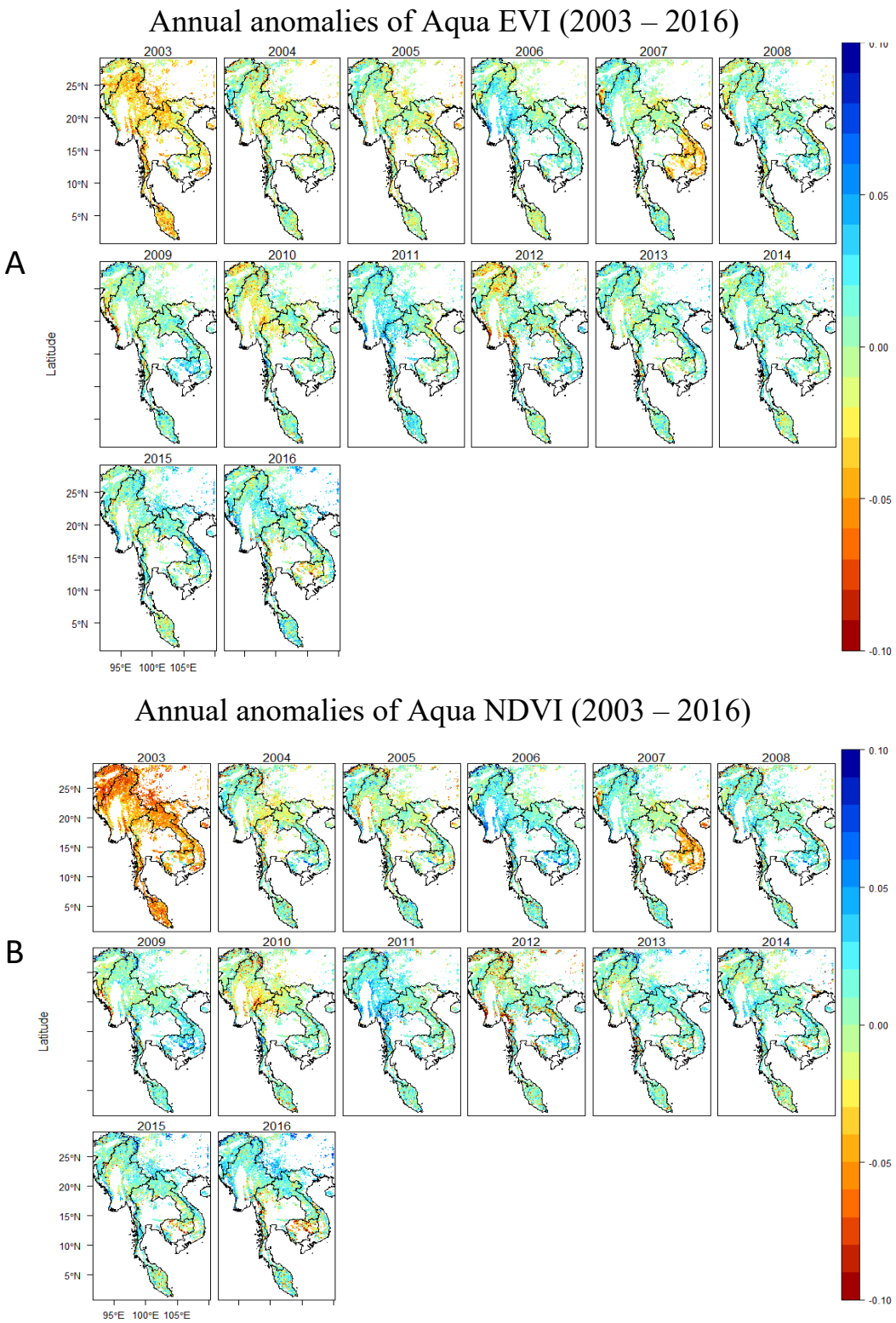

Figure 4.11. *Annual anomalies of forest areas for 14 years (2003–2016) of MODIS Aqua VI generated from MODIS Aqua CMG monthly VI data. A. EVI B. NDVI.*

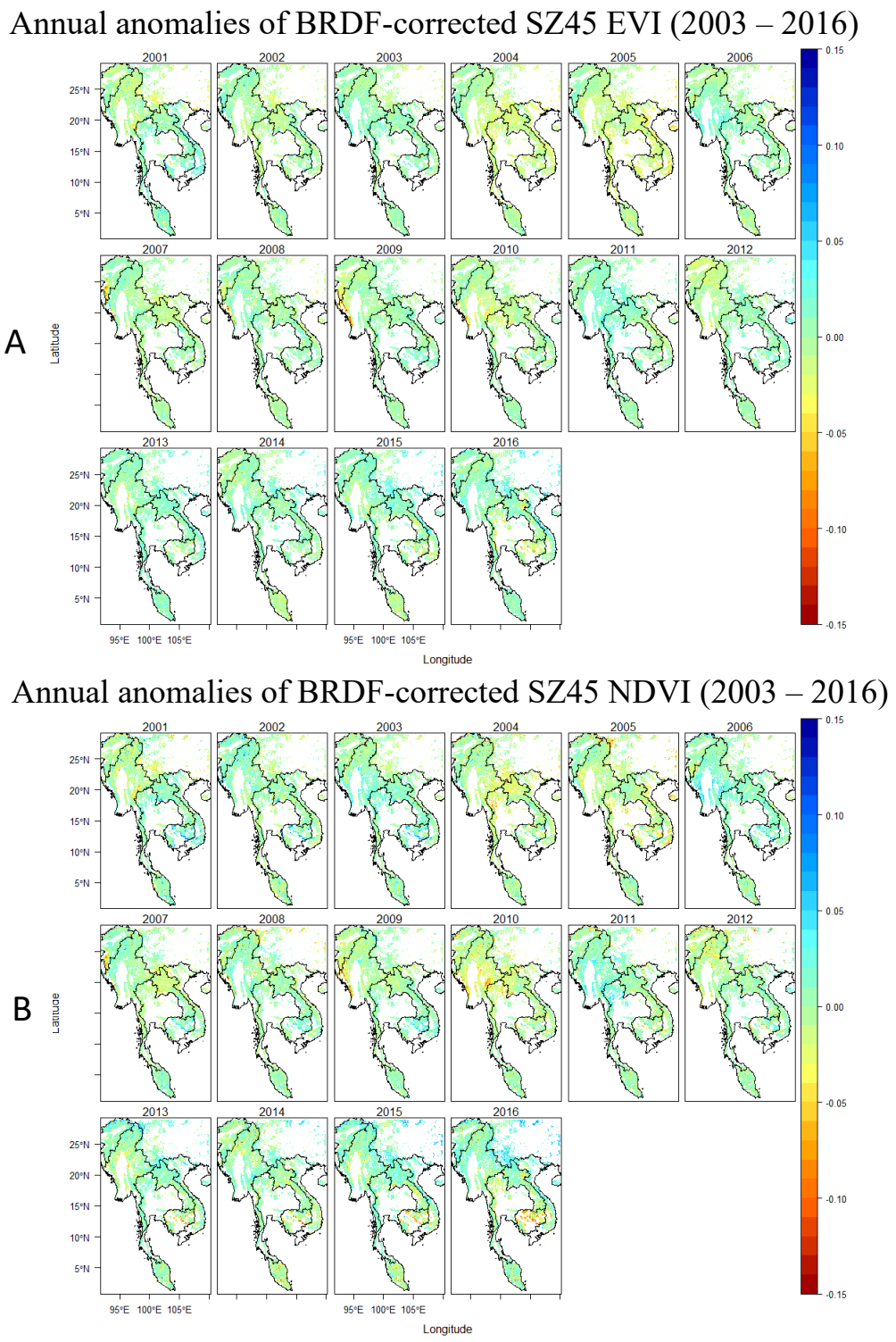

Figure 4.12. *Annual anomalies of forest areas for 16 years (2001–2016) of VI fixing at SZ 45 degrees and nadir view. Data were derived from MODIS BRDF/Albedo CMG data and converted from daily data to monthly data. A. EVI B. NDVI.*

To understand how forest VI changed annually and the BRDF influences on these annual changes, average yearly VI anomalies of SEA forest areas between BRDF-corrected and uncorrected VI (Figure 4.13) were plotted. From 2004 to 2016, anomalies between BRDF-uncorrected (Terra and Aqua) and BRDF-corrected VI were similar and the differences were minor. However, yearly anomalies of BRDF-uncorrected VI yielded abnormal values in 2001 (Terra) and 2003 (Aqua). For MODIS Terra, EVI anomalies increased from –0.04 (2001) to zero (2002), while NDVI anomalies jumped to zero in 2002 from the lower –0.06 value. A similar change occurred with Aqua VI from 2003 to 2004, as VI anomalies rose to 0.02 (EVI) and 0.05 (NDVI). This finding suggests that BRDF-uncorrected VI data caused individual anomalous results, although the general patterns remained intact for the long term.

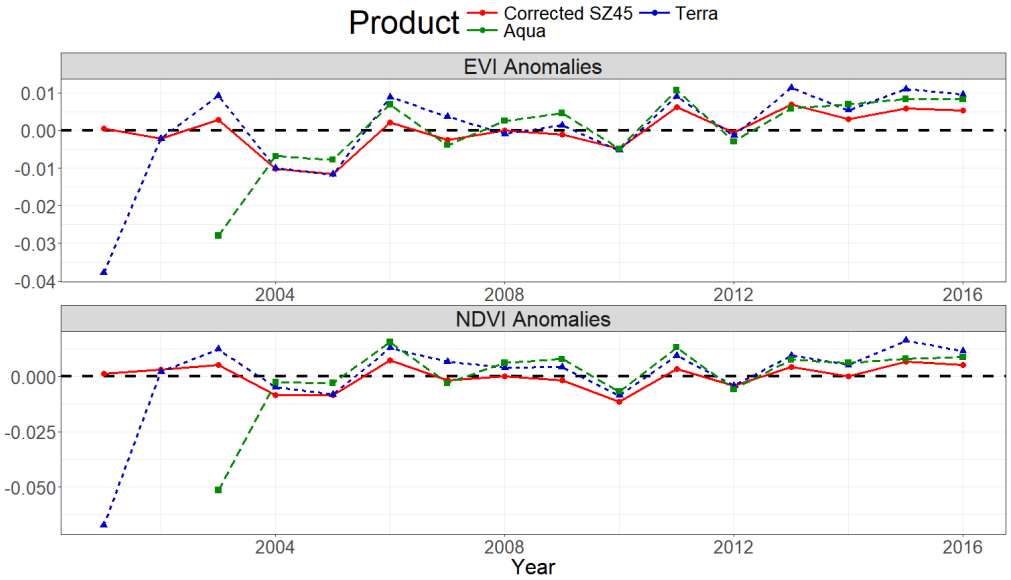

Figure 4.13. *Averaged SEA forest VI anomalies of CMG (0.05 degree) resolution between MODIS Terra/Aqua and BRDF-corrected SZ45 EVI (top) and NDVI (bottom) from 2001 to 2016.*

Aside from trend and annual anomaly maps, the inter-annual coefficient of variation (CV) or relative standard deviation was calculated to show relative yearly variations of SEA tropical forests (Figure 4.14). CV measurements calculated from BRDF-uncorrected VI time series were highest in the forests along the border of Burma and Thailand. Parts of Cambodian forests had high CV values from 2001 to 2016. High CV values indicate that annual changes in these forests are highest compared to forests in other regions.

Compared with CV maps retrieved from BRDF-corrected VI time series, it was found that BRDF-corrected CV measurements were lower than BRDF-uncorrected VI ones for most continental SEA forests (Figures 4.14.I.C and 4.14.II.C). In contrast, CVs derived from BRDF-corrected and uncorrected VIs are similar in some forested areas, especially over Cambodian jungles. These differences suggest that CVs calculated from BRDF-uncorrected VI data may amplify the annual changes in SEA forest VI and cause misinterpretation of results.

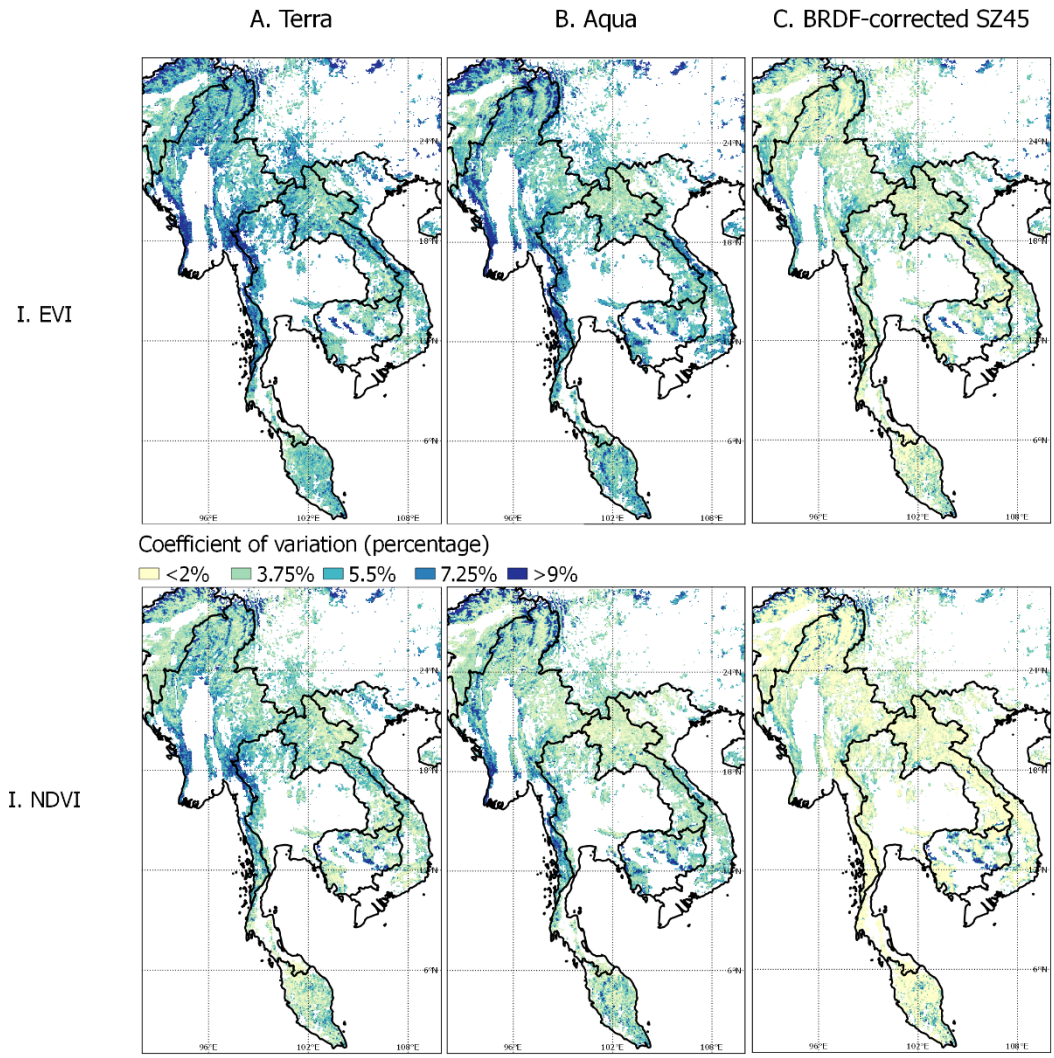

Figure 4.14. *Inter-annual VI CV (relative standard deviation) of forest areas from 2001 to 2016 for both EVI (top) and EVI (bottom). A. Terra, B. Aqua, C. BRDF-corrected SZ45.*

4.3.2.2. Comparison VI anomalies between undisturbed and mixed CMG forests

The comparison of VI anomalies between undisturbed forests at a 500 m scale and CMG 'disturbed influenced' forests showed that VI anomalies between the two forest

types were similar regardless of BRDF correction (Figure 4.15). EVI of both undisturbed and mixed CMG forests decreased significantly during the period from 2004 to 2005, while NDVI anomalies exhibited significant declines during the periods from 2004 to 2005 and 2009 to 2010. The similarity of VI anomalies suggests that disturbed and undisturbed forests in peninsular SEA had the same VI anomalies during this study period.

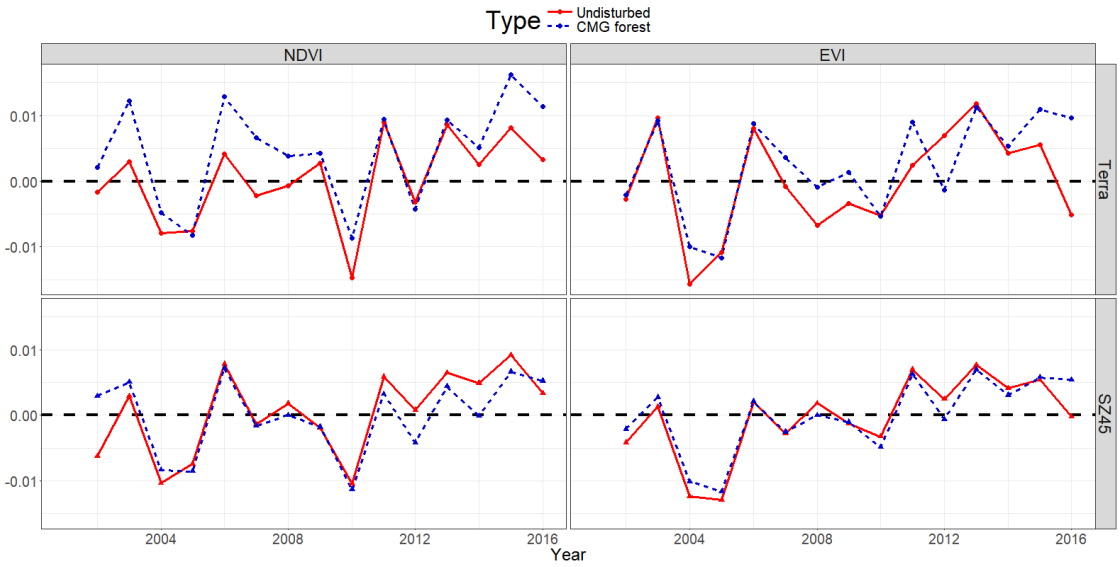

Figure 4.15. *Comparison of BRDF-corrected and uncorrected VI anomalies between undisturbed forests (500 m) and mixed CMG forests (0.05 degree).*

Regarding VI anomalies without BRDF correction, it was observed that there were significant differences between the two forest types (Figure 4.15). For example, NDVI anomalies in SEA tropical forests at CMG resolution were substantially higher than for undisturbed forests at a 500 m scale. Inter-annual EVI anomalies in undisturbed forests fluctuated in comparison with mixed CMG forests from 2008 to 2016. This indicated the need for BRDF correction to capture precise VI anomalies for continental SEA forests.

The VI anomalies of forests with various dry season lengths were compared across continental SEA (Figure 4.16). The inter-annual VI anomalies between forest types shown in Figure 4.16 were similar, with averaged VI anomalies shown in Figure 4.15, except for the EVI of wet forests represented zero to two months of dry season. In 2014, undisturbed EVI of moist forests dropped substantially, while EVI anomalies of other forests were higher than the average EVI for the entire study period.

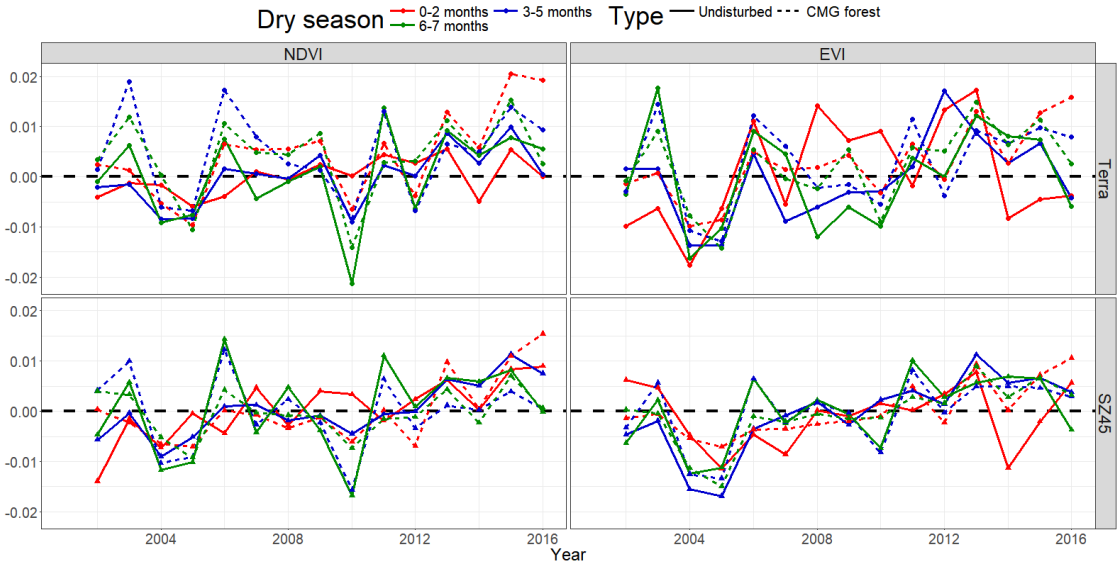

Figure 4.16. *Comparison of BRDF-corrected and uncorrected VI anomalies between undisturbed forests (500 m) and mixed CMG forests (0.05 degree) with various dry season lengths.*

4.3.3. Inter-annual variations of climate factors and the relationship between VI and climate variability

4.3.3.1. Climate trends and their relationship with VI trends

Trend maps of rainfall data derived from monthly CHIRPS datasets show that rainfall had no significant trends for continental SEA forests, except some forested areas on the border of Laos–Vietnam and southern Myanmar in the dry season periods (Figure 4.17). Considering absolute Z-score values derived from the SMK test, SEA rainfall tended to increase but dry season rainfall tended to decline, indicating that SEA rainfall in the dry season appeared to be more intensified, although these changes were insignificant, at 90 per cent confidence ($p < 0.05$).

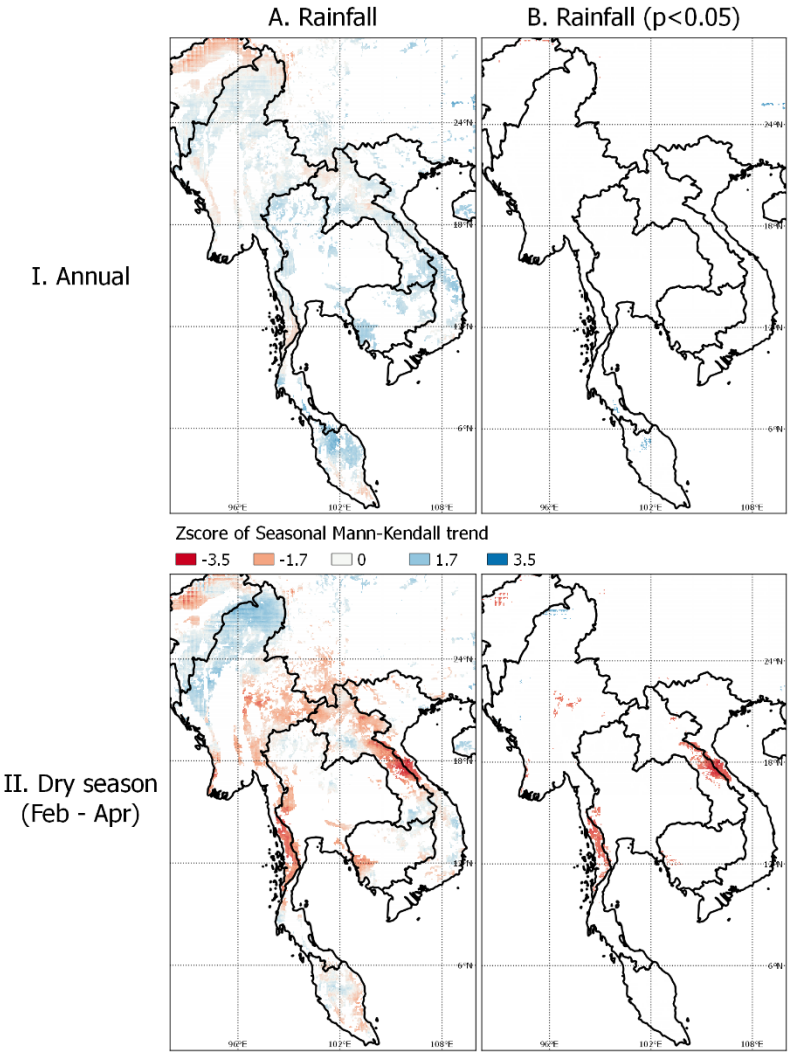

Figure 4.17. *Z-score of the SMK test calculated from monthly CHIRPS rainfall for SEA forest areas. I. Top row. Z-score maps derived from whole rainfall time series. A. All available values. B. 90 per cent confidence. II. Bottom row. Z-score maps derived from dry season (February–April) rainfall time series. A. All available values. B. 90 per cent confidence.*

Trend maps of GRACE TWSA data revealed that water storage of continental SEA increased in Laos and peninsular Malaysia, while dropping across other regions (Figure 4.18A). During the dry season, most forests in continental SEA experienced downtrends during the period from 2002 to 2016 (Figure 4.19A). Combined with rainfall trends. This finding suggests that water supplies across peninsular SEA tended to be more limited in the dry season.

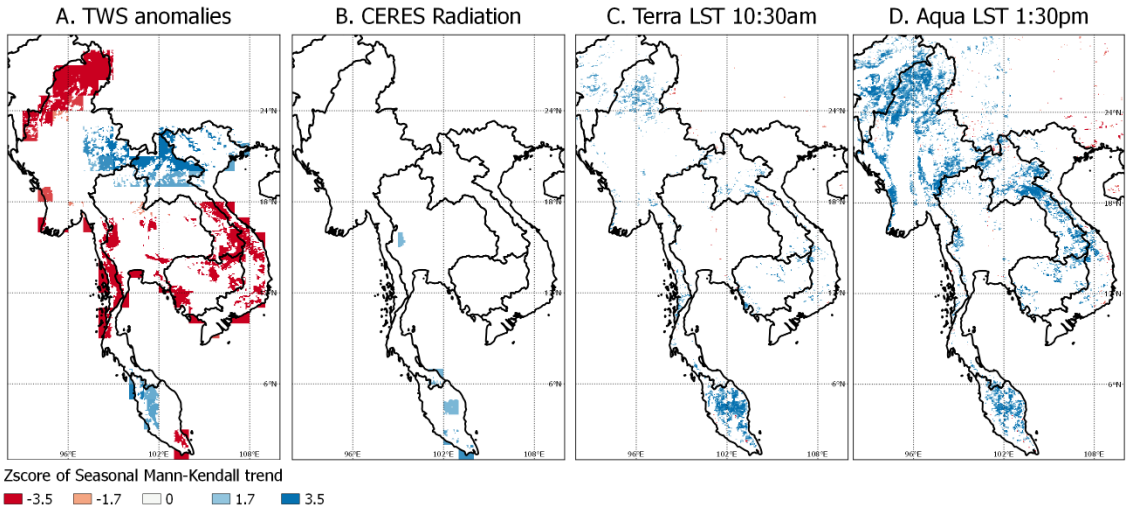

***Figure 4.18**. Z-scores of the SMK test calculated from monthly climate variables for SEA forest areas with 90 per cent confidence ($p < 0.05$). A. TWSA (one degree–110 km). B. CERES shortwave radiation (one degree–110 km). C. LST 10.30am (0.05 degree). D. LST 1.30pm (0.05 degree).*

Radiation trends derived from CERES shortwave solar radiation increased during the dry season; while inter-annual trends showed significant upward trends across a small part of mainland SEA (Figures 4.18B and 4.19B). In contrast, MODIS LST trend maps exhibited more significant upward trends during the dry season than inter-annual LST trends (Figures 4.18C and 4.19C).

LST trend Z-score map show that SEA forest LST increased after 16 years for 2001 – 2016 duration period (Figures 4.18C and 4.18D). However, there are differences between trending scores retrieved from MODIS Terra and Aqua LST daytime time series data. While Terra LST trend maps illustrate a significant upward trend in peninsular Malaysia, Myanmar and Laos (Figure 4.18C), the majority of SEA forest areas experienced upward trends, at 90 per cent confidence with Aqua LST daytime data (Figure 4.18D). As MODIS Terra and Aqua sensors take images at 10.30 am and 1.30 pm local time, the results mean that forest LST increased in the hottest hours of the day (1.30 pm), rather than in the morning (10.30 am).

Comparing annual and dry season trends, increasing LST during the dry season appeared to be less significant than the annual trend (Figures 4.19C and 4.19D). In peninsular Malaysia, the sizes of forest areas with strong upward trends were smaller during the dry season for both Terra and Aqua LST. In other regions, Aqua trends in dry season showed a substantial positive trend in northern Myanmar and parts of Laos (Figure

4.19D), while annual Aqua SMK trends illustrated uptrends for the majority of SEA forest areas (Figure 4.19D).

Connecting the rainfall and forest VI trends, it was discovered that the relationship between trends in forest VI and rainfall varied with forest location. Forest areas with significant downward trends (Laos and Myanmar) of precipitation in the dry season also experienced downward VI trends over the same time (Figures 4.17 and 4.2). In northern Myanmar, where rain tended to increase marginally, some forests suffered downward trends of VI, while the majority of forests in the area had VI upward trends during the study period (2001–2016).

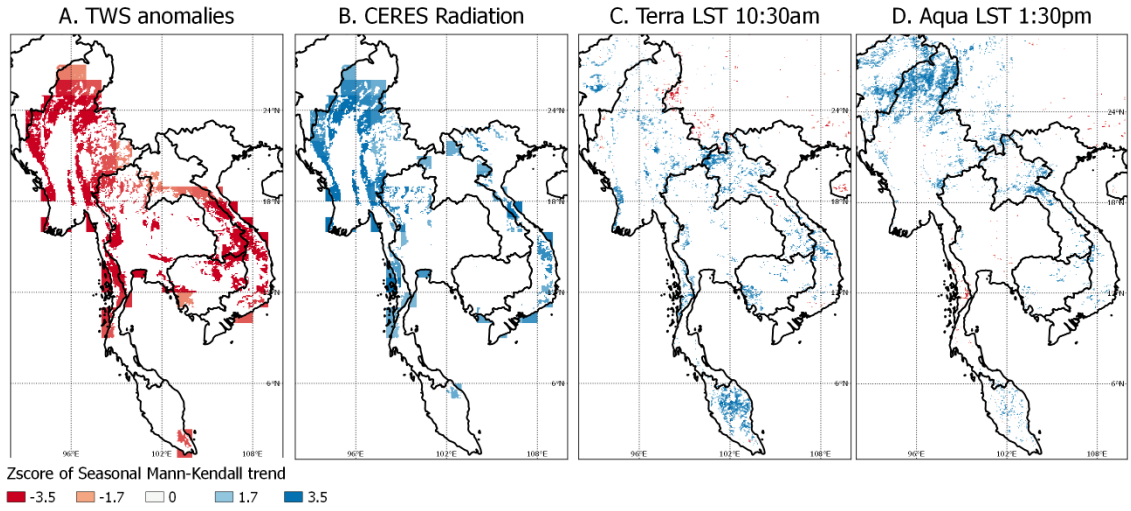

Figure 4.19. *Z-scores of the SMK test calculated from monthly climate variables of dry season periods (February–April) for SEA forest areas with 90 per cent confidence ($p < 0.05$). A. TWSA (one degree—110 km). B. CERES shortwave radiation (one degree—110 km). C. LST 10.30am (0.05 degree). D. LST 1.30pm (0.05 degree).*

4.3.3.2. Trending comparison between forest VI, rainfall and LST

SSS of BRDF-corrected VI, rainfall and LST of chosen sites was calculated at a 500 m scale to analyse the specific relationship between forest VI trends and climate trends. Figure 4.20 shows the correlated plot between the SSS score of BRDF-corrected VI and rainfall. In general, VI slopes indicate that forest VI increased for both NDVI and EVI, as most of the SSS values were positive. However, following the correlation figure, VI increasing trends had no apparent relationship with rainfall trends, as rainfall slopes are the mixed and regression lines of VI and rainfall are nearly horizontal.

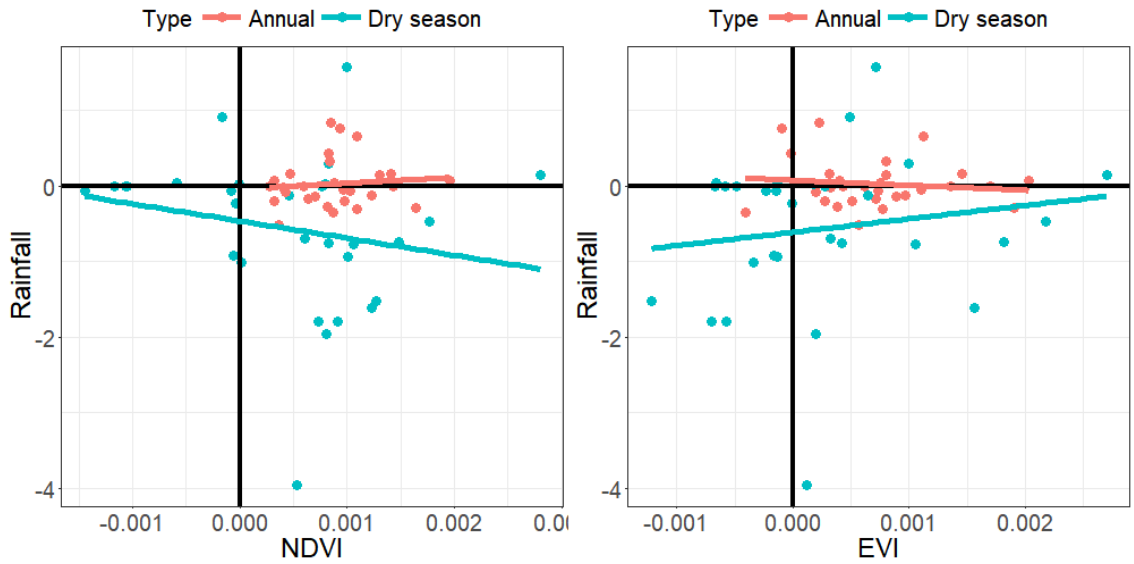

Figure 4.20. *Correlation plot between SSS of CHIRPS rainfall and BRDF-corrected VI of undisturbed forests (500 m) at SZ45 during the period from 2001 to 2016. A. NDVI v. rainfall. B. EVI v. rainfall.*

During the dry season, rainfall tended to decrease, as the majority of rainfall slope values were lower than zero. Forest VI trends in dry periods illustrate VI dependence on rainfall. However, the reliance of NDVI and EVI is variable. While EVI changes are positively correlated with rainfall changes, NDVI trends are negatively correlated with rainfall trends.

Correlation between forest VI and LST trends is presented in Figure 4.21. In contrast to rainfall, LST exhibited a significant impact on forest VI. Forest NDVI and EVI measurements tended to decrease as LST increased. This phenomenon is a surprising result, in consideration of the fact that both LST and VI of SEA forests significantly increased during the study period from 2001 to 2016. This means that the greening of SEA forests was not the consequence of LST increasing. Rising forest LST limited the greening of SEA forests.

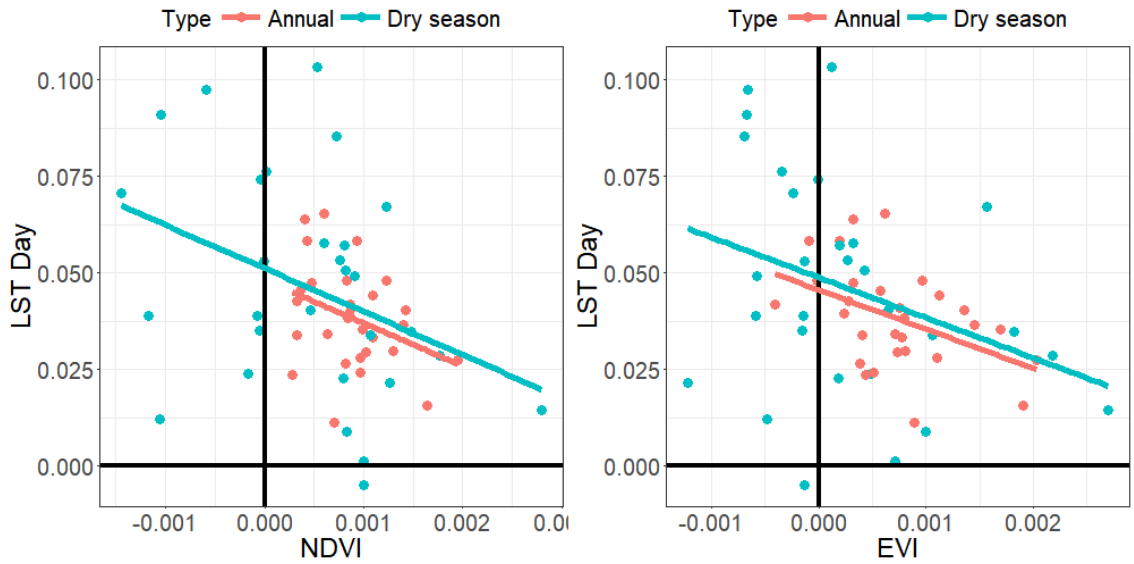

Figure 4.21. *Correlation plot between SSS of MODIS Terra LST and BRDF-corrected VI of undisturbed forests (500 m) at SZ45. A. NDVI v. LST daytime. B. EVI v. LST daytime.*

4.3.3.3. Anomalies in rainfall and LST and their relationship with forest VI

Spatial annual anomaly maps of precipitation are shown in Figure 4.22. They present low anomaly precipitation caused by the El Niño event for the period from 2014 to 2015. The 2009 El Niño decreased rainfall in Myanmar, northern Thailand and northern Laos. Compared with forest VI inter-annual variations (Figures 4.10–4.12), Cambodia was the only region where rainfall variation from 2014 to 2015 had a significant influence. In other forest regions, the effect of low precipitation from 2014 to 2015 was marginal.

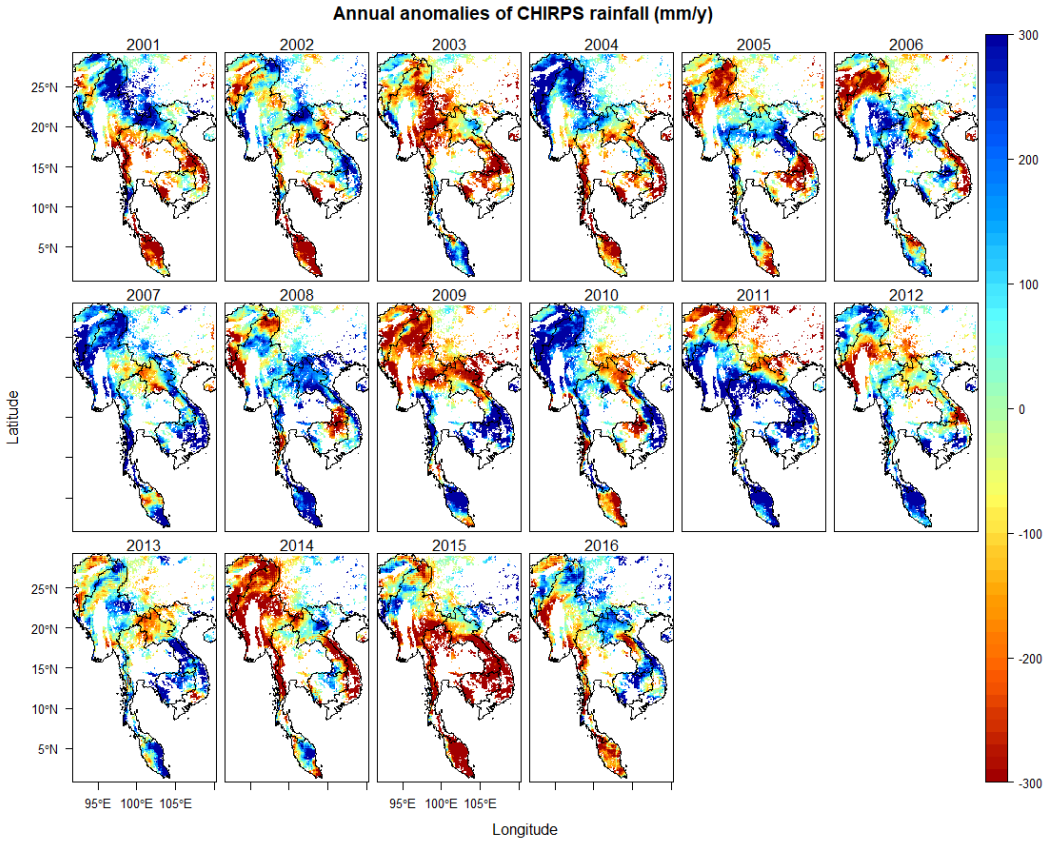

Figure 4.22. *Inter-annual rainfall anomalies of SEA tropical forests between 2001 and 2016, derived from CHIRPS monthly data.*

To understand the relationship between SEA forest VI and climate variability, averaged annual anomalies of forest EVI and other climate variables were plotted in Figure 4.23. Precipitation appeared to be negatively correlated with the ENSO index from 2001 to 2016. Rainfall decreased with an increase in the ENSO ONI index. Nevertheless, forest EVI anomalies showed no apparent relationship with rainfall or ENSO events. For example, the 2014 to 2016 ENSO event was considered one of the strongest El Niño events since 1950 (Becker, 2016) and its effect was reflected in the negative rainfall anomalies. However, forest EVIs declined marginally for both BRDF-corrected and uncorrected EVI from 2014 to 2016. The result suggests that SEA tropical forests were resilient against extreme rain events.

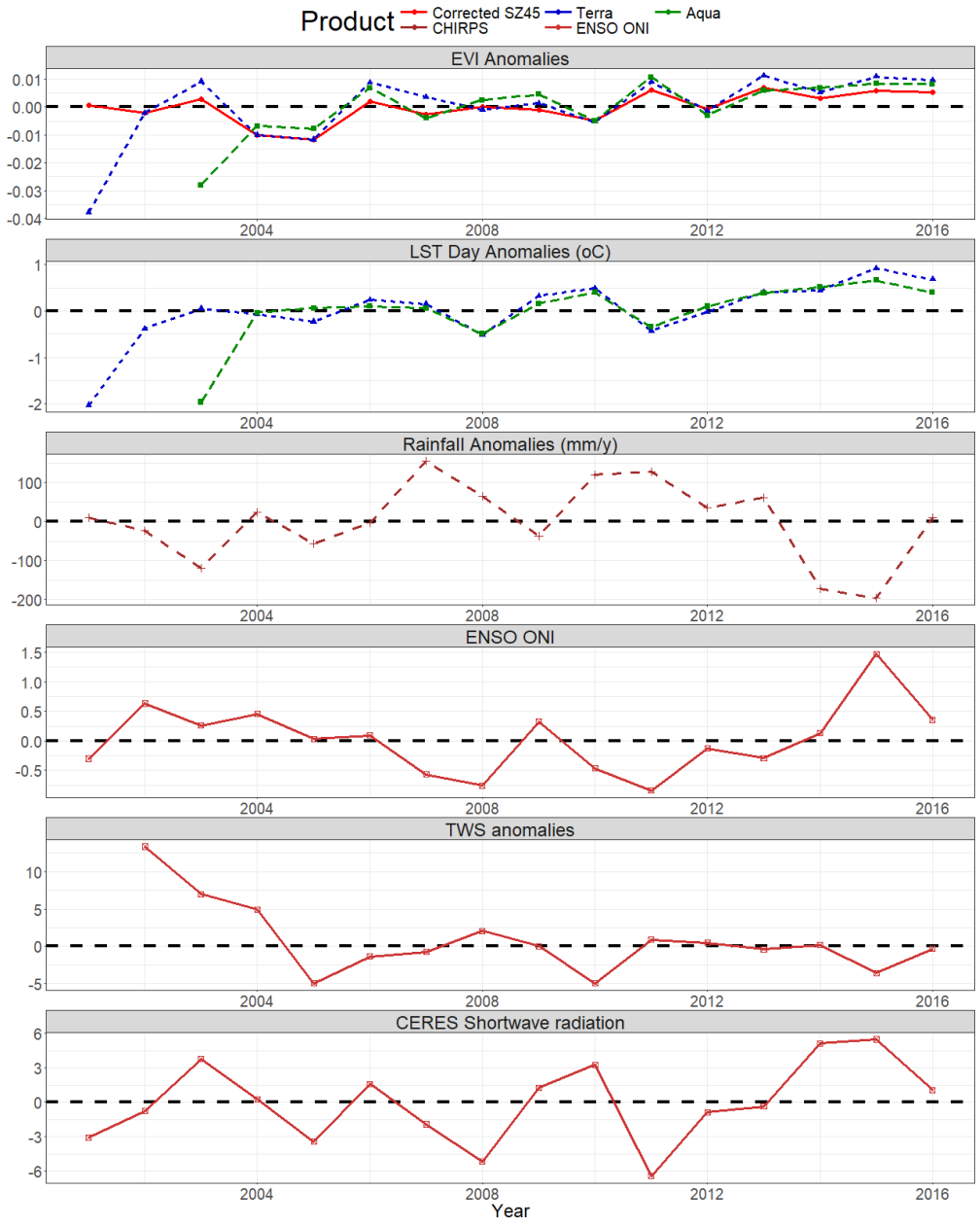

Figure 4.23. *Inter-annual anomalies of CMG forest EVI and climate factors from 2001 to 2016.*

Unlike rainfall, inter-annual TWSA decreased significantly from 2002 to 2005 and changed minimally after. During the period from 2002 to 2005, forest EVI also fell substantially, similarly to total water storage (TWS) changes. Rainfall tended to increase in the same period. This finding suggests that SEA forest greenness is dependent on TWS, with significant inter-annual variations, not just precipitation.

Regarding anomalies in other factors, CERES radiation anomalies were generally correlated with ENSO ONI. Radiation anomalies and ENSO ONI decreased from 2001 to 2011 and increased from 2011 to 2016. Additionally, LST anomalies showed their dependence on the ENSO index, as annual LST anomalies matched ENSO ONI

variations. LST increased for the period from 2011 to 2016, which is associated with the rise in the ENSO index. An increase in ONI or incoming radiation potentially caused the increase in LST. During the period from 2011 to 2016, it appeared that LST and shortwave radiation increase was positively correlated with EVI increase.

4.3.3.4. Relationship between inter-annual climate variability and VI anomalies of forests with differing dry season lengths

Selected forest sites were classified into categories to analyse inter-annual EVI of different forest types based on rain conditions. Figure 4.24 shows the inter-annual anomalies of BRDF-corrected EVI, rainfall and LST of forest types based on the length of their dry seasons. EVI anomalies of all forest types indicated that EVI decreased from 2004 to 2005. This decline was unrelated to rainfall changes, as rain tended to increase during the same period. However, this decrease in EVI was well correlated with TWS anomalies during the same period.

During ENSO in the 2014 to 2016 period, rainfall of all forest types declined significantly, especially wet forests that had a dry season length of zero to two months. Annual forest EVI of wet forests dropped considerably in 2014, while annual EVI of other forest types declined insignificantly from 2014 to 2016. The different responses of SEA tropical forests suggest the resilience of forests with pronounced dry seasons and the sensitivity of forests with short or no dry seasons with inter-annual rainfall variability.

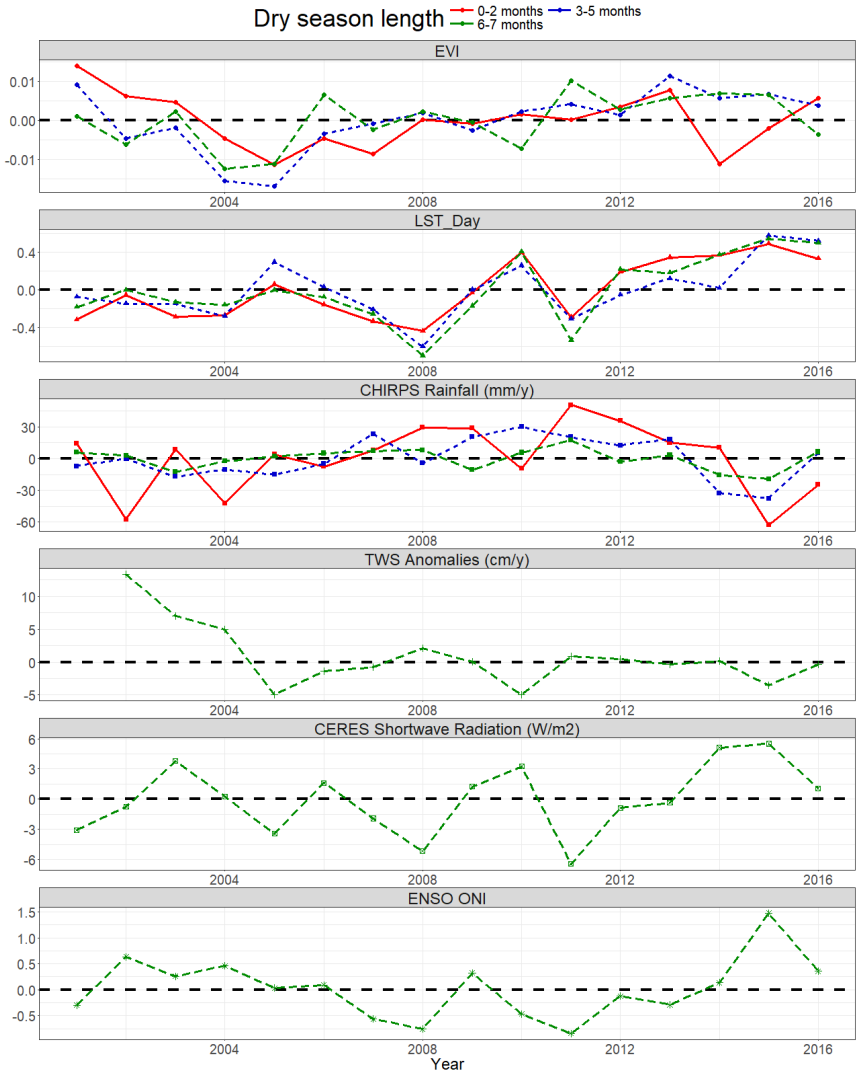

Figure 4.24. *Annual anomalies of VI (NDVI and EVI) at 500 m resolution, rainfall, LST, CERES shortwave radiation and TWS of forests with dry seasons of various lengths. TWS and CERES radiation anomalies are single lines because of their coarse spatial resolution.*

4.4. Discussion

4.4.1. Inter-annual VI variability of SEA tropical forests and the influence of BRDF on results

One of the primary goals of this chapter is to investigate the inter-annual variation of forest VI across continental SEA. The trend results reveal that forest NDVI and EVI increased during the study period from 2001 to 2016 (Figures 4.2 and 4.3). However, VI upward trends were insignificant for inter-annual dry season periods. The mixed VI trends of SEA tropical forests during the dry season periods suggests that VI of SEA tropical forests increased considerably from 2001 to 2016 due to greening during the wet periods, rather than the dry periods.

Zhang et al. (2016) concluded that SEA forest NDVI continuously declined during the dry seasons, while the results revealed that only a small portion of SEA tropical forests experienced NDVI downtrends during the study period. As Zhang used MODIS Terra VI Collection 5 (C5) data with two other remote-sensed datasets for his analyses, his results are likely to be unreliable. Terra-C5 VI were considered to overestimate decreases in trending. Large portions of browning areas in the tropics discovered by Terra-C5 VI were not evident in Terra-C6 VI (Zhang, Song, Band, Sun & Li, 2017).

Considering the effect of BRDF on VI trends, the results of the SMK test derived from BRDF-corrected EVI found forested areas with significant upward trends, in comparison to BRDF-uncorrected EVI (Figure 4.2). The BRDF influence on the dry season trends was similar to annual trends, as trend maps retrieved from EVI fixed at SZ45 showed more pixels with significant trends than standard, uncorrected VI products (Terra and Aqua). Further, slope comparisons revealed that BRDF-uncorrected EVI underestimated trends for forests with a dry season length of zero to two months, while it reversed with forests with longer dry season lengths. In contrast, NDVI was resilient to BRDF influences.

The difference in results derived from BRDF-corrected and uncorrected VI measurements was further evidenced by inter-annual VI anomalies (Figures 4.8–4.11). Although MODIS Terra and Aqua VI illustrated strange VI anomalies in 2001 and 2003, BRDF-corrected VI appeared to eliminate those abnormal VI anomalies. The VI anomaly

comparison between undisturbed and mixed CMG forests illustrated BRDF influence. The VI anomalies between two forest types were similar with BRDF correction, while anomalies in BRDF-uncorrected were fluctuating.

As MODIS satellites observed landscapes at the same local time everyday, variations of inter-annual sun angles were marginal. In contrast, satellite positions, which were variable, caused the higher inter-annual variations of observed VZA (section 2.3.2 of chapter 2). These VZA variations could be the main possible reason for the inter-annual differences between BRDF-corrected and -uncorrected VI. Another plausible reason is the different algorithms of MODIS VI and MODIS Albedo/BRDF parameter products. The VI products choose the best observation of all 16-day data to represent landscape greenness (Didan et al., 2015). As such, the inter-annual VI values captured at different DOYs within the 16-day window. In contrast to MODIS VI, MODIS Albedo/BRDF parameters are calculated from the entire 16-day reflectance data surrounding the day of interest, with weight factors (Strahler & Muller, 1999). Therefore, BRDF-corrected VI values can minimise uncertainties caused by inter-annual VZA variations and different DOY choosing.

4.4.2. SEA inter-annual changes in climate factors for SEA tropical forest areas and the relationship between forest VI and climate variability

Another objective of this chapter is to investigate the relationship between inter-annual VI changes and climate variability. Using trending analysis, it was observed that rainfalls of SEA tropical forests were insignificant during the study period (Figure 4.17). This result contrasts with the Suepa study (2016), which demonstrated significant downtrends from 2001 to 2010 for the majority of the continental SEA region, although the averaged inter-annual rainfall anomalies do not show downward trends from 2001 to 2010 (Figure 4.22). Different rainfall datasets potentially caused the disagreement between this study and Suepa. While Suepa used the TRMM dataset without a description of the version used, the present study used the CHIRPS precipitation dataset that combined the latest version of TRMM (v7) with in-situ data to retrieve more accurate rainfall information over land areas (Funk et al., 2015).

Considering inter-annual changes, rainfall patterns in continental SEA forested areas demonstrated their dependence on ENSO events. A previous study by Thirumalai

et al. (2017) using modelled data showed that ENSO events drove anomalous circulation and caused rainfall reductions in April. The results of this study revealed that annual precipitation substantially dropped during the period from 2014 to 2015 due to the influence of one of the strongest El Niño events in history. As the frequency of extreme El Niño events increases due to greenhouse warming (Cai et al., 2014), rainfall anomalies are likely to occur in addition to ENSO events.

Regarding forest VI response to rainfall variations, it was found that, despite the insignificant trends of rainfall, SEA forests became greener during the study period (Figures 4.2, 4.4 and 4.5). The investigation of particular sites at a 500 m scale revealed similar results, and thus there was an unclear relationship between forest VI and precipitation in terms of trends.

Inter-annual changes in rainfall increased during the period from 2001 to 2011 (Figures 4.13 and 4.19). This gradual increase in rainfall is presumed to have caused the increase in forest VI. However, rainfall decreased for the remaining study duration from 2012 to 2015 because of the effect of the one of the strongest El Niño events in history. Rainfall significantly decreased as a result of the El Niño event but SEA VI forests responded differently depending on the lengths of their dry seasons. The EVI of forests with short dry seasons declined substantially, while VI decreases in forests with prolonged dry seasons were marginal. The findings of this study suggest that dry SEA tropical forests are adapted to their long dry seasons and were able to resist droughts by accessing subsoil water with their deep roots. Conversely, rainforests may be sensitive to droughts (Borchert, 1994). More importantly, Mendivelso et al. (2014) discovered that tropical forests in the Amazon were tolerant to short-term droughts, although they were sensitive to multi-annual droughts. In SEA, precipitation recovery was observed after the drought from 2014 to 2015. It is presumed that the forest resisted the two-year drought until precipitation returned to normal.

One abnormal aspect of SEA forests is that EVI tended to decrease from 2004 to 2005, while rainfall appeared to increase during the same period. It was realised that the decreasing forest EVI was correlated with decreases in GRACE TWSA, rather than rainfall changes (Figures 4.19 and 4.20). As SEA is a tropical region with limited snow coverage, TWS represents surface and groundwater related to subsoil water that is

accessible to forested trees. This result suggests that TWS could influence forest phenology.

However, the relationship between forest VI and groundwater requires further analysis due to the coarse spatial resolution of GRACE sensors and the decreasing forest EVI during 2004 – 2005 period was also correlated with decreases in CERES solar radiation. As rainfall increased during the period from 2004 to 2005, SEA forests supplied extra precipitation could be radiation-limited, a fact that evident from previous studies of Amazon and SEA tropical forests (Guan et al., 2015; Huete et al., 2002, 2008).

In contrast, LST of SEA forests show an increasing trend in most of peninsular SEA from 2001 to 2016, especially at 1.30 pm (Aqua) (Figure 4.3). Additionally, the anomalies in LST and shortwave radiation demonstrate a positive correlation between MODIS LST and the El Niño event from 2014 to 2016, as most forests in continental SEA increased their LST and radiation during the period from 2014 to 2015. The findings of the present study are supported by a previous study by Thirumalai et al. (2017), which concluded that global warming amplified extreme climates that were caused by El Niño events in SEA (Thirumalai et al., 2017).

The comparison with SSS calculation in this study indicated that LST changes were negatively correlated with VI changes (Figure 4.18). The results suggest that LST rises limited forest activity represented as VI. Forest EVI was more sensitive to LST variability than to rainfall. This finding was supported by the Cuba study (2013), which showed that Mexican deciduous tropical forests were more closely associated with hot temperature than rainfall variations.

4.5. Conclusion

In this chapter, the influences of BRDF on VI inter-annual variations of SEA tropical forests was analysed by comparing trends and anomalies derived from BRDF-corrected and uncorrected VI time series. The VI inter-annual changes of different forest types were inspected based on the lengths of their dry seasons to understand the relationship between forest inter-annual greenness and various rainfall conditions. The relationship between forest VI inter-annual variations and climate variability was then examined.

The results revealed that BRDF influenced EVI trends, though its effect on NDVI trends was insignificant. BRDF also affected VI anomalies as BRDF correction minimised abnormal anomaly NDVI and EVI values occurred in BRDF-uncorrected VI anomalies. The different algorithms in choosing or calculating reflectance and VI are presumed to be the main cause of these variations.

Using inter-annual variations of forest EVI and climate variables, it was found that inter-annual forest EVI anomalies depended on both rainfall, TWS and radiation changes. Although forest EVI appeared to correlate with long-term precipitation, it substantially declined with significant decreases in TWS and solar radiation in the short term.

4.6. References

Allen, K., Dupuy, J. M., Gei, M. G., Hulshof, C., Medvigy, D., Pizano, C., … Powers, J. S. (2017). Will seasonally dry tropical forests be sensitive or resistant to future changes in rainfall regimes? *Environmental Research Letters*, *12*(2), 23001. Retrieved from http://stacks.iop.org/1748-9326/12/i=2/a=023001

Becker, E. (2016). ENSO Blog: February 2016 El Niño update: Q & A...and some Thursday-morning quarterbacking. Retrieved from https://www.climate.gov/news-features/blogs/enso/february-2016-el-niño-update-q-a…and-some-thursday-morning-quarterbacking

Bhandari, S., Phinn, S., & Gill, T. (2011). Assessing viewing and illumination geometry effects on the MODIS vegetation index (MOD13Q1) time series: implications for monitoring phenology and disturbances in forest communities in Queensland, Australia. *International Journal of Remote Sensing*, *32*(22), 7513–7538. https://doi.org/10.1080/01431161.2010.524675

Borchert, R. (1994). Soil and Stem Water Storage Determine Phenology and Distribution of Tropical Dry Forest Trees. *Ecology*, *75*(5), 1437–1449. https://doi.org/10.2307/1937467

Brando, P. M., Goetz, S. J., Baccini, A., Nepstad, D. C., Beck, P. S. A., & Christman, M. C. (2010). Seasonal and interannual variability of climate and vegetation indices across the Amazon. *Proceedings of the National Academy of Sciences*, *107*(33), 14685–14690. https://doi.org/10.1073/pnas.0908741107

Brohan, P., Kennedy, J. J., Harris, I., Tett, S. F. B., & Jones, P. D. (2006). Uncertainty estimates in regional and global observed temperature changes: A new data set from 1850. *Journal of Geophysical Research Atmospheres*, *111*(12), 1–21. https://doi.org/10.1029/2005JD006548

Cai, W., Borlace, S., Lengaigne, M., Van Rensch, P., Collins, M., Vecchi, G., … Jin, F. F. (2014). Increasing frequency of extreme El Niño events due to greenhouse warming. *Nature Climate Change*, *4*(2), 111–116. https://doi.org/10.1038/nclimate2100

Chadwick, R., Good, P., Martin, G., & Rowell, D. P. (2015). Large rainfall changes consistently projected over substantial areas of tropical land. *Nature Climate Change*, *6*(2), 177–181. https://doi.org/10.1038/nclimate2805

Cuba, N., Rogan, J., Christman, Z., Williams, C. A., Schneider, L. C., Lawrence, D., & Millones, M. (2013). Modelling dry season deciduousness in Mexican Yucatán forest using MODIS EVI data (2000–2011). *GIScience & Remote Sensing*, *50*(1), 26–49. https://doi.org/10.1080/15481603.2013.778559

de Beurs, K. M., & Henebry, G. M. (2005). A statistical framework for the analysis of long image time series. *International Journal of Remote Sensing*, *26*(8), 1551–1573. https://doi.org/10.1080/01431160512331326657

Didan, K. (2015a). *MOD13A1 MODIS/Terra Vegetation Indices 16-Day L3 Global 500m SIN Grid V006 [Data set]. NASA EOSDIS LP DAAC*. https://doi.org/10.5067/MODIS/MOD13A1.006

Didan, K. (2015a). MOD13C2 MODIS/Terra Vegetation Indices Monthly L3 Global 0.05Deg CMG V006. NASA EOSDIS LP DAAC. https://doi.org/10.5067/MODIS/MOD13C2.006

Didan, K. (2015b). *MYD13A1 MODIS/Aqua Vegetation Indices 16-day L3 Global 500m SIN Grid V006*. https://doi.org/10.5067/MODIS/MYD13A1.006

Didan, K. (2015b). MYD13C2 MODIS/Aqua Vegetation Indices Monthly L3 Global 0.05Deg CMG V006. NASA EOSDIS LP DAAC. https://doi.org/10.5067/MODIS/MYD13C2.006

Didan, K., Munoz, A. B., & Huete, A. (2015). MODIS Vegetation Index User ' s Guide (MOD13 Series), *2015*(June).

Dong, J., Xiao, X., Sheldon, S., Biradar, C., Zhang, G., Duong, N. D., … Moore, B. (2014). A 50-m forest cover map in Southeast Asia from ALOS/PALSAR and its application on forest fragmentation assessment. *PLoS ONE*, *9*(1). https://doi.org/10.1371/journal.pone.0085801

Famiglietti, J. S., & Rodell, M. (2013). Water in the Balance. *Science*, *340*(6138), 1300–1301. https://doi.org/10.1126/science.1236460

Fischer, E. M., Beyerle, U., & Knutti, R. (2013). Robust spatially aggregated projections of climate extremes. *Nature Climate Change*, *3*, 1033. Retrieved from http://dx.doi.org/10.1038/nclimate2051

Friedl, M., & Sulla-Menashe, D. (2015). MCD12C1 MODIS/Terra+Aqua Land Cover Type Yearly L3 Global 0.05Deg CMG V006 [Data set]. NASA EOSDIS Land Processes DAAC. https://doi.org/10.5067/MODIS/MCD12C1.006

Fu, R., Yin, L., Li, W., Arias, P. A., Dickinson, R. E., Huang, L., … Myneni, R. B. (2013). Increased

dry-season length over southern Amazonia in recent decades and its implication for future climate projection. *Proceedings of the National Academy of Sciences*, *110*(45), 18110–18115. https://doi.org/10.1073/pnas.1302584110

Funk, C., Peterson, P., Landsfeld, M., Pedreros, D., Verdin, J., Shukla, S., … Michaelsen, J. (2015). The climate hazards infrared precipitation with stations—a new environmental record for monitoring extremes. *Scientific Data*, *2*, 150066. Retrieved from http://dx.doi.org/10.1038/sdata.2015.66

Greve, P., Orlowsky, B., Mueller, B., Sheffield, J., Reichstein, M., & Seneviratne, S. I. (2014). Global assessment of trends in wetting and drying over land. *Nature Geoscience*, *7*, 716. Retrieved from http://dx.doi.org/10.1038/ngeo2247

Guan, K., Pan, M., Li, H., Wolf, A., Wu, J., Medvigy, D., … Lyapustin, A. I. (2015). Photosynthetic seasonality of global tropical forests constrained by hydroclimate. *Nature Geoscience*, *8*(4), 284–289. https://doi.org/10.1038/ngeo2382

Hannah, L. (2015). Chapter 4 - Phenology: Changes in Timing of Biological Events Due to Climate Change. In *Climate Change Biology* (pp. 83–102).

Hirsch, R., Slack, J., & Smith, R. (1982). Techniques of trend analysis for monthly water quality data. *Water Resources Research*, *18*(1), 107–121. https://doi.org/10.1029/WR018i001p00107

Huang, B., P. W. T. (2017). Extended Reconstructed Sea Surface Temperature version 5 (ERSSTv5), Upgrades, validations, and intercomparisons. J. J. Climate. https://doi.org/10.1175/JCLI-D-16-0836.1

Huete, A. R., Restrepo-Coupe, N., Ratana, P., Didan, K., Saleska, S. R., Ichii, K., … Gamo, M. (2008). Multiple site tower flux and remote sensing comparisons of tropical forest dynamics in Monsoon Asia. *Agricultural and Forest Meteorology*, *148*(5), 748–760. https://doi.org/10.1016/j.agrformet.2008.01.012

Huete, Didan, K., Miura, T., Rodriguez, E. P., Gao, X., & Ferreira, L. G. (2002). Overview of the radiometric and biophysical performance of the MODIS vegetation indices. *Remote Sensing of Environment*, *83*(1–2), 195–213. https://doi.org/10.1016/S0034-4257(02)00096-2

Huffman, G. J., Bolvin, D. T., Nelkin, E. J., Wolff, D. B., Adler, R. F., Gu, G., … Stocker, E. F. (2007). The TRMM Multisatellite Precipitation Analysis (TMPA): Quasi-Global, Multiyear,

Combined-Sensor Precipitation Estimates at Fine Scales. *Journal of Hydrometeorology*, *8*(1), 38–55. https://doi.org/10.1175/JHM560.1

Landerer, F. W., & Swenson, S. C. (2012). Accuracy of scaled GRACE terrestrial water storage estimates. *Water Resources Research*, *48*(4), 1–11. https://doi.org/10.1029/2011WR011453

Linderholm, H. W. (2006). Growing season changes in the last century. *Agricultural and Forest Meteorology*, *137*(1–2), 1–14. https://doi.org/10.1016/j.agrformet.2006.03.006

Long, D., Yang, Y., Wada, Y., Hong, Y., Liang, W., Chen, Y., … Chen, L. (2015). Deriving scaling factors using a global hydrological model to restore GRACE total water storage changes for China's Yangtze River Basin. *Remote Sensing of Environment*, *168*, 177–193. https://doi.org/10.1016/j.rse.2015.07.003

Loo, Y. Y., Billa, L., & Singh, A. (2015). Effect of climate change on seasonal monsoon in Asia and its impact on the variability of monsoon rainfall in Southeast Asia. *Geoscience Frontiers*, *6*(6), 817–823. https://doi.org/10.1016/j.gsf.2014.02.009

Loveland, T. R., & Belward, A. S. (1997). The IGBP-DIS global 1km land cover data set, DISCover: First results. *International Journal of Remote Sensing*, *18*(15), 3289–3295. https://doi.org/10.1080/014311697217099

Marek, G. W., Baumhardt, R. L., Brauer, D. K., Moorhead, J. E., Gowda, P. H., & Mauget, S. A. (2018). Evaluation of the Oceanic Niño Index as a decision support tool for winter wheat cropping systems in the Texas High Plains using SWAT. *Computers and Electronics in Agriculture*, *151*(July 2017), 331–337. https://doi.org/10.1016/j.compag.2018.06.030

Mendivelso, H. A., Camarero, J. J., Gutiérrez, E., & Zuidema, P. A. (2014). Time-dependent effects of climate and drought on tree growth in a Neotropical dry forest: Short-term tolerance vs. long-term sensitivity. *Agricultural and Forest Meteorology*, *188*, 13–23. https://doi.org/10.1016/j.agrformet.2013.12.010

Moura, Y. M., Galvão, L. S., dos Santos, J. R., Roberts, D. A., & Breunig, F. M. (2012). Use of MISR/Terra data to study intra- and inter-annual EVI variations in the dry season of tropical forest. *Remote Sensing of Environment*, *127*, 260–270. https://doi.org/https://doi.org/10.1016/j.rse.2012.09.013

Nagai, S., Ichii, K., & Morimoto, H. (2007). Interannual variations in vegetation activities and climate variability caused by ENSO in tropical rainforests. *International Journal of Remote*

Sensing, *28*(6), 1285–1297. https://doi.org/10.1080/01431160600904972

Pennington, R. T., & Ratter, J. A. (2006). *Neotropical Savannas and Seasonally Dry Forests: Plant Diversity, Biogeography, and Conservation*. CRC Press.

Portillo-Quintero, C. A., & Sánchez-Azofeifa, G. A. (2010). Extent and conservation of tropical dry forests in the Americas. *Biological Conservation*, *143*(1), 144–155. https://doi.org/10.1016/j.biocon.2009.09.020

Riebeek, H. (2010). Global Warming. Retrieved from https://earthobservatory.nasa.gov/Features/GlobalWarming/

Rouse, J. W., Hass, R. H., Schell, J. A., & Deering, D. W. (1973). Monitoring vegetation systems in the great plains with ERTS. *Third Earth Resources Technology Satellite (ERTS) Symposium*, *1*, 309–317. https://doi.org/citeulike-article-id:12009708

Sánchez-Azofeifa, G. A., Quesada, M., Rodríguez, J. P., Nassar, J. M., Stoner, K. E., Castillo, A., … Cuevas-Reyes, P. (2005). Research priorities for neotropical dry forests. *Biotropica*, *37*(4), 477–485. https://doi.org/10.1111/j.1744-7429.2005.00066.x

Schaaf, C. B., Gao, F., Strahler, A. H., Lucht, W., Li, X., Tsang, T., … Roy, D. (2002). First operational BRDF, albedo nadir reflectance products from MODIS. *Remote Sensing of Environment*, *83*(1–2), 135–148. https://doi.org/10.1016/S0034-4257(02)00091-3

Schaaf, C. B., Liu, J., Gao, F., & Strahler, A. H. (2011). Aqua and Terra MODIS Albedo and Reflectance Anisotropy Products. In B. Ramachandran, C. O. Justice, & M. J. Abrams (Eds.), *Land Remote Sensing and Global Environmental Change: NASA's Earth Observing System and the Science of ASTER and MODIS* (pp. 549–561). New York, NY: Springer New York. https://doi.org/10.1007/978-1-4419-6749-7_24

Schaaf, C., & Wang, Z. (2015a). MCD43A1 MODIS/Terra+Aqua BRDF/Albedo Model Parameters Daily L3 Global - 500m V006. NASA EOSDIS Land Processes DAAC.

Schaaf, C., & Wang, Z. (2015b). MCD43C1 MODIS/Terra+Aqua BRDF/AlbedoModel Parameters Daily L3 Global 0.05Deg CMG V006 [Data set]. NASA EOSDIS Land Processes DAAC. https://doi.org/10.5067/MODIS/MCD43C1.006

Sen, P. K. (1968). Estimates of the Regression Coefficient Based on Kendall's Tau. *Journal of the American Statistical Association*, *63*(324), 1379–1389. Retrieved from http://www.jstor.org/stable/2285891

Strahler, A., Gopal, S., Lambin, E., & Moody, A. (1999). MODIS Land Cover Product Algorithm Theoretical Basis Document (ATBD) MODIS Land Cover and Land-Cover Change. *Change*, (May), 72. Retrieved from http://modis.gsfc.nasa.gov/data/atbd/atbd_mod12.pdf

Strahler, A. H., & Muller, J. P. (1999). MODIS BRDF Albedo Product : Algorithm Theoretical Basis Document. *MODIS Product ID: MOD43*, *Version 5.*(April), 1–53. https://doi.org/http://duckwater.bu.edu/lc/mod12q1.html

Strugnell, N. C., Lucht, W., Hyman, A. H., & Meister, G. (1998). Continental-scale albedo inferred from land cover class, field observations of typical BRDFs and AVHRR data. In *Geoscience and Remote Sensing Symposium Proceedings, 1998. IGARSS '98. 1998 IEEE International* (Vol. 2, pp. 595–597 vol.2). https://doi.org/10.1109/IGARSS.1998.699522

Suepa, T., Qi, J., Lawawirojwong, S., & Messina, J. P. (2016). Understanding spatio-temporal variation of vegetation phenology and rainfall seasonality in the monsoon Southeast Asia. *Environmental Research*, *147*, 621–629. https://doi.org/10.1016/j.envres.2016.02.005

Swenson, S., & Wahr, J. (2006). Post-processing removal of correlated errors in GRACE data. *Geophysical Research Letters*, *33*(8), 1–4. https://doi.org/10.1029/2005GL025285

Tan, Z., Zhang, Y., Deng, X., Song, Q., Liu, W., Deng, Y., … Yang, L. (2015). Interannual and seasonal variability of water use efficiency in a tropical rainforest: Results from a 9 year eddy flux time series. *Jounal of Geophysical Research: Atmospheres*, *120*(1), 465–479. https://doi.org/10.1002/2014JD022535.Received

Thirumalai, K., DiNezio, P. N., Okumura, Y., & Deser, C. (2017). Extreme temperatures in Southeast Asia caused by El Niño and worsened by global warming. *Nature Communications*, *8*, 15531. https://doi.org/10.1038/ncomms15531

Tyukavina, A., Hansen, M. C., Potapov, P. V., Krylov, A. M., & Goetz, S. J. (2016). Pan-tropical hinterland forests: Mapping minimally disturbed forests. *Global Ecology and Biogeography*, *25*(2), 151–163. https://doi.org/10.1111/geb.12394

Wan, Z. (2013). MODIS Land Surface Temperature Products Users' Guide. https://doi.org/10.5067/MODIS/MOD11B3.006

Wan, Z., Hook, S., & Hulley, G. (2015a). MOD11A2 MODIS/Terra Land Surface Temperature/Emissivity 8-Day L3 Global 1km SIN Grid V006 [Data set]. NASA EOSDIS LP DAAC. https://doi.org/10.5067/MODIS/MOD11A2.006

Wan, Z., Hook, S., & Hulley, G. (2015b). MOD11C3 MODIS/Terra Land Surface Temperature/Emissivity Monthly L3 Global 0.05Deg CMG V006 [Data set]. NASA EOSDIS LP DAAC. https://doi.org/10.5067/MODIS/MYD11C3.006

Wan, Z., Hook, S., & Hulley, G. (2015c). MYD11A2 MODIS/Aqua Land Surface Temperature/Emissivity 8-Day L3 Global 1km SIN Grid V006 [Data set]. NASA EOSDIS LP DAAC. https://doi.org/10.5067/MODIS/MYD11A2.006

Wan, Z., Hook, S., & Hulley, G. (2015d). MYD11C3 MODIS/Aqua Land Surface Temperature/Emissivity Monthly L3 Global 0.05Deg CMG V006 [Data set]. NASA EOSDIS LP DAAC. https://doi.org/10.5067/MODIS/MYD11C3.006

Wang, X., Jiang, D., & Lang, X. (2017). Future extreme climate changes linked to global warming intensity. *Science Bulletin*, *62*(24), 1673–1680. https://doi.org/10.1016/j.scib.2017.11.004

Wang, Z., Schaaf, C. B., Chopping, M. J., Strahler, A. H., Wang, J., Román, M. O., … Shuai, Y. (2012). Evaluation of Moderate-resolution Imaging Spectroradiometer (MODIS) snow albedo product (MCD43A) over tundra. *Remote Sensing of Environment*, *117*, 264–280. https://doi.org/https://doi.org/10.1016/j.rse.2011.10.002

Wanner, W., Strahler, A. H., Hu, B., Lewis, P., Muller, J.-P., Li, X., … Barnsley, M. J. (1997). Global retrieval of bidirectional reflectance and albedo over land from EOS MODIS and MISR data: Theory and algorithm. *Journal of Geophysical Research: Atmospheres*, *102*(D14), 17143–17161. https://doi.org/10.1029/96JD03295

Wielicki, B. A., Barkstrom, B. R., Baum, B. A., Charlock, T. P., Green, R. N., Kratz, D. P., … Welch, R. M. (1998). Clouds and the earth's radiant energy system (CERES): Algorithm overview. *IEEE Transactions on Geoscience and Remote Sensing*, *36*(4), 1127–1141. https://doi.org/10.1109/36.701020

Wolfgang, L., & Crystal, S. (2001). A global albedo data set derived from AVHRR data for use in climate simulations. *Geophysical Research Letters*, *28*(1), 191–194. https://doi.org/doi:10.1029/2000GL011580

Xie, Z., Huete, A., Restrepo-Coupe, N., Ma, X., Devadas, R., & Caprarelli, G. (2016). Spatial partitioning and temporal evolution of Australia's total water storage under extreme hydroclimatic impacts. *Remote Sensing of Environment*, *183*, 43–52. https://doi.org/10.1016/j.rse.2016.05.017

Yan, H., Huang, J., Minnis, P., Wang, T., & Bi, J. (2011). Comparison of CERES surface radiation fluxes with surface observations over Loess Plateau. *Remote Sensing of Environment*, *115*(6), 1489–1500. https://doi.org/10.1016/j.rse.2011.02.008

Yue, S., Pilon, P., & Cavadias, G. (2002). Power of the Mann-Kendall and Spearman's rho tests for detecting monotonic trends in hydrological series. *Journal of Hydrology*, *259*(1–4), 254–271. https://doi.org/10.1016/S0022-1694(01)00594-7

Zhang, Y., Song, C., Band, L. E., Sun, G., & Li, J. (2017). Reanalysis of global terrestrial vegetation trends from MODIS products: Browning or greening? *Remote Sensing of Environment*, *191*, 145–155. https://doi.org/10.1016/j.rse.2016.12.018

Zhang, Y., Zhu, Z., Liu, Z., Zeng, Z., Ciais, P., Huang, M., … Piao, S. (2016). Seasonal and interannual changes in vegetation activity of tropical forests in Southeast Asia. *Agricultural and Forest Meteorology*, *224*, 1–10. https://doi.org/10.1016/j.agrformet.2016.04.009

Chapter 5. Conclusions

As the least studied and one of the most disturbed regions in the world, understanding the tropical forest phenology of SEA is critical. Optical satellite-based data are suitable for investigating SEA tropical forest phenology because of their capacity to provide extended spatial and temporal resolution observations. However, varying illumination angles and viewing geometries of observed data have the potential to cause variations in surface reflectances and VI that are disassociated from vegetation canopy activities. Therefore, it is necessary for studies to examine SEA forest phenology and its relationship with climate variability and disturbance, as well as to address the effect of BRDF on derived results from satellite data.

In this thesis, the intra and inter-annual forest dynamics were studied across continental SEA, alongside an investigation of BRDF and disturbance effects on retrieved phenology for 16 years (2001–2016). The thesis objectives were completed using satellite data and statistical methods. Based on standardising forest reflectances and VI at fixed sun-view settings and comparing BRDF-uncorrected observations, BRDF influences on SEA forest phenology were analysed in relation to disturbance and climate variability. MODIS VI and BRDF/Albedo products were used as the primary data sources, with various other satellite observations retrieved from CHIRPS, GRACE, CERES and other gridded products, such as LCT, forest cover change or non-disturbed forest maps.

First, inter-seasonal phenology of SEA non-disturbed tropical forests was analysed from 2001 to 2016. The influence of BRDF on VI seasonal profiles was investigated and phenological metrics were retrieved between BRDF-corrected and uncorrected VI time series. The effect of disturbance on SEA forest dynamics was highlighted. Further, inter-annual changes over SEA tropical forests and the BRDF effect on forest VI inter-annual variations were examined during this study period. Finally, the investigation of climate variability and the relationship with forest inter-annual dynamic activities were produced.

5.1. Summary of Key Methodology and Results

5.1.1. Chapter two

Inter-seasonal dynamics and the effect of BRDF on SEA non-disturbed forests were analysed using MODIS satellite data. Undisturbed forest areas were selected to avoid the disturbance effect. SEA forests were then sorted into three classes based on dry season lengths to understand seasonal forest dynamics with various water conditions. QA filtering was considered to balance data availability and data quality, the typical issue in tropical regions. In contrast to most SEA phenology studies, this study produced and compared annual VI profiles and derived phenological metrics from BRDF-corrected and uncorrected VI time series from MODIS BRDF/Albedo and VI products. This enabled an understanding of the effect of BRDF on derived phenological parameters (or forest annual dynamics) with a different water deficit during dry periods. Statistical methods of cross-site correlation analysis were applied to quantify the effect of BRDF on phenological metrics.

The results revealed that:

1. NDVI was resilient to the BRDF effect but was not suitable to monitor SEA forest dynamics due to the issue of saturation. EVI was better at capturing inter-seasonal forest phenology but was sensitive to the influence of BRDF, which was mainly caused by seasonal observed SZA changes. EVI sensitivity was evident due to the different patterns and magnitudes of annual EVI profiles derived from BRDF-corrected and uncorrected EVI time series.
2. Phenophase timings occurred later, with BRDF-corrected EVI time series, considering the BRDF effect on derived phenological metrics. The shifting was varied from several days to up to nearly two months. The lengths of the greening season were underestimated without BRDF correction, as BRDF-corrected EVI time series showed a longer growing season than BRDF-uncorrected EVI time series. These significant differences can alter the understanding of SEA tropical forest phenology and suggest the need for BRDF correction to capture precise seasonal forest dynamics.
3. The VI seasonality of SEA forests depended on the length of the dry season, as forests with shorter dry seasons had weaker seasonality, with higher

minimum EVI and lower maximum EVI. In addition, forests with the shortest dry seasons began their growing seasons earlier than other forests. Moreover, the seasonal VI profiles among forest types were more distinguishable after standardising VI at fixed sun-angles.

4. The phenological results with various sun-view angle settings revealed the insignificance of choosing different standardised viewing and illumination geometries, as the phenological variations were marginal.

5.1.2. Chapter three

The effects of disturbances on tropical forests were evaluated across continental SEA. To determine the forests influenced by disturbance, this study derived forest type coverage from a MODIS land cover map and represented those forests as mixed forests of both disturbed and non-disturbed forests, since coarse resolution LC maps do not distinguish between disturbed and non-disturbed forests. Disturbed forest sites were manually selected based on the 30-m Hansen Forest Cover Map to compare their phenology with adjacent undisturbed forests. This study extracted and compared VI time series, seasonal profiles and phenological metrics between undisturbed and disturbed forests to analyse disturbance influence on forest phenology. The effect of BRDF on the analyses between non-disturbed and disturbed forests was also considered.

The results demonstrated that:

1. The disturbance influence on forest seasonal phenology varied based on the lengths of their dry seasons. Although the EVI of disturbed forests with zero to two months of dry season was higher than non-disturbed forests, disturbed forests with longer dry seasons had higher maximum and lower minimum EVI values than undisturbed forests. This outcome demonstrates the different responses of disturbed forests associated with younger, regenerating plants and their sensitivity to the water deficit during dry seasons (possible due to their undeveloped and shallow rooting systems).
2. Phenological comparisons of disturbed forests showed a later onset of the greening season, rather than early green-up as in intact forests, due to the predominance of secondary forest canopies. Continuous disturbance, preventing forest maturity, was the primary cause of this phenomenon.

3. The effect of disturbance on seasonal VI profiles was different on each site at the 30 m scale. Although some forests altered their annual VI profiles after the time of their most disturbed state, other forests recovered their seasonal greenness within the 16-year study period, with insignificant forest percentage loss.
4. The BRDF influence on disturbed forests was amplified, which was related to the changes in forest canopy structure to more porous conditions. The NDVI of disturbed forests was significantly sensitive to the BRDF effect, unlike non-disturbed forests, which showed NDVI resilience to the BRDF influence. In some cases, the amplification of the BRDF effect helped to separate VI patterns between disturbed and non-disturbed forests, while BRDF-uncorrected VI time series were identical between forest types.

5.1.3. Chapter four

This chapter investigated the VI trends and anomalies of SEA tropical forests and the relationship between VI inter-annual variations and climate variability. The BRDF influence on VI trends and anomalies was considered by comparing results derived from BRDF-corrected and uncorrected VI time series. Trend slopes of undisturbed forests at a 30 m scale and mixed forests of CMG 0.05 degree spatial resolution were generated to compare trends between non-disturbed and disturbed forests, respectively. Using multiple satellite data sourced in relation to climate variables, such as rainfall (CHIRPS), total water storage (GRACE), solar radiation (CERES) and LST (MODIS), trends and anomalies of climate variables were calculated and the relationship with inter-annual VI changes of tropical forests over the continental SEA region was analysed.

The results presented that:

1. SEA forest greening occurred during the study period (2001–2016). However, the VI greening represented as annual trend maps and trend slopes was significant, while upward trends during the dry season periods were found to be insignificant. Moreover, non-disturbed forests had lower trend slopes than forests influenced by disturbance.

2. BRDF influenced both VI trends and anomalies in SEA tropical forests. BRDF-corrected EVI produced trend maps with extended significant positive trending areas and higher positive trends than BRDF-uncorrected EVI. In some cases, BRDF-corrected EVI yielded negative trend slopes while BRDF-uncorrected EVI yielded positive trend slopes. Although inter-annual VI anomalies of BRDF-uncorrected VI contained abnormal values, BRDF correction could minimise those uncertainties caused by the BRDF effect.
3. Forest EVI anomalies were dependent on inter-annual rain, TWS and solar radiation anomalies. Solar radiation and LST anomalies demonstrated an association with ENSO events. Negative correlation of trend slopes between LST and VI suggest the increasing LST limited forest vegetation activities.

5.2. General Future Research Directions

Chapter 2 provided a better understanding of BRDF influence on seasonal VI profiles and phenological metrics derived from satellite-observed VI. The substantial effect of BRDF suggests that standardising reflectance and VI at fixed sun-view angles is an essential process to analyse tropical forest phenology in continental SEA. BRDF correction can help avoid unnecessary controversy related to the effect of varying illumination angles and viewing geometries of satellite-based observations. However, there are other BRDF factors that may affect satellite observations, such as landscape topography. BRDF correction applied to optical satellite data, such as Landsat or Sentinel-2, must consider the effect of landscape topography, as topographic effects significantly influence the retrieval of vegetation dynamics for high spatial resolution satellite data.

Chapter 3 investigated the disturbance effect on SEA forest dynamics and examined the effect of BRDF on disturbed forest VI observations. However, the complexity of the disturbance effect requires further study. This study only used optical satellite observations for the analyses, with limited knowledge of tree species and disturbance types. Although various disturbance types and degrees may influence forest VI dynamics differently, future fieldwork is crucial to collect ground measurements to validate the findings of this study and clarify the role of disturbance types on forest seasonal and inter-annual phenology. As the results demonstrated, evidence of the

amplifying effect of BRDF on disturbed forest observations, fieldwork studies can help to understand BRDF influences caused by canopy structure changes.

Chapter 4 examined inter-annual VI variations of SEA tropical forests and the relationship with climate variability. Although this study compared VI trends and anomalies between undisturbed and mixed forests, detailed analyses of the disturbance effect on inter-annual dynamics must be conducted. Moreover, some datasets related to climate variables were provided at coarse spatial resolutions (~100 km) at which observations are only appropriate for quantifying changes over areas larger than the observed footprint. Although this study produced phenological analyses on MODIS data at 500 m and 0.05 degree scales, the different spatial resolution may cause uncertainties in the results. Finally, cross-correlation analysis may be essential to explain the relative importance of the climate factors to VI inter-annual dynamics across tropical forests of continental SEA.

Overall, future phenology research using optical satellite data was recommended to apply BRDF correction for phenological information retrieval. Moreover, additional studies are required to understand the effect of disturbance and BRDF on SEA tropical forest phenology.

5.3. Conclusion

This thesis analysed SEA tropical forest responses to climate seasonality, disturbance and sun-angle geometries using satellite observations. All objectives were met, and the investigations were conducted using suitable methodology and essential criteria. Given the importance of understanding SEA forest phenology and minimising the uncertainties of outcomes derived from optical satellite observations, particularly under the influences of varying sun-view observed angles, this thesis makes an essential and considerable contribution to that purpose.